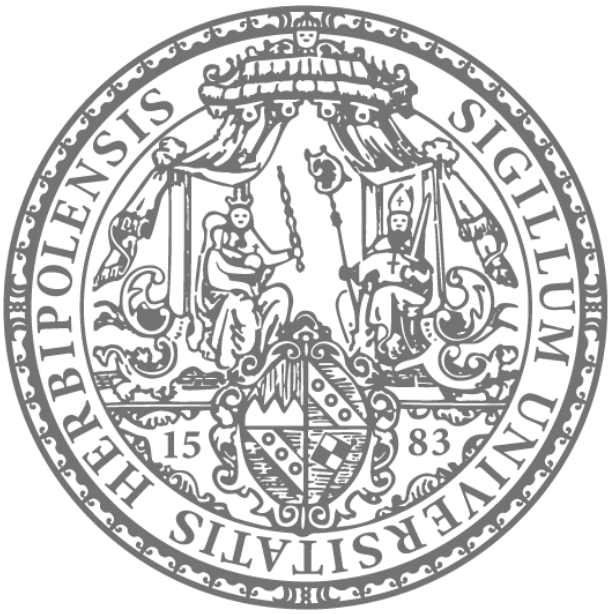

The Bacterial Exo- and Endo-Cytoskeleton Spatially Confines Functional Membrane Microdomain Dynamics in *Bacillus subtilis*

Das bakterielle Außen- und Innenskelett begrenzt die Mobilität funktionaler Membranmikrodomänen in *Bacillus subtilis* räumlich

Doctoral thesis for a doctoral degree at the Graduate School of Life Sciences,
Julius-Maximilians-Universität Würzburg, Section Infection and Immunity

submitted by

Rabea Marie Wagner

born in **Freiburg i. Br., Germany**

Würzburg, July 2020

Submitted on:

Members of the Thesis Committee

Chairperson:	**Prof. Dr. Thomas Rudel**
Primary Supervisor:	**Dr. Daniel Lopez**
Supervisor (Second):	**Prof. PhD Samuel Wagner**
Supervisor (Third):	**Prof. Dr. Nicolai Siegel**

Date of Public Defense:

Date of Receipt of Certificates:

Affidavit

I hereby confirm that my thesis entitled '**The Bacterial Exo- and Endo-Cytoskeleton Spatially Confines Functional Membrane Microdomain Dynamics in *Bacillus subtilis***' is the result of my own work. I did not receive any help or support from commercial consultants. All sources and/or materials applied are listed and specified in the thesis.

Furthermore, I confirm that this thesis has not yet been submitted as part of another examination process neither in identical nor in similar form.

Place, Date Signature

Eidesstattliche Erklärung

Hiermit erkläre ich an Eides statt, die Dissertation '**Das bakterielle Außen- und Innenskelett begrenzt die Mobilität funktionaler Membranmikrodomänen in *Bacillus subtilis* räumlich**' eigenständig, d. h. insbesondere selbstständig und ohne Hilfe eines kommerziellen Promotionsberaters, angefertigt und keine anderen als die von mir angegebenen Quellen und Hilfsmittel verwenden zu haben.

Ich erkläre außerdem, dass die Dissertation weder in gleicher noch in ähnlicher Form bereits in einem anderen Prüfungsverfahren vorgelegen hat.

Ort, Datum Unterschrift

TABLE OF CONTENTS

1 ABBREVIATIONS

aa	Amino acids
AMP	Ampicillin
APS	Ammonium persulfate
BN-PAGE	Blue native polyacrylamide gel electrophoresis
BNZ	Benzyl alcohol
C, Ctrl	Control condition
CFU	Colony forming units
DDM	n-Dodecyl-B-D-maltoside
Δ	Delta; deletion mutation
DiI-C12	1,1'-Didodecyl-3,3,3',3'-tetramethylindocarbocyanine perchlorate
$DiOC_2(3)$	3,3'-Diethyloxacarbocyanine iodide
DRM	Detergent resistant membrane
DSM	Detergent sensitive membrane
DTT	Dithiothreitol
EA	aa glutamate and alanine
ELISA	Enzyme-linked immunosorbent assay
EPI	Epifluorescence microscopy
Exp	Experimental condition
FL	Fluorescein
FMM	Functional Membrane Microdomains
FOS	Fosfomycin
GFP	Green Fluorescent Protein
HRP	Horseradish peroxidase
LTA	Lipoteichoic acids
MAR	Membrane-anchor region
MIC	Minimal Inhibitory Concentration
MIP	Maximum Intensity Projection
MRSA	methicillin-resistant *Staphylococcus aureus*
MSD	Mean Square Displacement
NA	Numerical Aperture
NAG	N-acetylmuramic acid
NAM	N-acetylglucosamine
NIS	Nisin
OD_{600}	Optical density at 600 nm
ONC	Overnight culture
PBP	Penicillin-binding protein
PCR	Polymerase Chain Reaction
PHB	Prohibitin homologues protein domain
RIF	Regions of Increased Fluidity

ABBREVIATIONS

RT	Room temperature
SDS-PAGE	Sodium dodecyl sulfate polyacrylamide gel electrophoresis
TIRFM	Total Internal Reflection Fluorescence Microscopy
TG	Transglycosylation
TP	Transpeptidation
TUN	Tunicamycin
V	Volume
VAL	Valinomycin
VAN	Vancomycin
WT	Wild Type
WTA	Wall teichoic acids

2 SUMMARY

Cellular membranes form a boundary to shield the inside of a cell from the outside. This is of special importance for bacteria, unicellular organisms whose membranes are in direct contact with the environment. The membrane needs to allow the reception of information about beneficial and harmful environmental conditions for the cell to evoke an appropriate response. Information gathering is mediated by proteins that need to be correctly organized in the membrane to be able to transmit information. Several principles of membrane organization are known that show a heterogeneous distribution of membrane lipids and proteins. One of them is functional membrane microdomains (FMM) which are platforms with a distinct lipid and protein composition. FMM move within the membrane and their integrity is important for several cellular processes like signal transduction, membrane trafficking and cellular differentiation. FMM harbor the marker proteins flotillins which are scaffolding proteins that act as chaperones in tethering protein cargo to FMM. This enhances the efficiency of cargo protein oligomerization or complex formation which in turn is important for their functionality. The bacterium *Bacillus subtilis* contains two flotillin proteins, FloA and FloT. They form different FMM assemblies which are structurally similar, but differ in the protein cargo and thus in the specific function.

In this work, the mobility of FloA and FloT assemblies in the membrane was dissected using live-cell fluorescence microscopy techniques coupled to genetic, biochemical and molecular biological methods. A characteristic mobility pattern was observed which revealed that the mobility of both flotillins was spatially restricted. Restrictions were bigger for FloT resulting in a decreased diffusion coefficient compared to FloA. Flotillin mobility depends on the interplay of several factors. Firstly, the intrinsic properties of flotillins determine the binding of different protein interaction partners. These proteins directly affect the mobility of flotillins. Additionally, binding of interaction partners determines the assembly size of FloA and FloT. This indirectly affects the mobility, as the endo-cytoskeleton spatially restricts flotillin mobility in a size-dependent manner. Furthermore, the extracellular cell wall plays a dual role in flotillin mobility: its synthesis stimulates flotillin mobility, while at the same time its presence restricts flotillin mobility. As the intracellular flotillins do not have spatial access to the exo-cytoskeleton, this connection is likely mediated indirectly by their cell wall-associated protein interaction partners. Together the exo- and the endo-cytoskeleton restrict the mobility of FloA and FloT.

Similar structural restrictions of flotillin mobility have been reported for plant cells as well, where the actin cytoskeleton and the cell wall restrict flotillin mobility. These similarities between eukaryotic and prokaryotic cells indicate that the restriction of flotillin mobility might be a conserved mechanism.

3 ZUSAMMENFASSUNG

Zelluläre Membranen bilden eine Barriere um das Zellinnere von dem -äußeren abzuschirmen. Das ist insbesondere bei Bakterien wichtig, einzellige Organismen, deren Membranen in direktem Kontakt zu ihrer Umgebung stehen. Die Membran muss es ermöglichen, Informationen über mögliche vorteilhafte oder schädliche Einflüsse in der Umgebung wahrzunehmen, damit die Zelle dementsprechend eine Reaktion initiieren kann. Die Informationsaufnahme und die resultierenden Reaktionen werden von Membranproteinen in Gang gesetzt, deren Organisation in der Membran Voraussetzung für ihre Funktionalität ist. Mehrere Prinzipien zur Membranorganisation sind bekannt, die alle eine heterogene Verteilung von Proteinen und Lipiden zu Grunde legen. Ein Beispiel für ein solches Prinzip sind funktionelle Membranmikrodomänen (FMM), Plattformen mit einer besonderen Lipid- und Proteinzusammensetzung. FMM bewegen sich in der Membran und ihre Integrität ist für viele zelluläre Prozesse wichtig, zum Beispiel für Signaltransduktion, Membrantransport oder zur zellulären Differenzierung. Flotilline sind Markerproteine für FMM. Sie bilden eine Art Gerüst und funktionieren als Chaperone, indem sie die sogenannten Frachtproteine in den FMM binden. Dort wird die Effizienz der Oligomerisierung oder Komplexbildung der Frachtproteine gesteigert, was für ihre Funktionalität und die ihrer assoziierten Prozesse von Bedeutung ist. In dem Bakterium *Bacillus subtilis* gibt es zwei Flotilline, FloA und FloT. Diese formen FMM Plattformen, die zwar strukturell ähnlich sind, sich aber in ihren Frachtproteinen und somit auch in ihren spezifischen Funktionen unterscheiden.

In dieser Arbeit wurde die Mobilität der FloA- und FloT-abhängigen Plattformen in der Membran untersucht. Dafür wurden Technologien der Fluoreszenzmikroskopie mit genetischen, biochemischen und molekularbiologischen Ansätzen kombiniert. Charakteristische Bewegungsmuster wurden beobachtet, die zeigten, dass die Beweglichkeit beider Flotilline räumlich begrenzt war. Dabei war die Einschränkung für FloT größer, und dementsprechend der Diffusionskoeffizient kleiner verglichen mit FloA. Die Mobilität von FloA und FloT hängt von dem Zusammenspiel mehrerer Faktoren ab. Zum einen bestimmen intrinsische Eigenschaften der Flotillinproteine ihre Fähigkeit verschiedene Interaktionspartner zu binden. Diese wirken sich dann direkt auf die Mobilität von Flotillinen aus. Des Weiteren bestimmt die Bindung verschiedener Interaktionspartner auch die Größe der FloA- und FloT-abhängigen Plattformen. Die resultierenden Größen beeinflussen die Mobilität indirekt, da das zelluläre Innenskelett die Flotillinmobilität räumlich in größenabhängiger Weise begrenzt. Außerdem spielt das Außenskelett der Zelle, die Zellwand, eine zweifache Rolle: die Zellwandsynthese fördert die Mobilität der Flotilline, während die Zellwand an sich gleichzeitig die Mobilität der Flotilline einschränkt. Da Flotilline räumlich keine Verbindung zum Außenskelett haben, wird diese Verbindung wahrscheinlich durch ihre Zellwand-assoziierten Interaktionspartner übermittelt. Zusammenfassend beschränken das Außen- und das Innenskelett die Mobilität von FloA und FloT.

In Pflanzen wurden ähnliche strukturelle Beschränkungen der Mobilität von Flotillinen durch das Aktin-Zytoskelett und die Zellwand beschrieben. Diese Ähnlichkeit zwischen prokaryotischen und eukaryotischen Zellen deutet darauf hin, dass die Beschränkung der Mobilität der Flotillin-Plattformen ein konservierter Mechanismus sein könnte.

Especially in small unicellular organisms, a high level of subcellular organization in time and space needs to be provided for an efficient organization of all cellular processes. Membranes form the structural barrier to the environment and fulfill the functional communication with the outside world. Within membranes, lipid- and protein-interactions arrange membrane components into dynamic microdomains that are important for the functionality of cellular processes. How microdomains are spatio-temporally organized in bacterial membranes and which molecular mechanisms underlie their dynamics will be addressed here.

4 INTRODUCTION

4.1 Compartmentalization in Biology

Organization in space and time is essential for life to exist and proliferate. This principle includes compartmentalization and is valid throughout a wide scale in biology, ranging from organs in our body to organelles in our cells. Organelles fulfil the function of spatially and temporally separating cellular processes by creating specific microenvironments that can concentrate components or spatially isolate opposing reactions and consequently lead to an increase in efficiency. Apart from the cell being compartmentalized into organelles, the membrane surrounding the cells is compartmentalized as well. Membranes form the border between the intracellular components and the extracellular environment. They are essential for life and are crowded by proteins and cellular machineries (Grecco et al., 2011; Simons and Sampaio, 2011). The original fluid mosaic model postulated a homogeneous distribution of membrane lipids and proteins (Singer and Nicolson, 1972). It has gradually been updated with findings showing a more complex organization underlying the cellular membrane leading to the formation of microdomains, so-called lipid rafts (Pike, 2009; Krapf, 2018). New characterizations were enabled by microscopy advances reaching increasing spatial and temporal resolutions (Rajendran and Simons, 2005; Kusumi et al., 2010, 2012; Klammt and Lillemeier, 2012; Krapf, 2018). Super resolution microscopy revealed underlying principles of membrane organization and compartmentalization which are of great importance for the cell to be able to quickly react and adapt to extracellular stimuli and ultimately to survive and proliferate.

4.2 Membrane compartmentalization in eukaryotic cells

The plasma membrane in eukaryotic cells is organized in different levels. Its compartmentalization can be achieved structurally and functionally (Klammt and Lillemeier, 2012; Krapf, 2018). The most recognized models of membrane compartmentalization in eukaryotic cells are the picket-fence model and lipid rafts. The picket-fence model describes structural membrane compartmentalization and lipid rafts describe functional membrane compartmentalization (Chichili and Rodgers, 2009; Krapf, 2018). The structure and function of both will be explained in more detail.

4.2.1 Picket-fence model – unspecific structural membrane organization

Membrane components are dynamic and move within the membrane. While studying the dynamics of membrane molecules a substantial 20-fold discrepancy between diffusion coefficients in the plasma membrane of intact cells and in artificial membranes was observed (Murase et al., 2004; Kusumi et al.,

2010, 2012). This difference was not only detected for transmembrane proteins, but also for lipids residing in the extracellular leaflet of the membrane (Fujiwara et al., 2002; Morone et al., 2006). Cells must contain components or structures that can account for these differences. In membranes blebs, an increase in mobility of membrane components compared to the native membrane can be observed as well which rules out that the membrane composition can account for the differences (Kusumi et al., 2010, 2012). Rather, cellular structures that can influence the mobility of membrane components must be the reason. To explain these observations, the picket-fence model was proposed. It links membrane components with underlying cytoskeletal structures to explain the reduced mobility in native membranes.

One of the main structural components in eukaryotic cells is the actin cytoskeleton. It forms a dense meshwork of filaments at the cytoplasmic interface of the plasma membrane and covers the entire cell (Morone et al., 2006). The meshwork is in close association with the plasma membrane by interacting with membrane-integrated proteins, either directly or indirectly but specifically via connecting molecules (Kusumi et al., 2012). The consequence of these interactions is a membrane-actin distance of <1 nm (Morone et al., 2006). The actin meshwork partitions the plasma membrane into small nanometer-sized

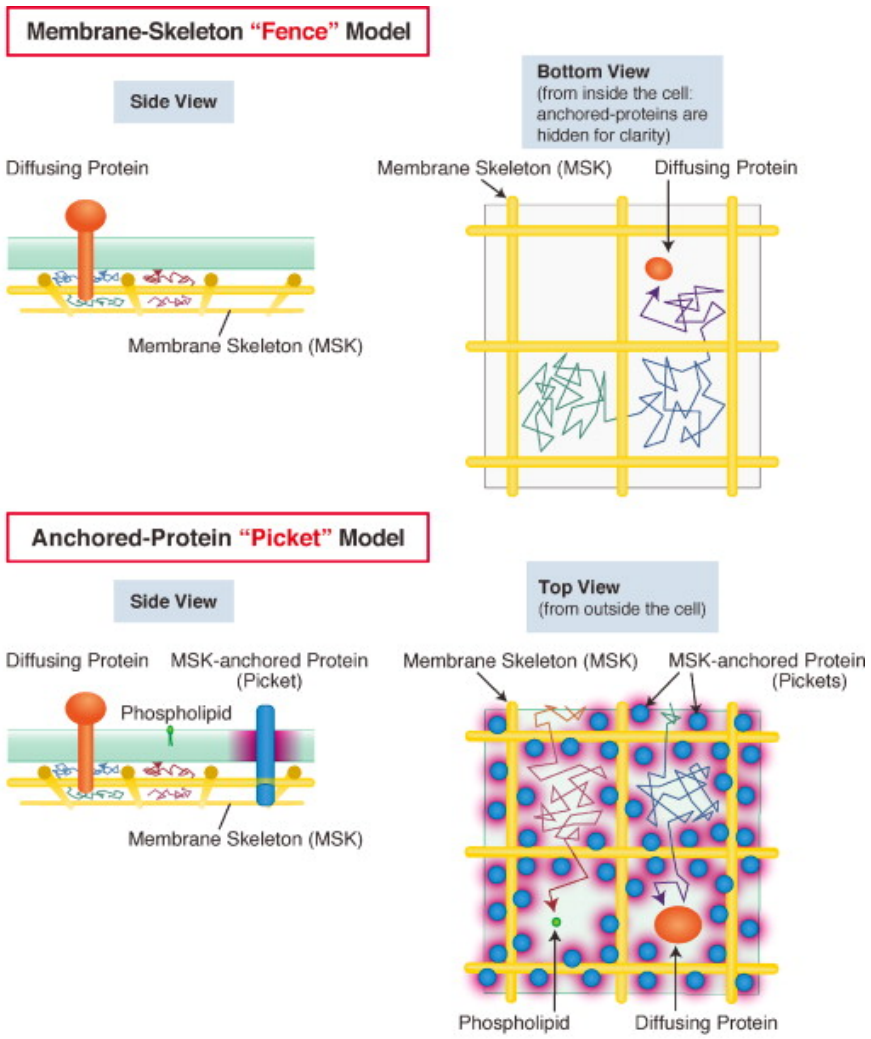

Figure 1: Hop-diffusion can be explained with the picket-fence model. The actin cytoskeleton forms a meshwork in close proximity to the inner side of the membrane and partitions it into several compartments and is therefore regarded as the fence (top). Membrane skeleton (MSK) anchored transmembrane proteins are regarded as the pickets (bottom). Together the cytoskeleton and the transmembrane proteins impact the diffusion of membrane components, leading to hop-diffusion. Image adapted with permission of the publisher, original publication by Kusumi et al., 2012.

compartments which resembles a fence-like structure. Compartment sizes depend on the cell type and reach 40-300 nm in diameter (Kusumi et al., 2012; Andrade et al., 2015) that increase upon actin depolymerization (Klammt and Lillemeier, 2012; Fujiwara et al., 2016; Krapf, 2018). This close proximity and the structural order profoundly affects the diffusion of transmembrane proteins: they must collide with the actin cytoskeleton with their cytosolic domains and this collision induces a temporary confinement of the protein inside the compartment (Figure 1 top) (Sako and Kusumi, 1994; Kusumi et al., 2010). The actin cytoskeleton is structurally and functionally integrated into the plasma membrane and forms a cage- or fence-like structure underneath the membrane that hinders the free diffusion of transmembrane proteins in a protein-unspecific manner (Kusumi et al., 2010). The compartmentalization of the membrane by the actin cytoskeleton on the cytoplasmic surface of the plasma membrane explains the reduced diffusion of transmembrane proteins in cells compared to artificial membranes (Kusumi et al., 2012). Nevertheless, even membrane lipids residing in the outer leaflet of the membrane show a reduced diffusion (Fujiwara et al., 2002; Morone et al., 2006), although direct interaction with the actin cytoskeleton is impossible (Weisswange et al., 2005; Kusumi et al., 2010, 2012; Klammt and Lillemeier, 2012). This can be explained by transmembrane proteins that are interacting with the actin cytoskeleton in a stable or temporary manner. They form a barrier against the free diffusion of lipids and resemble the pickets of a fence (Figure 1 bottom) (Fujiwara et al., 2002; Murase et al., 2004). This not only includes the steric hindrance of the proteins themselves, but also the hydrodynamic friction effect at their surface, as the membrane lipids adjacent to the immobile proteins shows increased viscosity (Figure 1 bottom, pink area) (Bussell et al., 1994, 1995). The combination of the actin cytoskeleton at the cytoplasmic surface of the plasma membrane (=fence) and the transmembrane proteins linked to the actin (=pickets) form a unspecific temporal semipermeable restriction barrier that physically limits the free diffusion of membrane molecules.

The underlying cellular structures of the picket-fence model lead to a characteristic diffusion pattern for proteins and lipids called hop-diffusion (Kusumi et al., 2010, 2012), which has also been studied theoretically (Powles et al., 1992; Kalay et al., 2008; Kenkre et al., 2008; Niehaus et al., 2008; Novikov et al., 2011). Membrane components diffuse freely within single compartments (microdiffusion) eventually hopping into a neighboring compartment (macrodiffusion) (Figure 1) (Kusumi et al., 2010). This can be explained with a temporal and local dissociation of the actin cytoskeleton from the plasma membrane (Tomishige et al., 1998). Microdiffusion values were found to be comparable to those in artificial membranes, and macrodiffusion values are comparable to those in native cell membranes (Klammt and Lillemeier, 2012; Kusumi et al., 2012). The bottleneck to distinguish between macrodiffusion and hop-diffusion in the plasma membrane is the temporal resolution of image acquisition. Fast single-molecule imaging at high frame rates of 0.02 ms (corresponding to 50,000 frames per second) is required to be able to detect hop-diffusion, as hopping events occur every 1-50 ms and can only be detected at a 100-fold temporal resolution (Kusumi et al., 2010, 2012). Membrane components undergo unrestricted diffusion within compartments combined with restricted diffusion at the compartment barriers. At the cellular level, this leads to an overall reduced mobility which explains the 20-fold diffusion difference between the plasma membrane and artificial membranes (Kusumi et al., 2012).

The plasma membrane organization by the picket-fence model should impact the function of membrane molecules and thus provide benefits for the cell. The order created by the actin filaments regulates the distribution and interaction of receptors for signal transduction in either inhibiting (Wang et al., 2001; Lajoie et al., 2007; Treanor et al., 2010) or enabling (Gómez-Móuton et al., 2001; Rodgers and Zavzavadjian, 2001; Baumgartner et al., 2003) interactions. The frequency of two receptors dimerizing for signal transduction is the same with or without compartments seen over the whole cell membrane (Kusumi et al., 2012). Receptor clustering is decreased when receptors are located in different compartments, but it is highly increased if two receptors end up in the same compartment (Saxton, 2001; Kusumi et al., 2012). There, interaction reactions are locally enhanced. A specific function of the membrane compartments induced by the actin cytoskeleton is the oligomerization-induced trapping which leads to local polarized signaling events. The diffusion of molecules decreases due to an increase in size upon oligomerization into larger complexes. The diffusion is further reduced as larger complexes are more likely to be bound to the actin cytoskeleton (Kusumi and Sako, 1996; Iino et al., 2001; Kusumi et al., 2010). Monomers can hop comparably easy between compartments, whereas oligomers are restricted to a single compartment for a longer time and exhibit a slower hop rate (Kusumi et al., 2012). Environmental stimuli can lead to oligomerization of membrane proteins that are then temporarily trapped. This can serve the cell as a kind of memory function which can be important for cellular processes such as chemotaxis (Kusumi et al., 2010, 2012). The picket-fence-model suggests that cells unspecifically compartmentalize their membrane leading to specific protein diffusion patterns that favor protein interaction-dependent signaling events (Gupta et al., 2006; Lajoie et al., 2007; Krapf, 2018).

4.2.2 Lipid Rafts – specific functional membrane organization

In addition to the unspecific membrane organization by picket-fence model, lipid rafts functionally organize several cellular processes in lipid rafts. Lipid rafts are laterally mobile, nanosized membrane regions that organize and regulate membrane components (Krapf, 2018) and have been found to be involved in many cellular processes, like cell signaling, membrane trafficking and migration (Rajendran and Simons, 2005; Stuermer, 2010; Otto and Nichols, 2011). Lipid rafts form membrane platforms tightly packed with lipids and proteins and can be biochemically enriched for molecular analysis. After non-ionic detergent treatment (Triton X-100 at 4°C) of the membrane, it can be separated into detergent sensitive membrane (DSM) and detergent resistance membrane (DRM) fractions. The DRM fraction is enriched in lipid rafts and used as an approximation for their analysis. Due to the compact lipid packaging, the DRM fraction floats at low density during membrane gradient centrifugation which led to the name lipid rafts (Yu et al., 1973; Brown and Rose, 1992; Edidin, 2003). The lipid raft-enriched DRM fraction can be used to perform biochemical and molecular analyses of lipid rafts (Heerklotz, 2002; Munro, 2003; Rajendran and Simons, 2005; Chichili and Rodgers, 2009; Pike, 2009; Kusumi et al., 2012). Following this protocol, structural and functional components of lipid rafts have been characterized. The constituent lipids and the flotillin proteins are structural components whereas the protein cargo is the functional component.

Biological membranes contain a variety of different lipid species that laterally segregate into distinct regions due to their physico-chemical properties (Cronan, 2003; van Meer et al., 2008; Lingwood and Simons, 2010; Coskun and Simons, 2011; Simons and Sampaio, 2011). The lipid components of eukaryotic lipid rafts are mainly cholesterol and glycosphingolipids (Figure 2) (Brown and Rose, 1992; Pike et al., 2002). The amphipathic properties as well as conical and inverse-conical shapes of cholesterol and sphingolipids, respectively, allow for tight packaging, as the voids created by sphingolipid assemblies are filled with cholesterol (Simons and Ikonen, 1997). This leads to the formation of stable lipid-lipid interactions creating ordered, submicroscopic, highly-dynamic assemblies that float within the membrane (Rajendran and Simons, 2005).

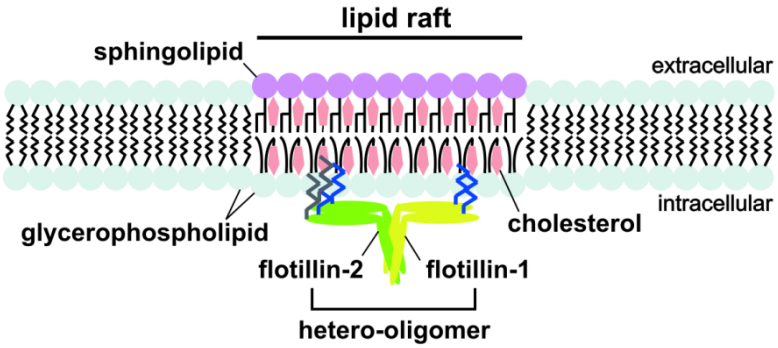

Figure 2: Structural components of lipid rafts. The lipid components (glycosphingolipids and cholesterol) and the flotillin proteins are displayed, together creating lipid rafts. Image credits: Kurrle et al., 2012, published under CC-BY-3.0.

Analyses of lipid rafts not only consistently identified the constituent lipids described above but also proteins. The same proteins were identified in floating DRM fractions of different cell types under different conditions. They were named flotillins and are considered to be marker proteins of lipid rafts (Bickel et al., 1997; Pike, 2009; Stuermer, 2010). Two homologous flotillins exist in mammalian cells, flotillin-1 and flotillin-2 (Figure 2). Flotillins are part of a protein family characterized by a prohibitin homology domain (PHB; also called SPFH domain from stomatin, prohibitin, flotillin and HflK/C) (Liu et al., 2005; Browman et al., 2007) which is commonly found in integral membrane proteins that oligomerize to stabilize lipid rafts (Otto and Nichols, 2011). The PHB domain of flotillin is located at the N-terminal half of the protein which confers membrane association mediated by a hydrophobic stretch, acylation sites and hydrophobic hairpins (Morrow et al., 2002; Neumann-Giesen et al., 2004; Morrow and Parton, 2005; Stuermer, 2010). The C-terminal half contains the flotillin domain: an alpha-helix forming a coiled-coil structure (Schulte et al., 1997) important for the oligomerization of flotillins into homo- and hetero-tetramers (Figure 2) (Babuke and Tikkanen, 2007; Solis et al., 2007; Kurrle et al., 2012). This domain is conserved and exclusive in all flotillins (Browman et al., 2007). Both, the PHB domain and the flotillin domain are necessary to confer localization of flotillins to the DRM fraction (Solis et al., 2007).

Flotillins are ubiquitously present across the evolutionary spectrum, including plants (Borner et al., 2005), bacteria (Hinderhofer et al., 2009) and fungi (Takeshita et al., 2012) and are considered an ancient protein family. Due to their importance in many different cellular processes (Babuke and Tikkanen, 2007), it is likely that they regulate basic cellular functions by possessing a structural scaffolding function which has been proposed in several studies (Rajendran and Simons, 2005; Stuermer, 2010). Overall, flotillins provide molecular scaffolding and chaperone activity in lipid rafts and

facilitate compartmentalization and functional specialization within the membrane. In this manner, they promote the assembly, interaction and oligomerization of signaling partners and cell surface proteins to aid in signal transduction (Stuermer, 2010).

Lipid rafts assemble by the heterogeneous distribution of different lipid species in the membrane because of lipid-lipid immiscibility due to their physico-chemical properties (Mouritsen and Bloom, 1984; Rajendran and Simons, 2005; Bernardino de la Serna et al., 2016). As the lipids of lipid rafts are enriched in longer saturated hydrocarbon chains, this allows tight packaging and leads to the formation of platforms of less fluid states that are thicker than the surrounding membrane (Kuzmin et al., 2005; Rajendran and Simons, 2005). Proteins locate to rafts due to their affinity for the unusual lipid composition (Bretscher and Munro, 1993; Baumgart et al., 2007) which allows their selective exclusion and inclusion (Nykjaer et al., 1994; Field et al., 1995; Simons and Sampaio, 2011). Thus, this lipid environment provides unspecific scaffolding activity that facilitates the concentration of proteins. The association of proteins to lipid rafts is a flexible and dynamic process that is often of transient nature. Lipid rafts mostly do not exceed sizes of 5-20 nm and are extremely dynamic due to weak interactions and consequently have a short lifetime (Kusumi et al., 2012). Upon physiological stimulation by extracellular signals, protein-protein interactions appear and stabilize leading to the formation of spatially and temporally stable clusters that can exceed the size of lipid rafts before stimulation (Kusumi et al., 2012). The natural lipid raft in the plasma membrane is the transient unstable state which turns into stable functional rafts upon stimulation. All of these lipid-lipid, lipid-protein, and protein-protein interactions together play key roles in the formation and proper functioning of lipid rafts (Klammt and Lillemeier, 2012).

Many different proteins are detected in lipid rafts in addition to flotillins, called the protein cargo, that constitute the functional component of lipid rafts. These proteins share some structural similarities as they are often associated with the lipid rafts with a GPI-anchor or by palmitoylation or myristoylation (Brown and Rose, 1992; Zacharias et al., 2002; Smotrys and Linder, 2004; Rajendran and Simons, 2005; Levental et al., 2010). Apart from structural similarities, their functions are more diverse, reflecting the different cellular processes that lipid rafts are involved in. The localization of proteins to lipid rafts plays a role in the proteins' correct functionality (Klein et al., 1995; Mutoh et al., 1995) and thus the protein cargo reveals information about the underlying cellular processes. Many proteins related to signal transduction and adhesion have been found to be associated with lipid rafts and accordingly, studies showed the importance of lipid rafts for cell signaling, membrane trafficking, cell-cell adhesion, endocytosis, migration, polarization and more (Rajendran and Simons, 2005; Stuermer, 2010; Otto and Nichols, 2011). The formation of lipid rafts allows the cell to manage membrane components to trigger favorable mechanisms by locally increasing concentrations but also to avoid unwanted reactions by segregating membrane components. Together, this tight regulation of membrane components enables highly specific biochemical functions (Krapf, 2018). Severe consequences have been reported to occur once lipid rafts are perturbed, in single cells and even the whole organism. Lipid raft perturbance has been related to Alzheimer's and Parkinson's disease. In this sense, the functionality of lipid rafts can have far-reaching implications (Michel and Bakovic, 2007).

4.2.3 The dynamics of lipid rafts in the picket-fence model

As stated above, the membrane is structurally compartmentalized by the cytoskeleton (picket-fence model) and functionally compartmentalized by protein- and lipid-interactions that lead to the formation of lipid rafts. These two principles of plasma membrane organization do not exclude each other, they can coexist (Pralle et al., 2000; Klammt and Lillemeier, 2012; Kusumi et al., 2012). The size of unstimulated lipid rafts of 5-20 nm fits well into the compartments created by the picket-fence model with sizes of 40-300 nm (Kusumi et al., 2012). Additionally, the transient and unstable nature of unstimulated lipid rafts allows their components to independently move between compartments. Lipid rafts can coexist within the actin cytoskeleton-induced compartments of the plasma membrane, but their mobility and stability are likely to be affected by the diffusion barriers (Figure 3). Therefore, it is not surprising that the DRM was found to be enriched in cytoskeletal proteins, including actin, tubulin and myosin (Nebl et al., 2002; Yu et al., 2008) and that flotillin was found to interact with actin (Langhorst et al., 2007; Neumann-Giesen et al., 2007). The stabilization and expansion of lipid rafts upon stimulation and possible raft coalescence is limited by the compartment barriers (Baumgart et al., 2007; Kusumi et al., 2012). However, raft proteins binding the actin cytoskeleton exist that can overcome its barrier function which can lead to the formation of larger rafts (Rodgers and Zavzavadjian, 2001; Viola and Gupta, 2007; Goswami et al., 2008; Chaudhuri et al., 2011; Kusumi et al., 2012). Thus, the actin cytoskeleton keeps individual lipid rafts apart or stabilizes and enlarges them, depending on their protein content and the respective functionality (Kusumi et al., 2010). The flotillin-cytoskeleton interaction has been shown to be important for cellular processes like cell migration or T-cell activation (Chichili and Rodgers, 2009; Ludwig et al., 2010).

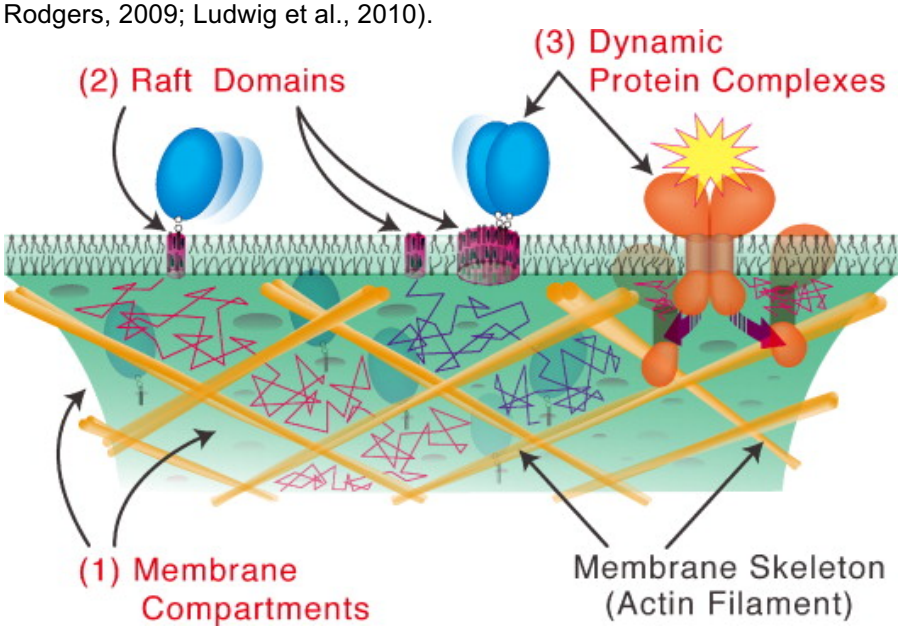

Figure 3: Lipid rafts can coexist within the picket-fence model. Raft domains of different sizes and protein oligomers are displayed within the compartments created by the actin cytoskeleton. Image displayed with permission of the publisher, original publication Kusumi et al., 2012.

4.2.4 The cell wall impacts lipid raft dynamics in plants

Eukaryotic cells of animals and plants are structurally different. In addition to the endo-cytoskeleton inside of cells, plant cells are surrounded by an exo-cytoskeleton as well, the cell wall. The call wall protects the cell from bursting due to internal turgor pressure. A recent paper studying flotillin dynamics in the plant *Arabidopsis thaliana* has shown that not only does the microtubules cytoskeleton spatially

restrict flotillin localization (Daněk et al., 2019). Additionally, the synthesis and structure of the cell wall is important for flotillin dynamics. In this study, the dynamics of flotillins was increased when the cell wall was partially removed enzymatically which lead the authors to postulate structural components linking cell wall and membrane that play an important role in flotillin-mediated cellular processes (Daněk et al., 2019).

4.2.5 Impact of membrane compartmentalization

The interplay of the structural cytoskeleton and the functional lipid rafts organize the plasma membrane in eukaryotic cells. These two principles work together to ensure a dynamic and complex plasma membrane where all molecules function together to achieve the best physiological response to any environmental stimuli. The integrity of the whole cell depends on the correct organization of the membrane. This is of special importance in unicellular organisms where all reactions are taking place in the same cellular entity (Rudner and Losick, 2010). Nevertheless, the existence of lipid rafts has long been considered an important step in the evolution of eukaryotic cells. Bacteria were believed to be organisms too simple to acquire such differentiation (Bramkamp and Lopez, 2015; Wagner et al., 2017). But indeed, several principles of membrane organization were discovered in the bacterium *Bacillus subtilis* including regions of increased fluidity (RIF) (Strahl et al., 2014) and functional membrane microdomains (FMM) (López et al., 2010) which will be explained in more detail.

4.3 The bacterium *Bacillus subtilis* as model organism for cellular biology

B. subtilis is a Gram-positive, rod-shaped, motile bacterium belonging to the phylum Firmicutes. It is relatively large in size with a length of around 3 µm, and a width of around 0.6 µm. As a facultative anaerobe, it naturally occurs in the upper layers of the soil (Earl et al., 2008), a habitat that is prone to constant and drastic environmental changes leaving the cells exposed to various stresses including nutrient limitation. Adaptation to these conditions is owed to its natural competence (Earl et al., 2008) and to the genetic program of cellular differentiation leading to the formation of endospores that can endure heat, drought, salinity, radiation, solvents and extreme pH (Earl et al., 2008; McKenney et al., 2013). Due to this interesting cellular differentiation and the possibility of the genetic manipulation making use of its natural competence, *B. subtilis* turned into a widely used model for cellular biology that is considered to be the best-characterized Gram-positive bacterium (Earl et al., 2008). Furthermore, itself being non-pathogenic and non-toxicogenic with phylogenetic proximity to the opportunistic pathogenic families Staphylococcaceae and Listeriaceae renders importance to *B. subtilis* for molecular biological and medical research. *B. subtilis* was one of the first organisms whose genome was completely sequenced (Kunst et al., 1997) and many regulatory and metabolic pathways are well studied (van Dijl and Hecker, 2013). *B. subtilis* is used in agriculture as a soil inoculant functioning as a biological fertilizer and fungicide (Ngugi et al., 2005; Earl et al., 2008; Swain and Ray, 2009) and its spores are used in the industry as indicator of successful sterilization processes. Additionally, its ability to secrete high yields of molecules and proteins has it being used in the biotechnological industry (van Dijl and Hecker, 2013). Recently, the use of bacterial lipid rafts for biotechnological productions was proposed (Lv et al., 2020a, 2020b, 2020c). The extensive knowledge and easy tractability make *B. subtilis* a

suitable model organism. Therefore, it is not surprising that several principles of membrane compartmentalization and organization were first discovered in *B. subtilis* and are most studied in this organism.

4.4 Membrane compartmentalization in *B. subtilis*

Bacterial membranes are composed of different lipid species. This opened the possibility for heterogeneous membrane organization which might lead to the formation of membrane domains as observed in eukaryotes (White and Frerman, 1967; Parsons et al., 2013). The membrane lipid cardiolipin was found to be important for chemotaxis when enriched at division sites and at the cell poles in *B. subtilis* and *Escherichia coli* membranes (Mileykovskaya and Dowhan, 2000; Kawai et al., 2004). This was one of the first indications that a heterogeneous membrane organization exists in bacteria. Additional membrane organization principles that were discovered include functional membrane microdomains (FMM) (López et al., 2010) that are structurally and functionally similar to eukaryotic lipid rafts (Bramkamp and Lopez, 2015; Lopez and Koch, 2017; Yokoyama and Matsui, 2020), and regions of increased fluidity (RIF) (Strahl et al., 2014). It became clear that the membrane components of bacteria are heterogeneously distributed and create specific nano- or micro-environments with specialized functions: bacterial membranes are compartmentalized.

4.4.1 Regions of increased fluidity in *B. subtilis*

Regions of increased fluidity (RIF) exist in membranes of *B. subtilis* (Strahl et al., 2014). The existence of distinct fluid regions rather than a homogeneous membrane distribution was discovered with the specific fluorescent membrane dye DiI-C12 that harbors a high affinity for areas of increased fluidity due to its relatively short acyl chains (Baumgart et al., 2007; Zhao et al., 2013). The formation of RIF has been shown to depend on cytoskeletal proteins and it seems likely that the lipids that constitute these RIF are carrier lipids of precursors for cell wall synthesis (Strahl et al., 2014; Schirner et al., 2015; Oswald et al., 2016). The accumulation of fluid lipids in RIF affects the global lipid homeostasis leading to a decrease in the overall membrane fluidity. Likewise, the formation of RIF impacts membrane protein localization as proteins disperse due to their preference for specific lipid environments (Strahl et al., 2014). Lipid and protein assembly into RIF is one important principle of membrane organization in bacteria.

4.4.2 Functional membrane microdomains in *B. subtilis*

Another principle of membrane organization are functional membrane microdomains (FMM). They represent the opposite of RIF as they show decreased fluidity and thus an increased rigidity. FMM are the bacterial counterpart to eukaryotic lipid rafts. These microdomains differ from the surrounding membrane in a distinct lipid and protein composition (Bramkamp and Lopez, 2015). FMM were initially discovered in *B. subtilis* membranes during investigation of biofilm formation. In wild type (WT) cells, KinC dimerizes upon stimulation by the autoinducer surfactin and phosphorylates the global activator of biofilm formation Spo0A. The process of dimerization is favored in the presence of the *B. subtilis* flotillins FloA and FloT. Flotillin functionality in turn depends on the lipids synthesized by YisP. A *yisP* deletion abrogates KinC activation by flotillin destabilization and thus prevents downstream signaling to induce

biofilm formation (López et al., 2010). This discovery revealed that bacterial cells harbor the components necessary for lipid raft-like membrane domains, specific lipids, flotillins and the cargo proteins. In many subsequent studies these findings were characterized further and several other cellular processes apart from biofilm formation were also found to be dependent on FMM (Donovan and Bramkamp, 2009; Dempwolff et al., 2012; Bach and Bramkamp, 2013; García-Fernández et al., 2017; Mielich-Süss et al., 2017).

4.4.2.1 Polyisoprenoid lipids and flotillins are structural components of FMM

The structural components of FMM, namely the lipids and the flotillin proteins, play an important role in functional maintenance of FMM and their associated cellular processes, represented by the protein cargo (Figure 4).

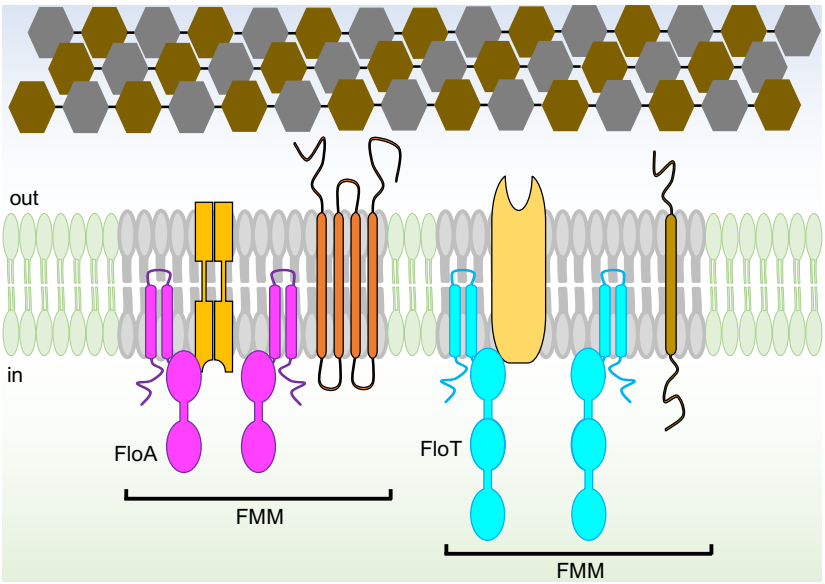

Figure 4: FMM in *B. subtilis*. Schematic representation of FMM in *B. subtilis*. FMM consist of a lipid environment that differs from the surrounding membrane and contain FloA or FloT and additional cargo proteins.

Bacterial membranes contain different lipid species that assemble due to their physico-chemical properties which lead to the formation of microdomains. Eukaryotic lipid rafts contain cholesterol which is absent in most bacteria. It is therefore likely that bacterial FMM lipids are sterol surrogates (Bramkamp and Lopez, 2015; Wagner et al., 2017). Based on the knowledge obtained from eukaryotic lipid rafts, these lipids possibly self-aggregate into rigid, compact and hydrophobic ordered microdomains. Nevertheless, due to the high diversity of bacteria and their environmental niches, the membrane composition is likely to be diverse as well. The exact nature of FMM lipids is probably species-dependent (Lopez and Koch, 2017) and so far, only few examples have been identified. An indication to play a role as a FMM lipid is lent to the lipid cardiolipin (Donovan and Bramkamp, 2009), a diphosphatidylglycerol that is synthesized from two molecules of phosphatidylglycerol. In a cardiolipin mutant the modulation of membrane composition in stress adaptation is severely impaired which might result from an impaired stability of FMM (Donovan and Bramkamp, 2009). Cardiolipin is known to impact lipid ordering in membranes and is enriched in the DRM fraction, and might thus be a constituent lipid of FMM in *B. subtilis* (Donovan and Bramkamp, 2009). A more direct hint for involvement in *B. subtilis* FMM lipid synthesis was presumed for YisP (López et al., 2010). FMM lipids are synthesized from farnesol, the

product from YisP activity (Feng et al., 2014) that are probably further processed to form derivates of polyisoprenoid lipids. Polyisoprenoid lipids come in two conformations, cyclic and non-cyclic. Both have a hydrophobic molecular structure and are planar allowing for a dense packaging resulting in a rigid membrane area (Sohlenkamp and Geiger, 2016; Lopez and Koch, 2017). Cyclic polyisoprenoid lipids are hopanoids or sporulenes and have been found to be important for membrane integrity, stress adaptation, signal transduction and division (Kannenberg and Poralla, 1982; Moreau et al., 1997; Poralla et al., 2000; Bosak et al., 2008). Non-cyclic polyisoprenoid lipids are called carotenoids that exist in high diversities and have been found to be important for membrane rigidity (Bramkamp and Lopez, 2015). In *Staphylococcus aureus*, carotenoids (staphyloxanthin and its derivates) have been found to be part of the FMM lipids, as their deletion (Δ*crt*) results in FMM-related physiological phenotypes (García-Fernández et al., 2017). A structural role in FMM has been proposed for polyisoprenoid lipids as they confer hydrophobic properties leading to compact ordering and increased membrane rigidity (Bramkamp and Lopez, 2015; Lopez and Koch, 2017). The exact nature of the polyisoprenoid lipid species in *B. subtilis* FMM, however, as well as a possible interplay with cardiolipin, are still unknown.

Apart from the constituent lipids described above, flotillins form the other structural component of FMM, similar to eukaryotic lipid rafts. Flotillins represent marker proteins that play an essential role in FMM organization (Browman et al., 2007; Bramkamp and Lopez, 2015). Flotillins are anchored to the membrane with the N-terminus, followed by the PHB domain and a flotillin domain with a characteristic coiled-coil region at the C-terminal part of the protein (Bramkamp and Lopez, 2015; Schneider et al., 2015a). Prokaryotic and eukaryotic flotillins show a high degree of structural and functional similarity. Unlike eukaryotic flotillins, in prokaryotes, flotillins are not lipid-modified for membrane localization, instead, they probably form a hairpin loop in the N-terminus which anchors the protein in the membrane (membrane anchor region, MAR) (Bach and Bramkamp, 2015). Similar to eukaryotic flotillins, the PHB domain in the flotillin of *S. aureus* was shown to play an important role in lipid recognition as a flotillin variant lacking the PHB domain lost the ability for staphyloxanthin binding, a *S. aureus* FMM lipid (García-Fernández et al., 2017). However, a purified *B. subtilis* PHB domain did not bind to liposomes of *B. subtilis* membranes (Bach and Bramkamp, 2015). Therefore, the involvement of PHB in lipid recognition and binding remains debatable. The C-terminal flotillin domain contains a coiled-coil region consisting of characteristic repetitions of the amino acids glutamate and alanine (EA repeats). These repetitions have been found to be important for protein-protein interactions and are responsible for intra- and inter-molecular oligomerization events of flotillin (Dempwolff et al., 2012; Schneider et al., 2015a). Overall, flotillins are anchored to the membrane with their N-terminus and form oligomers with their C-terminus.

In prokaryotes, genes are organized in operon structures, where multiple genes are expressed from the same promotor. Flotillin is usually the second gene of its respective operon (Hinderhofer et al., 2009). The gene encoded upstream of flotillin is a NfeD-protein (nodulation formation efficiency D) that only occurs in bacteria and archaea (Green et al., 2004). Moreover, in several species, the flotillin operon contains another gene downstream of flotillin which encodes a putative protein but does not show any homology with known proteins (Lopez and Koch, 2017). The number of flotillin-containing operons varies

between species, but almost all bacteria have at least one such operon in their genome. When two flotillins exist in a bacterium, they usually differ and one flotillin contains an extended C-terminus (Bramkamp and Lopez, 2015).

The genome of *B. subtilis* encodes two flotillins, FloA (331 aa) and FloT (509 aa) (formerly YqfA and YuaG, respectively). They are found in typical flotillin operon structures with a *nfeD* as the first gene, flotillin as the second gene, and a third gene of unknown function (Figure 5a). Both flotillins contain the typical domains of flotillin proteins: MAR at the N-terminus followed by a PHB domain and the flotillin domain at the C-terminus (Bramkamp and Lopez, 2015) (Figure 5b, c). Although structurally similar, FloA and FloT show differences as FloT contains an extended C-terminus (Dempwolff et al., 2012; Schneider et al., 2015a).

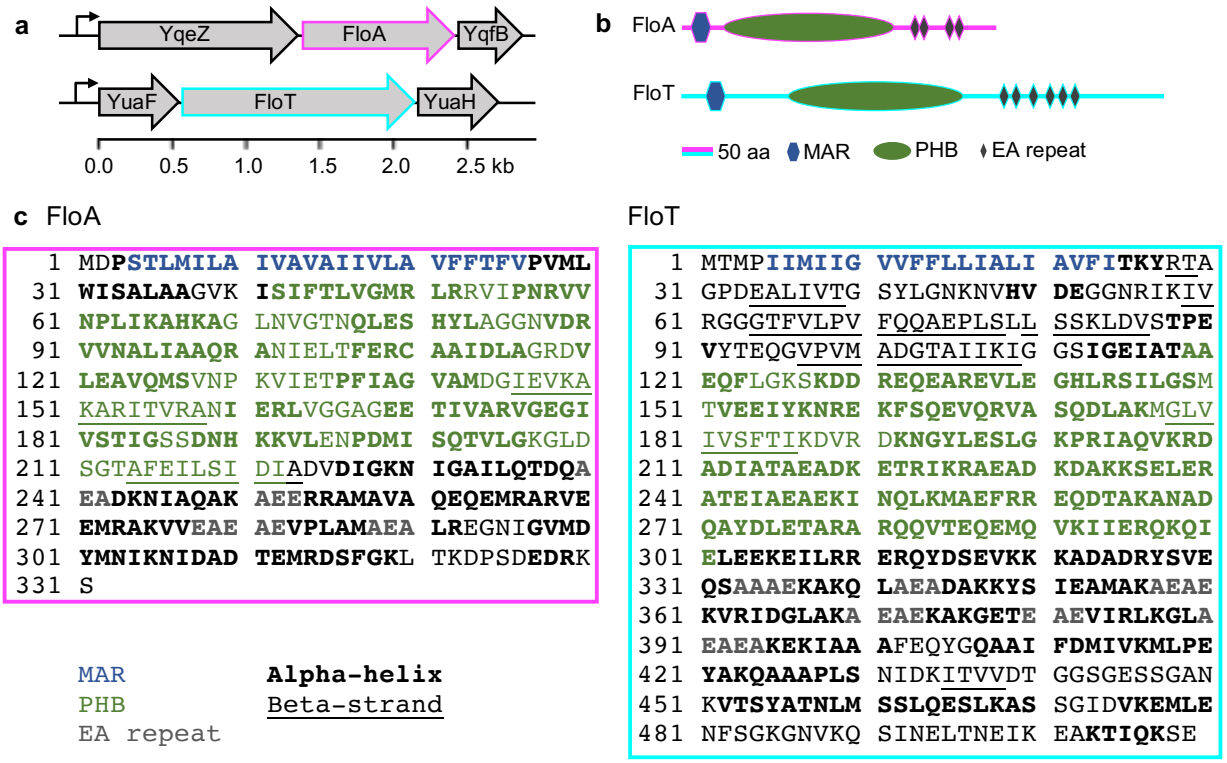

Figure 5: Operon, primary and secondary structure of FloA and FloT. a) Operon structure of FloA (top) and FloT (bottom) of *B. subtilis*. The first gene of the operon encodes a NfeD protein, the second gene encodes flotillin and the third gene is unknown. The operon of FloA encodes a long-NfeD and a short flotillin, the operon of FloT encodes a short NfeD and a long flotillin. b) Domain structure of FloA (top) and FloT (bottom) of *B. subtilis* as predicted with SMART (see chapter 9.3 APPENDIX I) (Letunic et al., 2015; Letunic and Bork, 2018). Both flotillins contain a membrane-anchor region (MAR) in the N-terminus, followed by a PHB domain. The C-terminal part consists of the flotillin domain that contains various repeats of glutamate and alanine (EA repeat). c) Primary and secondary structure of FloA (left) and FloT (right) including the domains. Magenta = FloA, cyan = FloT, blue = membrane anchor region (MAR), green = PHB domain, grey = EA repeats, bold = alpha-helix, underlined = beta-strand. Secondary structure was predicted with Phyre^2 (see chapter 9.3 APPENDIX I) (Kelley et al., 2015).

FloA and FloT are intrinsically subjected to different genetic programs. The operon *of floA* is constitutively expressed throughout growth (Schneider et al., 2015a), whereas the expression of the *floT* operon is increased upon entry into stationary growth phase (Donovan and Bramkamp, 2009; Dempwolff et al., 2012; Schneider et al., 2015a). Accordingly, each flotillin has been found to tether proteins involved in different cellular processes, FloA is involved in general cell wall turnover and FloT is involved in adaptation to stationary phase, including siderophore uptake and protein secretion (Schneider et al.,

2015a). Nevertheless, it has been proposed that FloA and FloT share redundant functions, as more severe phenotypes arise upon double deletions compared to individual deletions. A Δ*floA* Δ*floT* double deletion strain has been shown to be defective in cell growth and morphology, signal transduction, cellular differentiation (motility, biofilm formation, sporulation), protein secretion and competence (Donovan and Bramkamp, 2009; López et al., 2010; Dempwolff et al., 2012; Yepes et al., 2012; Bach and Bramkamp, 2013; Mann et al., 2013). Additionally, upregulation of FloA and FloT also impacts cellular functions pointing to the existence of an optimal concentration of flotillins in the bacterial membrane to ensure correct functionality of cellular processes (Mielich-Süss et al., 2013; Schneider et al., 2015a, 2015b). FloA and FloT physically interact with each other, and with other protein interaction partners (López et al., 2010; Yepes et al., 2012; Bach and Bramkamp, 2013; Schneider et al., 2015a), however, these interactions mostly occur in a transient manner (Dempwolff et al., 2016). FloA and FloT form spatially and temporally distinct FMM subpopulations that nevertheless show functional similarities as both play an important role in the organization and the integrity of the membrane (Dempwolff et al., 2012; Schneider et al., 2015b).

Flotillins localize to FMM likely due to their MAR along with the PHB domains which recognize the specific FMM lipid environment. In FMM, flotillins act as scaffolding proteins that are thought to function as chaperons in recruiting proteins which require this specific membrane environment for correct functionality. Flotillins promote efficient protein-protein interactions and complex formation. The close proximity of proteins in FMM increases their likelihood of interaction and enhances the efficiency of FMM-dependent cellular processes (Good et al., 2011; Bramkamp and Lopez, 2015; Lopez and Koch, 2017). An additional role for flotillins consists in the prevention of protein-protein interactions that are non-specific and possibly harmful for the integrity of cellular processes (Daley, 2008; Schneider et al., 2015b; Lopez and Koch, 2017). With these supporting actions, flotillins play an essential role in organizing and maintaining the correct FMM architecture and ensure the activity and efficiency of many membrane proteins (Bramkamp and Lopez, 2015).

4.4.2.2 FMM functionality is determined by the protein cargo

Many different studies that analyzed FMM not only showed structural similarities to lipid rafts in eukaryotic cells, but also several functional similarities have been detected (Bramkamp and Lopez, 2015; Lopez and Koch, 2017). Like in eukaryotic membranes, FMM resist detergent solubilization and thus the isolation and analysis of DRM fractions is a good starting point to identify proteins associated with FMM, the protein cargo. Nevertheless, candidate proteins should be further evaluated for their dependence on FMM integrity (Brown, 2002; Shah and Sehgal, 2007; Bramkamp and Lopez, 2015; Wagner et al., 2017). It was found that FMM protein cargo composition depends on the physiological state of the cell and consequently on the experimental conditions (Bramkamp and Lopez, 2015; García-Fernández et al., 2017). Despite the differences in experimental conditions, the marker protein flotillin is always detected. Additionally, many proteins have been identified to reside in DRM fractions and to depend on the presence of flotillin for their activity. The protein cargo has been extensively studied in *B. subtilis* (López et al., 2010; Yepes et al., 2012; Bach and Bramkamp, 2013; Schneider et al., 2015a, 2015b) and *S. aureus* (García-Fernández et al., 2017; Koch et al., 2017; Mielich-Süss et al., 2017), but

recently several other bacterial strains like *Borrelia burgdorferi* (Toledo et al., 2015), *E. coli* (Guzmán-Flores et al., 2019) and *Helicobacter pylori* (Hutton et al., 2017) have also been investigated. The identified proteins are functionally diverse, but a common feature of the protein cargo is their multimeric nature (Lopez and Koch, 2017). Proteins involved in signal transduction, membrane trafficking and regulation of the metabolism have been detected in the cargo which impact cellular processes like biofilm formation, sporulation, protein secretion, virulence and protease activity (Donovan and Bramkamp, 2009; López et al., 2010; Dempwolff et al., 2012; Yepes et al., 2012; Bach and Bramkamp, 2013; Mielich-Süss et al., 2013, 2017; Schneider et al., 2015a; García-Fernández et al., 2017).

4.4.2.3 Perturbation of FMM integrity impedes associated cellular processes

The functionality of the protein cargo-associated cellular processes depends on the localization to and the structural integrity of FMM. Perturbation of FMM lipid composition impairs the correct oligomerization and functionality of flotillins and equally, the absence of flotillins reduces the heterogeneity of lipids and leads to coalescence. Influencing one structural component impacts FMM functionality. Consequently, perturbation of FMM lipids or flotillins causes impairments of microdomain-associated cellular processes (Bramkamp and Lopez, 2015). As shown above, a deletion of *yisP* in *B. subtilis* disrupts biofilm formation via KinC and Spo0A signal transduction. A similar signaling-abrogated phenotype can be observed in the flotillin mutant background (Δ*floA* Δ*floT*) (López et al., 2010). Similarly, the antibiotic resistance of methicillin-resistant *S. aureus* (MRSA) depends on FMM flotillins and lipids. MRSA beta-lactam resistance is owed to the alternative penicillin-binding protein PBP2a that has low affinity for these antibiotics. Activity of PBP2a depends on its localization in FMM and its oligomerization. Consequently, a flotillin mutation in MRSA (Δ*sa1402*) reduces its antibiotic resistance in a PBP2a-dependent manner, as does the deletion of the FMM lipids carotenoids (Δ*crt*) (García-Fernández et al., 2017). The exact nature of FMM lipids is strain specific, but they are all synthesized by similar pathways with the intermediate product isopentenyl pyrophosphate (IPP) (Bramkamp and Lopez, 2015). IPPs are then condensated into different polyisoprenoid molecules resembling eukaryotic sterols. Late stages of sterol synthesis in mammals, plants, fungi, bacteria and archaea can be universally inhibited by squalestatins like zaragozic acid, a natural product of fungi (Bergstrom et al., 1993). Treatment with zaragozic acids leads to a dispersal of FMM, causing the protein cargo to diffuse and to lose their functionality (López et al., 2010). Zaragozic acid treatment hence results in similar physiological phenotypes as shown for deletions of flotillin or the strain-specific constituent lipids: KinC-induced biofilm formation is abrogated (López et al., 2010) and MRSA strains show reduced PBP2a-dependent beta-lactam antibiotic resistances (García-Fernández et al., 2017). Increased susceptibility of MRSA due to zaragozic acid treatment could also be demonstrated in mouse experiments (García-Fernández et al., 2017) and clinical studies detected beneficial role of cholesterol-lowering statins in microbial infection outcomes (Liappis et al., 2001; Falagas et al., 2008; Kopterides and Falagas, 2009). It is therefore possible to successfully perturb FMM integrity externally by the addition of a small, natural molecule. Importantly, targeting FMM simultaneously inhibits many physiological processes without posing a direct threat on viability which makes the development of resistances unlikely (Bramkamp and Lopez, 2015).

4.5 FMM dynamics and possible influencing factors

Membrane proteins and lipids are mobile and move within the membrane which also includes the assembled FMM. To visualize FMM, GFP-labeled fusion proteins of the FMM marker proteins FloA and FloT are used. Their observation revealed distinct localization patterns as FloA and FloT form a punctate pattern along the cell membrane distributed in 13 or 6 foci, respectively (Schneider et al., 2015a). Studies revealed that flotillins influence membrane fluidity (Dempwolff et al., 2012; Lee et al., 2012; Bach and Bramkamp, 2013; Zielińska et al., 2020) which might also impact the mobility of membrane components. Flotillins foci themselves are highly dynamic as well, as they randomly move within the membrane (Dempwolff et al., 2012; Schneider et al., 2015a). This also includes splitting and merging of individual foci showing that they can be interchangeable. The movement of FloA and FloT is not actively driven, as no differences are visible upon ATP depletion. Both flotillins diffuse freely in the membrane (Dempwolff et al., 2012) where FloA was found to be faster than FloT (Dempwolff et al., 2016).

As stated previously with the picket-fence model, the dynamics of eukaryotic lipid rafts depends on cytoskeletal structures. The actin cytoskeleton forms a stable meshwork underneath the membrane leading to the formation of membrane compartments that impact membrane dynamics (Kusumi et al., 2012). Additionally, in plant cells, the extracellular cell wall was shown to influence the mobility of lipid rafts as well (Daněk et al., 2019). Similar cellular structures exist in bacteria as well which raises the possibility that FMM mobility might also depend on the cytoskeleton and the cell wall.

Bacteria come in a variety of different shapes and despite large genetic and phenotypic differences, the building blocks that shape the cell are well conserved among bacteria (Sauvage et al., 2008; Dion et al., 2019; Vigouroux et al., 2020). The cell wall outside of the cell, also known as the exo-cytoskeleton, establishes cell shape and avoids further cellular expansion caused by internal turgor pressure (Sauvage et al., 2008). On the inner side of the membrane, the endo-cytoskeleton is guiding cell wall synthesis. Cell shape is maintained by structural stability of the exo-cytoskeleton and its carefully balanced synthesis is led by the endo-cytoskeleton. A close connection and interplay of the endo- and exo-cytoskeleton is crucial for cellular survival and proliferation.

4.5.1 The bacterial cell wall – the exo-cytoskeleton

Bacteria are surrounded by a cell wall which protects the cell from certain environmental influences and from the intracellular turgor pressure and thus maintains cell shape and cellular integrity (Sauvage et al., 2008). In addition to providing physical integrity to the cell, the cell wall needs to be porous to allow diffusion of macromolecules and solutes, and flexible enough to facilitate dynamic cell growth and division. This balance of rigidity and flexibility of the cell wall needs to be tightly regulated to maintain cellular integrity (Bhavsar and Brown, 2006; Zhao et al., 2017).

The bacterial cell wall is a single complex macromolecule that is comprised of mostly parallel peptidoglycan strands crosslinked by peptide bonds and modified by anionic polymers and proteins creating a stable 3D-meshwork (Zhao et al., 2017). The overall structure of the cell wall is quite similar in all bacteria, but crucial differences exist between the cell envelope structure of Gram-positive and

Gram-negative bacteria. Whereas in Gram-negative bacteria the cell wall is rather thin and surrounded by an additional outer membrane, the Gram-positive cell wall is much thicker and in direct contact with the environment. The cell wall consists of long crosslinked strands of peptidoglycan. Peptidoglycan is a polymer comprised of repeating units of the β(1-4)-linked N-acetylmuramic acid and N-acetylglucosamine (NAM-NAG) disaccharide. A pentapeptide is attached to each NAM and can be crosslinked with the pentapeptide of a neighboring peptidoglycan strand (Bhavsar and Brown, 2006; Sauvage et al., 2008). The basic structure of the peptidoglycan is very similar in most bacteria and only varies in the details, e.g. the pentapeptide composition or the glycan chain length (Zhao et al., 2017).

Cell wall synthesis can be divided into three main stages: the precursor synthesis in the cytosol, the incorporation of the precursor into the existing peptidoglycan, and the maturation of the cell wall (Figure 6) (Zhao et al., 2017). The MurA-MurF proteins synthesize the NAM-pentapeptide precursor in the cytosol (Lovering et al., 2012). MraY then links NAM-pentapeptide to the undecaprenyl (C55) carrier lipid (UDP) generating lipid I, the first intermediate linked to the membrane. NAG is ligated to lipid I by MurG creating the peptidoglycan precursor lipid II (Lovering et al., 2012). Lipid II is flipped to the outer leaflet of the membrane with the flippase MurJ (Ruiz, 2008; Sham et al., 2014; Meeske et al., 2015) where it is polymerized onto an existing peptidoglycan strand by transglycosylation (TG) reactions. The lipid carrier undecaprenyl-pyrophosphate is released and recycled in the cytoplasm (Zhao et al., 2017). In the last step, the newly incorporated peptidoglycan-subunit can then be modified further and pentapeptides can be crosslinked with a neighboring strand by D,D-transpeptidation (TP) reactions using the D-Ala-D-Ala-termini of the pentapeptides (Lovering et al., 2012).

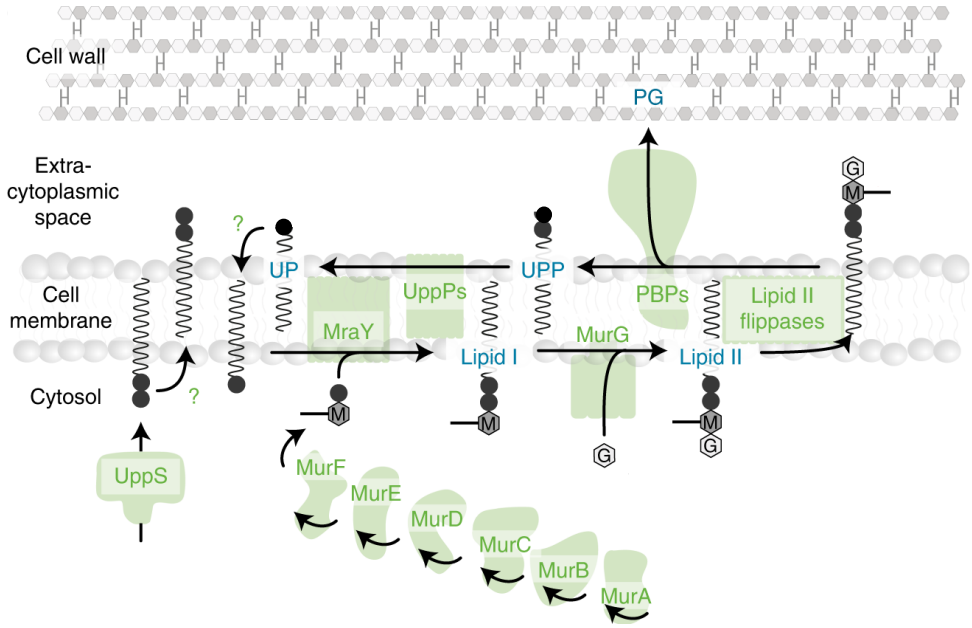

Figure 6: Schematic representation of cell wall synthesis. The precursor of the cell wall, lipid II, is synthesized in the cytosol, flipped across the membrane and then incorporated into the existing cell wall with PBPs. The lipid anchor is recycled. Adapted from Piepenbreier et al., 2019, published under CC-BY-4.0.

Lipid II molecules are incorporated into the existing peptidoglycan with TG and TP reactions. These are mostly mediated by penicillin-binding proteins (PBPs) (Sauvage et al., 2008). Class a PBPs (aPBPs) are capable of performing both TG and TP reactions, whereas class b PBPs (bPBPs) only possess TP

activity (Zhao et al., 2017). Although not possessing any PBPs able to catalyze the crucial TG step, a strain lacking all aPBPs is still able to grow (Ishino et al., 1986; McPherson and Popham, 2003). Because of that, other enzymes catalyzing TG reactions were suspected to exist for many years, until the SEDS (shape, elongation, division, and sporulation) proteins have been found to harbor TG activity (Cho et al., 2016; Meeske et al., 2016; Emami et al., 2017). Usually, several PBPs coexist in bacteria that partly contain specific functions and partly contain redundant functions. The number of PBPs found varies species-dependent with *B. subtilis* encoding 16 PBPs, 4 aPBPs (PBP1, PBP2c, PBP2d, PBP4), 6 bPBPs (PBP2a, PBP2b, PBP3, PBP4b, PbpH, SpoVD) and 6 PBPs with carboxy- (PBP4a, PBP5, PBP5*, DacF) or endopeptidase (PBP4*, PbpX) activity (Sauvage et al., 2008). Additionally, *B. subtilis* contains the three SEDS proteins RodA, FtsW, SpoVE important for cell elongation, division, and spore formation, respectively (Meeske et al., 2016; Emami et al., 2017).

The cell wall is a cellular structure that is specific for bacteria. This specificity is being exploited in the fight against pathogenic bacteria. Antibiotics targeting the bacterial cell wall are harmless for human cells but target an essential bacterial structure. Penicillin-binding proteins are targets for beta-lactam antibiotics, including penicillin, giving PBPs their name. Beta-lactam antibiotics covalently bind the active site of the TP domain of PBPs rendering them inactive, thus preventing cell wall synthesis and bacterial proliferation (Sauvage et al., 2008; Lovering et al., 2012).

During bacterial growth, cell wall synthesis occurs in distinct cellular locations. At midcell, cell wall is synthesized by the divisome leading to the formation of the septum and ultimately daughter cell separation (Zhao et al., 2017). Independently, lateral cell wall is synthesized to allow cell growth and elongation prior to cell division (Meeske et al., 2016). Two distinct cell wall synthesis systems are responsible for lateral cell growth, aPBPs and the Rod complex (Figure 7). Independent behavior of aPBPs and the Rod complex has been detected via single-molecule dynamic studies revealing distinct mobility patterns (Figure 7) (Domínguez-Escobar et al., 2011; Cho et al., 2016). The two cell elongation systems complement each other, as absence of either one drastically reduces incorporation of new cell wall material (Cho et al., 2016). Furthermore, counterbalance of these two systems is important to maintain cell width as cells lacking aPBPs are thinner and cells with reduced Rod complex' activity are thicker than WT cells. Reasons include the longer and oriented peptidoglycan strands synthesized by the Rod complex in comparison to the shorter unoriented strands synthesized by aPBPs (Dion et al., 2019). In *B. subtilis*, the Rod complex consists of RodA, the bPBPs PBP2a and/or PbpH, RodZ, and the cytoskeleton proteins MreBCD (Schirner et al., 2015).

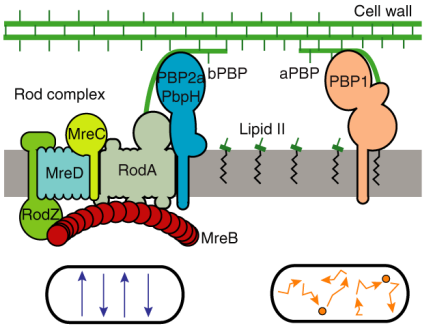

Figure 7: Lateral cell wall is synthesized independently by the Rod-complex and aPBPs. Incorporation of new cell wall precursors into the existing cell wall requires TP and TG reactions. aPBPs catalyze both reactions. The Rod-complex contains bPBPs for TP and RodA for TG reactions and additional structural proteins, like the MreB cytoskeleton. Mobility patterns of the Rod-complex and aPBPs are displayed in the bottom. Image displayed with permission of the publisher, original publication from Dion et al., 2019.

4.5.2 The actin-homolog cytoskeleton – the endo-cytoskeleton

Bacteria contain intracellular structural proteins that resemble the eukaryotic actin cytoskeleton (van den Ent et al., 2001). The actin-homolog cytoskeletal protein MreB is present in bacteria with complex non-spherical cell shapes (Errington, 2015). MreB polymerizes *in vivo* into short filaments at the inner leaflet of the membrane (Swulius et al., 2011; Errington, 2015; Dion et al., 2019), associated through interaction with its transmembrane operon partner proteins MreCD. The submembranous filaments are highly curved and orient along greatest membrane curvature perpendicular to the cell axis. MreB seems to be the coordinator of cell wall synthesis as its intrinsic filament orientation guides the Rod complex to move circumferentially around the cell width (Hussain et al., 2018; Wong et al., 2019). The Rod-complex moves directionally and its movement is driven by peptidoglycan incorporation conferred by RodA-bPBP activity (Domínguez-Escobar et al., 2011; Garner et al., 2011; Van Teeffelen et al., 2011). Most Gram-positive bacteria contain various MreB isoforms, and only MreB is encoded in an operon with *mreCD*. In *B. subtilis*, in addition to the MreB cytoskeletal protein two heterologous proteins exist, Mbl (MreB-like) and MreBH (MreB homolog) (Errington, 2015). They have largely redundant functions in cell morphogenesis (Kawai et al., 2009) and are essential under growth conditions with low levels of magnesium (Schirner and Errington, 2009). Despite their functional overlap in organization of lateral peptidoglycan synthesis, single deletion mutants demonstrate relatively mild but slightly different morphological defects. These contrast double and triple deletion mutants which show more severe phenotypes. A triple deletion mutant shows a spherical shape and is only viable under specific conditions (Schirner and Errington, 2009).

As mentioned previously, it has been shown that MreB organizes membrane regions of increased fluidity (RIF) in *B. subtilis* (see chapter 4.4.1). RIF are likely to contain the peptidoglycan precursor lipid II (Strahl et al., 2014; Schirner et al., 2015) which facilitates cell wall synthesis by the Rod-complex. MreB has an impact on lipid homeostasis by concentrating fluid lipids to RIF, leading to a decrease in the overall membrane fluidity (Strahl et al., 2014). In this manner, MreB is involved in the distribution of lipids and proteins in the membrane. MreB movement, and consequently the movement of RIF, might facilitate membrane protein diffusion through continuous mixing of membrane components which might ultimately favor their interaction (Strahl et al., 2014).

MreB is connected to the cell wall via the Rod-complex. Cell wall synthesis drives MreB dynamics (Domínguez-Escobar et al., 2011; Garner et al., 2011; Van Teeffelen et al., 2011) whose orientation in turn coordinates peptidoglycan incorporation (Hussain et al., 2018). Interference with any component of the Rod-complex stops the motion of the remaining components and leads to a reduction of cell wall synthesis. The cytoskeleton and the cell wall are highly intertwined cellular structures that depend on each other (Zhao et al., 2017). The MreB cytoskeleton has also been shown to influence membrane organization. Consequently, the mobility of FloA and FloT might be affected by MreB and its strong interplay with the cell wall.

4.6 Fluorescence microscopy

Cellular components can be monitored in their natural cellular environment with fluorescence microscopy. This makes live-cell fluorescence microscopy one of the widely used methods to gain understanding in protein localization and dynamics. Biochemical and molecular biological methods generally use cellular components outside their natural cellular environment which might lead to artefacts. Fluorescence microscopy samples can be extrinsically labeled by the addition of molecules carrying fluorescent dyes or intrinsically by genetic introduction of fluorescent proteins. Samples are usually fully labeled prior to microscope imaging, immobilized on a microscope slide and overlaid with a cover slip. For visualization of the fluorescence the fluorophores need to be excited at their specific excitation wavelength. The light emitted at the fluorophore-specific emission wavelength is then detected with specific filters (Coling and Kachar, 1997). Excitation of fluorophores involves the absorption of light energy, occasionally accompanied by irreversible decomposition due to chemical damage. This process is called photobleaching and is visible as a decrease in signal intensity over time (Combs, 2010; Shashkova and Leake, 2017). Therefore, for each fluorophore and application an equilibrium of emission signal intensity and photobleaching needs to be carefully assessed, both conversely depending on excitation intensity and time (Combs, 2010).

4.6.1 Resolution limit

Despite the technological developments of optical microscopes leading to improved image qualities, the optical resolution is limited by the diffraction limitation of light. It describes the minimal distance between two objects to be able to be distinguished independently by the optical setup. It is dictated by a fundamental set of physical laws depending on the wavelength and the numerical aperture (NA) of the objective (Shashkova and Leake, 2017). Usually the resolution limit is roughly half the excitation wavelength which results in a maximum lateral (x- and y-plane) resolution of around 200 nm point-to-point distance and an axial (z-plane) resolution of 500 nm (Coling and Kachar, 1997; Combs, 2010). Below this distance, individual objects cannot be separately resolved and appear as one joint object. However, super-resolution light microscopy has been developed by taking advantage of natural loopholes in the physical laws that dictate resolution limits (Shashkova and Leake, 2017). Sub-diffraction resolution is reached by use of specialized optical configurations.

4.6.2 Microscopy techniques

A set of different fluorescent microscopy techniques exist. As the different techniques have different requirements and capacities, their suitability for the respective application purpose needs to be determined individually. A selection of microscopy techniques including those used in this study are described below (Combs, 2010).

Epifluorescence microscopy

Epifluorescence microscopy is the traditional standard microscopy technique which most other techniques are based on with some critical modifications. Here, light is filtered to leave the light source at the excitation wavelength which travels through the objective to excite the specimen at a 90° angle. Most of the excitation light transmits through and excites fluorophores within the whole specimen (Figure

8 left) (Coling and Kachar, 1997). Emitted fluorescence is then transmitted through a dichroic mirror and an emission filter before collection at the detector. Excitation and emission filters as well as the dichroic mirror depend on the fluorophore to be visualized (Coling and Kachar, 1997; Combs, 2010). If two fluorophores need to be visualized in the same specimen, this is carried out sequentially. The magnification is fixed by the specific objective that is used, but the resolution can be increased up to the diffraction limit of light by using objectives with increased numerical aperture (Coling and Kachar, 1997). As the whole specimen is excited, relatively good fluorescent signal intensities can be collected, but fluorescence noise from unfocused z-planes (>500 nm) can scatter into the focal plane. Nevertheless, this technique allows the whole specimen to be visualized at the same time and is therefore useful for live-cell imaging (Combs, 2010).

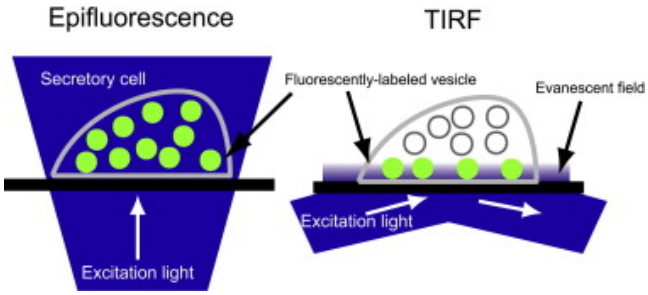

Figure 8: Differences in sample excitation between epifluorescence microscopy and TIRFM. In epifluorescence microscopy fluorophores in the whole sample are excited with light at a 90° angle (left). In TIRFM only the fluorophores at the glass/water interface are excited with the evanescent wave arising from the angle of light (right). Image credits: Ravier et al., 2008, published under CC-BY-3.0.

Total internal reflection fluorescence microscopy

A more restricted but directed view on the specimen is possible with total internal reflection fluorescence microscopy (TIRFM), where only fluorophores at the surface of the specimen are visualized (Ravier et al., 2008; Combs, 2010; Shashkova and Leake, 2017). To manage this selective imaging, the excitation light is not exciting the specimen at a 90° angle, but at a low angle for which objectives with high numerical aperture (NA > 1.45) are needed (Combs, 2010). The specific angle leads to a total internal reflection of the light at the specimen-cover slip interface (water/glass) and needs to be determined for each sample individually. Despite the whole excitation light being reflected, a quantum physical phenomenon called evanescent wave still penetrates up to 250 nm into the sample, and selectively excites fluorophores therein (Figure 8 right) (Combs, 2010). The fluorescent emission signal is then collected as in epifluorescence microscopy. TIRFM selectively considers the surface of the specimen and penetration depths can be modified within a range of 90 nm to 250 nm, thus reducing the background noise of the z-plane and increasing the resolution to the penetration depth (Combs, 2010; Shashkova and Leake, 2017). As reduced photon energy reaches the sample, bleaching events are reduced, thereby opening the possibility for long-term live-cell imaging at high frequency. Furthermore, owed to the addition of optical image splitting systems in the camera, TIRFM extensions exist to monitor different fluorophores simultaneously. TIRFM is limited to fluorescence of the surface area and offers great signal-to-noise ratios. Therefore, it is especially used for single-molecule tracking in membranes to characterize and quantify diffusion behaviors.

Confocal laser scanning microscopy

Higher resolution can be obtained by using confocal microscopy. Here, the excitation light passes a spatial pinhole leading to a focused light beam exciting the specimen. Emitted fluorescence then passes

another spatial pinhole to eliminate out-of-focus signal before reaching the detector (Combs, 2010; Shashkova and Leake, 2017). In this way, fluorescent emission is only detected close to the focal plane leading to an increase in resolution, especially in the z-plane. This point illumination is spatially restricted to a small area and is used to raster scan the specimen in the horizontal plane. Individual images are combined to reconstruct 2D (x- and y-plane) or 3D (x-, y- and z-plane) images of the specimen (Combs, 2010). As much of the emitted fluorescence is blocked by the pinhole, signal intensities are very low, and increased excitation times are often necessary. Furthermore, as the whole sample is imaged sequentially and not at the same time, confocal microscopy is not suitable to study dynamic behaviors but is usually used for localization studies with high signal-intensity fluorophores.

Super resolution microscopy techniques

Super resolution light microscopes reach resolutions below the diffraction limit of light by use of technically demanding setups (Schermelleh et al., 2010). One method of super resolution light microscopy is the structured illumination microscopy (SIM). Sub-diffraction resolution is archived by a combination of spatially modulated illumination and computational image reconstruction. SIM can improve the x- and y-plane resolution to around 100 nm, and the z-plane resolution to approximately 200 nm (Shashkova and Leake, 2017). Another method of super resolution microscopy is stimulated emission depletion (STED) microscopy which is based on confocal microscopy. STED uses two laser pulses, one focal spot to excite the specimen and a second laser selectively deactivating fluorophores of the first excitation in a doughnut-shape, resulting in the detection of the signal from a small area corresponding to the hole of the doughnut. Resolutions to sub-diffraction limits of around 20 nm in the lateral (x and y) plane and 100 nm in z-plane are reached (Klar et al., 2000; Combs, 2010). However, STED is not suitable for weak signal intensities and dynamic observations.

4.6.3 Fluorescent proteins

For live-cell imaging of proteins, fluorescent fusion proteins are usually used. The fluorescent proteins most commonly used in bacteria are GFP (green fluorescent protein), mCherry and their derivates (Doherty et al., 2010). In *B. subtilis* GFP stably emits fluorescence at satisfactory intensities during a decent time interval. Unfortunately, the fluorescent emission of mCherry is rather weak and photobleaching occurs rapidly. Therefore, usually GFP is the fluorescent protein of choice and is only accompanied by mCherry in conditions that require imaging of two fluorescent proteins at the same time. In previous studies it has been shown that FloA- and FloT-GFP translational fusion proteins are functional, as their sole expression in the cell prevents the severe phenotypes seen in Δ*floA* Δ*floT* double mutant strains (Dempwolff et al., 2012).

Fluorescent microscopy techniques with suitable fluorophores allow the visualization of cellular structures in live-cell imaging applications. It is a powerful tool complementing other biochemical and molecular biological techniques to study cellular processes. In this work, epifluorescence microscopy was used as the main source of fluorescent imaging. In specific cases, TIRFM was also used to obtain more detailed information on protein dynamics in the membrane.

4.7 Objective

Previous studies revealed the importance of FMM in membrane organization and highlighted a specific role for flotillins. The activity of several cellular processes is assured by the correct assembly and dynamics of FMM in the membrane. If, how and why bacteria organize the dynamics of FMM remains unknown, but molecular mechanisms and a biological significance are likely to underlie this membrane organization principle.

The model organism *B. subtilis* is used to study FMM dynamics of FloA and FloT in this work. Its phylogenetic proximity to opportunistic pathogens and its use in industrial settings makes the organism an interesting study object with implications for society. Furthermore, the wide knowledge gathered leading to a relative ease in genetic manipulation and the understanding of metabolic pathways allow for directed and cognizant procedures.

It has been shown that perturbance of FMM can have severe influences on cellular integrity caused by disturbance of the involved cellular processes. Understanding the underlying mechanisms of flotillin mobility with more profundity might lead to additional key factors that can be modified when exploiting FMM. This is of interest for the possibility to reduce virulence in close-related opportunistic pathogens. Additionally, this knowledge could be used to improve biotechnological processes in cellular factories. The more detailed the characterization of FMM, the more successful specific requirements can be customized. Being able to control FMM opens many possibilities to manipulate *B. subtilis* for desired applications.

Live-cell fluorescence microscopy and molecular biological, genetic and biochemical methods were used to understand and characterize the molecular mechanisms underlying FMM mobility in *B. subtilis.*

5 RESULTS

5.1 Distinct oligomerization profiles of FloA and FloT in *B. subtilis*

The genome of *B. subtilis* contains two genes encoding the flotillin proteins FloA and FloT. Fluorescently labeled constructs were generated and their functionality confirmed by observing known parameters: the formation of a punctate membrane pattern monitored by fluorescence microscopy and the cellular localization in the detergent-resistant membrane (DRM) fraction (Donovan and Bramkamp, 2009; López et al., 2010; Bach and Bramkamp, 2015). To not interfere with flotillin-membrane binding of the N-terminus, C-terminal GFP-fusion proteins were generated. They have previously been shown to be functional, as a flotillin double mutant only expressing a GFP-tagged flotillin fusion protein did not demonstrate the severe double-mutant phenotypes (Dempwolff et al., 2012).

The localization pattern of FloA and FloT was studied with fluorescently labeled proteins. FloA-GFP (RW77) or FloT-GFP (RW88) were expressed under their native promoter at the neutral *lacA* locus in the genome. These GFP-labeled strains were used to monitor flotillin localization pattern with total internal reflection fluorescence microscopy (TIRFM) (Ambrose, 1956) and with epifluorescence microscopy (EPI). TIRFM only excites fluorophores in close proximity to the cell surface, making it possible to observe a continuous membrane area (Figure 9, left). Epifluorescence microscopy excites fluorophores in the whole sample, resulting images display fluorophores in the lateral membranes (Figure 9, right). As expected, FloA and FloT showed the formation of assemblies leading to a punctate pattern in the membrane (Figure 9a). Quantification of the foci of FloA and FloT revealed on average

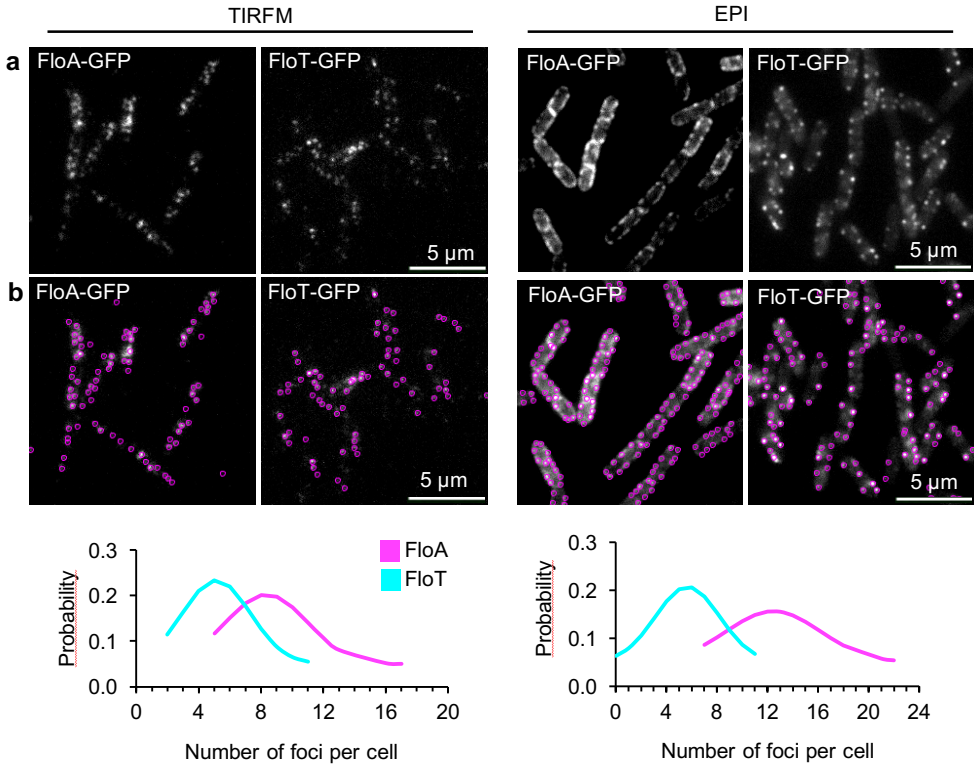

Figure 9: GFP-labeled FloA and FloT show distinct localization patterns. Analysis of the localization pattern of GFP-labeled FloA and FloT with TIRFM (left) and epifluorescence microscopy (right). a) Field showing cells expressing FloA-GFP (left) or FloT-GFP (right). b) Image displaying the automatic detection of membrane foci of FloA- (left) and FloT-GFP (right) with the plugin Trackmate (Tinevez et al., 2017) of Fiji (Schindelin et al., 2012) (top) and quantification of the number of foci per cell (bottom).

more FloA foci per cell (Figure 9b). Differences between TIRFM (Figure 9, left; FloA 8 foci, FloT 5 foci) and epifluorescence microscopy (Figure 9, right; FloA 12 foci, FloT 6 foci) possibly result from the fraction of the membrane that is excited during image acquisition which is smaller during TIRFM. The results obtained with both techniques probably display a lower limit of the total foci number per cell, as only parts of the cells are monitored. Due to the physical diffraction limit, the size of the flotillin foci cannot be determined accurately. However, the signal intensity of FloT foci was in general higher than that of FloA foci. This observation is in accordance with the bigger size of FloT foci obtained with super-resolution microscopy (Schneider et al., 2015a; Dempwolff et al., 2016).

Flotillin membrane localization was confirmed with cellular fractionation assays. FloA- (RW77) or FloT-GFP (RW88) cell cultures were harvested and lysed (cell extract) before separation of membrane and cytosol with ultracentrifugation. SDS-PAGE coupled to western blot and immuno-detection of GFP showed that FloA and FloT were detected in the membrane fraction (Figure 10a). The membrane extract was further treated with anionic detergents to separate the detergent-resistant from the detergent-sensitive membrane fraction (DRM and DSM) (Brown, 2002). The samples were subjected to SDS-PAGE, western blot and immunodetection of GFP and showed that FloA- and FloT-GFP were mainly associated to the DRM fraction of the membrane (Figure 10b), as expected from previous reports (Donovan and Bramkamp, 2009; López et al., 2010; Bach and Bramkamp, 2015). These results confirm that constructs are functional and can be used for further analysis.

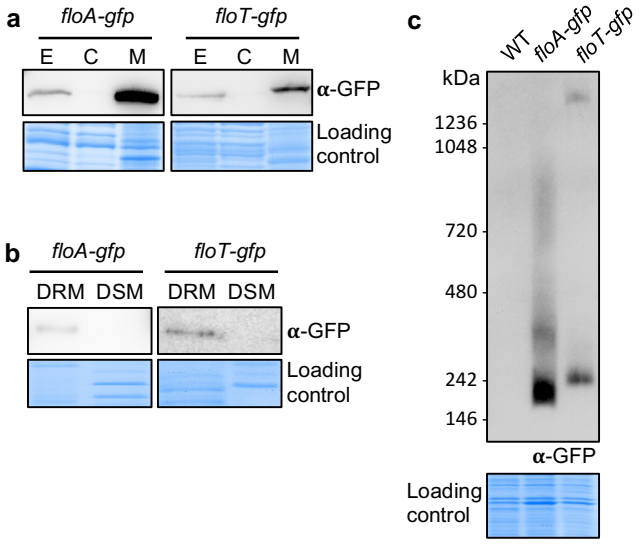

Figure 10: FloA and FloT preferentially localize in the DRM fraction and form oligomers. a) Western blots of cellular fractionation of FloA- (left) and FloT-GFP (right) labeled cells. A Coomassie stained gel is used as a loading control. E = whole cell extract, C = cytosol, M = membrane. b) Western blots of membrane separation into DRM and DSM fractions. c) Western blot of blue-native PAGE of membranes of FloA- or FloT-GFP labeled cells and unlabeled cells.

The oligomeric state of flotillin assemblies was then monitored with native blots. Membranes were solubilized overnight with detergent (0.1 % DDM) and then subjected to blue-native (BN-) PAGE coupled to western blot and GFP-immunodetection. A stable oligomer of high molecular weight (> 1 MDa) was consistently found for FloT and additional oligomers of low molecular weight (< 300 kDa) were found for both, FloA and FloT (Figure 10c). FloA additionally formed oligomers of intermediate molecular weight (< 1 MDa). These were not as defined as the other bands but diffusive and extended to broad molecular weight range. Overall, the oligomers of FloT are of higher molecular weight than the oligomers of FloA.

5.2 FloA diffuses faster than FloT

To monitor the mobility of FloA and FloT, live-cell TIRFM imaging was performed using cells expressing FloA- (RW396) and FloT-GFP (RW392) from the native promotor on a replicative plasmid. Images were collected at 200 ms frame rate for 20 s. The live-cell imaging movie can be found in the supplemental material of Wagner et al., 2020 (movie 7). Example pictures of 0 s and 20 s revealed that FloA and FloT foci were dynamic (Figure 11a). Flotillin mobility was then analyzed with three different complementary approaches: kymographs, trajectories and mean square displacement (MSD) analysis (Figure 54).

A kymograph is a method to display mobility in a single image representing distance (x-direction) over time (y-direction). For each time point, the signal of the same specific membrane area, usually a row of pixels, is monitored. The signal corresponding to one time point is plotted underneath the signal of the previous time point thus creating vertical tracks that represent the actual signal. The resulting image shows the mobility within the membrane area monitored (Figure 11b). Kymographs depend on the membrane area under observation and the direction of movement of the assembly in relation to the membrane area. Straight tracks correspond to no mobility, diagonal tracks correspond to uniform movement in one direction and less ordered tracks correspond to more random movements. The next sections will provide examples for all types of movement.

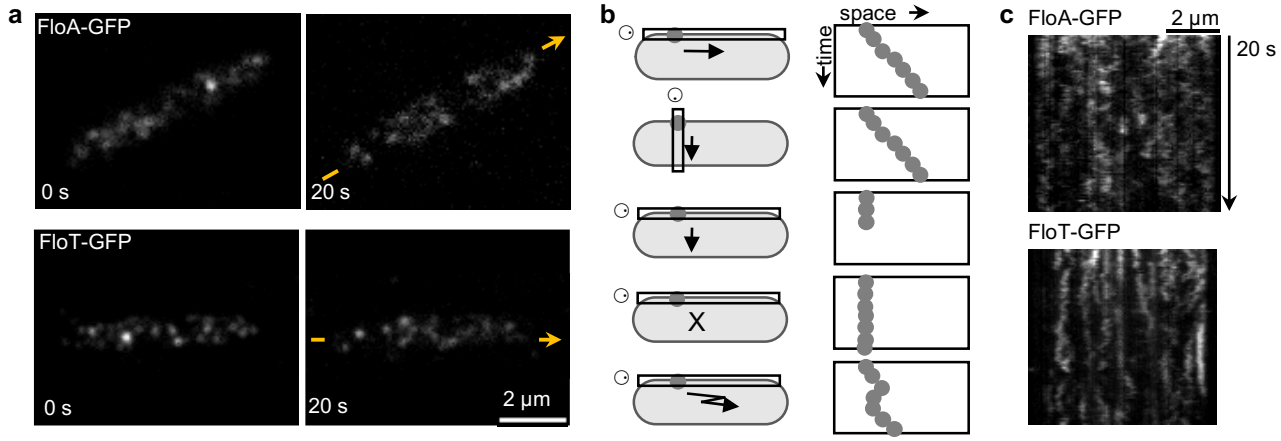

Figure 11: FloA and FloT are mobile. a) TIRF microscope images of FloA- (top) and FloT-GFP (bottom) labeled cells at 0 s (left) and 20 s (right). b) Schematic representation of the analysis of mobility with kymographs. Several different mobility patterns that will occur throughout this work are exemplified here. Several different mobility patterns are illustrated (left) which result in the corresponding kymographs (right). Different tracks of the signal are shown. The results of kymographs depend on the direction of mobility (illustrated by the arrow) and the direction of observation (illustrated by the black box and the simplified eye). c) Kymograph analysis of FloA- (top) and FloT-GFP (bottom) labeled cells. Kymographs were generated using the membrane signal along the long axis of the cell obtained with TIRF microscopy indicated in the 20 s image with a yellow arrow. A corresponding movie can be found in the supplemental material of Wagner et al., 2020 (movie 7).

The fluorescent signal (Figure 11a, right, yellow arrows) of the flotillin foci along the long axis of the cell (x-direction) was plotted over time (y-direction) (Figure 11c). In the kymographs the FloA and FloT signal formed tracks that showed lateral displacements: tracks formed a wave-like pattern. Individual tracks were separated from each other which is especially noticeable for FloT. The overall patterns of FloA and FloT were similar, but they differed in the lateral displacements, as the ‘waves‘ of FloA were bigger than those of FloT. Flotillins movement showed lateral displacements (waves) in a confined membrane area (separation between individual tracks) (Figure 11c). FloT foci are less dynamic than FloA foci.

To be able to project the movement of FloA and FloT foci, the collected fluorescent images were analyzed with the plugin Trackmate (Tinevez et al., 2017) of the software Fiji (Schindelin et al., 2012). Depending on input parameters, Trackmate automatically detects spots according to signal intensities, and spatially and temporally links them into trajectories which can then be depicted on top of the fluorescent signal (Figure 54c). In this way, the trajectories of the individual flotillin foci can be portrayed.

As flotillins cover most of the membrane surface within 20 s (corresponds to 100 frames), the trajectories were split into intervals of 20 frames to increase differentiability between individual trajectories (Figure 12a). Trajectories revealed that flotillin movement was occurring in all directions, and that FloA moved more than FloT. Observing the complete trajectories (Figure 12b) showed that flotillin foci move back and forth in a restricted area of the membrane, and this area seemed to be larger for FloA than for FloT which is in accordance with the kymograph results.

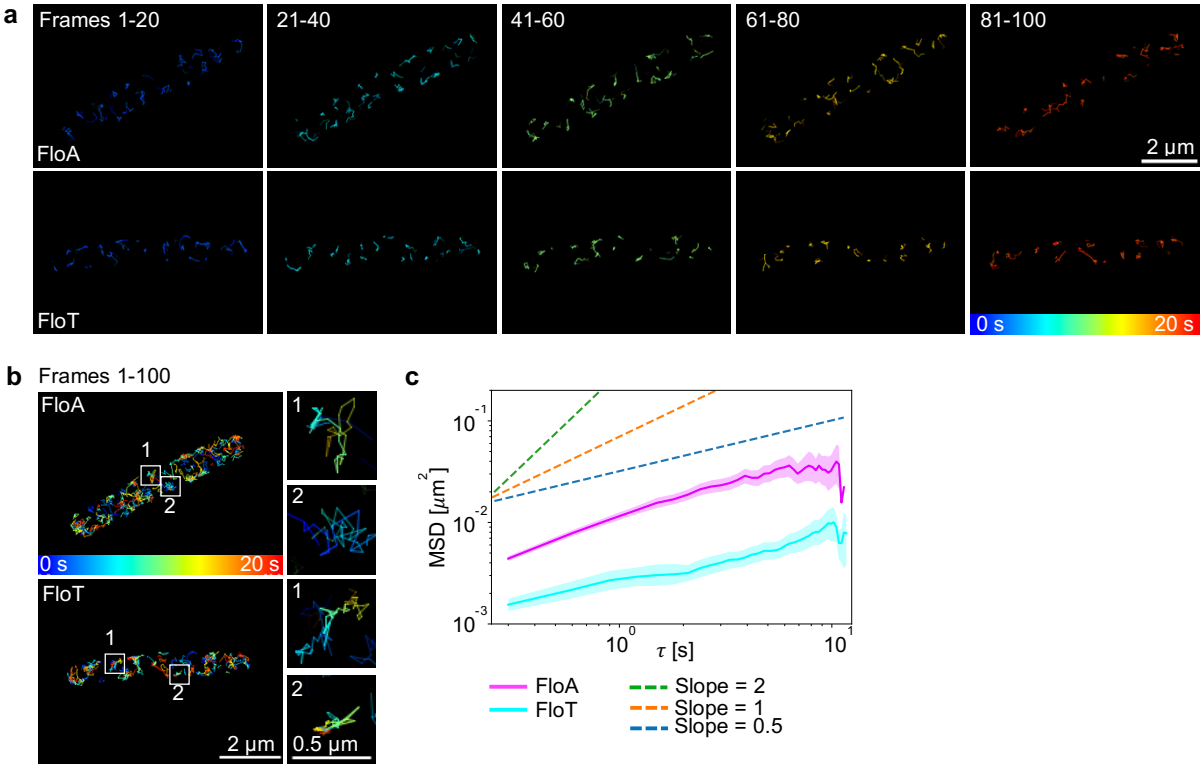

Figure 12: The mobility of FloA is faster than the mobility of FloT. a) Images showing the trajectories of FloA (top) and FloT (bottom) generated from TIRF microscopy every 200 ms for 20 s. To increase visibility, trajectories are split into several images containing a frame depth of 20 images each, corresponding to 4 s. Frames are indicated in the top. Colors indicate elapsing times from blue = 0 s to red = 20 s. b) Combined trajectories of FloA (top) and FloT (bottom) with a frame depth of 100 images, corresponding to the whole 20 s of image acquisition. Representative trajectories are highlighted. c) Plot showing the MSD analysis of FloA- and FloT-GFP. Plot shows the means with shaded areas representing the 95% confidence intervals. N≥765 trajectories.

The information that Trackmate uses to project trajectories contains x-, y-, and t-coordinates for the focus belonging to one trajectory. This information can be used to determine the mean square displacement (MSD) of flotillin foci (Figure 54d) which allows the quantification of flotillin foci mobility. MSD characterizes the mobility behavior of particles. It indicates the area a particle covers within a given time interval and can be used to determine if a particle moves by simple Brownian diffusion, or if additional forces are involved. For this purpose, MSD is plotted against the time interval. The resulting

graphs are intrinsically most reliable at early time scales. Interpretation of MSD plots concentrates on two characteristics, the y-intercept and the slope of the graphs. The y-intercept of the graph at the earliest time point determines the level of the movement, i.e. the diffusion coefficient. The slope of the graph characterizes the type of the movement, i.e. the diffusivity. Diffusivity is usually analyzed at early and intermediate time scales. Later time scales are intrinsically less reliable as they comprise fewer data points due to variable lengths of the trajectories. A slope of <1 corresponds to subdiffusion, a slope of =1 to normal diffusion, and a slope >1 corresponds to superdiffusion (Saxton, 2007). Subdiffusion results from obstructions reducing diffusivity and superdiffusion occurs by a local increase of diffusivity. For MSD analysis a collaboration was established with biophysicists from the laboratory of Prof. PhD Ned Wingreen at Princeton University who contributed with the bioinformatic tools and generated MSD plots. The plots show the means with the 95 % bootstrap confidence interval represented as shaded areas. MSD depends on the information generated with Trackmate according to specific input parameters. Those were carefully chosen, inspected and found to be appropriate, but might nevertheless not represent the exact nature of FloA and FloT foci mobility. Therefore, no absolute diffusion coefficients are claimed but instead comparisons are used to draw conclusions.

MSD analysis of FloA and FloT revealed that both showed a diffusive behavior (Figure 12c). The diffusion coefficient of FloA was bigger than that of FloT, meaning that FloA diffused faster than FloT. Additionally, at intermediate time scales (~1 s) the diffusivity of FloT was reduced hinting to an increased steric restriction. Overall, the methods used for mobility analysis – kymographs, trajectories and MSD analysis – are consistent regarding the increased mobility of FloA foci in comparison to FloT.

Results for flotillin foci mobility obtained with TRIFM were compared to epifluorescence microscopy. For that, images of FloA- (RW77) or FloT-GFP (RW88) labeled strains were acquired every 300 ms for 9 s. The live-cell imaging movie can be found in the supplemental material of Wagner et al., 2020 (movie 1). Localization patterns of 0 s and 9 s showed differences confirming flotillin mobility (Figure 13a). The mobility was further analyzed with kymographs, trajectories and MSD analysis. Kymographs showed individual tracks clearly separated from each other (Figure 13b). Lateral displacements of FloA were bigger revealing increased mobility. Trajectories showed that within 9 s FloA covered large membrane areas, whereas FloT only covered limited membrane areas (Figure 13c). The movement of individual foci were restricted to limited membrane areas which were smaller for FloT. MSD analysis revealed diffusive behavior for FloA and FloT foci with increased mobility for FloA. At larger time scales FloT shows a less diffusive behavior (Figure 13d).

The diffusion coefficients determined using epifluorescence microscopy showed the same tendency as the diffusion coefficients determined with TIRFM. The overall diffusion coefficients were lower in TIRFM, possibly due to increased temporal resolution during image acquisition. As the objective is to directly compare different conditions without stating any absolute values, epifluorescence microscopy analysis revealed results comparable to TIRFM data. Epifluorescence microscopy depicts flotillin foci mobility with good approximation and in addition, the analysis displays the results of kymographs and trajectories more clearly and plainly. Therefore, flotillin mobility will mainly be analyzed with epifluorescence microscopy and TIRFM will only be used in specific cases that demand more detailed membrane

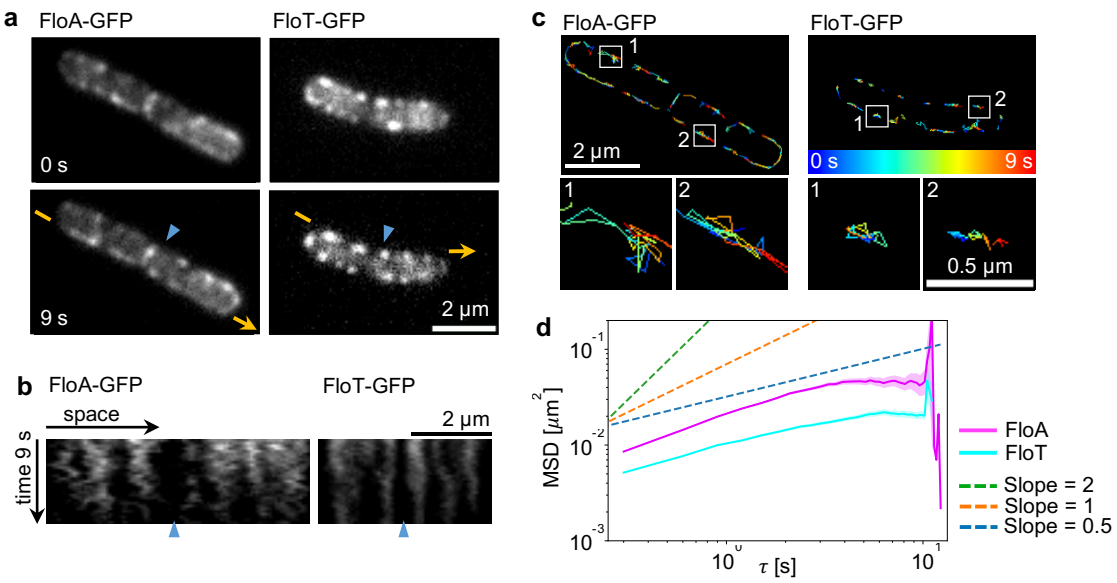

Figure 13: Mobility analysis of FloA and FloT with epifluorescence microscopy. a) Microscope images of FloA- (left) and FloT-GFP (right) labeled cells at 0 s (top) and 9 s (bottom). Triangles indicate neighboring cell poles. b) Kymograph analysis of the mobility of FloA- (left) and FloT-GFP (right). The membrane signal used is indicated in the 9 s image with a yellow arrow. Blue triangles indicate cell poles of neighboring cells. c) Images of the trajectories that FloA- (left) or FloT-GFP (right) foci follow during 9 s. Representative trajectories are highlighted. Colors indicate elapsing time from blue = 0 s to red = 9 s. d) Plot showing the MSD analysis of FloA- and FloT-GFP. Plot shows the means with shaded areas representing the 95% confidence intervals. N≥13988 trajectories from 16 different experimental controls. A corresponding movie can be found in the supplemental material of Wagner et al., 2020 (movie 1).

observations. FloA will be compared to FloT and each with (experiment) or without (control) exposure to different physiological or genetic conditions. Generally, graphs of the experimental condition will only be compared to their specific control (within one plot) and graphs of different experiments (different plots) will not be compare to each other. The mobility of FloA and FloT is always monitored within their assemblies, as the mobility of individual proteins cannot be monitored. Therefore, whenever flotillin mobility is mentioned in any way, this always implies the mobility of the observed foci. Please note that ‘tracks’ always refer to kymograph analyses and ‘trajectories’ always refer to the analysis performed with Trackmate. Additionally, it has to be noted that the analysis of trajectories and MSD depend on the information generated with Trackmate according to specific input parameters and kymographs use the actual fluorescent signal. Kymograph is a direct analysis, whereas trajectories and MSD analysis are indirect measures. Nevertheless, they all agree in their results and complement each other. For some key experiments all three analyses will be presented, for others, only the most meaningful analysis will be selected and the reader is referred to chapter 9.6 APPENDIX I to find the complete analyses for every experiment. Corresponding movies were published on a preprint server (Wagner et al., 2020) and are linked to in the respective chapter.

In summary, oligomers of FloT were of higher molecular weight and formed bigger assemblies than those of FloA. FloA and FloT diffuse in the membrane and FloA diffuses faster than FloT. Additionally, a spatial restriction in flotillin mobility was detected which was more pronounced in FloT. Differences in FloA and FloT mobility confirmed previous studies (Dempwolff et al., 2016), nevertheless, these existing studies did not focus on the characterization of the mobility of FloA and FloT and their differences.

Therefore, understanding the underlying molecular mechanisms that influence flotillin mobility is strived for in this work.

5.3 Flotillin mobility is independent of membrane fluidity but changes throughout growth

5.3.1 Flotillin mobility does not depend on the other flotillin operon

Genes encoding FloA and FloT are organized in conserved operon structures with genes encoding NfeD proteins (Figure 5a). It has been shown before that FloT and its operon-partner NfeD (NfeD2) showed similar mobility patterns and colocalized frequently, whereas this was not the case for FloA and its NfeD (NfeD1b) (Dempwolff et al., 2012). Furthermore, FloA and NfeD1b behaved independently, whereas the absence of NfeD2 affected the localization of FloT which, nevertheless, remained functional and dynamic (Dempwolff et al., 2012). Apart from the described influence of the operon partners, the possible effect that the absence of the whole flotillin operon has on the mobility of the other flotillin was examined. Previous reports already showed that the localization pattern is independent of the presence of the other flotillin (Dempwolff et al., 2012), but this study did not focus on the mobility. Strains expressing FloA-GFP in a Δ*floT*-operon background (RW521) or likewise FloT-GFP in Δ*floA*-operon background (RW522) were used to analyze the mobility of the labeled flotillins. No difference was visible for FloT-GFP in the absence of the FloA-operon (Figure 14). FloA-GFP showed a minor increase in mobility when the FloT-operon was deleted. This shows that the mobility of flotillins is largely independent from the other flotillin.

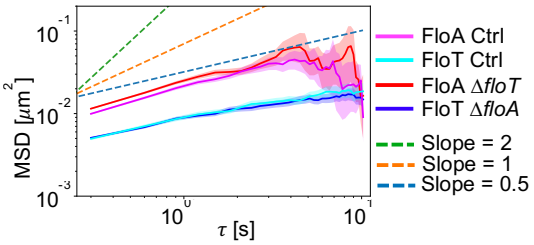

Figure 14: Flotillin mobility is independent of the other flotillin operon. Plot showing the MSD analysis of FloA- and FloT-GFP in WT background cells (Ctrl) and in mutants of the other flotillin operon, FloA in Δ*floT* and FloT in Δ*floA*. Plot shows the means with shaded areas representing the 95 % confidence intervals. N≥1538 trajectories.

5.3.2 Membrane fluidity does not influence flotillin mobility

FloA and FloT are membrane proteins that form oligomers moving within the membrane. Previously, it has been shown that flotillins are influencing the overall membrane fluidity (Bach and Bramkamp, 2015; Zielińska et al., 2020). It was monitored if in turn the fluidity of the membrane also has an effect on flotillin mobility. Benzyl alcohol (BNZ) increases the fluidity of the membrane rapidly (Strahl et al., 2014). Upon treatment with BNZ, the membrane hydration is increased resulting in disordering of the membrane structure which ultimately leads to alterations in membrane permeability (Konopásek et al., 2000). FloA- (RW77) and FloT-GFP (RW88) labeled cells were treated with BNZ (30 mM, 5 min) and flotillin mobility was monitored with epifluorescence microscopy every 300 ms for 9 s. The live-cell imaging movie can be found in the supplemental material of Wagner et al., 2020 (movie 2). Increasing the membrane fluidity did not influence flotillin mobility (Figure 15a, left). Additional perturbation of other properties of the membrane were performed to see if any effect on flotillin mobility can be observed. Nisin (NIS, 30 µM, 90 min) forms pores in the membrane and valinomycin (VAL, 60 µM, 90 min) is an ionophore that selectively transports potassium-ions across the membrane and in this manner abolishes the membrane potential. No differences in flotillin mobility upon NIS treatment was observed (Figure 15a, middle).

Similarly, VAL treatment did not affect FloA mobility, whereas an increase was observed for FloT mobility (Figure 15a, right) which will be explained in the progress of this work (see chapter 5.8). Overall, perturbations of membrane properties have little effect on flotillin mobility and especially membrane fluidity does not affect flotillin mobility at all.

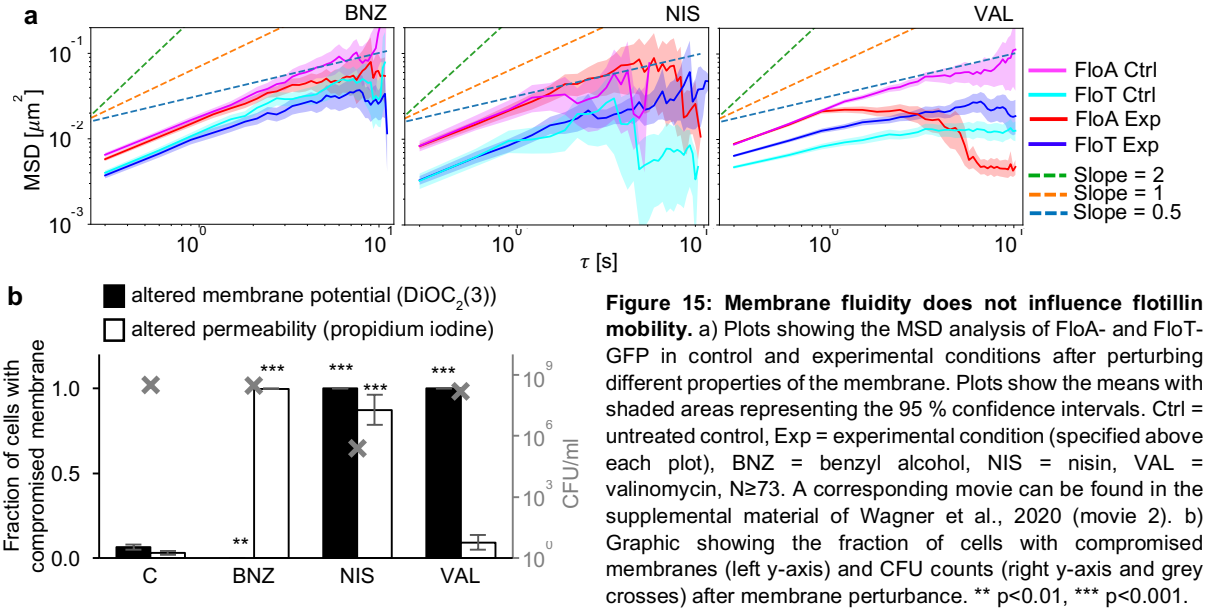

Figure 15: Membrane fluidity does not influence flotillin mobility. a) Plots showing the MSD analysis of FloA- and FloT-GFP in control and experimental conditions after perturbing different properties of the membrane. Plots show the means with shaded areas representing the 95 % confidence intervals. Ctrl = untreated control, Exp = experimental condition (specified above each plot), BNZ = benzyl alcohol, NIS = nisin, VAL = valinomycin, N≥73. A corresponding movie can be found in the supplemental material of Wagner et al., 2020 (movie 2). b) Graphic showing the fraction of cells with compromised membranes (left y-axis) and CFU counts (right y-axis and grey crosses) after membrane perturbance. ** p<0.01, *** p<0.001.

To confirm the efficiency of the treatments, several control experiments were performed with WT cells (RW3). Colony forming units (CFU) were counted after the treatment and cellular dyes were used to observe differences in membrane properties. The dye $DiOC_2(3)$ indicates alterations in the membrane potential and the dye propidium iodine indicates differences in membrane permeability. These control experiments confirmed that upon treatments with BNZ, NIS or VAL, different properties of the membrane are affected and that bacterial viability was reduced after NIS treatment (Figure 15b). Flotillin mobility is generally not affected when different membrane properties are changed.

5.3.3 Flotillin mobility changes during growth

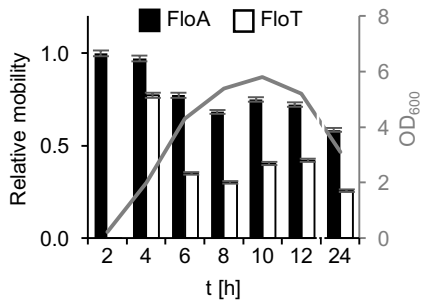

Figure 16: Flotillin mobility decreases during growth and FloA is always faster than FloT. Graphic showing flotillin mobility (right y-axis) monitored during growth in regard to OD_{600} (left y-axis and grey graph). Bar chart shows means±sem, N=400.

As previously observed, FloT expression is induced upon entry into stationary phase, whereas FloA is constitutively expressed (Donovan and Bramkamp, 2009; Dempwolff et al., 2012; Schneider et al., 2015a). Therefore, experiments of this study monitored the localization pattern of FloA-GFP in early-exponential phase (4.5 h growth) and of FloT-GFP in late-exponential – early-stationary phase (7.5 h growth). To understand if these different growth conditions might determine the differences in mobility, the mobility of flotillins during cell growth indicated by OD_{600} in 2 h intervals was monitored. Throughout the whole growth the mobility of FloA was higher than that of FloT (Figure 16). For both, FloA- (RW77) and FloT-GFP (RW88), the mobility decreased at

late-exponential growth and upon entry into stationary phase. Differences in flotillin mobility are intrinsic but are additionally steered by the growth phase.

5.4 The mobility of flotillin is determined by its C-terminus

5.4.1 Construction of chimeric flotillins

Flotillins contain a PHB domain in their N-terminus important for lipid binding and a flotillin domain in their C-terminus important for protein binding (Dempwolff et al., 2012; Schneider et al., 2015a). To determine if either the membrane composition or the FMM protein cargo might influence flotillin mobility, the N- and C-termini of flotillins were monitored independently by using chimeric versions. Chimeras contain the N-terminus of one ond the C-terminus of the other flotillin (Figure 17a, b) and were expressed under the control of the promotor of the N-terminal flotillin at a neutral locus in the genome and transcriptionally labeled with GFP (Schneider et al., 2015a). $FloT_{nt}A_{ct}$-GFP (RW323) showed stable protein production and fluorescence signal, whereas $FloA_{nt}T_{ct}$-GFP (RW326) repeatedly could not be detected. Secondary structure prediction for FloA, FloT and $FloA_{nt}T_{ct}$ with Phyre[2] (Kelley et al., 2015)

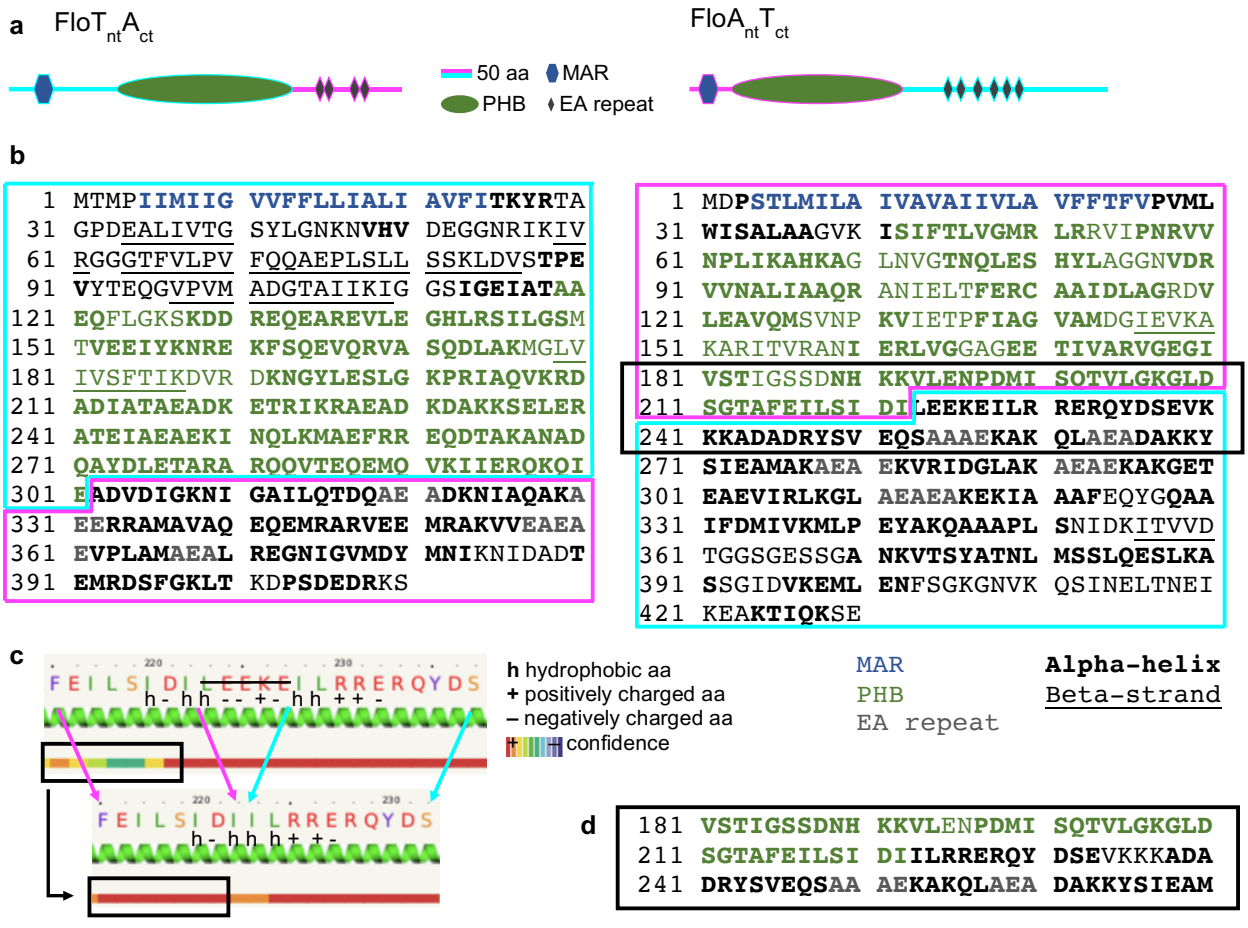

Figure 17: Primary and secondary structure of $FloT_{nt}A_{ct}$ and $FloA_{nt}T_{ct}$. a) Schematic representation of the domains of $FloT_{nt}A_{ct}$ (left) and $FloA_{nt}T_{ct}$ (right). Domains of FloA and FloT were predicted with SMART (Figure 5b, c and chapter 9.3 APPENDIX I) (Letunic et al., 2015; Letunic and Bork, 2018). b) Primary and secondary structure of $FloT_{nt}A_{ct}$ (left) and $FloA_{nt}T_{ct}$ (right, RW326) including the domains. Magenta = FloA origin, cyan = FloT origin, blue = membrane anchor region (MAR), green = PHB domain, grey = EA repeats, bold = alpha-helix, underlined = beta-strand. Secondary structure was predicted with Phyre[2] (see chapter 9.3 APPENDIX I) (Kelley et al., 2015). The FloA-to-FloT transition of $FloA_{nt}T_{ct}$ is framed with a black box. c) The primary and secondary structure of the FloA-to-FloT transition of $FloA_{nt}T_{ct}$ is displayed (top, RW326). A reduced confidence of secondary structure at the end of the N-terminus of FloA is marked with a black box. Adjustment of the transition by removing 5 charged amino acids (LEEKE) from the beginning of the C-terminus of FloT increases secondary structure confidence (bottom, RW375). d) Resulting sequence of the FloA-to-FloT transition of $FloA_{nt}T_{ct}$ (RW375).

was performed (see chapter 9.3 APPENDIX I). In FloA, the PHB domain is predicted to end with a beta-strand, and the C-terminus is predicted to start with an alpha-helix (Figure 5c). In FloT, the area of transition from N- to C-terminus is predicted to form an united alpha-helix (Figure 5c). Therefore, the transition of the $FloT_{nt}A_{ct}$ construct contains two alpha-helixes that seem to have connected easily. In the transition of the $FloA_{nt}T_{ct}$ construct, the end of a beta-strand is connected to an alpha-helix that lacks its beginning and might be destabilized (see chapter 9.3 APPENDIX I). This hypothesis is supported by a reduced secondary structure confidence at the end of the FloA N-terminus in the $FloA_{nt}T_{ct}$ strain (Figure 17c top). In order to improve the stability of $FloA_{nt}T_{ct}$, the transition was facilitated by joining stretches of hydrophobic amino acids. Instead of L302, the C-terminus of FloT was started with I307, eliminating a stretch of five charged amino acids (Figure 17c bottom, d). This version of $FloA_{nt}T_{ct}$ (RW375, 425 aa) showed protein production and fluorescence signal and was used for further analysis.

5.4.2 Oligomerization, localization and mobility analysis of chimeric flotillins

To confirm the possible functionality of the chimeric flotillins, biochemical assays to examine cellular localization of $FloT_{nt}A_{ct}$ and $FloA_{nt}T_{ct}$ were used. Cellular fragmentation analyzed with SDS-PAGE, western blot and immunodetection of GFP showed that $FloT_{nt}A_{ct}$- and $FloA_{nt}T_{ct}$-GFP were associated with the membrane fraction (Figure 18a). In further separation of the membrane into DRM/DSM fractions, the chimeric flotillins mostly localized in the DRM fraction (Figure 18b), like the native flotillins. Overall, the chimeric flotillins behave like the native flotillins in the cellular environment.

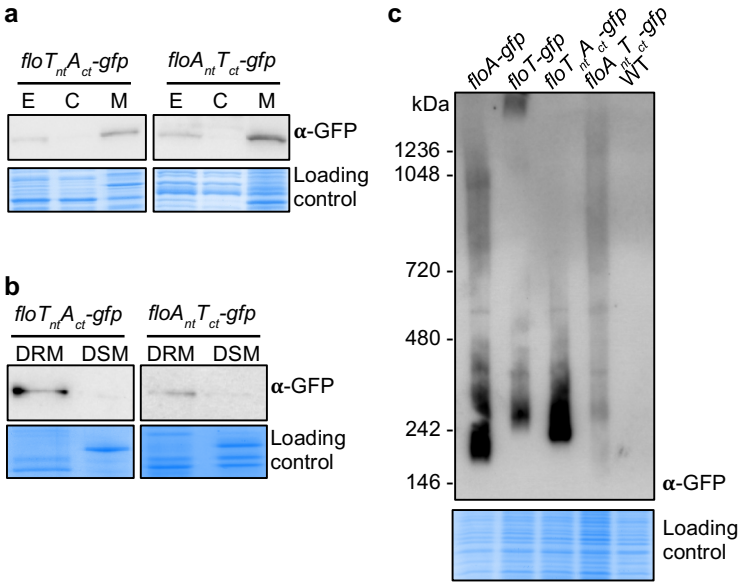

Figure 18: The chimeric flotillins $FloT_{nt}A_{ct}$ and $FloA_{nt}T_{ct}$ preferentially localize in the DRM fraction and form oligomers. a) Western blots show the cellular fractionation of $FloT_{nt}A_{ct}$- (left) and $FloA_{nt}T_{ct}$-GFP (right). A Coomassie stained gel is used as a loading control. E = whole cell extract, C = cytosol, M = membrane. b) Western blots show the membrane separation into DRM and DSM fractions. c) Western blot of blue-native PAGE of membranes of native and chimeric flotillins.

Furthermore, differences in the natural oligomerization state of $FloT_{nt}A_{ct}$- and $FloA_{nt}T_{ct}$-GFP were analyzed with BN-PAGE, western blot and GFP-immunodetection. The $FloA_{nt}T_{ct}$ signal was diffusive and did not form clear bands however still showed signal of higher molecular weight (> 1 MDa) (Figure 18c). The signal of $FloT_{nt}A_{ct}$ was rather restricted to lower molecular weights (< 300 kDa). Like FloT, the oligomers of $FloA_{nt}T_{ct}$ are of higher molecular weight than the oligomers of FloA and $FloT_{nt}A_{ct}$, respectively. The oligomerization profiles of FloA were comparable to that of $FloT_{nt}A_{ct}$ and the oligomerization profiles of FloT were comparable to that of $FloA_{nt}T_{ct}$. The C-terminus of the flotillin seems to determine its oligomeric state.

Next, the localization pattern of the chimeric variants of the flotillins was analyzed with epifluorescence microscopy. Both showed a punctate membrane localization (Figure 19a). On average $FloT_{nt}A_{ct}$-GFP formed 11 assemblies and $FloA_{nt}T_{ct}$-GFP formed 6 assemblies (Figure 19b), similar to what was observed for FloA and FloT, respectively (Figure 9). This shows that the C-terminus of the flotillin determines its localization pattern.

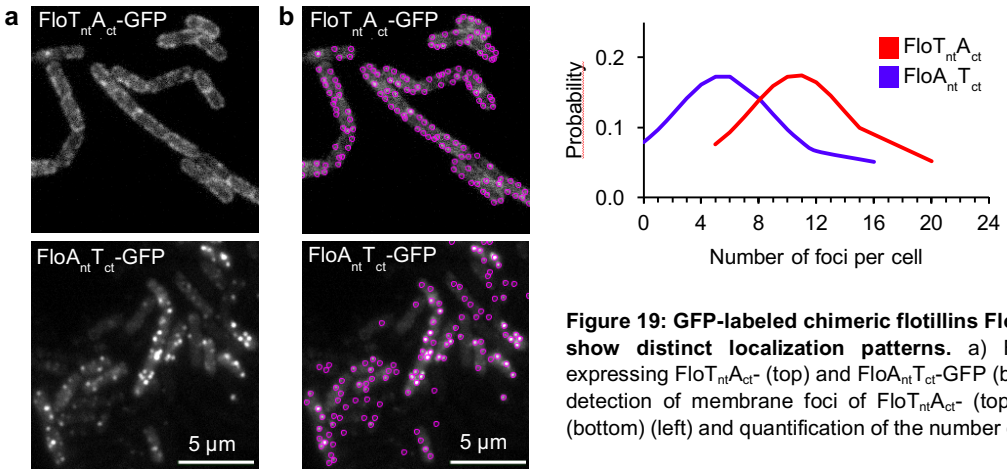

Figure 19: GFP-labeled chimeric flotillins $FloT_{nt}A_{ct}$ and $FloA_{nt}T_{ct}$ show distinct localization patterns. a) Field showing cells expressing $FloT_{nt}A_{ct}$- (top) and $FloA_{nt}T_{ct}$-GFP (bottom). b) Automatic detection of membrane foci of $FloT_{nt}A_{ct}$- (top) and $FloA_{nt}T_{ct}$-GFP (bottom) (left) and quantification of the number of foci per cell (right).

Then, the mobility of the GFP-labeled chimeric flotillins was monitored by epifluorescence microscopy acquiring images every 300 ms for 9 s. The live-cell imaging movie can be found in the supplemental material of Wagner et al., 2020 (movie 3). The images from 0 s and 9 s revealed that both $FloT_{nt}A_{ct}$- and $FloA_{nt}T_{ct}$-GFP were mobile, as differences in the localization patterns can be seen (Figure 20a). The image sequences were further used to analyze the mobility with kymographs, trajectories and MSD. Kymographs revealed that the $FloT_{nt}A_{ct}$-GFP signal formed tracks with higher lateral displacement than $FloA_{nt}T_{ct}$-GFP (Figure 20b), similar to what was observed for FloA and FloT, respectively. In both cases, tracks were separated from one another and confined to a specific membrane area.

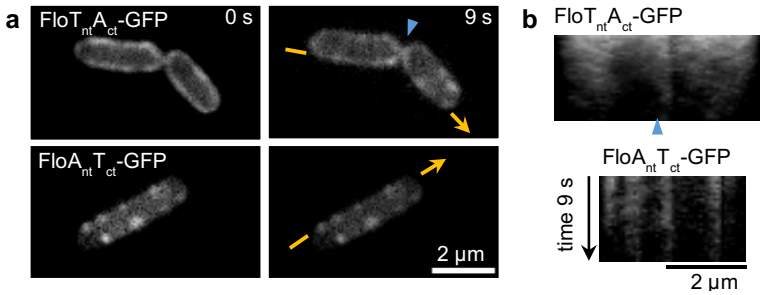

Figure 20: Kymographs show that $FloT_{nt}A_{ct}$ is more dynamic than $FloA_{nt}T_{ct}$. a) Microscope images of $FloT_{nt}A_{ct}$- (left) and $FloA_{nt}T_{ct}$-GFP (right) labeled cells at 0 s (top) and 9 s (bottom). Arrows indicate the signal used for kymographs, and triangles indicate neighboring cell poles. b) Kymograph analysis of the mobility of $FloT_{nt}A_{ct}$- (left) and $FloA_{nt}T_{ct}$-GFP (right). The membrane signal used is indicated by a yellow arrow in a). Blue triangles indicate cell poles of neighboring cells. A corresponding movie can be found in the supplemental material of Wagner et al., 2020 (movie 3).

Similarly, trajectories showed spatial restrictions in the membrane area they move within (Figure 21a). $FloT_{nt}A_{ct}$-GFP was shown to be more mobile than $FloA_{nt}T_{ct}$-GFP, as the foci of $FloT_{nt}A_{ct}$ moved within lager membrane areas. Likewise, MSD analysis revealed that both $FloT_{nt}A_{ct}$ and $FloA_{nt}T_{ct}$ showed diffusive behavior with decreasing diffusivity at longer time scales (> 1 s), indicating increased restriction

of mobility. The diffusion coefficient of $FloT_{nt}A_{ct}$ was higher than that of $FloA_{nt}T_{ct}$, confirming that $FloT_{nt}A_{ct}$ was more mobile (Figure 21b). Furthermore, at early time scales MSD analysis showed that the mobility of $FloT_{nt}A_{ct}$ was comparable to the mobility of FloA and equally, $FloA_{nt}T_{ct}$ was comparable to FloT. These results show that the C-terminus is responsible for the mobility behavior of the flotillins.

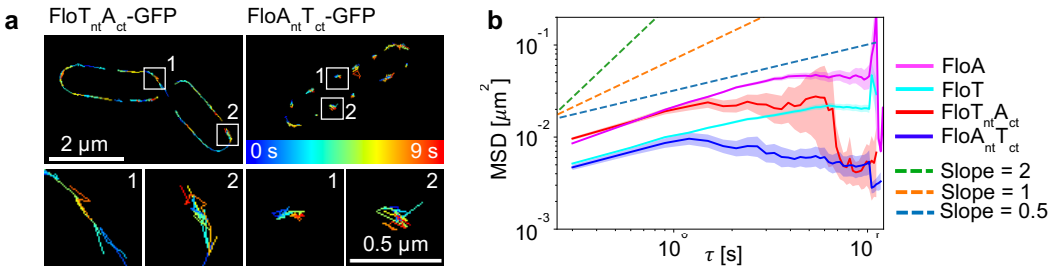

Figure 21: Trajectories and MSD analysis reveal that $FloT_{nt}A_{ct}$ is more dynamic than $FloA_{nt}T_{ct}$. a) Images of the trajectories that $FloT_{nt}A_{ct}$- (left) and $FloA_{nt}T_{ct}$-GFP (right) foci follow during 9 s. Representative trajectories are highlighted. Colors indicate elapsing time from blue = 0 s to red = 9 s. b) Plot showing the MSD analysis of FloA-, FloT-, $FloT_{nt}A_{ct}$- and $FloA_{nt}T_{ct}$-GFP. Plot shows the means with shaded areas representing the 95 % confidence intervals. N≥946 trajectories.

5.5 Flotillin mobility is influenced by cell wall-associated proteins

The C-terminus containing the flotillin domain has been shown to be important for oligomerization (Dempwolff et al., 2012; Schneider et al., 2015a), and thus, protein interaction partners are likely to play a role in flotillin mobility. To get a better understanding of possible mechanisms involved in flotillin mobility, the protein interaction partners of all flotillin variants were analyzed.

5.5.1 Pull-down analysis of flotillin variants

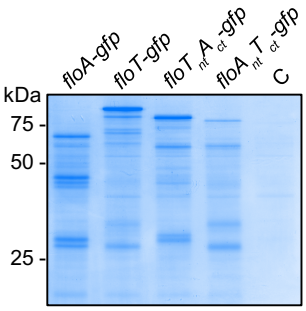

Figure 22: Pull-down analysis shows similarities of $FloT_{nt}A_{ct}$ with FloA and of $FloA_{nt}T_{ct}$ with FloT. Coomassie stained gel of the elution fractions of the pull-down analysis of FloA-, FloT-, $FloT_{nt}A_{ct}$- and $FloA_{nt}T_{ct}$-GFP. C = control strain containing the empty pRW plasmid in the Δ*floA* Δ*floT* strain background.

Pull-down assays were performed with FloA- and FloT-GFP expressed under the native promotor from a replicative pRW plasmid (see chapter 7.3.11) in a Δ*floA* Δ*floT* strain background. The double mutant strain background was used to exclude the detection of indirect protein interaction partners mediated by the other flotillin, as FloA and FloT hetero-oligomerize (Schneider et al., 2015a). Proteins that coeluted from the GFP-resin with FloA- (RW404), FloT- (RW405), $FloT_{nt}A_{ct}$- (RW407) and $FloA_{nt}T_{ct}$-GFP (RW406) or the unlabeled GFP control (RW408) (Figure 22) were subjected to mass spectrometry and protein identification. The abundance of proteins was normalized to the control sample and the fold change enrichment compared to the control sample was determined. Detected membrane proteins were classified according to their functional category assigned by *Subti*wiki (Zhu and Stülke, 2018).

To have a global overview of all identified membrane proteins, a heatmap (Babicki et al., 2016) was generated that depicted their fold-change abundance compared to the control, transformed to $\log_{10}$ scale. The heatmap was clustered according to the functional categories and proteins that were not identified in one sample were manually set to the lowest value which was depicted in dark blue (Figure 23). The heatmap showed that the abundance of many proteins was very similar in all samples, visible

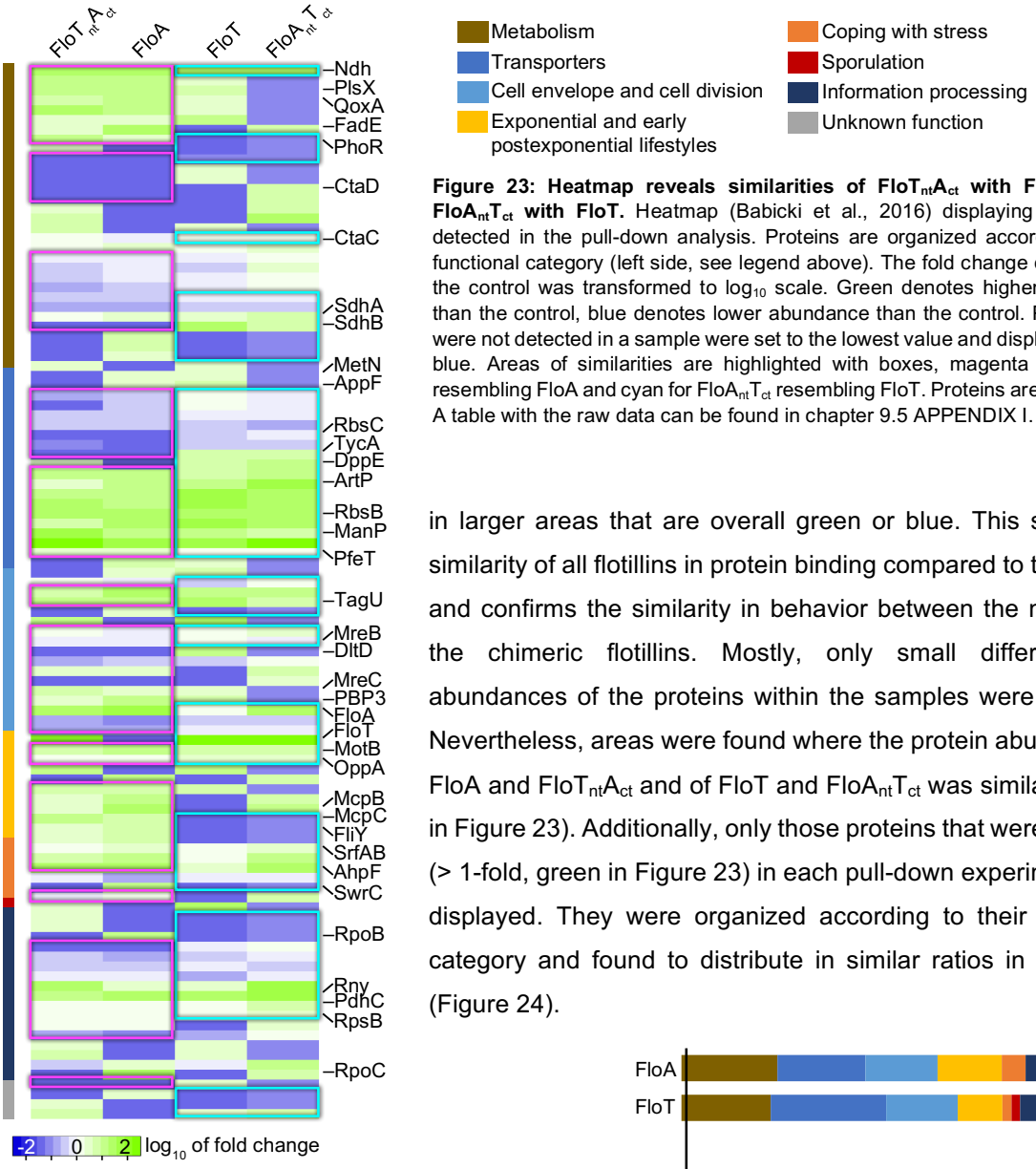

Figure 23: Heatmap reveals similarities of FloT$_{nt}$A$_{ct}$ with FloA and of FloA$_{nt}$T$_{ct}$ with FloT. Heatmap (Babicki et al., 2016) displaying all proteins detected in the pull-down analysis. Proteins are organized according to their functional category (left side, see legend above). The fold change compared to the control was transformed to log$_{10}$ scale. Green denotes higher abundance than the control, blue denotes lower abundance than the control. Proteins that were not detected in a sample were set to the lowest value and displayed in dark blue. Areas of similarities are highlighted with boxes, magenta for FloT$_{nt}$A$_{ct}$ resembling FloA and cyan for FloA$_{nt}$T$_{ct}$ resembling FloT. Proteins are highlighted. A table with the raw data can be found in chapter 9.5 APPENDIX I.

in larger areas that are overall green or blue. This shows the similarity of all flotillins in protein binding compared to the control and confirms the similarity in behavior between the native and the chimeric flotillins. Mostly, only small differences in abundances of the proteins within the samples were detected. Nevertheless, areas were found where the protein abundance of FloA and FloT$_{nt}$A$_{ct}$ and of FloT and FloA$_{nt}$T$_{ct}$ was similar (framed in Figure 23). Additionally, only those proteins that were enriched (> 1-fold, green in Figure 23) in each pull-down experiment were displayed. They were organized according to their functional category and found to distribute in similar ratios in all strains (Figure 24).

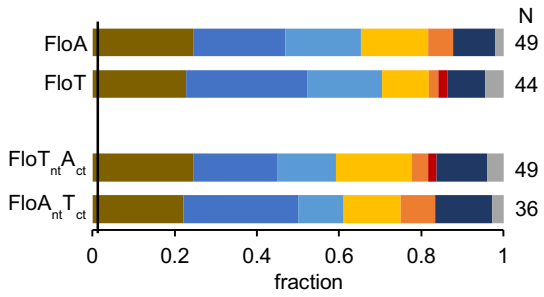

Figure 24: Enriched proteins distribute in similar ratios according to their functional categories. Bar chart showing the fraction of proteins organized according to their functional category (see Figure 23 for a legend) that are enriched in the pull-down analysis compared to the control. A table with the raw data can be found in chapter 9.5 APPENDIX I.

34 membrane proteins were found to preferentially interact with FloA, 23 preferentially interacted with FloT and 10 proteins did not show preferential interaction between FloA and FloT (Figure 25a). FloA interaction partners in general seemed to be associated to the active growth and environment surveillance. Proteins involved in chemotaxis (McpABC, CheA) and mobility (FliF and FliY) were detected. Furthermore, FloA was associated with protein synthesis proteins RpoBC, the general metabolism (FadE, PlsX, QoxA) and cell wall synthesis (PBP3, TagF). The interaction partners of FloT were part of transporter systems (DppE, OppAD, TcyA), the energy metabolism (SdhB, AtpG) and the cell wall metabolism (DltD, TagU, MinD) indicating adaptation to overcome starvation stresses during stationary phase. Interaction partners of both flotillins were associated to the general metabolism demonstrated by transporters (RbsAB, ArtP, MetN) and the cell envelope (MreC).

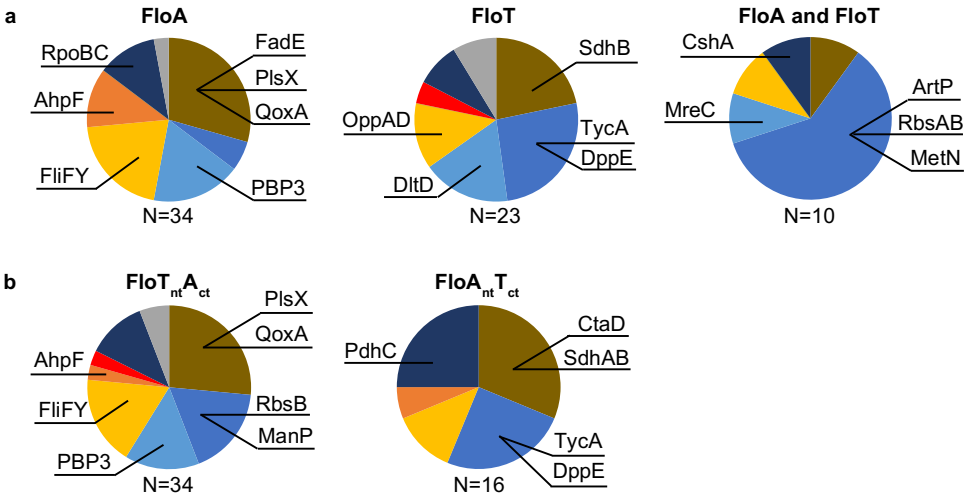

Figure 25: All flotillin variants interact with the same and with distinct proteins in pull-down experiments. Pie charts showing fractions of proteins organized according to their functional category (see Figure 23 for a legend) that preferentially interacted with FloA (left) or FloT (middle) and proteins that did not show preferential interaction with FloA or FloT (right). b) Pie charts showing proteins that preferentially interacted with $FloT_{nt}A_{ct}$ (left) and $FloA_{nt}T_{ct}$ (right). Proteins are organized according to their functional category. Representative proteins for the categories are highlighted. A table with the raw data can be found in chapter 9.5 APPENDIX I.

Similarly, 34 membrane proteins were found that preferentially interacted with $FloT_{nt}A_{ct}$ and 16 proteins that preferentially interacted with $FloA_{nt}T_{ct}$ (Figure 25b). Various proteins that preferentially interacted with $FloT_{nt}A_{ct}$ also interacted with FloA but not with FloT (PlsX, QoxA, FliF, FliY, PBP3), other proteins interacted with both, FloA and FloT (RbsB, ManP, MreC). Likewise, proteins interacting with $FloA_{nt}T_{ct}$ were also shown to interact with FloT (SdhB, DppE, TycA) whereas others interacted with FloA and FloT (ArtP, YxeB). Several proteins interacting with FloA also interacted with $FloT_{nt}A_{ct}$ and several proteins interacting with FloT also interacted with $FloA_{nt}T_{ct}$.

Overall, many interaction partners related to membrane transport and information processing were detected in this pull-down assay. A number of cell wall-related proteins were detected as well, all together confirming previous reports (López et al., 2010; Bach and Bramkamp, 2015; Schneider et al., 2015a). Cell wall synthesis has been shown previously to be responsible for the dynamics of membrane proteins (Domínguez-Escobar et al., 2011; Garner et al., 2011; Strahl et al., 2014). Therefore, the question was raised if the interaction partners PBP3 and DltD might influence the mobility of FloA and FloT, respectively.

5.5.2 PBP3 and FloA influence the mobility of each other

In the global pull-down analysis, PBP3 was found to preferentially interact with FloA (Figure 25). PBP3 is a class b penicillin-binding protein (PBP) performing transpeptidation (TP) reactions (Sauvage et al., 2008) independent of the Rod-complex and thus outside of RIF (Domínguez-Escobar et al., 2011; Strahl et al., 2014). PBP3-FloA interaction was confirmed by DRM localization and targeted pull-down analysis. For DRM/DSM analysis, cellular PBPs in the membrane of WT cells (RW3) were labeled with Bocillin-FL (Zhao et al., 1999), and subjected to DRM/DSM separation. Proteins were separated with SDS-PAGE and PBPs visualized under UV-light and identified with mass spectrometry fingerprinting (Figure 26a). PBP1 was identified to be mainly localized in the DSM fraction, and PBP3 and PBP5 to be mainly

localized in the DRM fraction. Overall, the interacting partners PBP3 and FloA (Figure 10) both localized in the DRM fraction of the membrane.

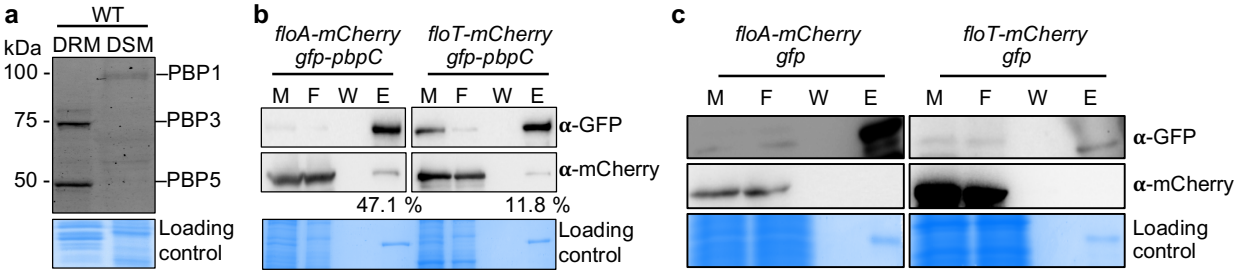

Figure 26: PBP3 localizes to the DRM and preferentially interacts with FloA. a) SDS-PAGE showing bocillin-FL labeled WT membranes subjected to DRM/DSM separation to visualize PBPs. Indicated PBPs were identified by mass spectrometry. Coomassie staining is used as a loading control. b) Western blots of targeted pull-down with FloA- (left) or FloT-mCherry (right) and GFP-PBP3 double-labeled strains. Numbers indicate the intensity of the mCherry signal in the elution fraction in relation to the normalized GFP signal in the elution fraction. M = membrane starting material, F = flowthrough, W = final wash, E = elution. c) Western blots of control pull-down experiments with FloA- (left) or FloT-mCherry (right) and untagged-GFP double-labeled strains.

Strains labeled with GFP-PBP3 and FloA- (RW452) or FloT-mCherry (RW455) were used for targeted pull-down analysis. All labeled proteins were expressed from a xylose inducible promotor (0.5 % xylose), GFP-PBP3 in the chromosome at the ectopic locus, flotillins from a replicative pRW plasmid. A resin to bind GFP was used and coelution of FloA- or FloT-mCherry was analyzed with SDS-PAGE, western blot and immunodetection. GFP-PBP3 stably bound to the resin, and FloA- and FloT-mCherry were coeluted with GFP-PBP3 (Figure 26b). The FloA-mCherry signal intensity was 47.1 % of the GFP signal intensity, whereas the FloT-mCherry signal intensity was only 11.8 % of the GFP signal intensity. Control strains expressing GFP without PBP3 did not show coelution of FloA- (RW434) or FloT-mCherry (RW435) (Figure 26c). With this, the results obtained from the global pull-down analysis were confirmed. PBP3 preferentially interacted with FloA.

To understand if PBP3 might have an influence on FloA, PBP3 localization and mobility were characterized first. The cellular localization pattern of PBP3 was monitored with a strain expressing GFP-PBP3 from a xylose inducible promotor at the ectopic locus (RW445, 0.5 % xylose). Epifluorescence microscopy showed a punctate pattern in the membrane (Figure 27a). To have a better understanding of PBP3 distribution and a picture of a continuous membrane area, TIRFM was used as well (Figure 27b). Quantification of the PBP3 foci detected in TIRFM images revealed on average 9 foci per cell (Figure 27c, d). Next, the mobility of PBP3 was analyzed with TIRFM by acquiring images every 300 ms for 9 s. The live-cell imaging movie can be found in the supplemental material of Wagner et al., 2020 (movie 5). PBP3 dynamics were obvious from localization patterns in images at 0 s and 9 s (Figure 27e, left). The mobility was analyzed with kymographs along the long axis of the cell, revealing tracks with lateral displacements of different margin (Figure 27e, middle). The strict separation of individual tracks as visible for FloA and FloT was not as pronounced here. Nevertheless, areas that were not covered by tracks for several frames were visible. Trajectory analysis of PBP3 used the same parameters as for flotillin analysis. Trajectories represented PBP3 foci randomly moving in all directions covering larger areas of the membrane (Figure 27e, right). MSD analysis revealed a diffusive behavior

with a diffusion coefficient in the same range as FloA and FloT, slower than FloA and faster than FloT (Figure 27f).

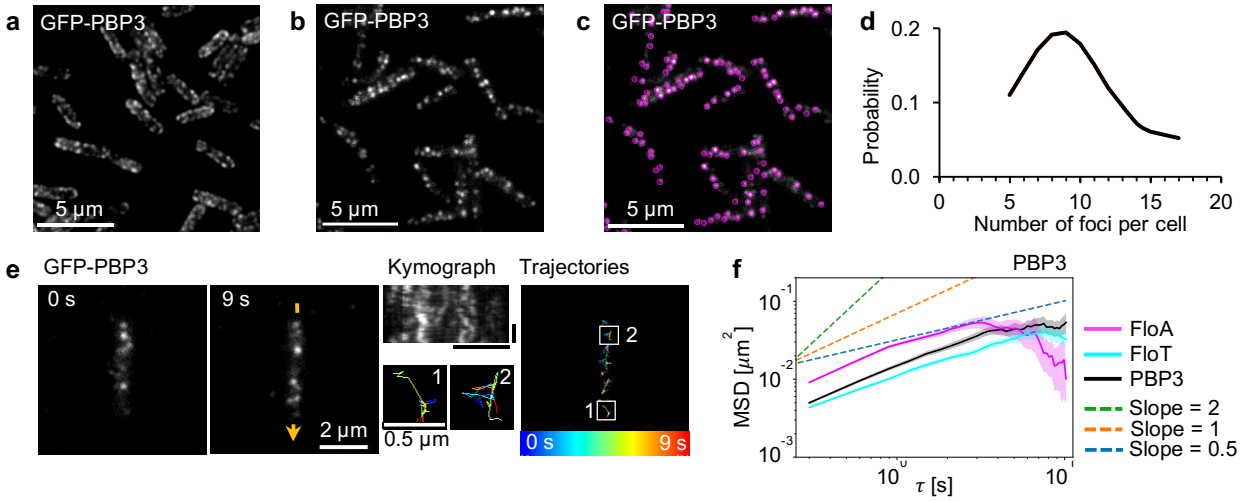

Figure 27: PBP3 localizes in a punctate patter that shows random mobility. a) Image showing a field of GFP-PBP3 labeled cells acquired with epifluorescence microscopy. b) Image showing a field of GFP-PBP3 labeled cells acquired with TIRFM. c) Image displaying the automatic detection of membrane foci of cells shown in b). d) Graphic showing the quantification of the number of PBP3 foci per cell. e) Images showing the mobility analysis of GFP-PBP3 with TIRFM. Images were acquired every 300 ms for 9 s. Shown are the localization patterns of GFP-PBP3 at 0 s and 9 s (left), mobility analysis with kymographs (middle) and mobility analysis with trajectories (right). Kymographs are generated using the membrane signal indicated with a yellow arrow in the 9 s image (horizontal scale bar represents 2 µm and vertical scale bar represents 3 s). Representative trajectories are highlighted. Colors indicate elapsing time from blue = 0 s to red = 9 s. f) Plot showing the MSD analysis of GFP-PBP3 in comparison to FloA- and FloT-GFP. Plot shows the means with shaded areas representing the 95 % confidence interval. N≥1275 trajectories. A corresponding movie can be found in the supplemental material of Wagner et al., 2020 (movie 5).

The cellular pattern of GFP-PBP3 looked similar to the cellular pattern of FloA and FloT: puncta distributed in the whole membrane. To understand if these puncta of PBP3 and FloA or FloT overlap, their colocalization was studied. Double-labeled strains were used expressing GFP-PBP3 from a xylose inducible promotor at the ectopic locus (0.5 % xylose), and FloA- (RW554) or FloT-mCherry (RW555) under the natural promotor at the neutral *lacA* locus in the genome. Epifluorescence microscopy was initially used to study colocalization (Figure 28a) but then expanded to TIRFM to view the cellular surface in more detail (Figure 28b). In general, only few flotillin foci were found to colocalize with PBP3 indicating a transient interaction. The Pearson correlation coefficient r for TIRFM-acquired colocalization images was determined: PBP3-FloA r=0.657, PBP3-FloT r=0.497. This confirms the observation that PBP3 only transiently interacts with flotillins. However, it also shows that the localization of PBP3 with FloA is higher than with FloT.

To understand if PBP3 influences flotillin mobility, a knockout mutation in *pbpC* (PBP3 is encoded by *pbpC*) was generated and the mobility of FloA- (RW307) and FloT-GFP (RW299) in this genetic strain background monitored. The Δ*pbpC* strain did not show any growth differences compared to the WT strain (Figure 28c). Images of flotillin-GFP labeled Δ*pbpC* strains were acquired every 300 ms for 9 s. The live-cell imaging movie can be found in the supplemental material of Wagner et al., 2020 (movie 4). Analysis with kymographs, trajectories, and MSD revealed a minor reduction in flotillin mobility in a

Δ*pbpC* strain background (Figure 28d). Additionally, a minor increase in the diffusivity of FloA was observed in the deletion mutant indicating that PBP3 was restricting the mobility of FloA to weak extent.

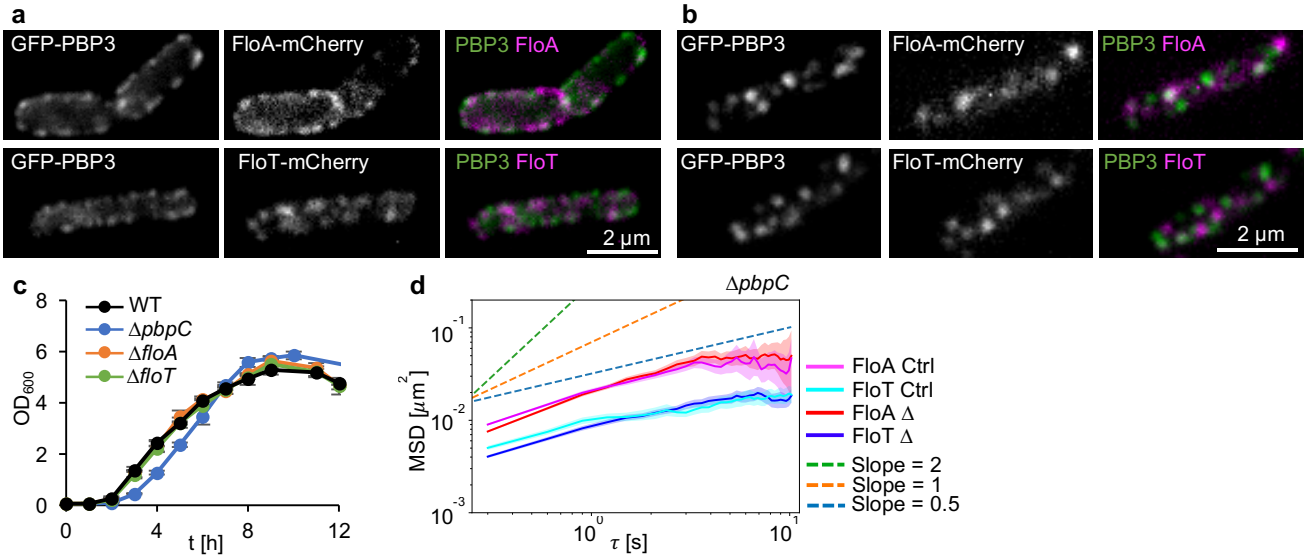

Figure 28: PBP3 preferentially localizes with FloA and slightly decreases its diffusivity. a) Epifluorescence microscopy images showing the colocalization of GFP-PBP3 and FloA- (top) or FloT-mCherry (bottom) double-labeled cells. b) TIRFM images showing the colocalization of GFP-PBP3 and FloA- (top) or FloT-mCherry (bottom) double-labeled cells. c) Growth curves of WT, Δ*pbpC* (encodes PBP3), Δ*floA* (whole operon deletion) and Δ*floT* (whole operon deletion) strain backgrounds. d) Plot showing the MSD analysis of FloA- and FloT-GFP in WT (Ctrl) and Δ*pbpC* strain backgrounds. Plot shows the means with shaded areas representing the 95 % confidence interval. N≥1275 trajectories. A corresponding movie can be found in the supplemental material of Wagner et al., 2020 (movie 4).

Next, it was tested if inversely, FloA and FloT also influence characteristics of PBP3. First, the cellular localization of PBPs was monitored with Bocillin-FL-labeled membrane extracts from WT (RW3), Δ*floA* (RW329), Δ*floT* (RW330) and Δ*floA* Δ*floT* (RW334) strain backgrounds (in all cases the whole flotillin operons were deleted) subjected to DRM/DSM separation. SDS-PAGE separation and UV-detection revealed that the amount of PBP3 was increased in the DRM of the Δ*floA* mutant backgrounds (Δ*floA* and Δ*floA* Δ*floT*) (Figure 29a). However, another preliminary study did not detect differences in PBP3 level in WT and Δ*floA* Δ*floT* whole membranes, using different laboratory strain backgrounds (Zielińska et al., 2020). Further, the mobility of GFP-PBP3 was analyzed in Δ*floA*- (RW482) and Δ*floT*-operon (RW488) deletion backgrounds. The Δ*floA* and Δ*floT* strain backgrounds did not show any growth differences compared to the WT strain (Figure 28c). GFP-PBP3 was expressed under a xylose-inducible promotor (0.5%) from the ectopic locus in the genome and its mobility analyzed in these strain backgrounds. Kymographs and trajectories showed that the absence of FloT did not seem to influence PBP3 mobility. The absence of FloA resulted in an increase in PBP3 dynamics. This was visible in kymographs displaying higher lateral displacements and trajectories that were temporally shorter (Figure 29b). Shorter trajectories denote the connection of fewer consecutive foci. This results from larger spatial distances of foci in between two consecutive time points because of a higher foci mobility. In the course of this, occasionally, foci exceed the spatial threshold to be considered part of the same trajectory. This results in temporally shorter tracks with longer spatial distances in between two time points. Apart from this, MSD analysis revealed a minor increase in diffusion coefficient of PBP3 in the Δ*floA* mutant background but not in the Δ*floT* background (Figure 29c). FloA and its interaction partner

PBP3 have an effect on each other: FloA impacts the mobility and the amount of PBP3 and conversely, PBP3 influences the mobility of flotillins.

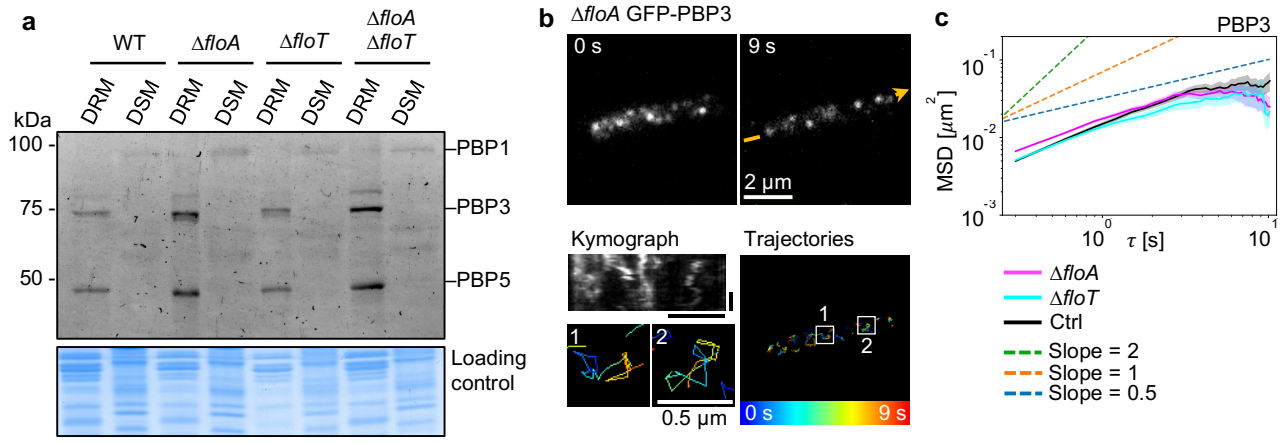

Figure 29: PBP3 abundance and mobility is influenced by FloA. a) SDS-PAGE showing bocillin-FL labeled membrane fractions to visualize PBPs from WT, Δ*floA*, Δ*floT* and Δ*floA* Δ*floT* strain backgrounds (always whole operon deletion) subjected to DRM/DSM separation. Indicated PBPs were identified with mass spectrometry. Coomassie staining is used as a loading control. b) Images showing the mobility analysis of GFP-PBP3 in Δ*floA* (whole operon deletion) strain background. Images were acquired every 300 ms for 9 s. Shown are the localization patterns of GFP-PBP3 at 0 s and 9 s (top), mobility analysis with kymographs (bottom left) and mobility analysis with trajectories (bottom right). Kymographs are generated using the membrane signal indicated in the 9 s image with a yellow arrow (horizontal scale bar represents 2 µm and vertical scale bar represents 3 s). Representative trajectories are highlighted. Colors indicate elapsing time from blue = 0 s to red = 9 s. c) Plot showing the MSD analysis of GFP-PBP3 in WT (Ctrl), Δ*floA* and Δ*floT* strain backgrounds (always whole operon deletion). Plot shows the means with shaded areas representing the 95 % confidence interval. N≥1275 trajectories. A corresponding movie can be found in the supplemental material of Wagner et al., 2020 (movie 5).

5.5.3 DltD and FloT influence the mobility of each other

In the global pull-down analysis, DltD was found to preferentially interact with FloT (Figure 25). DltD is encoded in the *dltABCDE* operon. The operon is responsible for modification of the anionic polymers in the cell wall (wall teichoic acids (WTA) anchored in the cell wall and lipoteichoic acids (LTA) anchored in the membrane). The addition of positively charged D-alanyl residues (Figure 30) (Perego et al., 1995; Rajagopal and Walker, 2017; McKay Wood et al., 2018) reduces the repulsive forces of the anionic polymers and leads to a more densely packed cell wall (Neuhaus and Baddiley, 2003). DltD is a membrane protein that is assumed to attach D-alanine to LTA. D-alanyl residues are then transferred from LTA to WTA (Haas et al., 1984; Reichmann et al., 2013).

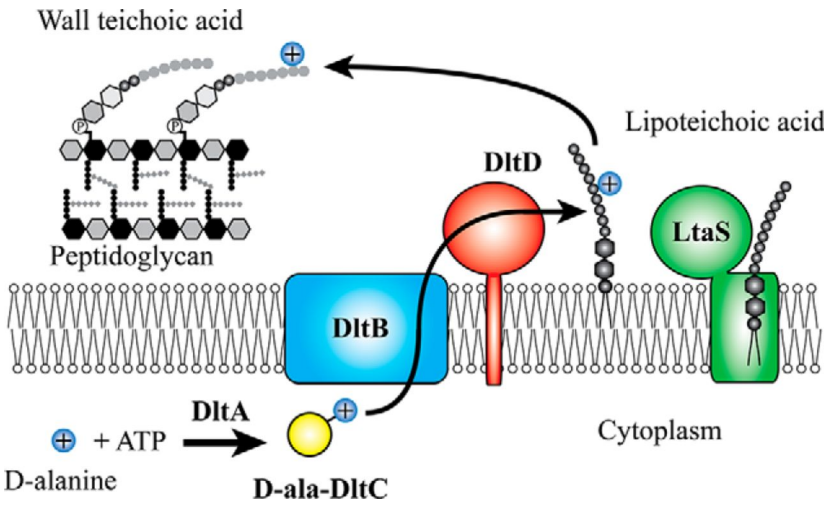

Figure 30: The DltABCDE proteins modify LTA and WTA in the cell wall. In the cytosol DltA transfers D-Ala to the DltC carrier protein. Then DltB transfers D-ala to the outer side of the membrane where to DltD further transfers it to LTA. DltE is not necessary for the incorporation of D-Ala and its function remains unknown. D-ala residues are first attached to LTA and then further transferred to WTA. Image displayed with permission of the publisher, original publication by McKay Wood et al., 2018.

FloT mobility is reduced in a Δ*dltA-E* deletion strain background

To confirm the localization of DltD in the DRM fraction and its interaction with FloT in a targeted pull-down analysis, double-labeled strains were used expressing GFP-DltD under a xylose-inducible promotor at the neutral *amyE* locus in the genome, and FloA- (RW500) or FloT-mCherry (RW502) under the xylose-inducible promotor from a replicative plasmid (0.5 % xylose). First, the membranes of these strains were subjected to DRM/DSM separation. SDS-PAGE, western blot and immunodetection of GFP or mCherry showed that both, DltD and flotillins, preferably located in the DRM fraction of the membrane (Figure 31a). The interaction of DltD and FloT was analyzed using a targeted pull-down assay. A GFP-binding resin was used and the co-elution of FloA- or FloT-mCherry with GFP-DltD was analyzed. SDS-PAGE, western blot and immunodetection confirmed GFP-DltD binding to the resin and the coelution of both FloA- and FloT-mCherry (Figure 31b). Quantification revealed that the FloA-mCherry signal intensity was 4.1 % of the GFP signal intensity, whereas the FloT-mCherry signal intensity was 14.5 % of the GFP signal intensity. This confirms the global pull-down analysis that showed preferential binding of DltD with FloT.

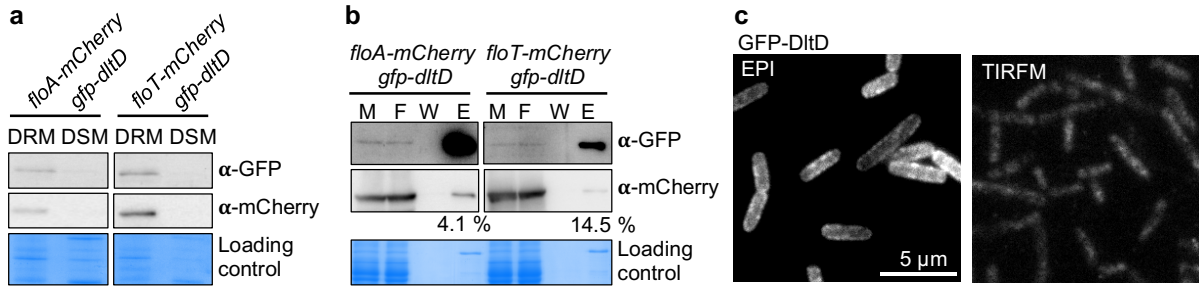

Figure 31: DltD localizes to the DRM and preferentially interacts with FloT. a) Western blots of DRM/DSM separation of GFP-DltD and FloA- (left) or FloT-mCherry (right) double-labeled strains. A Coomassie stained gel is used as a loading control. b) Western blots of targeted pull-down with FloA- (left) or FloT-mCherry (right) and GFP-DltD double-labeled strains. Numbers indicate the intensity of the mCherry signal in relation to the normalized GFP signal. M = membrane starting material, F = flowthrough, W = final wash, E = elution. A control pull-down can be seen in Figure 26c. c) Images showing a field of GFP-DltD labeled cells acquired epifluorescence microscopy (EPI, left) or TIRFM (right).

Next, to understand if DltD might have an influence on FloT mobility, DltD cellular localization was characterized. A GFP-DltD (RW498) labeled strain expressing GFP-DltD under a xylose-inducible promotor at the neutral *amyE* locus in the genome (0.5 % xylose) was used to monitor DltD cellular localization. In epifluorescence microscopy DltD is inhomogeneously distributed in the whole membrane. TIRFM was used to have a more detailed view on the surface distribution of DltD and showed a heterogeneous distribution with a homogeneous background signal and accumulations of higher signal intensities (Figure 31c). This membrane distribution differed from the punctate pattern of FloA and FloT and thus did neither allow quantification nor comparison to FloA and FloT.

Despite these differences, a possible colocalization between the accumulations of DltD and flotillin foci was studied. Double-labeled strains were used expressing GFP-DltD under a xylose-inducible promotor at the neutral *amyE* locus in the genome, and FloA- (RW556) or FloT-mCherry (RW557) under the xylose-inducible promotor at the neutral *lacA* locus in the genome (0.5 % xylose). Colocalization was analyzed with epifluorescence (Figure 32a) and TIRFM (Figure 32b) and showed that DltD accumulations mostly did not colocalize with flotillin foci, indicating a transient interaction. Analysis of

the TIRFM images revealed the following Pearson correlation coefficients: DltD-FloA r=0.62, DltD-FloT r=0.7. Flotillins only transiently interacted with DltD and the interaction of DltD with FloT was higher than the interaction with FloA. These results were not surprising, as differences in localization patterns made it unlikely to detect colocalization that exceeds transient interactions.

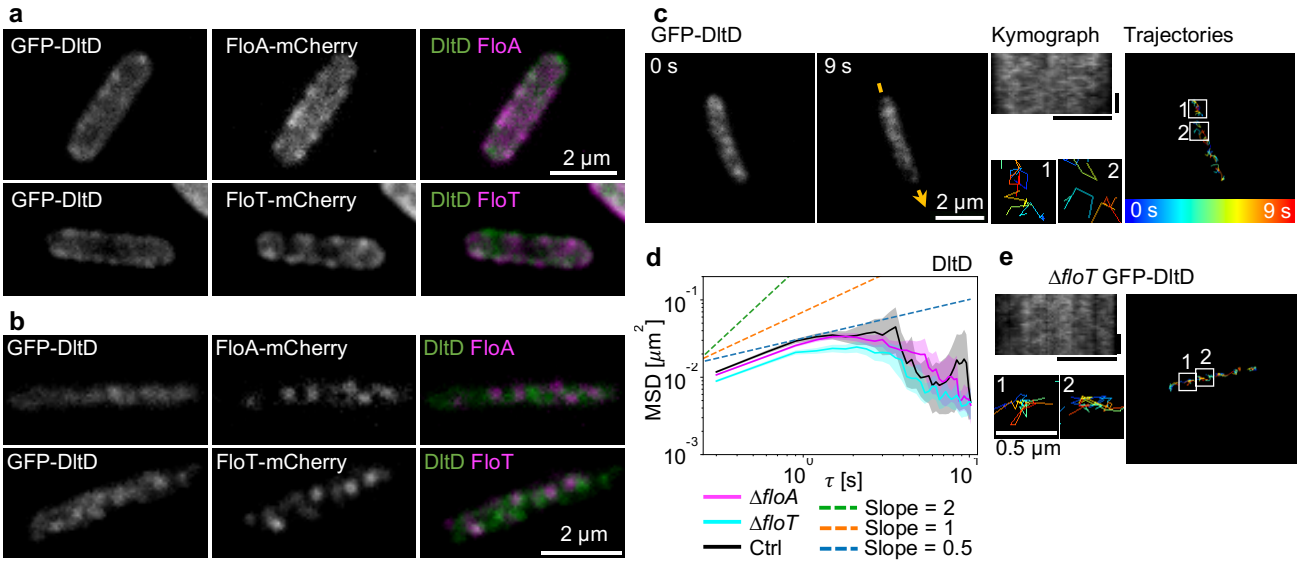

Figure 32: DltD preferentially localizes with FloT and depends on its presence for mobility. a) Epifluorescence microscopy images showing the colocalization of GFP-DltD and FloA- (top) or FloT-mCherry (bottom) double-labeled cells. b) TIRFM images showing the colocalization of GFP-DltD and FloA- (top) or FloT-mCherry (bottom) double-labeled cells. c) Images showing the mobility analysis of GFP-DltD. Images were acquired every 300 ms for 9 s. Shown are the localization patterns of GFP-DltD at 0 s and 9 s (left), mobility analysis with kymographs (middle) and mobility analysis with trajectories (right). Kymographs are generated using the membrane signal indicated in the 9 s image with a yellow arrow (horizontal scale bar represents 2 µm and vertical scale bar represents 3 s). Representative trajectories are highlighted. Colors indicate elapsing time from blue = 0 s to red = 9 s. d) Plot showing the MSD analysis of GFP-DltD in WT (Ctrl), Δ*floA* and Δ*floT* strain backgrounds (always whole operon deletion). Plot shows the means with shaded areas representing the 95 % confidence interval. N≥1061 trajectories. e) Images showing the mobility analysis of GFP-DltD in a Δ*floT* (whole operon deletion) strain background. Shown are the mobility analysis with kymographs (left) and mobility analysis with trajectories (right). Kymographs are generated using the membrane signal along the long axis of the cell (horizontal scale bar represents 2 µm and vertical scale bar represents 3 s). Representative trajectories are highlighted. Colors indicate elapsing time from blue = 0 s to red = 9 s. A corresponding movie can be found in the supplemental material of Wagner et al., 2020 (movie 5).

Next, the mobility of DltD was monitored with image acquisition of GFP-DltD (RW498, 0.5 % xylose) every 300 ms for 9 s. The live-cell imaging movie can be found in the supplemental material of Wagner et al., 2020 (movie 5). The images of 0 s and 9 s showed differences in DltD localization pattern and revealed that DltD accumulations are moving within the membrane (Figure 32c left). The mobility was further analyzed with kymographs along the cell axis which similarly showed a background noise with highlighted tracks corresponding to the signal of the accumulations (Figure 32c middle). These showed strong lateral displacements and random orientation. Some tracks rapidly moved a long stretch before changing direction or moving out of the membrane area observed, visible in nearly vertical lines. Similarly, trajectories were temporally very short with long spatial distances bridged within short time intervals (Figure 32c right). These observations revealed DltD accumulations to rapidly move within the membrane. Nevertheless, due to the heterogeneous membrane signal of DltD, Trackmate might not efficiently detect accumulations, as it is designed for spot detection. Therefore, DltD mobility was not compared with the mobility of FloA or FloT. As any possible error resulting from inappropriate Trackmate

analysis would be constant throughout different analyses, DltD can still be compared with itself after exposure to different conditions.

To analyze if flotillins have an impact on the mobility of DltD, strains were created that had a Δ*floA*- (RW514) or Δ*floT*-operon (RW513) deletion background and expressed GFP-DltD under a xylose-inducible promotor at the neutral *amyE* locus in the genome (0.5 % xylose). Image sequences were acquired every 300 ms for 9 s. The live-cell imaging movie can be found in the supplemental material of Wagner et al., 2020 (movie 5). MSD analysis revealed that the absence of FloA only had a minor influence on DltD mobility, whereas the absence of FloT decreased the DltD diffusion coefficient in a more pronounced manner (Figure 32d). Similarly, kymographs and trajectories showed a decreased mobility of DltD in Δ*floT* background, and no differences in the Δ*floA* background. The kymographs in Δ*floT* showed lateral displacements to a smaller extent indicating slower mobility (Figure 32e left). Trajectories were temporally longer and with spatially shorter distances (Figure 32e right) supporting the slower mobility observed with kymographs. The mobility of DltD is dependent on the FloT-operon as its absence reduces the mobility of DltD.

Next, to understand if convserely flotillins were also influenced by the *dltABCDE*-operon (*dltA-E*), a Δ*dltA-E* deletion strain was labeled with FloA- (RW104) or FloT-GFP (RW105) expressed from the native promotor at the neutral *lacA* locus in the genome. The Δ*dltA-E* strain did not show any growth differences compared to the WT strain (Figure 35a). Images were acquired every 300 ms for 9 s. The live-cell imaging movie can be found in the supplemental material of Wagner et al., 2020 (movie 4). Images at 0 s and 9 s showed that while the localization pattern of FloA was changed, the localization pattern of FloT remained consistent (Figure 33a left). Likewise, analysis of kymographs and trajectories showed no differences in FloA mobility, while FloT mobility was reduced in the Δ*dltA-E* strain background (Figure 33a middle and right). This was confirmed by MSD analysis which revealed no differences in FloA diffusion, but a reduction in the diffusion coefficient for FloT, accompanied by a decrease in diffusivity (Figure 33b). The reduced diffusivity of FloT in the Δ*dltA-E* strain background indicates that FloT is directly or indirectly shielded from influences restricting its diffusivity in the WT background mediated by DltA-E. At the same time, DltA-E promote the mobility of FloT, as the diffusion coefficient is reduced in their absence. The Δ*dltA-E* strain background showed reduced FloT mobility.

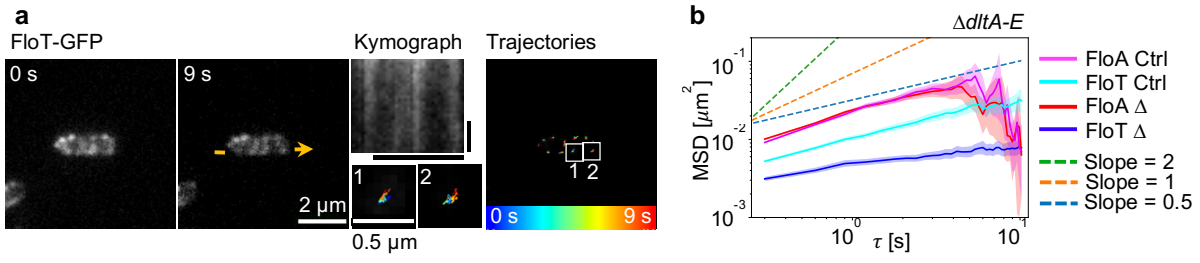

Figure 33: The mobility of FloT is reduced upon absence of DltA-E. a) Images showing the mobility analysis of FloT-GFP in Δ*dltA-E* deletion background. Images were acquired every 300 ms for 9 s. Shown are the localization patterns of FloT-GFP at 0 s and 9 s (left), mobility analysis with kymographs (middle) and mobility analysis with trajectories (right). Kymographs are generated using the membrane signal indicated in the 9 s image with a yellow arrow (horizontal scale bar represents 2 µm and vertical scale bar represents 3 s). Representative trajectories are highlighted. Colors indicate elapsing time from blue = 0 s to red = 9 s. b) Plot showing the MSD analysis of FloA- and FloT-GFP in WT (Ctrl) and Δ*dltA-E* strain backgrounds. Plot shows the means with shaded areas representing the 95 % confidence interval. N≥1134 trajectories. A corresponding movie can be found in the supplemental material of Wagner et al., 2020 (movie 4).

Changes in FloT mobility are not caused by the activity of DltA-E

In this Δ*dltA-E* strain background, the DltA-E proteins themselves are absent as well as their impingement on the cell wall. DltA-E modify the anionic polymers LTA and WTA with D-alanyl residues and thereby have an impact on the overall cell wall structure (Figure 30). To understand if either the proteins themselves or the cell wall differences can account for differences in FloT mobility, several control experiments were performed.

First, the possibility if WTA or LTA themselves might influence flotillin mobility was examined. While a simultaneous deletion of both polymers is lethal, each polymer itself is dispensable for the cell, albeit accompanied by severe defects in cellular growth (D'Elia et al., 2006; Schirner et al., 2009).

As WTA are covalently bound to the cell wall outside the cell and are not linked to the membrane where flotillins are localized, it seems unlikely that they affect flotillin mobility. Nevertheless, the WTA synthesis protein TagU was detected in the global pull-down analysis to preferentially interact with FloT, similarly to DltD. TagU is a membrane protein that, together with its paralogs TagT and TagV, attaches the teichoic acids to the cell wall. Δ*tagTUV* deletions are not viable unless rescued by an additional Δ*tagO* deletion (Kawai et al., 2011). Therefore, only the flotillin interaction partner TagU was mutated. The Δ*tagU* deletion strain background grew at WT levels, albeit growing as spheres (Figure 34a, c). It was labeled with FloA- (RW458) or FloT-GFP (RW456) and the mobility of flotillins was monitored every 300 ms for 9 s. Using kymographs, trajectories and MSD analysis, no differences in mobility were detected for FloA and only a minor reduction in FloT (Figure 34d). The Δ*tagU* deletion mutation is only an approximation for WTA deficiency, as TagTV are still able to carry out a certain amount of WTA synthesis. However, morphological differences in the Δ*tagU* deletion strain background confirm perturbance in WTA synthesis which did not result in differences in flotillin mobility.

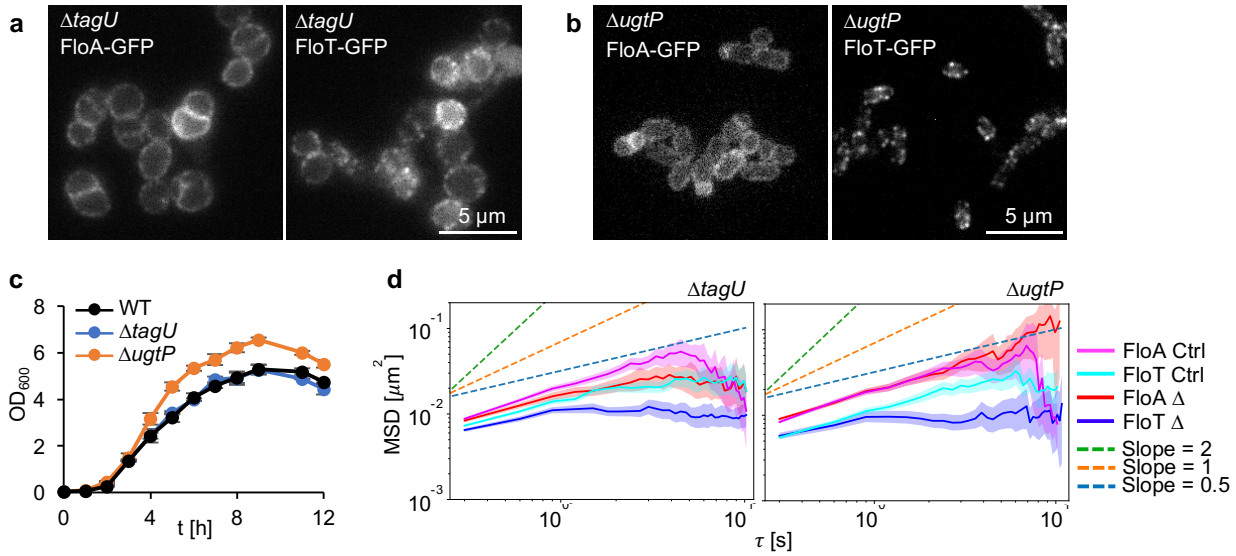

Figure 34: Differences in WTA and LTA do not affect flotillin mobility. a) Epifluorescence microscopy images of FloA- (left) and FloT-GFP (right) labeled cells in a Δ*tagU* strain background. b) Epifluorescence microscopy images of FloA- (left) and FloT-GFP (right) labeled cells in a Δ*ugtP* strain background. c) Growth curves of WT, Δ*tagU* and Δ*ugtP* strain backgrounds. d) Plots showing the MSD analysis of FloA- and FloT-GFP in WT (Ctrl) and Δ*tagU* (left) or Δ*ugtP* (right) strain backgrounds. Plots show the means with shaded areas representing the 95 % confidence interval. N≥627 trajectories.

In contrast to the cell wall-anchored WTA, LTA are anchored to the membrane and might impact flotillin mobility directly. As the complete absence of LTAs is accompanied by severe defects in cellular growth, mutations are constructed that impact LTA structure but do not show reduced growth rates. In initial synthesis steps, the membrane anchor of LTA is synthesized. UgtP (formerly YpfP) is a glycosyltransferase that catalyzes the final step of attaching glycosyl moieties to the lipid carrier, generating diglucosyl-diacylglycerol (Glc2-DAG) (Jorasch et al., 1998; Matsuoka, 2017). Upon *ugtP* deletion, cells become spherical (Price et al., 1997; Lazarevic et al., 2005) (Figure 34b, c) which has been reported in *S. aureus* to results from structural differences of LTA (Gründling et al., 2007). A Δ*ugtP* deletion strain background was generated and labeled with FloA- (RW119) or FloT-GFP (RW117) to monitor flotillin mobility in the absence of UgtP. Kymographs, trajectories and MSD analysis showed no differences for FloA and FloT mobility (Figure 34d). The Δ*ugtP* deletion is only an approximation for LTA deficiency. UgtP absence possibly results in differences in LTA structure, but LTA should still be partially functional, as their complete elimination is accompanied by severe defects in the level of cellular growth (Schirner et al., 2009). It has to be noted that in the absence of UgtP also glucolipids other than Glc2-DAG are absent (Matsuoka, 2017). Nevertheless, morphological differences in the Δ*ugtP* strain background point to an impaired LTA functionality. Flotillin mobility is not affected by these morphological differences upon LTA structural changes.

The mutations used to reduce the functionality of WTA and LTA are only approximations, and cannot completely exclude that the effect of Δ*dltA-E* on the cell wall leads to the difference in FloT mobility. Additional control experiments were performed to distinguish if the absence of the DltA-E proteins or the more negative surface net charge is responsible for the difference in FloT mobility in the Δ*dltA-E* deletion strain background. i) The Δ*dltA-E* deletion strain background was used and grown with addition of 25 mM $MgCl_2$ which is supposed to mimic the positive charges in the cell wall (García-Betancur et al., 2017). Several cell envelope mutations have been shown to be rescued by elevated levels of Mg^{2+}, e.g. *ponA* (Murray et al., 1998), *tagO* (D'Elia et al., 2006), *mreCD* (Leaver and Errington, 2005) or *mbl* (Schirner and Errington, 2009). In this condition, DltD is absent but the surface net charge is restored. ii) A Δ*dltA* deletion strain background (RW568) was used which still contains DltD but cannot modify the cell wall with D-alanyl residues (Perego et al., 1995; Wecke et al., 1996). iii) WT cells were grown in LB with a basic pH abolishing the surface charge and the incorporation of D-alanyl residues (Hyyryläinen et al., 2000). In this case, DltD is present but the D-alanyl residues are absent. In all conditions FloT-GFP was expressed under the native promotor at the neutral *lacA* locus in the genome. Cellular growth under these conditions did not cause pronounced growth differences (Figure 35a). Only Δ*dltA-E* + $MgCl_2$ caused a rapid decrease of OD_{600} upon entry into stationary phase. Nevertheless, the OD_{600} of all strains at the time of image acquisition was comparable. Cells grown in these conditions were imaged every 300 ms for 9 s and the mobility of FloT analyzed (Figure 35b). Kymographs, trajectories and MSD revealed that FloT mobility was independent of the surface net charge but was reduced when DltB-E were absent. The reduced FloT mobility in Δ*dltA-E* is possibly owed to the absence of the FloT interaction partner DltD. The mobility of FloT is influenced by DltD and likewise, DltD mobility is influenced by FloT.

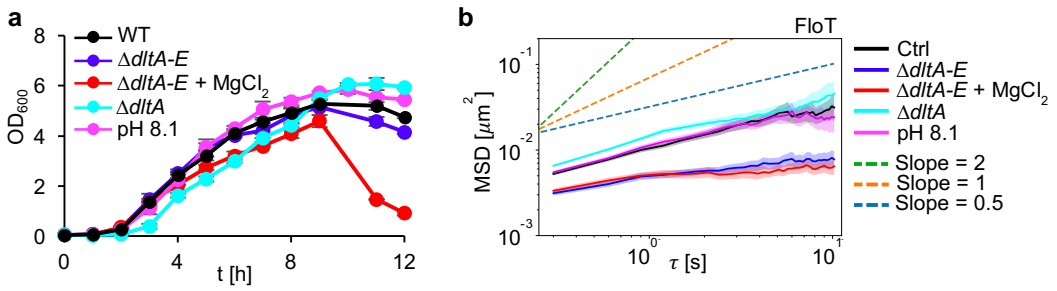

Figure 35: The reduced mobility of FloT depends not on cell wall changes but on the DltB-E proteins. a) Growth curves of WT, Δ*dltA-E*, Δ*dltA-E* + $MgCl_2$, Δ*dltA* strain backgrounds and at pH 8.1. b) Plot showing the MSD analysis of FloT-GFP in WT (Ctrl), Δ*dltA-E*, Δ*dltA-E* + $MgCl_2$, Δ*dltA* strain backgrounds and at pH 8.1. Plot shows the means with shaded areas representing the 95 % confidence interval. N≥1134 trajectories.

5.6 Cell wall synthesis promotes flotillin mobility

It was shown that the protein interaction partners PBP3 and DltD impact the mobility of FloA and FloT, respectively. The interaction partners are proteins that are important for the synthesis and the integrity of the cell wall. In previous studies, cell wall synthesis has been shown to impact the mobility of several membrane proteins (Domínguez-Escobar et al., 2011; Garner et al., 2011; Van Teeffelen et al., 2011; Strahl et al., 2014; Hussain et al., 2018). Therefore, the question was raised if cell wall synthesis in general might be involved in flotillin mobility as well.

5.6.1 Inhibition of cell wall synthesis reduces flotillin mobility

The most straightforward procedure to understand if FloA and FloT mobility is dependent on cell wall synthesis, is to inhibit cell wall synthesis with known antibiotics. Several antibiotics that inhibit intermediate steps in cell wall synthesis (Sarkar et al., 2017) were used to monitor flotillin mobility in cell wall synthesis-inhibiting conditions (Figure 36, Table 4). The cell wall is synthesized by polymerization of the precursor lipid II with transglycosylation and transpeptidation reactions. Fosfomycin (FOS,

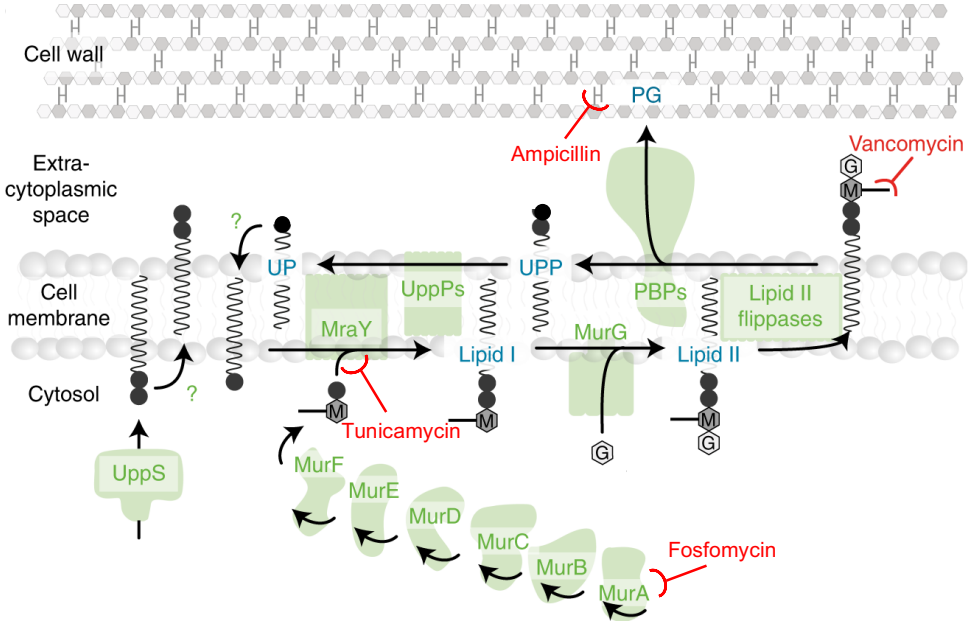

Figure 36: Schematic representation of antibiotic targets during cell wall synthesis. The precursor of the cell wall, lipid II, is synthesized in the cytosol, flipped across the membrane and then incorporated into the existing cell wall with PBPs. The lipid anchor is recycled. Several antibiotics are displayed that inhibit intermediate steps of cell wall synthesis. Adapted from Piepenbreier et al., 2019, published under CC-BY-4.0.

2.5 mg/ml) inhibits MurA, the first enzyme of lipid II synthesis (Silver, 2017). Tunicamycin (TUN, 2.5 µg/ml) inhibits the glycosylation of undecaprenyl phosphate with precursor molecules, the first membrane-bound step. TUN inhibits MraY and TagO with different affinities, involved in lipid II and WTA synthesis, respectively (Campbell et al., 2011). Ampicillin (AMP 1 mg/ml) and vancomycin (VAN 5 µg/ml) both inhibit the transpeptidation reaction of the last incorporation step of lipid II into the existing cell wall. AMP covalently binds to the active site for transpeptidation of PBPs (Kong et al., 2010) and VAN sterically inhibits transpeptidation by binding to the D-Ala-D-Ala of the acceptor pentapeptide (Kahne et al., 2005).

The mobility of FloA- (RW77) or FloT-GFP (RW88) expressed under their native promotor at a neutral locus in the genome was monitored every 300 ms for 9 s after 90 min exposure to cell wall synthesis inhibiting antibiotics. The live-cell imaging movie can be found in the supplemental material of Wagner et al., 2020 (movie 6). Analysis of kymographs, trajectories and MSD showed that the mobility of FloA and FloT was reduced upon inhibition of cell wall synthesis (Figure 37). Kymographs showed tracks without lateral displacements, trajectories were focused on a spot, and diffusion coefficients were reduced (Figure 37a). MSD analysis further exposed less diffusive behavior upon cell wall synthesis inhibition which was most pronounced after VAN treatment (Figure 37b). Possibly, a reduced diffusivity resulted from the general halt of cell wall synthesis complexes in the membrane upon treatment with these antibiotics (Domínguez-Escobar et al., 2011; Garner et al., 2011; Van Teeffelen et al., 2011).

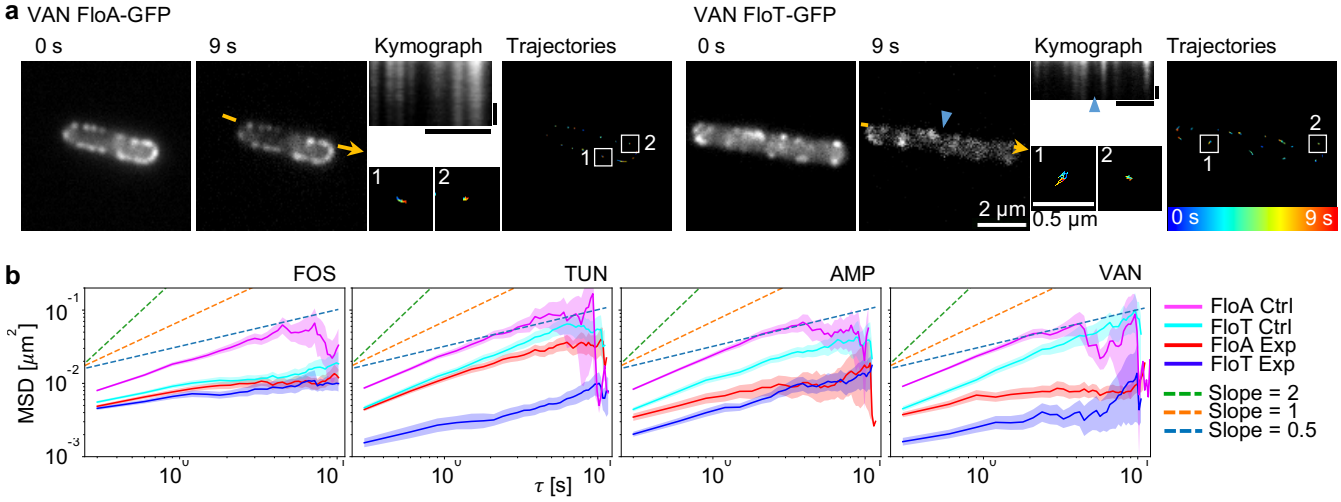

Figure 37: Inhibition of cell wall synthesis reduces flotillin mobility. a) Images showing the mobility analysis of FloA (left) and FloT-GFP (right) after treatment with vancomycin. Images were acquired every 300 ms for 9 s. Shown are the localization patterns at 0 s and 9 s (left), mobility analysis with kymographs (middle) and mobility analysis with trajectories (right). Kymographs are generated using the membrane signal indicated in the 9 s image with a yellow arrow (horizontal scale bar represents 2 µm and vertical scale bar represents 3 s). Blue triangles indicate cell poles of neighboring cells. Representative trajectories are highlighted. Colors indicate elapsing time from blue = 0 s to red = 9 s. b) Plots showing the MSD analysis of FloA- and FloT-GFP after cell wall inhibition with different antibiotics. Plots show the means with shaded areas representing the 95 % confidence interval. N≥297 trajectories. A corresponding movie can be found in the supplemental material of Wagner et al., 2020 (movie 6). Ctrl = untreated control, Exp = experimental condition (specified above each plot), VAN = vancomycin, FOS = Fosfomycin, TUN = tunicamycin, AMP = ampicillin.

Several control experiments were performed to further characterize this observation. First, cell death was excluded as the cause for changes in flotillin mobility upon antibiotic treatment. Plasmolysis occurs upon cell death, visible as the shrinkage of the cells (Korber et al., 1996) (Figure 38a). The cell width was measured after antibiotic exposure and confirmed that overall cells are not dead, although a small

reduction in cell width was visible after AMP treatment in early-exponential growth (Figure 38b, left y-axis). Note that an increase in cell width has been reported to result from inhibition of wall teichoic acid synthesis upon TUN treatment (D'Elia et al., 2006) and has also been reported for FOS treatment in *Listeria monocytogenes* (Harris and Theriot, 2016). The viability of cells exposed to antibiotics was confirmed with CFU counts as well (Figure 38b, right y-axis).

Then the impact of the inhibition by TUN on MraY and TagO was examined. TUN binds MraY with a lower affinity than TagO (Campbell et al., 2011), therefore higher concentrations of TUN are needed, to inhibit cell wall synthesis via MraY. At this concentration (TUN, 2.5 µg/ml), TagO is inhibited as well, but lower concentrations (TunWTA, 0.025 µg/ml) only inhibit TagO, whereas MraY is still functional. Upon TunWTA treatment TagO-dependent WTA synthesis was inhibited and only a minor decrease was visible for FloA and FloT mobility, revealing that only inhibition of MraY, and thus inhibition of cell wall synthesis, results in the mobility decrease after TUN treatment (Figure 38c top). Additionally, it was confirmed that the solvent of TUN, DMSO, did not account for the reduction of flotillin mobility (Figure 38c bottom).

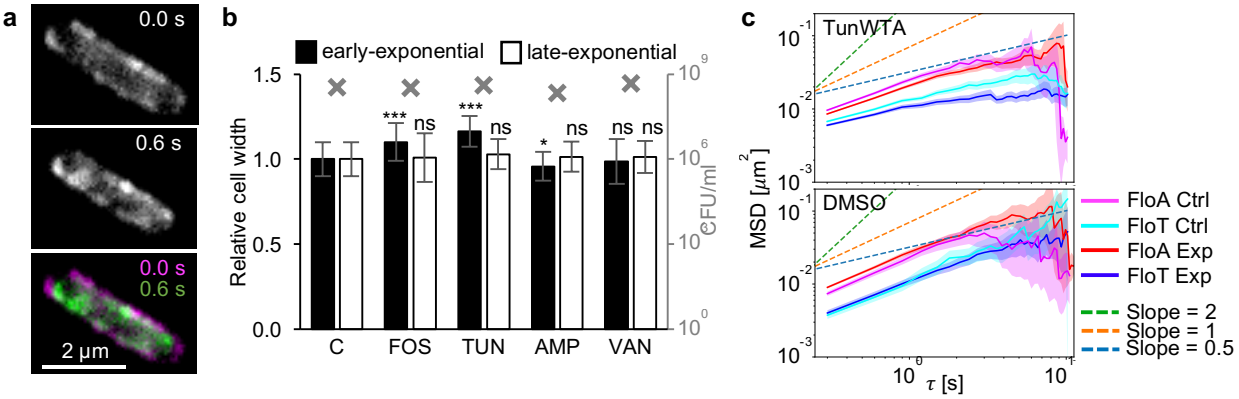

Figure 38: Reduced flotillin mobility upon inhibition of cell wall synthesis is not a result of cell death. a) Epifluorescence microscopy images illustrating cell shrinkage caused by plasmolysis. b) Bar chart showing the relative cell width (left y-axis) and CFU count (right y-axis and grey crosses) after treatment with cell wall synthesis inhibiting antibiotics. Bar chart shows means±SD, N≥28 cells, ns = not significant, * p<0.05, *** p<0.001. c) Plots showing the MSD analysis of FloA- and FloT-GFP after control treatments with low concentrations of TUN (TunWTA) inhibiting WTA synthesis only (top) and the solvent DMSO (bottom). Plots show the means with shaded areas representing the 95 % confidence interval. N≥151 trajectories. Ctrl = untreated control, Exp = experimental condition (specified in the top left corner of each plot).

5.6.2 Membrane differences do not correlate with mobility differences

Next, the question was raised if reduced flotillin mobility upon cell wall synthesis inhibition is a direct or an indirect effect. Inhibition of cell wall synthesis might lead to changes in the membrane which then in turn might impact flotillin mobility. Possible differences in the membrane composition and resilience were examined and correlated with differences in flotillin mobility in several experiments.

Polar lipids and fatty acid composition were analyzed using cells (RW3) treated with AMP and VAN as a positive control for mobility changes and with VAL as a negative control. Cells exposed to these antibiotics were lyophilized and analyzed by the German Collection of Microorganisms and Cell Cultures (DSMZ) in Braunschweig, Germany. Polar lipids and cellular fatty acids were extracted and analyzed. Upon antibiotic treatment the overall polar lipid pattern changed, especially the amount of cardiolipin

was increased (Figure 39a). This increase nevertheless did not correlate with differences in flotillin mobility, as the same increase was seen for AMP, VAN and VAL. Fatty acid composition was visualized as the ratio of C17/C15 and iso/anteiso and the different conditions compared among each other. No differences in cellular fatty acids that corresponds with differences in flotillin mobility could be detected (Figure 39b).

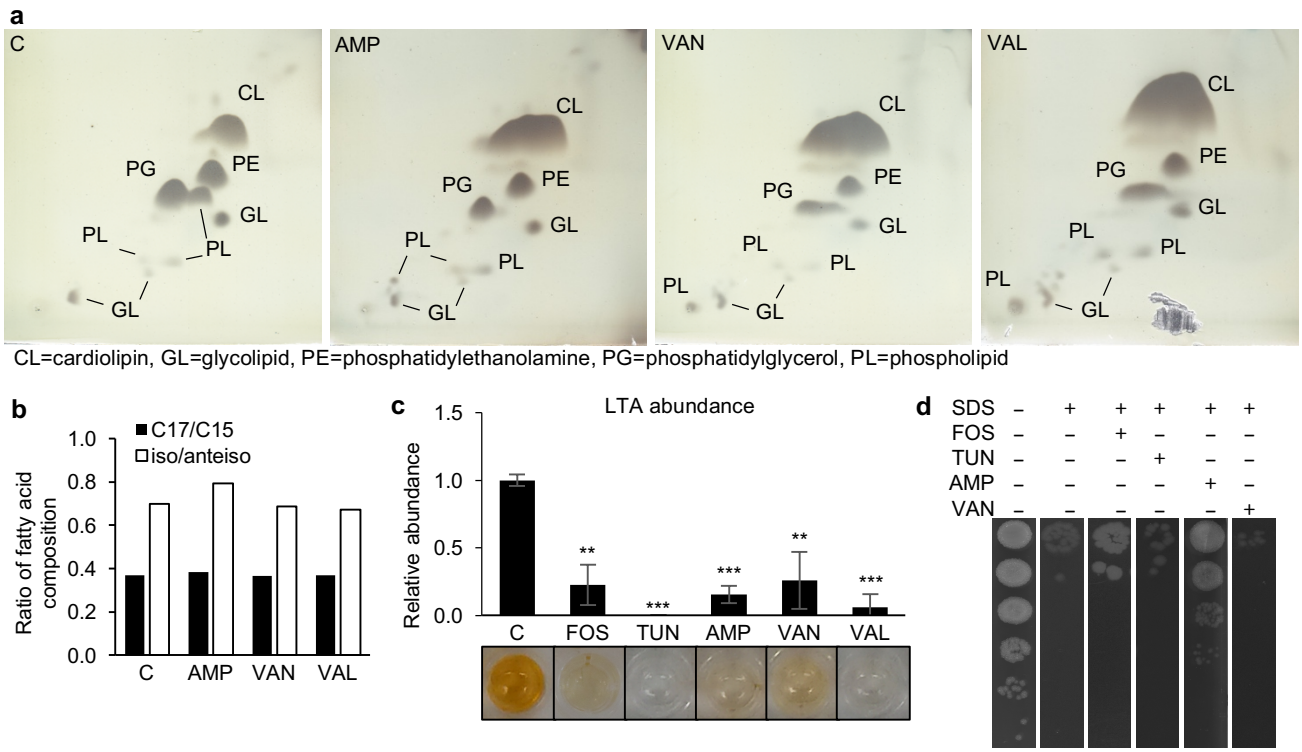

Figure 39: Differences in the membrane do not correlate with differences in flotillin mobility after antibiotic treatments. a) 2D-thin layer chromatography of cellular polar lipids of untreated cells and of cells treated with the antibiotics AMP or VAN that do affect flotillin mobility and with VAL that does not affect flotillin mobility. CL = cardiolipin, GL = glycolipid, PE = phosphatidylethanolamine, PG = phosphatidylglycerol, PL = phospholipid. b) Bar chart showing the ratio of fatty acid composition determined with mass spectrometry of untreated cells and of cells treated with the antibiotics AMP or VAN that do affect flotillin mobility and with VAL that does not affect flotillin mobility. Analysis in a) and b) were performed by the identification service of the German Collection of Microorganisms and Cell Cultures in Braunschweig, Germany. c) Bar chart showing the abundance of LTA of untreated cells and of cells treated with the antibiotics FOS, TUN, AMP or VAN that do affect flotillin mobility and with VAL that does not affect flotillin mobility. Bar chart shows means±SD, N=3, ** p<0.01, *** p<0.001. Images underneath show the corresponding color reaction in ELISA. d) Graphic showing the dilution series of WT strains with or without pre-treatment with the antibiotics FOS, TUN, AMP or VAN and subsequent exposure to the detergent SDS. C = untreated control, AMP = ampicillin, VAN = vancomycin, VAL = valinomycin, FOS = fosfomycin, TUN = tunicamycin.

Furthermore, possible differences in the abundance of LTA upon cell wall synthesis inhibition was analyzed and correlated to differences in flotillin mobility. LTA were isolated from WT cells (RW3) treated with FOS, TUN, AMP, VAN, reducing flotillin mobility, and VAL, not reducing flotillin mobility. Quantification of LTA was done by ELISA with a LTA-specific antibody and a HRP-mediated colorimetric reaction and showed that the levels of LTA were reduced after all antibiotic treatments (Figure 39c). Therefore, the reduction in the amount of LTA does not correlate with the decreased flotillin mobility.

Additionally, the resilience of the membrane was tested which might have changed after antibiotic treatment and thus might have affected flotillin mobility. Differences in detergent resistance after pre-treatment with the antibiotics FOS, TUN, AMP and VAN were monitored. Resistance to SDS was visible for AMP, whereas the other antibiotics did not trigger any resistant behavior (Figure 39d). This excludes

that membrane differences, that might account for resistance to detergents, causes the mobility of flotillins to decrease after cell wall synthesis inhibition.

Membrane differences that result from cellular responses to inhibition of cell wall synthesis do not correlate with differences in flotillin mobility. Flotillin mobility seems to directly depend on cell wall synthesis.

5.6.3 Re-evaluation of previous results

The effect of the cell wall precursor lipid II on flotillin mobility was examined. The resulting levels of lipid II should differ after inhibition of cell wall synthesis at different intermediate steps. Upon FOS and TUN treatment, the levels of lipid II should rapidly cease as no new lipid II is synthesized, AMP treatment should keep a constant level of lipid II. Even though most of its consumers – the PBPs harboring TP activity – are inhibited, PBPs with TG activity can still proceed lipid II consumption. VAN treatment should lead to an accumulation of lipid II as its TG and TP reactions are sterically prevented (Kohlrausch and Höltje, 1991; Lara et al., 2005; Piepenbreier et al., 2019). This means, as the cellular lipid II levels vary after inhibition of cell wall synthesis, they cannot account for the reduction in flotillin mobility. Instead, inhibition of cell wall synthesis decreases flotillin mobility independently of the availability of lipid II but due to an arrest in the activity of the cell wall synthesis machinery itself. Then NIS treatment should also temporarily decrease flotillin mobility (Figure 15) as it binds lipid II to form membrane pores. Therefore, in the early phase of NIS treatment, lipid II is sequestered and is not available for cell wall synthesis which should lead to a temporary arrest in the activity of the cell wall synthesis machinery. Flotillin mobility is expected to decrease upon NIS treatment at early time points before cellular lipid II levels are re-established. The mobility of FloA- and FloT-GFP was monitored after 10 min, 30 min and 90 min of treatment with NIS, FOS, TUN, AMP and VAN. An initial decrease in flotillin mobility was detected after NIS treatment which was then reverted to WT mobility (Figure 40). Flotillin mobility after treatments with the other antibiotics gradually decreased over time.

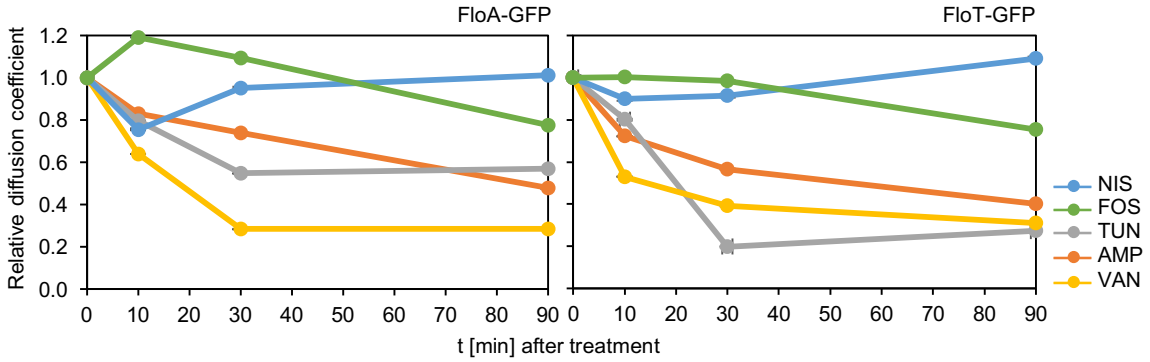

Figure 40: Nisin reduces flotillin mobility at early time points. Graphics showing the relative diffusion coefficients of FloA- (left) or FloT-GFP (right) at 0 min, 10 min, 30 min and 90 min after treatments with antibiotics. Points show means±sem. NIS = nisin, FOS = fosfomycin, TUN = tunicamycin, AMP = ampicillin, VAN = vancomycin, N≥73 trajectories.

Inhibition of cell wall synthesis reduces the mobility of FloA and FloT. This might also explain the reduced mobility of FloA and FloT upon entry into stationary phase (Figure 16). It results from decelerated cell

growth which is accompanied by a reduction in cell wall synthesis and might decrease flotillin mobility in a similar manner as cell wall synthesis inhibiting antibiotics.

5.7 MreB and flotillins are spatially separated from each other

Cell wall synthesis at the periphery of the cell is mediated by the Rod-complex. The movement of several proteins of the Rod-complex has been shown to cease upon exposure to vancomycin (Domínguez-Escobar et al., 2011; Garner et al., 2011). One of these proteins is MreB, the actin-homolog cytoskeleton in bacteria. MreB is known to orient the Rod-complex of cell wall synthesis perpendicular to the length axis of the cell (Hussain et al., 2018; Wong et al., 2019). Cell wall precursor incorporation fuels the movement of the whole Rod-complex, including MreB (Domínguez-Escobar et al., 2011; Garner et al., 2011; Van Teeffelen et al., 2011). It is thus obvious to assume that flotillins might form a structural part of the cell wall synthesis machinery. Especially as MreC, a MreB operon and interaction partner, was detected in the global pull-down analysis.

First, the mobility of MreB was analyzed to understand if it is comparable to flotillin mobility. A strain expressing GFP-MreB from a xylose-inducible promotor at the neutral *amyE* locus (RW38, 0.01 % xylose) was used to monitor MreB localization. MreB localized in filaments at the inner side of the membrane oriented perpendicular to the length axis of the cell. Differences were visible in images acquired with epifluorescence and TIRFM (Figure 41a). A helical pattern was visible in epifluorescence microscopy and a punctate or strand pattern was visible in TIRFM. TIRFM is generally used to monitor the mobility of MreB. Images were acquired every 1 s for 100 s. The live-cell imaging movie can be found in the supplemental material of Wagner et al., 2020 (movie 8). Images at 20 s intervals showed differences in localization pattern indicative of a mobile behavior of MreB (Figure 41b). Image sequences were analyzed with kymographs, trajectories and MSD analysis. Additionally, maximum intensity projections (MIP) were generated. MIP are images that summarize the signal intensities of an image

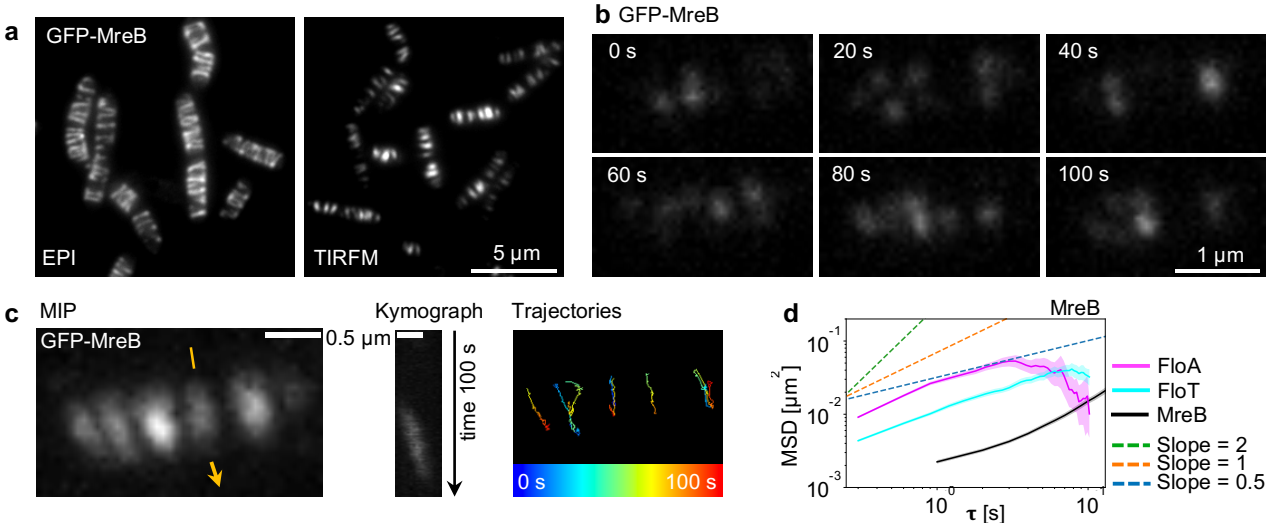

Figure 41: MreB movement orients perpendicular to the cell axis and is slower than flotillin mobility. a) Images showing a field of GFP-MreB labeled cells acquired by epifluorescence microscopy (EPI, left) or TIRFM (right). b) TIRFM images showing the localization of GFP-MreB in intervals of 20 s. c) Images showing the mobility analysis of GFP-MreB monitored every 1 s for 100 s. Shown are the maximum intensity projection (MIP) (left), mobility analysis with kymographs (middle) and mobility analysis with trajectories (right). Kymographs are generated using the membrane signal indicated in the MIP image with a yellow arrow. Colors in trajectories indicate elapsing time from blue = 0 s to red = 100 s. d) Plot showing the MSD analysis of GFP-MreB in comparison to FloA- and FloT-GFP. Plot shows the means with shaded areas representing the 95 % confidence interval. N≥850. A corresponding movie can be found in the supplementary material of Wagner et al., 2020 (movie 8).

sequence into a single image. MIP of MreB showed signal strands that oriented perpendicular to the axis of the cell (Figure 41c, left). They were separated from each other and did not overlap. Kymographs of the signal perpendicular to the cell axis showed a diagonal track indicative of directed movement (Figure 41c, middle). Similarly, the trajectories verified the previous observations as they were oriented perpendicular to the axis of the cell (Figure 41c, right), as MIP showed. Their orientation showed a directed movement from one lateral side of the cell to the other, as kymographs revealed. MSD comparison with flotillins show that the mobility of MreB is comparably slow (Figure 41d), whereas flotillins diffuse more randomly and faster. Because of these differences in mobility, it seems unlikely that flotillins are part of the Rod-complex of cell wall synthesis.

Nevertheless, the localization pattern of flotillins and MreB was analyzed in double-labeled strains expressing GFP-MreB under the xylose-inducible promotor at the neutral *amyE* locus (0.01 % xylose) and FloA- (RW422) or FloT-mCherry (RW423) under the native promotor from a replicative pRW plasmid. Image acquisition with epifluorescence showed the typical localization patterns for flotillins and MreB. FloA or FloT and MreB localization excluded each other (Figure 42a). To get a better look on a bigger membrane area TIRFM was used for image acquisition which resulted in the same pattern, flotillins and MreB localizing side by side (Figure 42b).

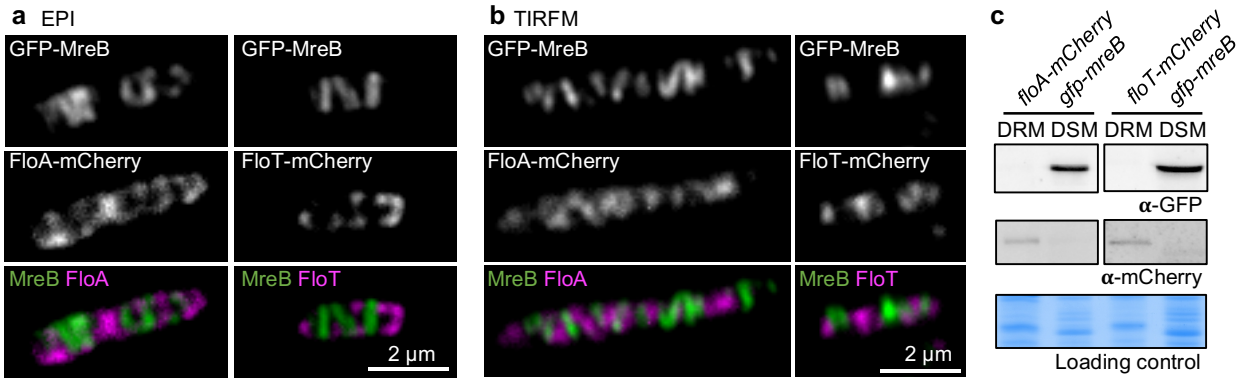

Figure 42: MreB and flotillin localization exclude each other. a) Epifluorescence microscopy (EPI) images showing the colocalization of GFP-MreB and FloA- (left) or FloT-mCherry (right) double-labeled cells. b) TIRFM images showing the colocalization of GFP-MreB and FloA- (left) or FloT-mCherry (right) double-labeled cells. c) Western blots of DRM/DSM separation of GFP-MreB and FloA- (left) or FloT-mCherry (right) double-labeled strains. A Coomassie stained gel is used as a loading control.

It was proposed previously that MreB creates membrane regions of increased fluidity (RIF) (Strahl et al., 2014). These are possibly enriched in the cell wall synthesis precursor lipid II (Ganchev et al., 2006; Schirner et al., 2015). RIF contrast FMM which are domains that are packed densely and thus provide reduced fluidity. Consequently, the question was raised if by separating the membrane in DRM and DSM fractions, flotillins would localize in the DRM and MreB in the DSM fraction, matching their respective membrane environment. DRM/DSM separation were performed with the membrane of the GFP-MreB and FloA- (RW422) or FloT-mCherry (RW423) double-labeled strains. As expected, FloA and FloT were detected to preferentially localize in the DRM fraction and MreB in the DSM fraction (Figure 42c). As already seen in the colocalization studies, flotillins and MreB localize in spatially distinct areas of the membrane. Therefore, flotillins do not form part of the MreB-containing Rod-complex of cell wall synthesis.

Then, it was hypothesized if instead, MreB might be responsible for the spatial restrictions in lateral displacements that was observe for flotillin mobility (Figure 13). This has been shown to apply for several membrane proteins in *E. coli*, whose diffusion is restricted by the MreB cytoskeleton (Oswald et al., 2016). Considering MreB as a restriction barrier for flotillin mobility, the global projection of the trajectories of FloA (RW396) and FloT (RW392) monitored with TIRFM was re-examined more thoroughly (Figure 12). Several areas per cell were observed that did not show any trajectories during the 20 s of image acquisition (Figure 43a). To confirm that these areas are devoid of flotillins, MIP was created which directly uses the signal of the image compared to the indirectly created trajectories. MIP also revealed membrane areas that did not show FloA or FloT signal (Figure 43b). The assumption arises whether this absence of flotillins is accompanied by the presence of MreB in these areas.

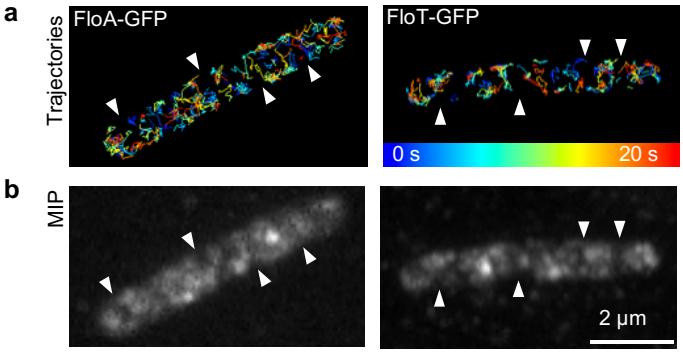

Figure 43: Flotillin membrane coverage reveals empty spaces. a) Images showing trajectories of FloA- (left) and FloT-GFP (right) acquired every 200 ms over 20 s with TIRFM (Figure 12). White triangles point to membrane areas that were not covered by flotillin within these 20 s. Colors indicate elapsing time from blue = 0 s to red = 9 s. b) MIP of these cells likewise reveal empty spaces.

TIRFM with simultaneous image acquisition of the green and red channels can be used to monitor the signals of fluorescently labeled MreB and FloA or FloT simultaneously. This microscopy setup implies that exposure times and frame rates of both channels are the same. Adversely, neither the mobility of flotillins and MreB nor the stability of the fluorescence signal of the green and red fluorophores are comparable. Simultaneous visualization of the mobility of flotillins and MreB was technically impossible. Thus, the mobility of MreB was monitored at longer frame intervals (2 s) and the respective localization of flotillins determined for every time point. In this way, a longer overall time interval was monitored (14 s) at several intermediate time points. Double-labeled strains were used that express mRFPruby-MreB from a xylose-inducible promotor at the neutral *amyE* locus in the genome (0.5 % xylose), and FloA- (RW552) or FloT-GFP (RW553) from the native promotor at the neutral *lacA* locus in the genome. mRFPruby has been reported to show minor advantages in signal intensity and stability compared to mCherry (Domínguez-Escobar et al., 2011). The mobility was monitored every 2 s for 14 s (resulting in 8 consecutive images) using 500 ms exposure times. For every time point, the colocalization of flotillin and MreB was visualized which generally did not demonstrate any overlap (Figure 44a, c). Additionally, kymographs were generated along the long axis of the cell to observe the time course of the localization. Colocalization kymographs generally did not show any signal overlap of flotillins and MreB. Due to the relatively long frame interval, only current positions could be observed for flotillin, but these could not be linked to tracks as information on the localization in between two consecutive images were missing. The signal of MreB was visible as straight tracks without any lateral displacement, as MreB moves perpendicular to the long axis of the cell and the kymographs did not capture the mobility in this direction. The normal behavior of MreB mobility was still confirmed with MIP, trajectories, and kymographs

perpendicular to the long axis of the cell (Figure 44b, d). Overall, the signals of flotillins and MreB did not colocalize but were excluding each other. These and previous results hint towards a spatial restriction of flotillin mobility by the MreB actin-homolog cytoskeleton.

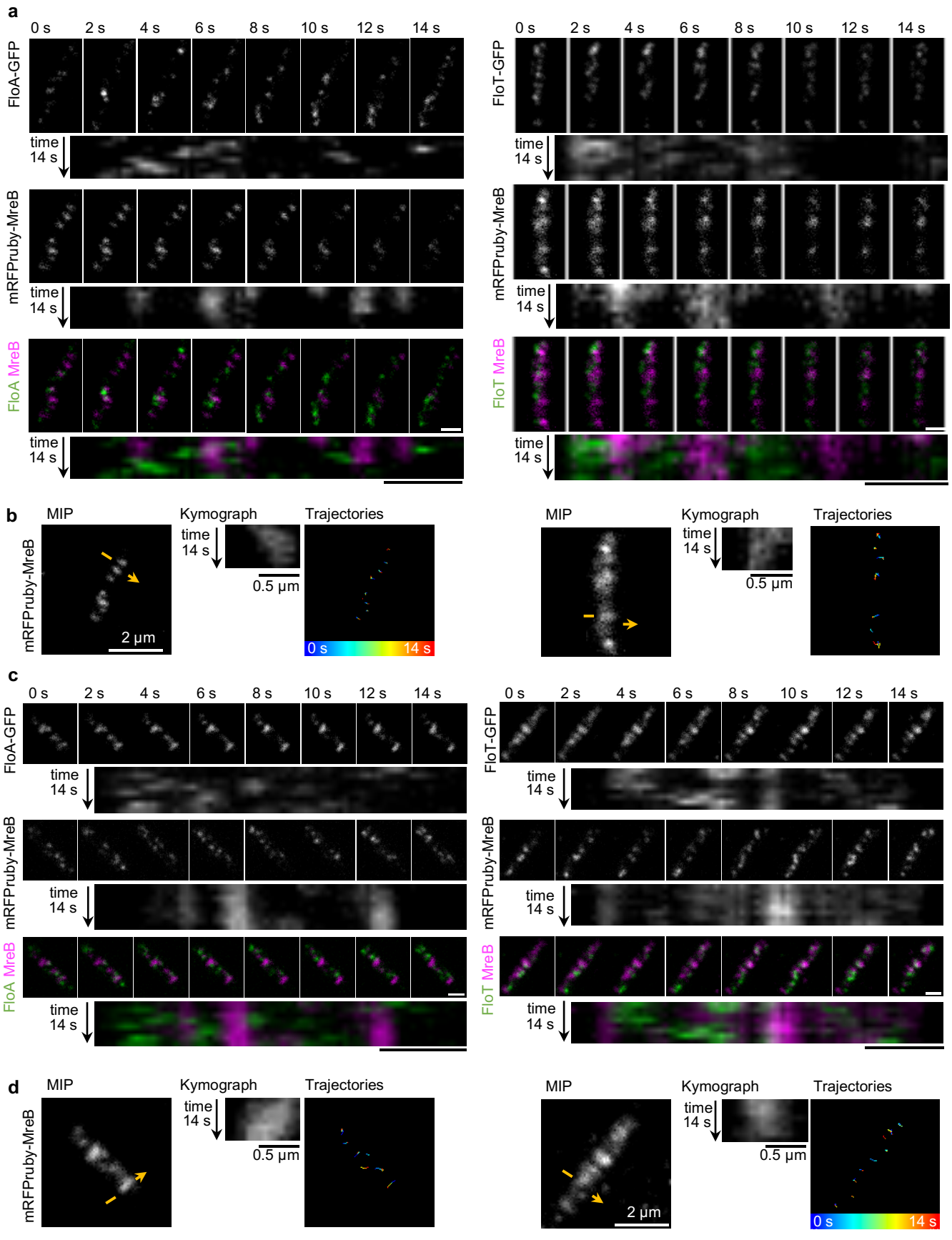

Figure 44: MreB and flotillins are spatially separated. a) Images of mRFPruby-MreB and FloA- (left) or FloT-GFP (right) double-labeled strains acquired by simultaneous TIRF microscopy in the red and green channels. Images were acquired every 2 s for 14 s. The individual frames of flotillins (top), MreB (middle) and their overlay (bottom) are shown with the corresponding kymographs generated with the signal along the longitudinal axis of the membrane. Scale bars represent 1 µm. b) Images show the mobility analysis of mRFPruby-MreB from microscope images of a) in double-labeled strains with FloA- (left) or FloT-GFP (right). Shown are the maximum intensity projection (MIP) (left), mobility analysis with kymographs (middle) and mobility analysis with trajectories (right). Kymographs are generated using the membrane signal indicated in the MIP image with a yellow arrow. Colors in trajectories indicate elapsing time from blue = 0 s to red = 14 s. c) and d) show an additional example of a) and b), respectively.

5.8 The actin-homolog cytoskeleton spatially restricts flotillin mobility

Correct localization of the MreB actin-homolog cytoskeleton requires an intact membrane potential (Strahl and Hamoen, 2010) which is maintained through the availability of nutrients and oxygen. Therefore, a depletion of those on the agarose slide results in the mislocalization and disruption of MreB, visible as the formation of big accumulations of the protein at the cell periphery. Strains expressing GFP-MreB (RW38) or its homologs GFP-MreBH (RW39) and -Mbl (RW40) under a xylose-inducible promotor at the neutral *amyE* locus in the genome were used to monitor their localization patterns (0.5 % xylose). Upon the creation of cytoskeleton-disrupting conditions, the depletion of LB and O_2, all three paralogs mislocalized (Figure 45a).

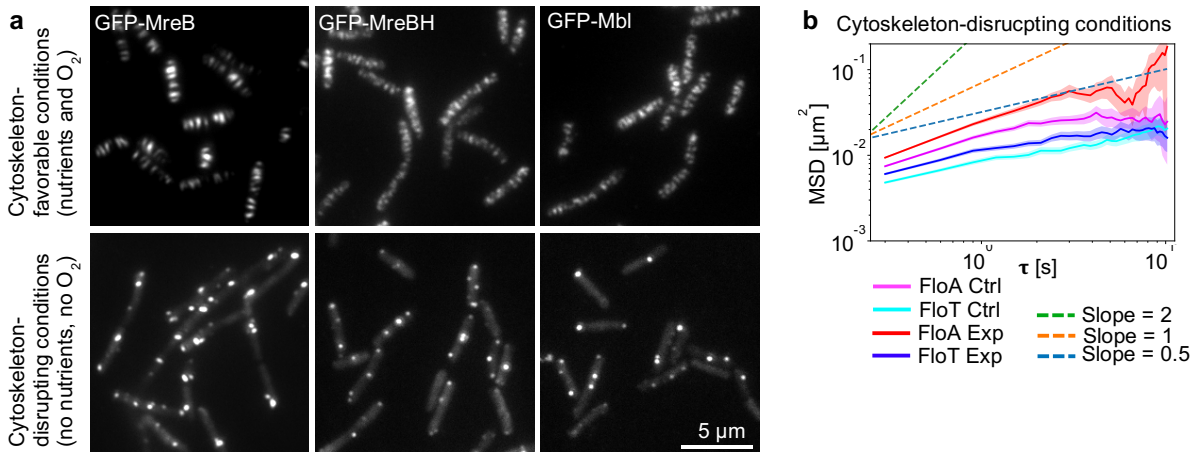

Figure 45: Flotillin mobility increases upon disruption of MreB and its homologs. a) TIRFM images of GFP-MreB (left), -MreBH (middle) and -Mbl (right) in cytoskeleton-favorable (top) and -disrupting conditions (bottom). b) Plot showing the MSD analysis of FloA- and FloT-GFP in cytoskeleton-favorable (Ctrl) and -disrupting (Exp) conditions. Plot shows the means with shaded areas representing the 95 % confidence interval. N≥1785 trajectories.

The same conditions were used to monitor FloA and FloT mobility when the actin-homolog cytoskeleton was disrupted. FloA- (RW77) or FloT-GFP (RW88) labeled strains were used and their mobility monitored upon depletion of LB and O_2. Kymographs, trajectories and MSD were analyzed of image sequences acquired every 300 ms for 9 s (Figure 45b). Upon the mislocalization of MreB and its homologs, the diffusion coefficients of FloA and FloT were increased. This provides a further hint that the cytoskeleton might spatially restrict the mobility of FloA and FloT. Nevertheless, other cellular structures are also affected by the absence of the membrane potential and these might also participate in the increase in flotillin mobility. The effect of the mislocalization of MreB and its homologs needs to be distinguished from a possible effect of other cellular structures.

The actin-homolog cytoskeleton is essential under normal growth conditions. To construct a deletion mutant that lacks all three homologs, MreB, MreBH and Mbl, an additional deletion of RsgI, the anti-sigma factor for SigI, and a supplementation of the medium with 20 mM $MgSO_4$ are necessary to maintain growth. SigI activity maintains cell envelope integrity and has an impact on cell morphology during heat stress (Schirner and Errington, 2009; Ramaniuk et al., 2018), thus contributing to overall cellular integrity. A strain containing these four deletion mutations from the laboratory of Jeff Errington was used (strain #4277 Δ*mreB* Δ*mreBH* Δ*mbl* Δ*rsgI*) (Schirner and Errington, 2009). It grows spherical and slower than the WT (Figure 46a, b). The absence of MreB and its homologs was shown to elevate membrane fluidity in a similar manner to BNZ (Strahl et al., 2014). However, previous experiments in this work (Figure 15) already excluded membrane fluidity from influencing flotillin mobility. Therefore firstly, labeled strains expressing FloA- or FloT-GFP at the ectopic locus in the genome were used and *rsgI* was deleted, creating strains RW610 and RW606, respectively. The mobility of flotillins in these strains was indistinguishable from the WT (Figure 46c), so that possible differences can be attributed to the absence of the actin-cytoskeleton alone.

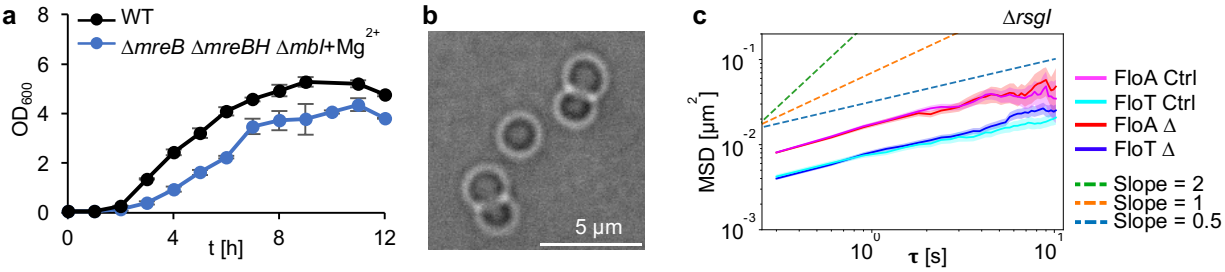

Figure 46: A triple mutant of MreB and its homologs reveals growth defects. a) Growth curves of WT and Δ*mreB* Δ*mreBH* Δ*mbl* strain backgrounds. The Δ*mreB* Δ*mreBH* Δ*mbl* mutant can only grow with an additional mutation in Δ*rsgI* and the addition of $MgSO_4$. b) Brightfield image of this Δ*mreB* Δ*mreBH* Δ*mbl* mutant. c) Plot showing the MSD analysis of FloA- and FloT-GFP in WT (Ctrl) and Δ*rsgI* strain backgrounds. Plot shows the means with shaded areas representing the 95 % confidence interval. N≥1196 trajectories.

Then the actin-homolog cytoskeleton deletions were consecutively added to these strains. The resulting strains were spherical and growth depended on the addition of $MgSO_4$. The FloA- (RW616) or FloT-GFP (RW617) labeled strains showed reduced signal intensity. Epifluorescence microscopy was used to monitor them every 300 ms for 9 s (Figure 47a) and to analyze flotillin mobility with kymographs,

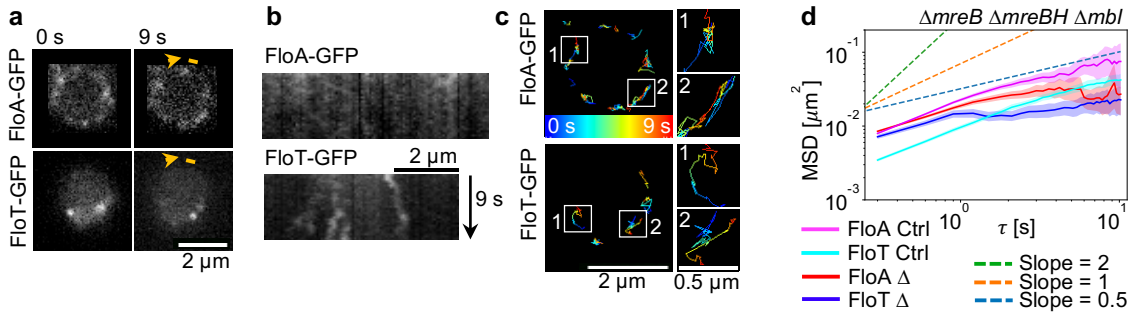

Figure 47: The triple mutant of MreB and its homologs releases FloT from restrictions. a) Images showing the localization pattern at of FloA- (top) and FloT-GFP (bottom) in the Δ*mreB* Δ*mreBH* Δ*mbl* strain background at 0 s and 9 s. b) Images showing the mobility analysis with kymographs of FloA- (top) and FloT-GFP (bottom) in the Δ*mreB* Δ*mreBH* Δ*mbl* strain background. Kymographs are generated using the membrane signal indicated in the 9 s image with a yellow arrow. c) Images showing the mobility analysis with trajectories of FloA- (top) and FloT-GFP (bottom) in the Δ*mreB* Δ*mreBH* Δ*mbl* strain background. Representative trajectories are highlighted. Colors indicate elapsing time from blue = 0 s to red = 9 s. d) Plot showing the MSD analysis of FloA- and FloT-GFP in the Δ*mreB* Δ*mreBH* Δ*mbl* strain background. Plot shows the means with shaded areas representing the 95 % confidence interval. N≥666 trajectories. A corresponding movie can be found in the supplemental material of Wagner et al., 2020 (movie6). Ctrl = Δ*rsgI* strain background control.

trajectories and MSD analysis. The live-cell imaging movie can be found in the supplemental material of Wagner et al., 2020 (movie 6). In kymographs, increased lateral displacements were visible for FloA, but trajectories and MSD analysis did not reveal any differences in FloA mobility (Figure 47b-c top). Analysis of FloT revealed increased mobility visible in lateral displacements of kymographs, the membrane area occupied by trajectories and the diffusion coefficient of MSD (Figure 47b-c bottom). The diffusion coefficient of FloT was approaching that of FloA in the Δ*mreB* Δ*mreBH* Δ*mbl* strain background (Figure 47d). The actin-homolog cytoskeleton restricts the mobility of flotillins, for FloA to a lesser extent than for FloT.

The restriction of the mobility of FloT by the actin-homolog cytoskeleton might explain the increased mobility after VAL treatment (Figure 15). VAL abolished the membrane potential which in turn mislocalizes MreB and its homologs, leading to a reduced restriction and an increase in FloT mobility.

5.9 Removal of the cell wall increases flotillin mobility to the same level

It was demonstrated that MreB and its homologs restrict the mobility of FloT. However, despite the reduced restriction, some level of restriction still persists which is visible from kymograph and trajectory analysis. Moreover, cell wall organization was previously demonstrated to also affects the mobility of flotillins, unspecifically by general cell wall synthesis and specifically by protein interaction partners. The cell wall thus represents an additional structure impacting flotillin mobility. It has been shown in eukaryotic plant cells that the cytoskeleton and the cell wall restrict flotillin mobility (Daněk et al., 2019). To further understand this interplay in *B. subtilis*, the whole cell wall was removed by lysozyme digestion in the presence of osmotically stabilizing medium, rendering protoplasts. As due to the loss of the cell wall, rods turn into spheres, the orientation of MreB along the highest membrane curvature loses its specification and is oriented randomly (Hussain et al., 2018). Furthermore, MreB mobility is driven by cell wall synthesis which has now ceased to exist (Domínguez-Escobar et al., 2011; Garner et al., 2011; Van Teeffelen et al., 2011).

The question was raised if the mobility of MreB changed in protoplasts. The mobility of GFP-MreB expressed under a xylose-inducible promotor at the neutral *amyE* locus in the genome (RW38, 0.01 % xylose) was monitored in protoplasts with TIRFM every 300 ms for 60 s (Figure 48a). The live-cell imaging movie can be found in the supplemental material of Wagner et al., 2020 (movie 8). Analysis of MreB mobility with kymographs, MIP, trajectories, and MSD was performed and revealed that MreB mobility was increased in protoplasts. MIP showed the whole cell to be covered by MreB (Figure 48b) and trajectories revealed that MreB did not move directed but randomly (Figure 48c). This was also supported by kymograph analysis (Figure 48d). MSD analysis verified an increased diffusion coefficient of MreB in protoplasts (Figure 48e).

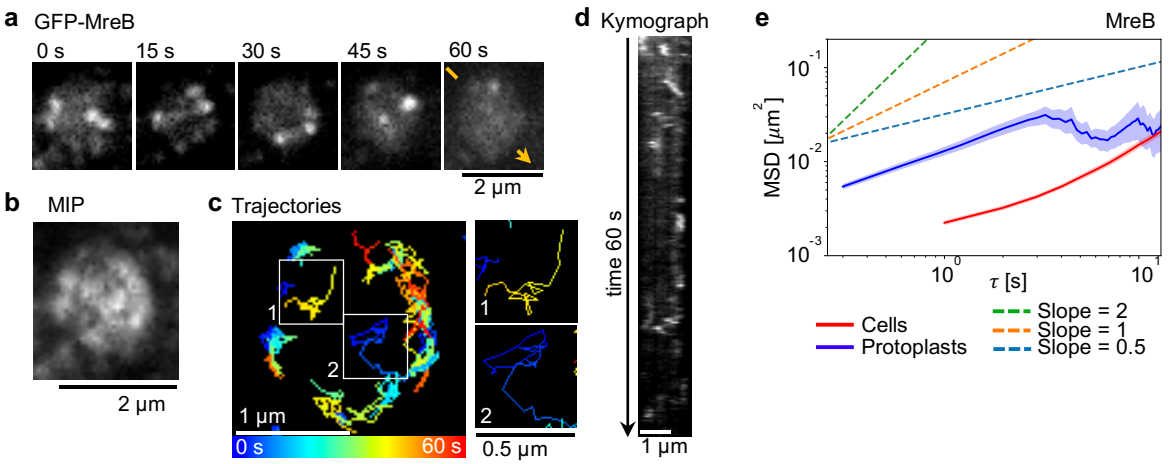

Figure 48: MreB mobility is increased in protoplasts. a) TIRFM images showing the localization of GFP-MreB in protoplasts in intervals of 15 s. b) Image shows the MIP of GFP-MreB in protoplasts. c) Images showing the mobility analysis with trajectories of GFP-MreB in protoplasts. Representative trajectories are highlighted. Colors indicate elapsing time from blue = 0 s to red = 60 s. d) Image showing the mobility analysis with kymographs of GFP-MreB in protoplasts. Kymographs are generated using the membrane signal indicated in the 60 s image with a yellow arrow. e) Plot showing the MSD analysis of GFP-MreB in the cells and protoplasts. Plot shows the means with shaded areas representing the 95 % confidence interval. N≥496 trajectories. A corresponding movie can be found in the supplemental material of Wagner et al., 2020 (movie 8).

Therefore, as the mobility of MreB is increased in protoplasts, most likely, its restrictive behavior towards FloT should be reduced as well. If the cell wall restricts flotillin mobility, an increase in flotillin mobility in protoplasts would be expected, exceeding that of the absence of MreB confinement alone. Further, the mobility restrictions that are still detectable in the absence of MreB and its homologs should be reduced. If in contrast, the mobility will not exceed that of the absence of MreB, the cell wall would not be restricting flotillin mobility and concurrently MreB is still restrictive in protoplasts. Thus, the mobility of FloA- (RW77) and FloT-GFP (RW88) labeled strains was monitored in protoplasts with epifluorescence microscopy every 300 ms for 9 s (Figure 49a) and flotillin mobility analyzed with kymographs, trajectories and MSD analysis. The live-cell imaging movie can be found in the supplemental material of Wagner et al., 2020 (movie 6). Kymographs showed increased lateral displacements that was only occasionally restricted for both FloA and FloT (Figure 49b). Trajectories covered large membrane areas (Figure 49c) and MSD analysis showed that the diffusion coefficients of FloA and FloT were increased and reached the same

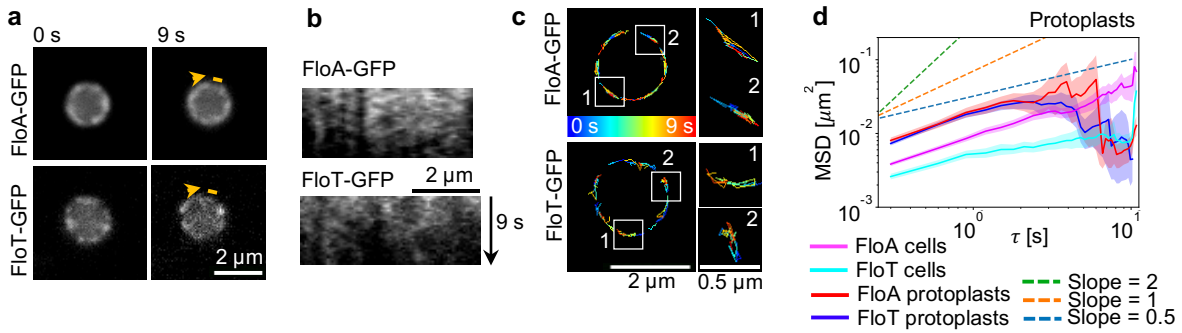

Figure 49: Protoplasts release FloA and FloT from spatial restrictions. a) Images showing the localization pattern at of FloA- (top) and FloT-GFP (bottom) in protoplasts at 0 s and 9 s. b) Images showing the mobility analysis with kymographs of FloA- (top) and FloT-GFP (bottom) in protoplasts. Kymographs are generated using the membrane signal indicated in the 9 s image with a yellow arrow. c) Images showing the mobility analysis with trajectories of FloA- (top) and FloT-GFP (bottom) in protoplasts. Representative trajectories are highlighted. Colors indicate elapsing time from blue = 0 s to red = 9 s. d) Plot showing the MSD analysis of FloA- and FloT-GFP in the cells and protoplasts. Plot shows the means with shaded areas representing the 95 % confidence interval. N≥236 trajectories. A corresponding movie can be found in the supplemental material of Wagner et al., 2020 (movie 6).

level (Figure 49d). Properties that were responsible for the differences in mobility of FloA and FloT in cells (interaction partners, assembly size, or others that are still unknown) ceased to influence flotillin mobility in protoplasts. Nevertheless, additional effects that the absence of the cell wall might have on other cellular structures influencing flotillin mobility, cannot be excluded. It is not possible to distinguish the effect of the cell wall from the effect of the reduced MreB restriction on FloT mobility. Concludingly, upon removal of the cell wall, the exo-cytoskeleton, FloA and FloT show an increased mobility.

5.10 PBP3 and DltD mobility likewise depends on the cell wall

FloA and FloT mobility depend on the cell wall and on their protein interaction partners PBP3 and DltD, respectively. The question was raised if the mobility of PBP3 and DltD also depends on the cell wall.

First, cells labeled with GFP-PBP3 (RW445) or -DltD (RW498) were treated with FOS, TUN, AMP and VAN and their mobility monitored. MSD analysis showed that inhibition of cell wall synthesis decreased the mobility of PBP3 and DltD (Figure 50), similar to what was observed for flotillins.

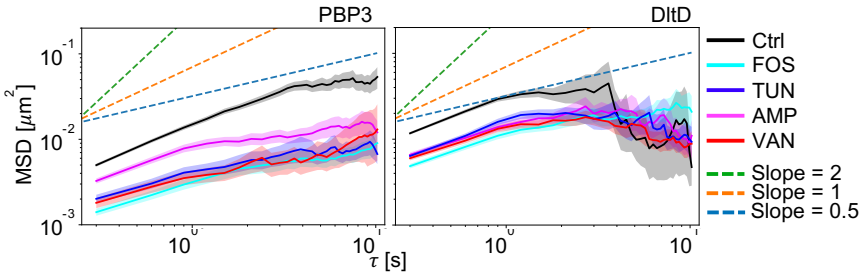

Figure 50: The mobility of PBP3 and DltD is reduced upon cell wall synthesis inhibition. Plots showing the MSD analysis of GFP-PBP3 (left) and -DltD (right) after cell wall inhibition with different antibiotics. Plots show the means with shaded areas representing the 95 % confidence interval. Ctrl = untreated control, AMP = ampicillin, VAN = vancomycin, VAL = valinomycin, FOS = fosfomycin, TUN = tunicamycin, N≥538 trajectories.

Next, the cell wall in cells labeled with GFP-PBP3 (RW445) or -DltD (RW498) was removed and their mobility in protoplasts monitored. MSD analysis showed an increase in the mobility of PBP3 and DltD in protoplasts compared to intact cells (Figure 51), similar to what was shown for FloA, FloT and MreB.

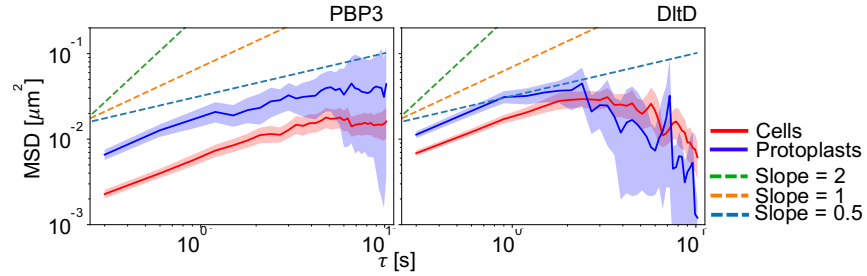

Figure 51: The mobility of PBP3 and DltD is increased in protoplasts. Plots showing the MSD analysis of GFP-PBP3 (left) and -DltD (right) in cells and protoplasts. Plots show the means with shaded areas representing the 95 % confidence interval. N≥284 trajectories.

6 DISCUSSION

Functional membrane microdomains describe dynamic compartments of the bacterial cell membrane that organize several cellular processes in space and time with the help of their scaffolding proteins FloA and FloT. It was shown here that FloA and FloT assemblies are mobile and diffuse in the membrane at distinct mobility patterns. The FloA diffusion coefficient revealed faster movement compared to FloT which additionally showed more restrictions obstructing free diffusion. The mobility of FloA and FloT depends on several factors. Firstly, the C-terminus determines the characteristic mobility patterns of FloA and FloT. It is responsible for the oligomerization and the interaction partners. FloA oligomers are smaller than FloT oligomers. Secondly, the interaction of FloA and FloT with different protein partners influence their mobility, as has been demonstrated for PBP3 and DltD, respectively. And thirdly, the intracellular MreB cytoskeleton and the extracellular cell wall play a role in spatially restricting flotillin mobility. This confinement is possibly mediated by the size of the oligomers and the protein interaction partners, respectively.

6.1 FloA and FloT are two distinct flotillins

FloA mobility was monitored at early-exponential growth and FloT mobility was monitored at late-exponential growth. These differences are based on the different genetic programs that control the expression of *floA* and *floT*. *floA* is constitutively expressed throughout cell growth, whereas *floT* expression is increased upon entry into stationary phase (Donovan and Bramkamp, 2009; Dempwolff et al., 2012; Schneider et al., 2015a). These different expression patterns are naturally accompanied by different cellular functions that are grasped by the protein cargo. The pull-down analysis showed that FloA interaction partners are involved in processes of active growth and environment surveillance, while FloT interaction partners are involved in adaptation to starvation stresses as indicated by transporters or proteins of the energy metabolism. Along with these differences, both flotillins interacted with proteins involved in cell wall synthesis which has been shown impact flotillin mobility. This might serve as an explanation for the reduction of FloA and FloT mobility upon entry into stationary phase. At that time, growth stops and cell wall synthesis is reduced, also slowing down flotillin mobility (see chapter 6.4). Additionally, in the course of the cellular growth FloA mobility is always faster than FloT mobility. This lower diffusion coefficient of FloT might be due to the larger size of the oligomers and assemblies which impacts diffusion (Stokes-Einstein equation (Einstein, 1905), and specified in Saffman-Delbrück model (Saffman and Delbrück, 1975)). And the size differences possibly also account for the restrictive effect of the MreB-cytoskeleton solely on FloT mobility (see chapter 6.5). Furthermore, intrinsic properties that might be responsible for a reduced mobility of FloT compared to FloA depend on their C-terminus which determines binding of different interaction partners.

6.2 Flotillins interact transiently with their protein interaction partners

The interaction of flotillins with the cell wall-associated proteins PBP3 and DltD that were detected using pull-down analysis to preferentially interact with FloA and FloT, respectively, was characterized. The mobilities of flotillins and their interaction partners depend on each other, but distinct mobility patterns

of all four proteins and only low levels of colocalization were observed. Therefore, it is unlikely that a stable interaction exists between FloA and PBP3 or FloT and DltD. Rather, transient interactions occur between flotillins and their interaction partners, as has been reported for other flotillin interactions partners, like KinC (Dempwolff et al., 2016). Nevertheless, this transient interaction with cell wall-associated proteins has profound influence on flotillin mobility. Especially the deletion of the *dltA-E* operon results in a decrease of the FloT diffusion coefficient and the diffusivity (Figure 33). These differences only occur because of the absence of DltB-E and not because of the differences in the cell wall they confer (Figure 35). DltD was the only proteins encoded within the *dltA-E* operon identified in the pull-down analysis. Thus, it is likely that mobility differences of FloT in Δ*dltA-E* deletion strain background depend on DltD itself or a DltD-specific mechanism. DltD seems to shield FloT from restricting influences that were shown to decrease FloT diffusivity in the absence of DltD. In addition to that, DltD also seems to stimulate FloT mobility which might be linked to the dual role of the cell wall described below (see chapter 6.4).

6.3 Possible role of FloA and FloT in cell wall synthesis

Interaction of flotillins with cell wall-associated proteins raises the question if FloA and FloT are involved in cell wall synthesis. However, mobility differences preclude FloA and FloT to be part of the Rod-complex of lateral cell wall synthesis. Lateral cell wall synthesis by aPBP protein PBP1 also showed a more random mobility pattern distinct of the Rod-complex (Figure 7) (Dion et al., 2019). Nevertheless, PBP1 was found to localize in the detergent-sensitive fractions of the membrane, spatially apart from FloA and FloT. Other aPBPs were not detected, neither in bocillin-FL stained DRM fraction nor with pull-down analysis. However, several other cell wall synthesis-associated proteins were identified that interacted with FloA and/or FloT (Table 6). Despite the interaction with these cell wall-associated proteins, FloA or FloT do not seem to have a profound influence on cell wall synthesis. The deletion of the cell wall synthesis-associated interaction partners PBP3 and DltD themselves does not reveal growth or morphology differences compared to WT cells. This shows that FloA and FloT might only have a minor possible influence on cell wall synthesis via PBP3 and DltD, respectively. In Δ*floA* or Δ*floT* strains the mobilities of PBP3 and DltD do not show substantial differences and cellular growth rates and morphologies do not differ from WT cells. However, Δ*floA* Δ*floT* double deletions showed reduced growth rates along with a twisted and irregular-shaped cellular morphology (Dempwolff et al., 2012), revealing a certain redundant influence of FloA and FloT on cell wall synthesis. An additional preliminary study detected a shift from the lateral cell wall synthesis to the division septum in the Δ*floA* Δ*floT* double deletion strain (Zielińska et al., 2020). The specific roles of FloA and FloT on cell wall synthesis remain unknown, but conversely, cell wall synthesis has shown to influence the mobility of flotillins.

6.4 The cell wall harbors a dual role in flotillin mobility

The cell wall plays a dual role in influencing flotillin mobility. Firstly, upon inhibition of cell wall synthesis with antibiotics, the mobility of FloA and FloT is reduced (Figure 37). Additionally, flotillin mobility in these conditions was hinting towards an increase in spatial restrictions. However, indirect effects of cell wall synthesis inhibition on flotillin mobility cannot be excluded. These might result from cellular responses leading to differences in the FMM protein cargo that might affect flotillin mobility. However, as several

studies showed similar reduction of membrane protein mobility upon cell wall synthesis inhibition (Domínguez-Escobar et al., 2011; Garner et al., 2011; Strahl et al., 2014), induced differences in FMM protein cargo seem unlikely. Cellular treatment with cell wall synthesis-inhibiting antibiotics lead to a halt of cell wall synthesis components including the Rod-complex in the membrane containing MreB (Domínguez-Escobar et al., 2011; Garner et al., 2011). A similar reduction was observed in the mobility of PBP3 and DltD upon inhibition of cell wall synthesis (Figure 50). The arrest of cell wall synthesis might lead to a general increase in membrane viscosity due to the increased hydrodynamic interactions adjacent to the halted cell wall synthesis components (Bussell et al., 1994, 1995). Restricting barriers are therefore reinforced and result in reduced flotillin mobility. Overall, cell wall synthesis stimulates the mobility of flotillins and their cargo proteins.

Secondly, upon removal of the whole cell wall, in protoplasts, the mobility of FloA and FloT is increased and reaches the same level for both flotillins (Figure 49). This indicates that the cell wall exerts restricting influences on the mobility of FloA and FloT. Physiologically a direct interaction between the cell wall and flotillins seems rather unlikely, as flotillins are localized at the cytosolic side of the membrane and do not reach into the extracellular space where the cell wall is located. It is thus likely that flotillin interaction partners confer the link between flotillins and the cell wall. An increase in the mobility of the cell wall-associated interaction partners of flotillins, PBP3 and DltD, was observed in protoplasts as well (Figure 51). Additionally, MreB mobility is randomized and increased in protoplasts (Figure 48). Upon cell wall removal, the connections between the membrane and the cell wall are possibly relieved from steric restraints. This general release from the friction of the cell wall might lead to the increased mobility of FloA and FloT and their observed equalization.

Together, the cell wall is restricting flotillin mobility (increase in protoplasts) while at the same time its synthesis is stimulating it (decrease upon cell wall synthesis inhibition). These two observations seem to be contradicting at first. On one hand, flotillin mobility restriction by the cell wall is likely mediated by cell wall-associated proteins. Steric restrictions that the cell wall is imposing on cell wall-associated proteins are transmitted to flotillins through their interaction. On the other hand, flotillin mobility stimulation by cell wall synthesis seems to be mediated by cell wall-associated interaction partners as well. Changes in cell wall synthesis directly affect the mobility of the cell wall-associated interaction partners which are further transmitted to flotillins through their interaction. Thereby, the cell wall exerts positive and negative effects on flotillin mobility. It is therefore likely that the cell wall is affecting flotillin mobility indirectly, mediated by transient interactions with cell wall-associated interaction partners.

The cell wall was shown to have the same impact on flotillins and on their interaction partners PBP3 and DltD: a reduced mobility upon antibiotic inhibition of cell wall synthesis and increased mobility upon cell wall removal. Previous reports already showed a similar reduction in membrane protein mobility upon inhibition of cell wall synthesis with vancomycin (Domínguez-Escobar et al., 2011; Garner et al., 2011; Strahl et al., 2014). Therefore, this might be a general principle that applies to various membrane proteins, independent of their function in cell wall synthesis (Strahl et al., 2014). The effect of the cell wall on the mobility of membrane proteins might be secondary and is possibly resulting from general

changes in viscosity in the membrane due to a release of cell wall interacting proteins from spatial restrictions of the cell wall.

6.5 Spatial restriction by the MreB-cytoskeleton is possibly assembly size-dependent

In addition to the cell wall, the bacterial actin-homolog cytoskeleton likewise restricts flotillin mobility – especially that of FloT. Deletion of MreB and its homologs results in an increase in the mobility of FloT (Figure 47). A reason for the differences that the restraining effect of the MreB cytoskeleton exerts on FloT and FloA possibly depends on the different sizes of their oligomers. The smaller FloA oligomers might circumvent MreB filaments more efficiently, while the larger FloT assemblies are affected by the restrictions for a longer time. These differences result in the distinct mobility pattern that were observed, FloT moving at lower diffusion coefficient and reduced diffusivity than FloA, and FloT showing less lateral displacements than FloA.

6.6 The cell wall and the cytoskeleton are intertwined structures

The cell wall and the MreB cytoskeleton are intertwined processes, the correct synthesis of the cell wall depends on MreB orientation (Hussain et al., 2018), and the mobility of MreB depends on cell wall synthesis (Domínguez-Escobar et al., 2011; Garner et al., 2011; Van Teeffelen et al., 2011). Therefore, it is rather difficult to differentiate the effect of one or the other on flotillin mobility. Nevertheless, MreB mutant cells still contain a cell wall, albeit probably structurally different as cells grow as spheres. Additionally, the mobility of MreB in protoplasts is increased, its restricting properties in cells should not exist in protoplasts. Therefore, while the absence of MreB only affects the mobility of FloT, the absence of the cell wall, which also includes a relieve from MreB confinement, alleviates both FloA and FloT from spatial restrictions and equalizes their mobility. Despite the interplay of the exo- and the endo-cytoskeleton, distinct roles in flotillin restriction could be specified.

6.7 A model illustrating flotillin mobility

A model that summarizes these findings is proposed. The mobility of FloA and FloT depends on the size of the assembly, the interaction partners, especially those associated with the cell wall and therefore the cell wall, and the MreB cytoskeleton. All of these aspects together can be summarized to FloA and FloT mobility depending on the size and composition of the oligomers which is depicted in the model (Figure 52). These factors working together result in the characteristic mobility patterns detectable for FloA and FloT: random movement with lateral displacements over short time scales with a reduced diffusivity over longer time scales, where FloT diffusivity is lower than FloA diffusivity.

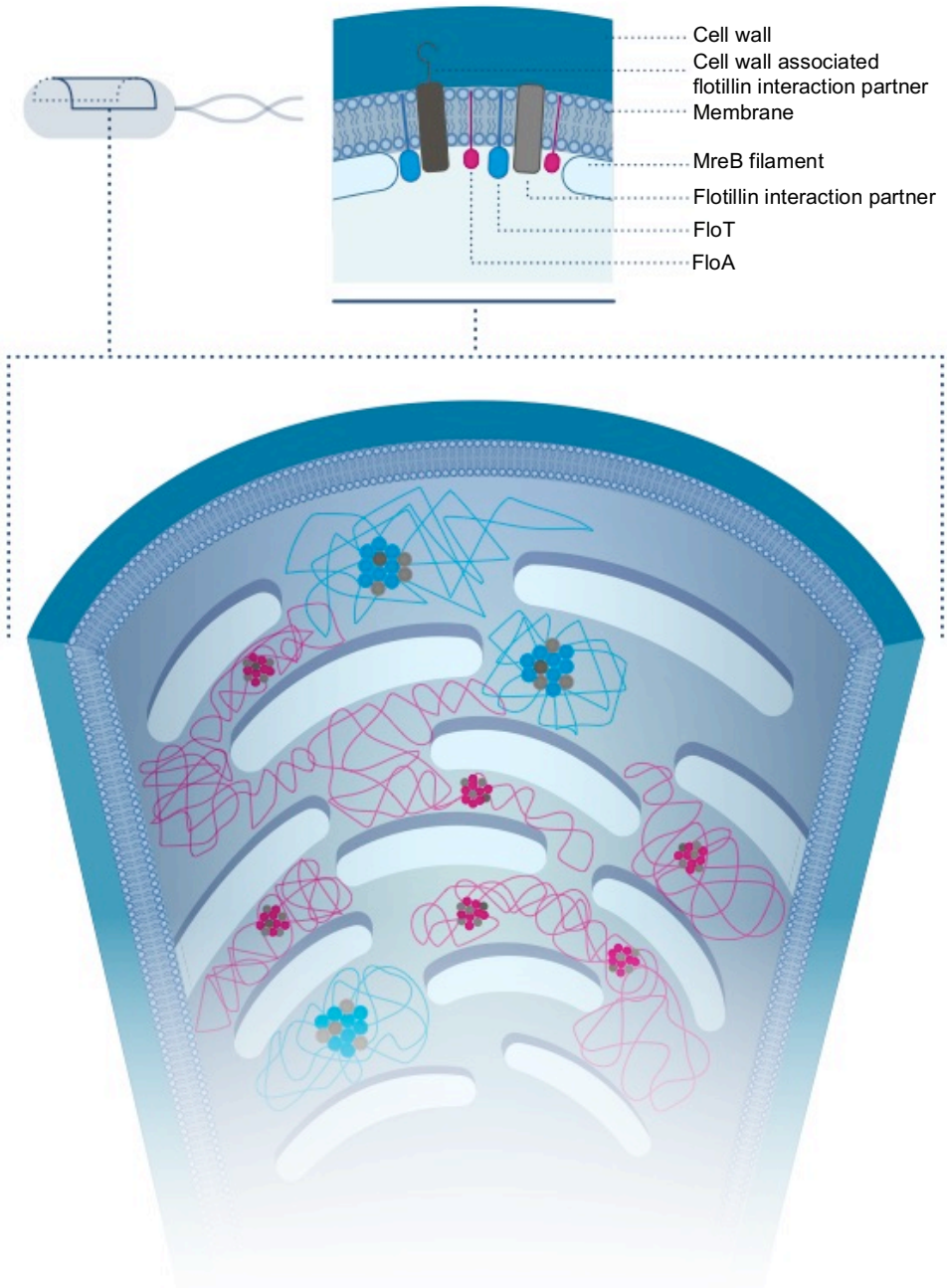

Figure 52: A model suggesting how the exo- and endo-cytoskeleton restricts flotillin mobility. The model shows the membrane looking from the inside of the cell towards the outside. MreB filaments are depicted. Small FloA (magenta) and bigger FloT (cyan) assemblies are displayed with their movement in between the MreB filaments. The assemblies contain several protein interaction partners (grey), some of which are associated with the cell wall (dark grey). Compared to flotillins, the mobility of MreB is very slow and thus not included in the model. Flotillin mobility depends on the restrictions of the exo- and endo-cytoskeleton mediated by the interaction partners and the size of their assemblies. Graphic implementation by scienseed.

6.8 Benefits from restricting flotillin mobility

What might be the benefit for the cell to restrict the mobility of flotillin in the membrane? It is assumed that FloA and FloT are scaffolding proteins that act as chaperons in facilitating protein interactions and complex formation. The constraining mechanism by the exo- and the endo-cytoskeleton might provide assistance in distributing FloA and FloT assemblies appropriately over the whole cell surface. As merging events of individual foci have been observed (Dempwolff et al., 2012), this cellular distribution might prevent the coalescence of individual assemblies into larger domains. The constraining

mechanism might facilitate the spatial distribution to ensure an efficient encounter with FMM cargo proteins to promote their oligomerization and thus secure the correct functionality of FMM. Through the efficient complex oligomerization of their proteins, FMM play an important role in bacterial processes like signal transduction, protein secretion, differentiation and protease activity (Donovan and Bramkamp, 2009; López et al., 2010; Dempwolff et al., 2012; Yepes et al., 2012; Bach and Bramkamp, 2013; Mielich-Süss et al., 2013, 2017; Schneider et al., 2015a; García-Fernández et al., 2017).

6.9 Does the eukaryotic picket-fence model exist in bacteria?

It Is apparent that bacteria harbor the necessary components that constitute the eukaryotic membrane compartmentalization principles that led to the postulation of the picket-fence model. It assumes that the actin cytoskeleton in close proximity to the cytosolic interface of the membrane and its associated transmembrane proteins are creating temporal restriction barriers for the mobility of membrane molecules. These restrictions cause membrane molecules to move at a hop-diffusion pattern, microdiffusion within a compartment and macrodiffusion while hopping from one compartment to another (Kusumi et al., 2010). Despite bacteria containing similar components, small differences exist that have profound impact on the likelihood of similar mobility restrictions. Whereas the eukaryotic actin meshwork persists over long distances and separates the whole membrane into distinct 2D compartments, the MreB cytoskeleton forms comparably short interrupted filaments (Billaudeau et al., 2019). It is therefore unlikely that MreB can compartmentalize the bacterial membrane in a similar manner. Consequently, it is also questionable if hop-diffusion can exist in bacterial membranes. The conditions used to analyze flotillin mobility (300 ms frame rate for 9 s) are restricted by biological limitations. These image acquisition conditions are a factor of 10^4 too slow to be able to detect hop diffusion (Kusumi et al., 2012). Besides that, the structural differences in MreB confinement make it unlikely that bacterial MreB can provoke hop-diffusion in membrane molecules. Nevertheless, the MreB cytoskeleton does still affect the mobility of membrane molecules, albeit differently. In addition to the MreB restriction that was demonstrated here, it has been shown in *E. coli* that inhibition of MreB filament polymerization increases the diffusion of transmembrane proteins. Authors reason that differences could either result from a physical restriction of mobility due to MreB or from RIF disassembly increasing the overall membrane fluidity (Oswald et al., 2016). Therefore, the actin-like cytoskeleton in bacteria can impact the mobility of membrane components, albeit not by the formation of distinct membrane compartments as proposed for eukaryotic cells.

6.10 Similarities to flotillin mobility in plant cells

In addition to the cytoskeletal restrictive network, it was recently found that in plant cells the mobility of flotillin is influenced by the cell wall as well (Daněk et al., 2019). In this study, the dynamics of flotillins was increased when the cell wall was partially removed enzymatically. The authors suggest that the restriction on flotillin mobility is indirect. Structural components that link the membrane with the cell wall are likely to be responsible for the restriction of the cell wall on flotillin mobility (Daněk et al., 2019). Flotillins in plants have been found to interact with membrane proteins that harbor extracellular domains and are involved in cell wall maintenance (Junková et al., 2018). Similar to the described restriction of flotillin mobility by the cell wall in plant cells, cell wall was found to play a role in restricting flotillin mobility

in *B. subtilis* in addition to the MreB cytoskeleton. The cell wall especially accounts for the differences in mobility between FloA and FloT. While the structure of the endo-cytoskeleton differs between eukaryotic and prokaryotic cells, the exo-cytoskeleton is structurally and functionally comparable. Flotillins are located inside the cell and are connected to the cell wall with protein interaction partners like PBP3 or DltD, similar to what has been proposed for plant cells (Daněk et al., 2019). Thus, the confinement of membrane domains is comparable between prokaryotic and eukaryotic cells which implies that cellular mechanisms limiting their lateral movement are conserved.

6.11 Possible implications of this work for the biotech industry

The involvement of FMM in many different cellular processes shows that they are functionally unspecific. This allows them to be used for different purposes that are not naturally occurring in the cell of *B. subtilis*. *B. subtilis* is widely used in biotechnological applications due to its non-toxicity and its ability to secrete proteins at high yields (van Dijl and Hecker, 2013). Initial studies have started to exploit FMM for this purpose (Lv et al., 2020a, 2020b, 2020c). Furthermore, projects in our laboratory focus on increasing production yields by positioning enzymes in FMM with the help of the scaffolding activities of FloA and FloT. The more detailed the understanding of the underlying processes is, the more success will be achieved by their manipulation and exploitation for desired processes. Therefore, understanding the structures that influence the mobility of FloA and FloT assemblies in the membrane offers another component to be used and exploited to control the desired production.

6.12 The exo- and endo-cytoskeleton spatially confines FMM

This work has shown that principles of restricting the diffusion of membrane microdomains depend on the exo- and the endo-cytoskeleton. In addition to this work, preliminary data from other labs have shown that flotillin organization influences membrane fluidity which in turn affects peptidoglycan synthesis and MreB movement (Zielińska et al., 2020). This further suggests a strong connection between flotillin assembly, cytoskeleton organization and cell wall synthesis. Continuing research will help to shed light onto this strong intertwined interplay of important cellular structures. The present work provides evidence that the spatial organization of membrane microdomains in bacterial cells is controlled by the exo- and the endo-cytoskeleton, similar to what has been described for eukaryotic plant cells. The exo- and endo-cytoskeleton provides a means of spatial membrane organization necessary for life to exist and proliferate.

7 MATERIALS AND METHODS

7.1 Materials

All chemicals were purchased from Sigma-Aldrich if not specified otherwise.

7.1.1 Buffers

PBS 1x	137 mM NaCl 2.7 mM KCl 10 mM Na_2HPO_4 1.8 mM KH_2PO_4 pH 7.4	TAE 1x	40 mM Tris base 0.114 % glacial acetic acid 1 mM EDTA pH 8
TBS-T 1x	20 mM Tris base pH 7.4 150 mM NaCl 0.05 % tween 20	Running buffer 1x	25 mM Tris base 192 mM glycine 0.1 % SDS
Transfer buffer 1x	25 mM Tris base 192 mM glycine 20 % MeOH	Phusion buffer 10x	100 mM Tris-HCl pH 8.8 500 mM KCl 25 mM $MgCl_2$ 0.8 % NP-4O
TFB1	100 mM RbCl 50 mM $MnCl_2$ 30 mM potassium acetate 10 mM $CaCl_2$ 15 % glycerol, pH 5.8	TFB2	10 mM RbCl 75 mM $CaCl_2$ 10 mM MOPS 15 % glycerol, pH 6.8
LTA buffer	100 mM sodium citrate pH 4.7		

7.1.2 Bacterial growth media

LB	1 % tryptone [a] 0.5 % yeast extract [a] 0.5 % NaCl (15 g/l Bacto Agar [a])	TY	LB supplemented with 10 mM $MgSO_4$ 100 µM $MnSO_4$ (15 g/l Bacto Agar [a])

MSgg	5 mM potassium phosphate pH 7 100 mM Mops pH 7 2 mM $MgCl_2$ 700 µM $CaCl_2$ 50 µM $MnCl_2$ 50 µM $FeCl_3$ 1 µM $ZnCl_2$ 2 µM thiamine 0.5 % glycerol 0.5 % glutamate 50 µg/ml tryptophan 50 µg/ml phenylalanine (15 g/l Bacto Agar [a])	MC	100 mM potassium phosphate pH 7 2 % glucose 0.1 % casein hydrolysate 0.2 % potassium L-glutamate 3 mM sodium citrate 22 µg/ml ferric ammonium citrate 3 mM $MgSO_4$ 50 µg/ml L-tryptophan 50 µg/ml L-phenylalanine 50 µg/ml L-threonine
GTE	50 mM glucose 10 mM EDTA 20 mM Tris-HCl pH 7.5	SM	0.5 M sucrose 20 mM $MgCl_2$ 10 mM potassium phosphate pH 6.8

[a] Tryptone, yeast extract and Bacto Agar were purchased from BD Biosciences.

7.1.3 Additional preparations

DNA gels and agarose-coated microscope slides	0.8 % agarose boiled in TAE buffer	DNA loading dye 3x	30 % glycerol Orange G
SDS sample buffer 4x	200 mM Tris-HCl pH 6.8 400 mM DTT 8 % SDS 0.4 % bromophenol blue 40 % glycerol	Fixative SDS-gels	4 V methanol 1 V acetic acid 5 V H_2O
Stacking gel 4%	0.125 M Tris-HCl pH 6.8 4 % acrylamide [a] 0.1% SDS 0.1% APS 0.01 % TEMED [a]	Resolving gel 12 %	0.375 M Tris-HCl pH 8.8 12 % acrylamide [a] 0.1 % SDS 0.1 % APS 0.01 % TEMED [a]
Fixative cells	2.5 % paraformaldehyde[a] 0.03% glutaraldehyde 10 mM sodium phosphate buffer pH 7.4 10 min RT, 50 min on ice	ELISA developing solution	50 mM sodium dihydrogen phosphate 25 mM citric acid 0.4 mg/ml O-phenylene-diamine dihydrochloride 0.4 µg/ml hydrogen peroxide, pH 5

[a] Acrylamide (Bio-Rad), TEMED (VWR) and paraformaldehyde (Carl Roth) were not purchased from Sigma-Aldrich.

7.1.4 Kits, enzymes and other specific products

Genomic DNA isolation	Phase Lock Gel Heavy, 5PRIME
Plasmid isolation	NucleoSpin® Plasmid, Macherey Nagel Biomass of 50 % agar plate or 3 ml ONC, elution in 50 µl
DNA clean-up	NucleoSpin® Gel and PCR Clean-up, Macherey Nagel PCR product or digestion in agarose gel, elution in 0.5 V
Phusion polymerase	In-house purification
dNTPs	Deoxynucleoside Triphosphate Set PCR Grade, Roche
Joining PCR	Expand™ Long Template PCR System, Roche
Restriction enzymes	New England Biolabs
Ligation	T4 DNA Ligase, New England Biolabs
DNA standard	5 µl, 1 kb DNA Ladder, New England Biolabs
DNA sequencing	Macrogen
DRM/DSM	CelLytic™ MEM Protein Extraction Kit, Sigma
SDS-PAGE and western blot systems	Bio-Rad
Protein standard SDS-PAGE	2 µl, Precision Plus Protein™ Dual Color Standards, Bio-Rad
SDS-PAGE staining	BlueSafe, NZYTech
Western blot developing	Clarity Western ECL Substrate, Bio-Rad
Blue-Native PAGE	NativePAGE^{TM} Novex system, Invitrogen
Protein standard BN-PAGE	7 µl, NativeMark™ Unstained Protein Standard, Invitrogen
Pull-down GFP	GFP-Trap Agarose, ChromoTek
LIVE/DEAD™ *Bac*Light™ Bacterial Viability Kit	Invitrogen
$DiOC_2(3)$	Sigma-Aldrich

7.1.5 Software and online tools

Several bioinformatic programs, software and online tools were used during this work. They are listed here and will be specified in their respective sections if necessary.

Molecular Biology

DNA cloning	SnapGene Viewer, continuously updated, latest v.5.1.3
Sequence alignments	EMBL-EBI MUSCLE
Protein domain prediction	SMART (Letunic et al., 2015; Letunic and Bork, 2018)
Secondary structure prediction	Phyre^2 (Kelley et al., 2015)

Fluorescence microscopy	
Leica Microscope DMI6000B	Leica Microsystems LAS X v.3.3
Leica Microscope DMi8 S	Leica Microsystems LAS X v.3.0
General image processing	Fiji (ImageJ) v.2.0.0-rc69/1.52p (Schindelin et al., 2012)
Cell width	Fiji Plugin: MicrobeJ v5.13l (Ducret et al., 2016)
Colocalization	Fiji Plugin: JACoP (Bolte and Cordelieres, 2006)
Mobility analysis	Fiji Plugin: Trackmate v.3.8.0 (Tinevez et al., 2017)
Biochemistry	
Global pull-down proteomics	Data collection (Analyst TF 1.7), processing (PeakView v.2.2) and identification (MASCOT v.2.6.1)
Fingerprinting proteomics	Data collection (ABi 4000 Series Explorer Spot Set Manager), processing (ABi 4000 Series Explorer v.3.6) and identification (MASCOP v.2.6.1)
Protein identification from provided accession numbers	NCBI, UniProt
Assigning of the functional category	*Subti*wiki (Zhu and Stülke, 2018)
Heatmap	Heatmapper (Babicki et al., 2016)
Statistics	R commander 2.5-1

7.2 Microbiology methods

7.2.1 Bacterial strains

The strains used in this study are derived from *Bacillus subtilis* PY79. *Escherichia coli* DH5α was used to shuttle plasmids. Strains used for each specific experiment are specified in the results. A complete list of strains can be found in Table 1 and Table 2.

Table 1: List of plasmids used in this study.

Strain		Genotype [a]	Reference	Construction [b]
Escherichia coli				
DL95	DH5α	Wild type	(Reusch et al., 1986)	
RW65	DH5α	pDR183 (*amp*/*mls*)	(Rudner Lab | Harvard Medical School)	
RW73	DH5α	pDR183-P_{yqeZ}-*floA-gfp*	This study	*Eco*RI/*Sph*I
RW114	DH5α	pDR183-P_{yuaF}-*floT-gfp*	This study	*Sal*I/*Sph*I
JS197	DH5α	pDR183-P_{yqeZ}-*floA-mCherry*	(Schneider et al., 2015a)	
JS182	DH5α	pDR183-P_{yuaF}-*floT-mCherry*	(Schneider et al., 2015a)	
RW371	DH5α	pDR183-P_{yqeZ}-*floA*$_{nt}$-(IL)*T*$_{ct}$-*gfp*	This study	*Eco*RI/*Xho*I

Strain		Genotype [a]	Reference	Construction [b]
RW430	DH5α	pSG1729 (*amp*/*spc*)	(Guerout-Fleury et al., 1996)	
RW494	DH5α	pSG1729-P_{xyl}-*gfp-dltD*	This study	*Xho*I/*Eco*RI
RW189	DH5α	pJL-sar-gfp (*amp*/*ermC*)	(Liese et al., 2013)	
RW197	DH5α	pRW01 (*amp*/*ermC*)	This study	*Sph*I/*Nar*I
RW420	DH5α	pRW01-P_{yqeZ}-*floA-mCherry*	This study	*Eco*RI/*Sph*I
RW421	DH5α	pRW01-P_{yuaF}-*floT-mCherry*	This study	*Kpn*I/*Sph*I
RW450	DH5α	pRW01-P_{xyl}-*floA-mCherry*	This study	*Sal*I/*Sph*I
RW453	DH5α	pRW01-P_{xyl}-*floT-mCherry*	This study	*Sal*I/*Sph*I
RW199	DH5α	pRW02 (*amp*/*km*)	This study	*Xho*I/*Apa*I
RW200	DH5α	pRW03 (*amp*/*tet*)	This study	*Xho*I/*Apa*I
RW201	DH5α	pRW04 (*amp*/*cm*)	This study	*Xho*I/*Apa*I
RW394	DH5α	pRW04-P_{yqeZ}-*floA-gfp*	This study	*Eco*RI/*Sal*I
RW390	DH5α	pRW04-P_{yuaF}-*floT-gfp*	This study	*Kpn*I/*Sal*I
RW391	DH5α	pRW04-P_{yuaF}-*floT*$_{nt}$*A*$_{ct}$-*gfp*	This study	*Kpn*I/*Sal*I
RW395	DH5α	pRW04-P_{yqeZ}-*floA*$_{nt}$*T*$_{ct}$-*gfp*	This study	*Eco*RI/*Sal*I
RW438	DH5α	pRW04-P_{xyl}-*floA-mCherry*	This study	*Sal*I/*Sph*I
RW439	DH5α	pRW04-P_{xyl}-*floT-mCherry*	This study	*Sal*I/*Sph*I

[a] Antibiotic resistance is specified in parentheses if necessary, first and second resistance correspond to *E. coli* and *B. subtilis*, respectively.

[b] Restriction enzymes used to construct the plasmids. The order of the restriction enzymes represents the coding direction of the insert. The corresponding primers can be found in Table 3.

Table 2: List of strains used in this study.

Strain [a]		Genotype	Reference	Construction [b]
Bacillus subtilis				
RW3	PY79	Wild type	(Youngman et al., 1984)	
RW88	PY79	Δ*lacA*::P_{yuaF}-*floT-gfp* (*mls*)	This study	RW3+RW114
RW77	PY79	Δ*lacA*::P_{yqeZ}-*floA-gfp* (*mls*)	This study	RW3+RW73
RW45	PY79	Δ*lacA*::P_{yqeZ}-*floA-mCherry* (*mls*)	(Schneider et al., 2015a)	
RW48	PY79	Δ*lacA*::P_{yuAF}-*floT-mCherry* (*mls*)	(Schneider et al., 2015a)	
RW396	PY79	pRW04-P_{yqeZ}-*floA-gfp* (*cm*)	This study	RW3+RW394
RW392	PY79	pRW04-P_{yuaF}-*floT-gfp* (*cm*)	This study	RW3+RW390
RW578	PY79	Δ*floA*::*floA-gfp-tet*	This study	Primers A
RW579	PY79	Δ*floT*::*floT-gfp-tet*	This study	Primers B
RW323	PY79	Δ*amyE*::P_{yuaF}-*floT*$_{nt}$*A*$_{ct}$-*gfp* (*spc*)	(Schneider et al., 2015a)	
RW326	PY79	Δ*lacA*::P_{yqeZ}-*floA*$_{nt}$*T*$_{ct}$-*gfp* (*mls*)	(Schneider et al., 2015a)	
RW375	PY79	Δ*lacA*::P_{yqeZ}-*floA*$_{nt}$-(IL)*T*$_{ct}$-*gfp* (*mls*)	This study	RW3+RW371

Strain [a]		Genotype	Reference	Construction [b]
RW329	PY79	Δ*floA*::*cm*	This study	Primers C
DL1237	168	Δ*floA*::*spc*	(López et al., 2010)	
RW330	PY79	Δ*floT*::*tet*	This study	Primers D
RW334	PY79	Δ*floA*::*cm* Δ*floT*::*tet*	This study	RW329+RW330
RW28	PY79	Δ*floA::mls* Δ*floT::spc*	(Yepes et al., 2012)	
RW521	PY79	Δ*floT*::*tet* Δ*lacA*::P_{yqeZ}-*floA-gfp* (*mls*)	This study	RW330+RW73
RW522	PY79	Δ*floA*::*cm* Δ*lacA*::P_{yuaF}-*floT-gfp* (*mls*)	This study	RW329+RW114
RW404	PY79	Δ*floA::mls* Δ*floT::spc* pRW04-P_{yqeZ}-*floA-gfp* (*cm*)	This study	RW28+RW394
RW405	PY79	Δ*floA::mls* Δ*floT::spc* pRW04-P_{yuaF}-*floT-gfp* (*cm*)	This study	RW28+RW392
RW406	PY79	Δ*floA::mls* Δ*floT::spc* pRW04-P_{yqeZ}-*floA*$_{Nt}$*T*$_{Ct}$-*gfp* (*cm*)	This study	RW28+RW395
RW407	PY79	Δ*floA::mls* Δ*floT::spc* pRW04-P_{yuaF}-*floT*$_{Nt}$*A*$_{Ct}$-*gfp* (*cm*)	This study	RW28+RW393
RW408	PY79	Δ*floA::mls* Δ*floT::spc* pRW04 (*cm*)	This study	RW28+RW201
RW433	PY79	Δ*amyE*::P_{xyl}-*gfp* (*spc*)	This study	RW3+RW430
RW434	PY79	Δ*amyE*::P_{xyl}-*gfp* (*spc*) pRW01-P_{yqeZ}-*floA-mCherry* (*ery*)	This study	RW3+RW420
RW435	PY79	Δ*amyE*::P_{xyl}-*gfp* (*spc*) pRW01-P_{yuaF}-*floT-mCherry* (*ery*)	This study	RW3+RW421
RW445	168	Δ*trpC2* Δ*pbpC*::pSG5045(P_{xyl}-*gfp-pbpC*)*cm*	(Scheffers et al., 2004)	
RW445b	PY79	Δ*pbpC*::pSG5045(P_{xyl}-*gfp-pbpC*)*cm*	This study	RW3+RW445
RW452	PY79	Δ*pbpC*::pSG5045(P_{xyl}-*gfp-pbpC*)*cm* pRW01-P_{xyl}-*floA-mCherry* (*ery*)	This study	RW445b+RW450
RW455	PY79	Δ*pbpC*::pSG5045(P_{xyl}-*gfp-pbpC*)*cm* pRW01-P_{xyl}-*floT-mCherry* (*ery*)	This study	RW445b+RW453
RW554	PY79	Δ*lacA*::P_{yqeZ}-*floA-mCherry* (*mls*) Δ*pbpC*::pSG5045(P_{xyl}-*gfp-pbpC*)*cm*	This study	RW45+RW445 (SPP1)
RW555	PY79	Δ*lacA*::P_{yuaF}-*floT-mCherry* (*mls*) Δ*pbpC*::pSG5045(P_{xyl}-*gfp-pbpC*)*cm*	This study	RW48+RW445 (SPP1)
RW312	PY79	Δ*pbpC*::*km*	This study	Primers E
RW307	PY79	Δ*pbpC*::*km* Δ*lacA*::P_{yqeZ}-*floA-gfp* (*mls*)	This study	RW312+RW73
RW299	PY79	Δ*pbpC*::*km* Δ*lacA*::P_{yuaG}-*floT-gfp* (*mls*)	This study	RW312+RW114
RW482	PY79	Δ*floA*::*spc* Δ*pbpC*::pSG5045(P_{xyl}-*gfp-pbpC*)*cm*	This study	RW445b+DL1237
RW488	PY79	Δ*floT*::*tet* Δ*pbpC*::pSG5045(P_{xyl}-*gfp-pbpC*)*cm*	This study	RW330+RW445 (SPP1)
RW498	PY79	Δ*amyE*::P_{xyl}-*gfp-dltD* (*spc*)	This study	RW3+RW494
RW500	PY79	Δ*amyE*::P_{xyl}-*gfp-dltD* (*spc*) pRW04-P_{xyl}-*floA-mCherry* (*cm*)	This study	RW498+RW438
RW502	PY79	Δ*amyE*::P_{xyl}-*gfp-dltD* (*spc*) pRW04-P_{xyl}-*floT-mCherry* (*cm*)	This study	RW498+RW439
RW556	PY79	Δ*amyE*::P_{xyl}-*gfp-dltD* (*spc*) Δ*lacA*::P_{yqeZ}-*floA-mCherry* (*mls*)	This study	RW498+RW73

Strain [a]		Genotype	Reference	Construction [b]
RW557	PY79	Δ*amyE*::P_{xyl}-*gfp-dltD* (*spc*) Δ*lacA*::P_{yuaF}-*floT-mCherry* (*mls*)	This study	RW498+RW114
DL469	168	Δ*dltA-E*::*tet*	(Lopez et al., 2009)	
RW124	PY79	Δ*dltA-E*::*tet*	This study	RW3+DL469
RW104	PY79	Δ*dltA-E*::*tet* Δ*lacA*::P_{yqeZ}-*floA-gfp* (*mls*)	This study	RW124+RW73
RW105	PY79	Δ*dltA-E*::*tet* Δ*lacA*::P_{yuaF}-*floT-gfp* (*mls*)	This study	RW124+RW114
RW514	PY79	Δ*floA*::*cm* Δ*amyE*::P_{xyl}-*gfp-dltD* (*spc*)	This study	RW329+RW494
RW513	PY79	Δ*floT*::*tet* Δ*amyE*::P_{xyl}-*gfp-dltD* (*spc*)	This study	RW330+RW494
RW569	PY79	Δ*dltA*::*tet*	This study	Primers F
RW568	PY79	Δ*dltA*::*tet* Δ*lacA*::P_{yuaF}-*floT-gfp* (*mls*)	This study	RW569+RW114
RW457	PY79	Δ*tagU*::*km*	This study	Primers G
RW458	PY79	Δ*tagU*::*km* Δ*lacA*::P_{yqeZ}-*floA-gfp* (*mls*)	This study	RW457+RW73
RW456	PY79	Δ*tagU*::*km* Δ*lacA*::P_{yuaG}-*floT-gfp* (*mls*)	This study	RW457+RW114
RW113	PY79	Δ*ugtP*::*km*	This study	Primers H
RW119	PY79	Δ*ugtP*::*km* Δ*lacA*::P_{floA}-*floA-gfp* (*mls*)	This study	RW113+RW73
RW117	PY79	Δ*ugtP*::*km* Δ*lacA*::P_{floT}-*floT-gfp* (*mls*)	This study	RW113+RW114
RW38	PY79	Δ*amyE*::P_{xyl}-*gfp-mreB* (*spc*)	(Soufo and Graumann, 2003)	
RW39	PY79	Δ*amyE*::P_{xyl}-*gfp-mreBH* (*spc*)	(Soufo and Graumann, 2003)	
RW40	PY79	Δ*amyE*::P_{xyl}-*gfp-mbl* (*spc*)	(Soufo and Graumann, 2003)	
RW422	PY79	Δ*amyE*::P_{xyl}-*gfp-mreB* (*spc*) pRW01-P_{yqeZ}-*floA-mCherry* (*ery*)	This study	RW38+RW420
RW423	PY79	Δ*amyE*::P_{xyl}-*gfp-mreB* (*spc*) pRW01-P_{yuaF}-*floT-mCherry* (*ery*)	This study	RW38+RW421
RW491	168	Δ*amyE*::P_{xyl}-*mRFPruby-mreB* (*spc*)	(Domínguez-Escobar et al., 2011)	
RW491b	PY79	Δ*amyE*::P_{xyl}-*mRFPruby-mreB* (*spc*)	This study	RW3+RW491
RW552	PY79	Δ*amyE*::P_{xyl}-*mRFPruby-mreB* (*spc*) Δ*lacA*::P_{yqfA}-*floA-gfp* (*mls*)	This study	RW491b+RW73
RW553	PY79	Δ*amyE*::P_{xyl}-*mRFPruby-mreB* (*spc*) Δ*lacA*::P_{yuaF}-*floT-gfp* (*mls*)	This study	RW491b+RW114
RW576	168	Δ*trpC2* Ω*neo3427* Δ*mreB* Δ*mbl*::*cm* Δ*mreBH*::*erm* Ω(*neo*::*spc*)Δ*rsgI*	(Schirner and Errington, 2009)	
RW610	PY79	Δ*floA*::*floA-gfp-tet* Ω(*neo*::*spc*)Δ*rsgI*	This study	RW578+RW576
RW606	PY79	Δ*floT*::*floT-gfp-tet* Ω(*neo*::*spc*)Δ*rsgI*	This study	RW579+RW576
RW616	PY79	Δ*floA*::*floA-gfp-tet* Ω*neo3427* Δ*mreB* Δ*mbl*::*cm* Δ*mreBH*::*erm* Ω(*neo*::*spc*)Δ*rsgI*	This study	RW578+RW576

Strain [a]		Genotype	Reference	Construction [b]
RW617	PY79	Δ*floT*::*floT-gfp-tet* Ω*neo3427* Δ*mreB* Δ*mbl*::*cm* Δ*mreBH*::*erm* Ω(*neo*::*spc*)Δ*rsgI*	This study	RW579+RW576

[a] Strains are sorted construct-specific according to the chronological order in this study.

[b] Information explains how strains were constructed. If strains were constructed by transformation of PCR-constructs, primers are referenced (Table 3). If strains were constructed with plasmids, genomic DNA or SPP1 phages, the acceptor (first strain number) and the donor strains (second strain number) are listed.

7.2.2 Culture conditions

B. subtilis cultures were grown in liquid LB (1 % tryptone, 0.5 % yeast extract, 0.5 % NaCl) at 37 °C or on MSgg minimal medium (Freese et al., 1979) plates at 30 °C. Media were supplemented with 0.5 % xylose (exception MreB 0.01 % xylose) and antibiotics if necessary (chloramphenicol 5 µg/ml, erythromycin 1 µg/ml, lincomycin 25 µg/ml, kanamycin 10 µg/ml, spectinomycin 100 µg/ml, tetracycline 5 µg/ml). *E. coli* cultures were grown in LB at 37°C supplemented with ampicillin 100 µg/ml if necessary.

7.2.3 Determination of antibiotic minimum inhibitory concentration

Minimum inhibitory concentrations (MIC) were determined in 96 well plates. Serial 1:1 dilutions of antibiotics in LB medium (0.025 µg/ml till 500 µg/ml) were inoculated with *B. subtilis* PY79 from ONC to a final OD_{600} = 0.05. Plates were incubated at 37 °C for 20 h without agitation. The lowest antibiotic concentration that showed no bacterial growth was regarded as the MIC. MIC were determined in triplicates.

7.3 Molecular biology methods

7.3.1 Plasmid and genomic DNA isolation

Plasmids were isolated from *E. coli* with the NucleoSpin® Plasmid kit (Macherey Nagel) according to instructions. Biomass from half an agar plate or 3 ml ONC were used per column and eluted in 50 µl elution buffer.

Genomic DNA from *B. subtilis* was isolated by resuspending biomass in 700 µl PBS and incubating it with 25 µl lysozyme (10 mg/ml, Carl Roth) and 10 µl RNAse (10 mg/ml) 15 min at 37 °C. 10 µl Proteinase K (10 mg/ml) was added before incubation at 52 °C for 15 min. 0.2 % of the detergent N-Lauroylsarcosine was added for complete lysis. After addition of 1 V phenol:chloroform:isoamyl alcohol (25:24:1) (saturated with 10 mM Tris pH 8, 1 mM EDTA) the whole mix was subjected to phase separation in phase lock tubes (Phase Lock Gel Heavy, 5PRIME) (17,000 x g, 10 min, RT). The upper aqueous phase was collected and DNA precipitated with the addition of 1 V isopropanol. DNA was pelleted (12,000 x g, 1 min, RT), washed with 2 V 70 % ethanol (12,000 x g, 1 min, RT), dried, and resuspended in ultrapure water.

7.3.2 PCR amplification and purification

PCR fragments were amplified for cloning in four simultaneous reactions that were later collected for further processing. To connect individual DNA fragments into a single DNA fragment, joining-PCRs were performed in a single preparation separated into two reactions (Expand™ Long Template PCR System, Roche) (Wach, 1996). Information for the reaction mixes and the incubation protocols are shown below. PCR and joining-PCR products used for cloning were purified with the NucleoSpin® Gel and PCR Clean-up kit (Macherey Nagel) and eluted in 0.5 V.

To perform colony-PCR 0.5 V of the PCR protocol were used per reaction and fragments of < 1 kb amplified, if possible. *E. coli* biomass was added directly to the PCR reaction. *B. subtilis* biomass was lysed prior to amplification by resuspending biomass in 10 µl 0.1 mg/ml lysozyme and incubation for 10 min at 37 °C. Subsequently, the mixture was boiled in the microwave at 800 W for 3 min and debris was pelleted. 1 µl supernatant was used as template in the colony-PCR.

PCR	5 µl 10x phusion buffer 1 µl dNTPs (10 mM each) 1 µl primer forward 5 µM 1 µl primer reverse 5 µM 1 µl Phusion polymerase 1 µl DMSO 1 µl template 39 µl H_2O	Protocol	1. 98 °C 5 min 2. 98 °C 30 s 3. 54 °C 30 s 4. 72 °C 30 s per 1 kb Repeat 2.-4. 34 x 5. 72 °C 10 min 6. 12 °C hold
Joining-PCR	10 µl 10x Expand Long Template Buffer 2 4 µl dNTPs (10 mM each) 4 µl primer forward 5 µM 4 µl primer reverse 5 µM 1.5 µl DNA polymerase mix 500 ng each fragment a.d. 100 µl H_2O	Protocol	1. 94 °C 5 min 2. 94 °C 30 s 3. 54 °C 30 s 4. 68 °C 2 min per 1 kb Repeat 2.-4. 10x Repeat 2.-4. 24x, increasing 4. by 20 s each repetition 5. 68 °C 10 min 6. 12 °C hold

Table 3: List of primers used in this study.

Purpose	Construct	Name	Sequence 5' - 3'
Replicative plasmid	pRW derivates	pRW-MCS_for	AAAAGCATGCTAGCAGATCTCCATGGTACCCGGGAGC
		pRW-MCS_rev	AAAAACTAGTGGCGCGCCGGCGCCGATATCGGATCCATATGACG
		km-ApaI_for	AAAAGGGCCCCAGCGAACCATTTGAGGTG
		km-XhoI_rev	AAAACTCGAGCGATACAAATTCCTCGTAGG

Purpose	Construct	Name	Sequence 5' - 3'
		tet-ApaI_for	TTTTGGGCCCTCTTGCAATGGTGCAGGTTG
		tet-XhoI_for	TTTTCTCGAGCTCTCCCAAAGTTGATCCC
		cm-ApaI_for	AAAAGGGCCCGCAATAGTTACCCTTATTATC
		cm-XhoI_rev	AAAACTCGAGCTGGAGCTGTAATATAAAAAC
Fluorescent-labeled strains	Flotillins	P_{yqfeZ}-EcoRI_for	TAATGAATTCGTGAGCAGTCAACTGTC
		P_{yuaF}-KpnI_for	AAAAGGTACCCGCAGCAGTCAGCTGC
		P_{yuaF}-SalI_for	AAAAGTCGACCGCAGCAGTCAGCTGC
		mCherry-SphI_rev	AAAAGCATGCTTACTTGTACAGCTCGTCCAT
		P_{xyl}-SalI_for	TTTTGTCGACTTTATTGCAATAACAGGTGCTTAC
		gfp-SalI_rev	TTTTGTCGACGTTATTTGTATAGTTC
		gfp-SphI_rev	AAAAGCATGCTTATTTGTATAGTTCATCCATGC
		gfp-XhoI_rev	TTTTTTCTCGAGTTATTTGTATAGTTCATC
	Chimera	nFloA-lLcFloT_rev	GTATTGACGTTCACGGCGAAGAATAATATCAATTGAGAGAATTTCAAAC
		lLcFloT-nFloA_for	GTTTGAAATTCTCTCAATTGATATTATTCTTCGCCGTGAACGTCAATAC
	Δ*floA*::*floA-gfp-tet*	floA_for	ATGGATCCGTCAACACTTATG
		gfp-tet_rev	CACATTTCACCCTCCAATAATGTTATTTGTATAGTTCATCCATG
	Primers A	tet-gfp_for	CATGGATGAACTATACAAATAACATTATTGGAGGGTGAAATGTG
		tet-yqfB_rev	CGTTCTCCCTTCTTAGAGAGATTAGAAATCCCTTTGAGAATG
		yqfB-tet_for	CATTCTCAAAGGGATTTCTAATCTCTCTAAGAAGGGAGAACG
		yqfB_rev	AAGGCATGTACATCCTGAAGC
	Δ*floT*::*floT-gfp-tet*	floT_for	ATGACAATGCCGATTATAATG
		tet-yuaH_rev	GGTTCTGCCCTTTCCTTACTCTTAGAAATCCCTTTGAGAATG
	Primers B	yuaH-tet_for	CATTCTCAAAGGGATTTCTAAGAGTAAGGAAAGGGCAGAACC
		yuaH_rev	CAAAGCAGGTCTTACTACAGG
	DltD	dltD-XhoI_for	AAAACTCGAGATGAAAAAGCGTTTTTTCGG
		dltD-EcoRI_rev	AAAAGAATTCGGATGAAGTGACTTTTCCGG
Deletions	Δ*floA*::*cm*	FloA-clean-U-SalI_for	AAAAGTCGACTAGTCGATTGGTGTATTCG

Purpose	Construct	Name	Sequence 5' - 3'
	Primers C	FloA-up-cm_rev	GATAATAAGGGTAACTATTGCTCAAGAATAATATGGTCTGC
		FloA-down-cm_for	GTTTTTATATTACAGCTCCAGCGTATGGTACAGGCAAGA
		FloA-down-BamHI_rev	AAAAGGATCCTTTCGGGCGACATCATTAA
		cm-floA-up_for	GCAGACCATATTATTCTTGAGCAATAGTTACCCTTATTATC
		cm-floA-down_rev	TCTTGCCTGTACCATACGCTGGAGCTGTAATATAAAAAC
	Δ*floT*::*tet*	FloT-clean-up-SalI_for	AAAAGTCGACCGGCTTTCGTCCGCCA
	Primers D	FloT-up-tet_rev	GAGAACAACCTGCACCATTGCAAGACAGAGGCAATACAAGTTCA
		FloT-down-tet_for	GGGATCAACTTTGGGAGAGAGTTCGCAAAAGGAGCGGAGTTT
		FloT-clean-down-BamHI_rev	AAAAGGATCCGCTGAGAGTGAGCGGTT
		tet-floT-up_for	TGAACTTGTATTGCCTCTGTCTTGCAATGGTGCAGGTTGTTCTC
		tet-floT-down_rev	AAACTCCGCTCCTTTTGCGAACTCTCTCCCCAAAGTTGATCCC
	Δ*pbpC*::*km*	pbpC-up-XhoI_for	AAAACTCGAGTGCGGTTATCATTATTATACTGG
	Primers E	pbpC-up-km_rev	CACCTCAAATGGTTCGCTGATGACTTTCCCCTGCCTTCC
		pbpC-down-km_for	CCTACGAGGAATTTGTATCGCGTTGAGAAAGCGAAAAAGC
		pbpC-down-EcoRI_rev	TTTTGAATTCCTTCTCAGGCAAATATGATTCC
		km-pbpC_for	GGAAGGCAGGGGAAAGTCATCAGCGAACCATTTGAGGTG
		km-pbpC_rev	GCTTTTTCGCTTTCTCAACGCGATACAAATTCCTCGTAGG
	Δ*dltA*::*tet*	dltA-up_for	ATAAGTTCGTCGCGATCTGG
	Primers F	dltA-up-tet_rev	GATTGTGAATAGGATGTATTCACCATAGTTATTCTCTCTCCAATTAG
		tet-dltA-up_for	CTAATTGGAGAGAGAATAACTATGGTGAATACATCCTATTCACAATC
		tet-dltA-down_rev	TCATACAAGAACCTCTTCGCCTTAGAAATCCCTTTGAGAATG
		dltA-down-tet_for	CATTCTCAAAGGGATTTCTAAGGCGAAGAGGTTCTTGTATGA
		dltA-down_rev	AGACATATGCCAGCGATTC
	Δ*tagU*::*km*	tagU-up-BamHI_for	AAAAGGATCCCGCAGTTTCGTATCGTGAAGC

Purpose	Construct	Name	Sequence 5' - 3'
	Primers G	tagU-up-km_rev	CACCTCAAATGGTTCGCTGCGTTTCTC ATCCTTTGCACC
		km-tagU-up_for	GGTGCAAAGGATGAGAAACGCAGCGA ACCATTTGAGGTG
		km-tagU-down_rev	CCGGATTCATTTACAGGCAAATCGATA CAAATTCCTCGTAGG
		tagU-down-km_for	CCTACGAGGAATTTGTATCGATTTGCC TGTAAATGAATCCGG
		tagU-down-EcoRI_rev	TTTTGAATTCGTTTCCGGAAGAGCTCA ATCG
	ΔugtP::*km*	ugtP-BamHI_for	AAAAGGATCCCTGCGAGAGAACACCTT G
	Primers H	ugtP-km_rev	CCTATCACCTCAAATGGTTCGCTGTTA GAAACTGTTACATGCTG
		km-ugtP_for	CAGCATGTAACAGTTTCTAACAGCGAA CCATTTGAGGTGATAGG
		km-ugtP_rev	CACTTCAGAGGAGTTTGCTCGATACAA ATTCCTCGTAGGCGCTCGG
		ugtP-km_for	CCGAGCGCCTACGAGGAATTTGTATCG AGCAAACTCCTCTGAAGTG
		ugtP-SalI_rev	TTTTGTCGACATCCGTAAAGCCGGTCT G

7.3.3 Agarose gel electrophoresis

To verify PCR reactions, DNA was separated by DNA agarose gel electrophoresis. 0.8 % agarose was boiled in TAE buffer for dissolving and then polymerized with 0.5 mg/ml ethidium bromide. DNA was diluted with 3x DNA loading dye, loaded on the agarose gel and run at 150 V. 1 kb ladder (New England Biolabs) was used as the standard. The DNA was visualized under UV light.

7.3.4 Digestion and purification

Plasmids and PCR products were digested with appropriate restriction enzymes (New England Biolabs). Information for the reaction mix and the incubation protocol are shown below. After digestion, fragments were purified from agarose gels subjected to electrophoresis as described above.

Digestion	5 µl 10x appropriate digestion buffer (enzyme dependent) 1 µl each restriction enzyme 30 µl template a.d. 50 µl H_2O	Protocol	2 h at 37 °C Clean-up with agarose gel

7.3.5 Ligation and dialysis

Digested plasmids and PCR products (inserts) were ligated according to the reaction mix and the incubation protocol shown below (New England Biolabs). If required for subsequent steps, the reaction mixes were subjected to dialysis with filter discs (Millipore) on H_2O for 20 min after ligation.

Ligation	1.5 µl 10x T4 DNA ligase buffer 0.8 µl T4 DNA ligase insert:vector at ratio 2:1 a.d. 15 µl H_2O	Protocol	3 h at RT Desalt with dialysis

7.3.6 Plasmid transformation in *E. coli*

Plasmids were transformed into previously prepared chemo- or electrocompetent *E. coli* cells.

Chemocompetent *E. coli*

To obtain chemocompetent cells, an *E. coli* LB culture was inoculated 1:100 from ONC and grown until OD_{600} = 0.4-0.5. Culture were chilled for 15 min, pelleted (2000 x g, 15 min, 4 °C), resuspended in 0.3 V ice-cold buffer TFB1 and chilled on ice for 5 min. Cells were then resuspended in 0.04 V ice-cold buffer TFB2, chilled on ice for 5 min, aliquoted in 50 µl, frozen in liquid nitrogen and stored at -80 °C until use. For transformation of plasmids, aliquots of chemocompetent cells were thawed on ice in the presence of 1 µl purified plasmid or 15 µl ligation product and incubated on ice for 30 min. Cells were heat-shocked at 42 °C for 30 s, chilled on ice for 5 min, incubated in 400 µl LB for 1 h at 37 °C before plating on LB supplemented with ampicillin (100 µg/ml) and grown overnight at 37 °C.

Electrocompetent *E. coli*

Electrocompetent *E. coli* were obtained by inoculating a LB culture 1:100 from ONC and growing it until OD_{600} = 0.5-0.6. Cultures were chilled for 15 min, pelleted (2000 x g, 20 min, 4 °C) and washed with 1 V and 0.5 V of ice-cold H_2O. The pellet was washed with 0.1 V 10 % ice-cold glycerol, the supernatant carefully removed, the pellet resuspended in 0.003 V 10 % ice-cold glycerol, 50 µl aliquots prepared and frozen in liquid nitrogen. Electrocompetent cells were stored at -80 °C until use. For transformation of plasmids, aliquots of electrocompetent cells were thawed on ice in the presence of 1 µl of purified plasmid or 4 µl of dialyzed ligation product. Cells were transferred to an electroporation cuvette (1 mm, cell projects), electroporated with one electric pulse (1.8 kV, 5 ms) and incubated in 400 µl LB for 1 h at 37 °C before plating on LB supplemented with ampicillin (100 µg/ml) and grown overnight at 37 °C.

7.3.7 Sequencing

Sequences of plasmids or joining-PCR products were confirmed by sequencing prior to transformation into *B. subtilis*. 5 µl primer (5 µM) and 5 µl template were mixed and sent for sequencing (Macrogen). Alignments to compare desired and real sequences were generated and analyzed.

7.3.8 Transformation of *B. subtilis*

B. subtilis PY79 recipient strains were grown in competence medium (MC) (Magnuson et al., 1994) at 37 °C until late-exponential, early-stationary phase to reach natural competence (~5-6 h). Donor genomic DNA, PCR products or plasmids were added to the competent cells and further incubated for 3 h at 37 °C. Integrative plasmids were linearized prior to transformation. These conditions allow DNA uptake into cells coupled to homologous recombination for chromosome integration. Cells were plated on LB supplemented with appropriate antibiotics at the following concentrations: chloramphenicol 5 µg/ml, erythromycin 1 µg/ml, lincomycin 25 µg/ml, kanamycin 10 µg/ml, spectinomycin 100 µg/ml, tetracycline 5 µg/ml.

7.3.9 *B. subtilis* SPP1 phage transduction

Donor strains were grown in TY medium until stationary phase (Yasbin and Young, 1974). 200 µl cells were incubated with 100 µl of SPP1 phage stock in different dilutions, incubated at RT for 30 min, and plated on TY with the addition of 3 ml TY soft agar (5 g/l Bacto Agar, BD Biosciences). After incubation overnight at 37 °C the phages were harvested from the plate that showed confluent lysis with plaques that were still visible. Phage harvest was done by addition of 5 ml liquid TY, scraping off of the soft agar, isolating phages form soft agar by vortexing and pelleting of the soft agar. The supernatant contains the phages and was filtered twice (0.22 µm, GE Healthcare).

Recipient strains were grown in TY medium until stationary phase. 1 ml culture was added to 9 ml prewarmed TY with 100 µl SPP1 phages and incubated at 37 °C for 1 h. Cells were pelleted and plated on LB 10 mM sodium citrate with appropriate antibiotics.

7.3.10 Cryoconservation of bacterial strains

Confirmed strains were grown on LB agar plates with appropriate antibiotics if necessary. The whole biomass was resuspended in 800 µl LB and then mixed with 200 µl 85 % glycerol. The cells were stored in cryogenic vials at -80 °C.

7.3.11 Construction of strains

In this work, several strategies were used to create different constructs. A plasmid replicative in Gram-positive bacteria, deletion mutants and fluorescently labeled proteins were generated. Information on the general methods are listed below and specific information can be found in the strain and primer lists. A complete list of plasmids and strains used in this study can be found in Table 1 and Table 2, respectively. Primers are listed in Table 3.

Design of a plasmid replicative in Gram-positive bacteria

To construct a replicative plasmid in *B. subtilis*, the backbone of the shuttle vector pJL-sar-gfp was used (Liese et al., 2013). It contains an ori and the ampicillin resistance cassette for selection in *E. coli*, and an ori and the erythromycin resistance cassette for selection in Gram-positive bacteria. The *sar-gfp* insert was replaced with the multiple cloning site originating from pMAD (Arnaud et al., 2004). Using this backbone, different variants of the plasmid were generated that contain distinct antibiotic-resistance

cassettes suitable for selection in Gram-positive bacteria (Figure 53) (see sequence in chapter 9.2 APPENDIX I).

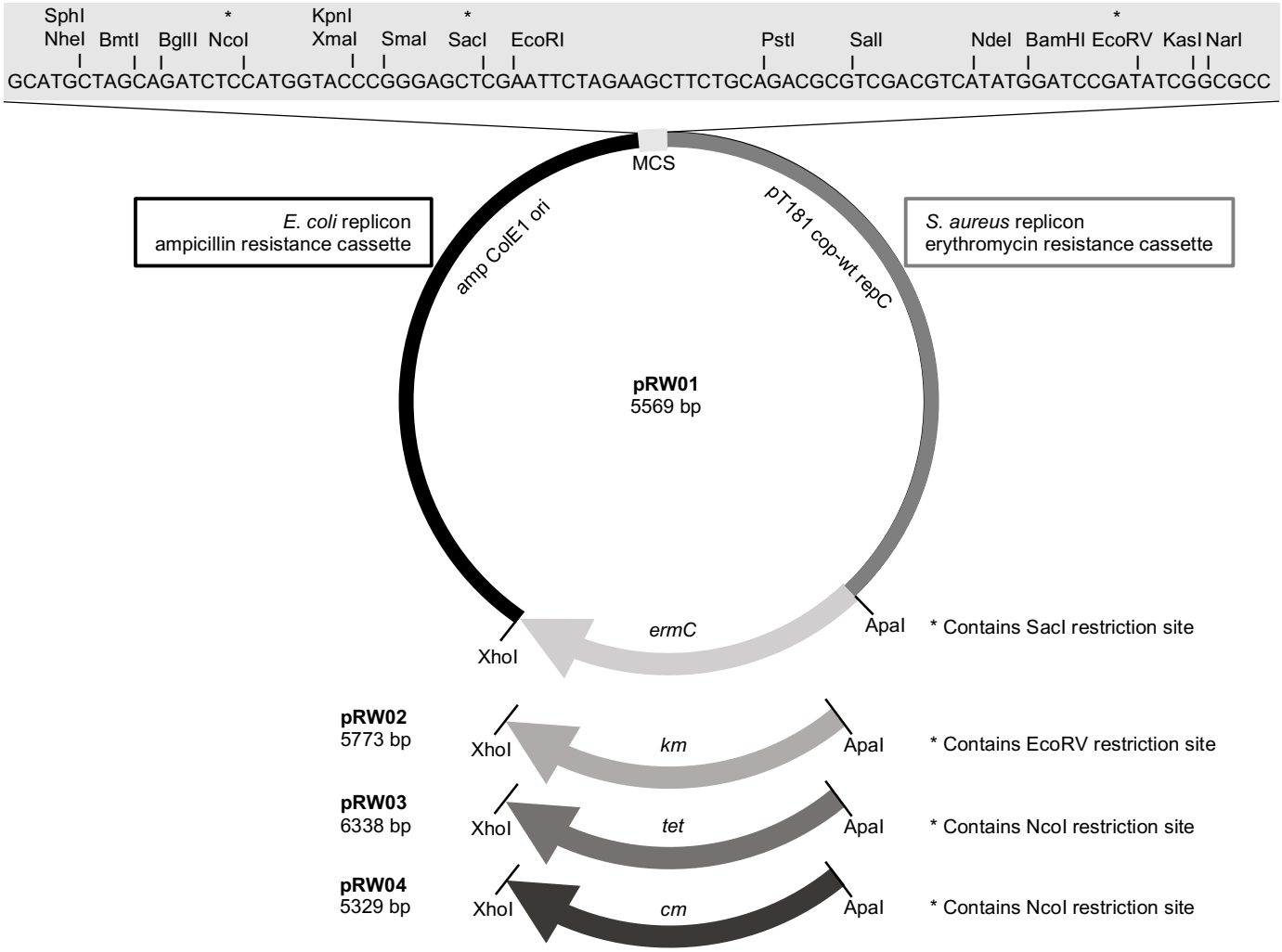

Figure 53: Design of a plasmid replicative in *B. subtilis*. The shuttle vector pJL-sar-gfp contains an ori with an ampicillin resistance for proliferation in *E. coli* and an ori with an erythromycin resistance for selection in Gram-positive bacteria (Liese et al., 2013). It was used as a backbone to replace the sar-gfp insert with a multiple cloning site (MCS) to generate pRW001. Several versions of the plasmid with different antibiotic resistance cassettes for Gram-positive bacteria were then constructed. The sequences of the plasmids can be found in chapter 9.2 APPENDIX I.

Joining of individual fragments – primer design

If individual PCR fragments needed to be joined into a single fragment, joining PCR was used. Primers were designed for the fragments to obtain 40 nt overlapping sequences, 20 nt belonging to the respective PCR product and 20 nt overlap of the upstream or downstream PCR product which will be amplified with the reverse complement primer. The forward primer of the most upstream fragment and the reverse primer of the most downstream fragment were then used during joining-PCR (see chapter 7.3.2).

Fluorescently labeled fusion-proteins

If proteins were to be expressed as a N- or C-terminal GFP-fusion under the xylose promotor at the neutral *amyE* locus, proteins were amplified and cloned into the pSG1729 or pSG1154 plasmid,

respectively. In other cases, promotor, protein and fluorescent marker were PCR amplified (for N-terminal labeling the stop codon of the marker was omitted, for C-terminal labeling the stop codon of the protein was omitted during primer design), joined and either transformed directly into *B. subtilis* (see chapter 7.3.8) or cloned into appropriate plasmids, if desired. Plasmid pDR183 integrates at the neutral *lacA* locus and pRW01-04 are replicative plasmids that do not integrate into the genome.

Deletion mutants

Mutants were constructed by PCR amplification of 0.7-1.0 kb regions flanking the gene to be deleted which was replaced by an antibiotic resistance marker. PCR products of upstream fragment, antibiotic resistance marker and downstream fragment were joined and joining-PCR products used directly for transformation in *B. subtilis* (see chapter 7.3.8).

The flotillin-labeled actin-homolog mutation strains were constructed by successively deleting individual genes in the flotillin-labeled strains RW578 and RW579. Genomic DNA of the Δ*mreB* Δ*mreBH* Δ*mbl* Δ*rsgI* donor strain (#4277 of the Errington laboratory (Schirner and Errington, 2009)) was added to the competent FloA- or FloT-GFP labeled strains and desired mutations enforced with appropriate antibiotics. Antibiotic pressure was reduced by omitting the addition of antibiotics of resistance cassettes that were present in donor and acceptor strains. The resulting strains were grown in LB supplemented with 20 mM $MgSO_4$. Despite genotypic confirmation of the deletions, the strain RW617 demonstrated an unstable phenotype. Repeatedly, a proportion of cells reverted to a rod-shaped phenotype for an unknown reason. For analysis, only spherical cells were used.

Chimeric flotillins

Flotillin domains were predicted using SMART (Letunic et al., 2015; Letunic and Bork, 2018) to construct chimeric flotillins. The sequence reaching as far as the end of the predicted PHB domain was defined as the N-terminus. The rest of the protein was defined as the C-terminus. Adaptation of the transition was performed according to secondary structure prediction analysis with Phyre^2 (Kelley et al., 2015). Using overlap PCR, the N-terminus of one flotillin was joined with the C-terminus of the other and cloned into appropriate plasmids. Chimeric flotillins were expressed under the native promoter of the N-terminal flotillin at the *amyE* or *lacA* neutral locus or from a replicative plasmid.

7.4 Fluorescence microscopy

7.4.1 Sample preparation

Samples were prepared according to different protocols depending on the experiment to be performed.

Sample preparation to visualize different strains and treatments

Cells were grown to early (FloA) or late (FloT) exponential phase in liquid LB, washed with PBS and mounted on agarose-coated microscope slides, covered with a coverslip of thickness #1.5 and imaged immediately. To maintain MreB functionality for an extended period of time, the agarose was supplemented with 10 % LB. Additionally, the agarose was carved into stripes (width ~5 mm) alternating with empty spaces allowing the access of oxygen. If required, cells were subjected to treatments with several compounds prior to image acquisition. In these cases, PBS and agarose was supplemented

with these compounds as well. Concentrations used are derived from appropriate studies published (Table 4). If not applicable, 10x MIC was used. Treatments lasted for 90 min, except for benzyl alcohol, where treatment lasted 5 min.

Table 4: Activity, MIC and concentration of antibiotics used in this work.

Target structure	Compound[a]	MIC[b]	Concentration[c]	Effect	Reference
Membrane					
Lipid bilayer	Benzyl alcohol (BNZ)	nd	30 mM	Increases membrane fluidity	(Strahl et al., 2014)
Lipid II	Nisin (NIS)	nd	30 µM	Membrane pore formation	(Strahl and Hamoen, 2010)
K^+-ions	Valinomycin (VAL)	nd	60 µM[d]	Abolishes electro-chemical gradients	(Strahl and Hamoen, 2010)
Cell wall					
MurA	Fosfomycin (FOS)	250 µg/ml	2.5 mg/ml	Inhibits first step in cell wall synthesis	
TagO MraY	Tunicamycin (TUN)	0.5 µg/ml	0.025 µg/ml 2.5 µg/ml	Inhibits glycosylation of UPP with WTA and Lipid II precursors	(Campbell et al., 2011)
Class b PBPs	Ampicillin (AMP)	100 µg/ml	1 mg/ml	Inhibits transpeptidation reaction of PBPs	
D-Ala-D-Ala of pentapeptide	Vancomycin (VAN)	0.5 µg/ml	5 µg/ml	Sterically inhibits transpeptidation	

[a] Parenthesis define abbreviations used in this study.

[b] nd = not determined

[c] If available, the same concentrations as in appropriate published studies were used, if not, 10x MIC was used. For tunicamycin, concentrations were extrapolated according to the MIC and the referenced study performed in *S. aureus*.

[d] Valinomycin was used in the presence of 300 mM KCl and 50 mM Hepes pH 7.5.

In each experiment of this work, a control sample was used as a reference for the specific day-conditions, called the respective control. After all treatments, flotillin mobility was analyzed and cell viability confirmed via CFU/ml counts. Additional control experiments were performed after specific treatments to check for possible changes in cell width, membrane permeability and potential, polar lipids, fatty acid composition, LTA abundance and detergent resistance. See below for details.

Sample preparation to visualize protoplasts

To generated protoplasts overnight cultures were resuspended in SM buffer (Renner et al., 2013) with lysozyme (200 µg/ml) and incubated at 37 °C for 30 min. Protoplasts were pelleted (4700 x g, 1 min, RT) and resuspended in SM buffer by carefully flicking the tube.

Sample preparation to visualize colocalization

To determine protein colocalization, cells were grown on MSgg plates for 24 h at 30 °C. Biomass was fixed (see chapter 7.1.3), washed three times with PBS, resuspended in GTE, and stored at 4 °C until image acquisition (maximum 1 week).

7.4.2 Fluorescence microscopes

Epifluorescence microscope

For epifluorescence image acquisition a Leica DMI600B epifluorescence system (equipped with a Leica CRT6000 illumination system, an HCX PL APO oil immersion objective [100 x 1.47], and a Leica DFC630FX color camera) or an epifluorescence Leica DMi8 S System (equipped with a CoolLED pE4000 illumination system, an HCX PL APO oil immersion objective [100 x 1.47], and a Hamamatsu Orca-Flash 4.0 sCMOS camera) was used.

The microscope setup to capture flotillin mobility was chosen to obtain an acceptable signal intensity that is maintained for a decent amount of time. Lower exposure times might increase the duration of the signal, but would decrease the signal intensity. This would preclude reliable analysis due to insufficient differences of the signal compared to the background noise. Therefore, to study the mobility of FloA- and FloT-GFP, pictures were taken every 300 ms for at least 9 s with 200 ms exposure time (Figure 54a).

Total internal reflection fluorescent microscope

For total internal reflection fluorescent microscopy (TIRFM) a Leica DMi8 S System (equipped with a TIRF Infinity HP module, a WSU unit with 488 nm and 561 nm solid state lasers [110 nm penetration depth], an HCX PL APO oil immersion objective [100 x 1.47], and a Hamamatsu Orca-Flash 4.0 sCMOS camera) was used. Samples were prepared as previously described. To monitor flotillin mobility, images were acquired every 200 ms over a 20 s period. To monitor the MreB movement, images were acquired every 1 s for 100 s in cells and every 300 ms for 60 s in protoplasts. PBP3 and DltD dynamics were acquired every 300 ms for 9 s and compared to flotillins whose signals were acquired with the same parameters.

For simultaneous TIRFM image acquisition, the Leica DMi8 S System was additionally equipped with a W-VIEW GEMINI image splitter (Hamamatsu) with a dichroic mirror and bandpass filters specific for GFP (525/50) and mCherry (630/60). Flotillins and MreB were imaged simultaneously, implying that exposure specifications for the green and the red channels are the same. Protein mobilities and fluorophore signal intensities differ. Short frame intervals (to monitor FloA and FloT) over a long time (to monitor MreB) would be necessary (≤300 ms for ~15 s) to visualize the mobility simultaneously. However, longer exposure times are necessary (~1 s) to obtain a suitable signal intensity of red fluorophores in *B. subtilis*. Exposure times still have to be kept as low as possible, to prevent blurring of the flotillin signal due to their faster mobility. Furthermore, fast bleaching of red fluorophores prevents image acquisition over a large number of frames (<10 frames). Therefore, simultaneous visualization of the mobility of flotillins and MreB was technically and biologically impossible. Images were acquired every 2 s for 14 s to monitor MreB mobility and contemporaneous flotillin location.

7.4.3 Image processing and mobility analysis

Microscopy images were analyzed and processed using Fiji software (Schindelin et al., 2012). Depending on the analysis, different functions and plugins were used.

Image processing

For cell width measurements the MicrobeJ plugin was used (Ducret et al., 2016). Brightfield images were used and cells detected (N≥30 cells per image) and their cell width determined automatically.

Colocalization was analyzed with Pearson correlation coefficient using the JACoP plugin (Bolte and Cordelieres, 2006). It is a means to measure the linear correlation, i.e. the degree of colocalization, of two parameters. A total positive linear correlation has the value 1 and 0 defines no linear correlation. This translates to colocalization studies in that the higher the value, the more colocalization.

Mobility analysis

Kymographs were generated by marking the membrane signal to be monitored with a line and using the 'Reslice' function of Fiji (parameters: no interpolation). Kymographs are space-time plots that display mobility in a single image (Figure 54b). For that, the signal of the lateral membrane was used and automatically plotted underneath the signal of the previous time point. Kymographs depend on the direction of movement in relation to the membrane area under observation (Figure 11). The resulting image allows the tracking of the mobility and is a direct analysis method. Corresponding membrane signals are specified in the respective figures.

Maximum intensity projection (MIP) images were generated with the 'Z Project…' function of Fiji. A temporal image sequence is summarized with MIP into a single image. Every pixel of the final image, depicts the pixel with the highest signal intensity throughout the whole image sequence. The resulting image summarizes the signals visible in the course of the image sequence and is a direct analysis method.

Mobility was analyzed quantitatively using the plugin Trackmate (Tinevez et al., 2017). Trackmate detects spots and temporally and spatially links them into individual trajectories according to input parameters and therefore, represents an indirect analysis method. Input parameters were set as follows: LOG detector 0.3 µm diameter spot detection (automatic spot quality filter, manually adjusted to include all visible foci, if applicable), LAP tracker (0.2 µm frame-to-frame linking distance, excluding gap closing, including splitting and merging), ≥ 4 foci per track; N≥400 tracks (Figure 54c). Trackmate overlays the individual trajectories with the fluorescent signal and thus allows visualization of the dynamics of individual flotillin foci. Trajectories were collected from several independent experiments (N of total trajectories is specified in the figure legends and in chapter 9.6 APPENDIX I).

Trackmate furthermore creates files that contain x- and y-positions of flotillin foci for each time point sorted according to the trajectories they are part of. For each trajectory the speed is also provided. The output values of Trackmate depend on the input parameters (listed above); accordingly, the absolute output values vary using different input parameters, but the relative values comparing controls to

experimental condition do not. To compare results from different experiments with each other the individual controls are normalized. All controls of FloA and all controls of FloT were averaged independently and plotted in relation to the average of FloA which was set to 1 (Figure 54d right) and the experimental condition was determined in relation to that.

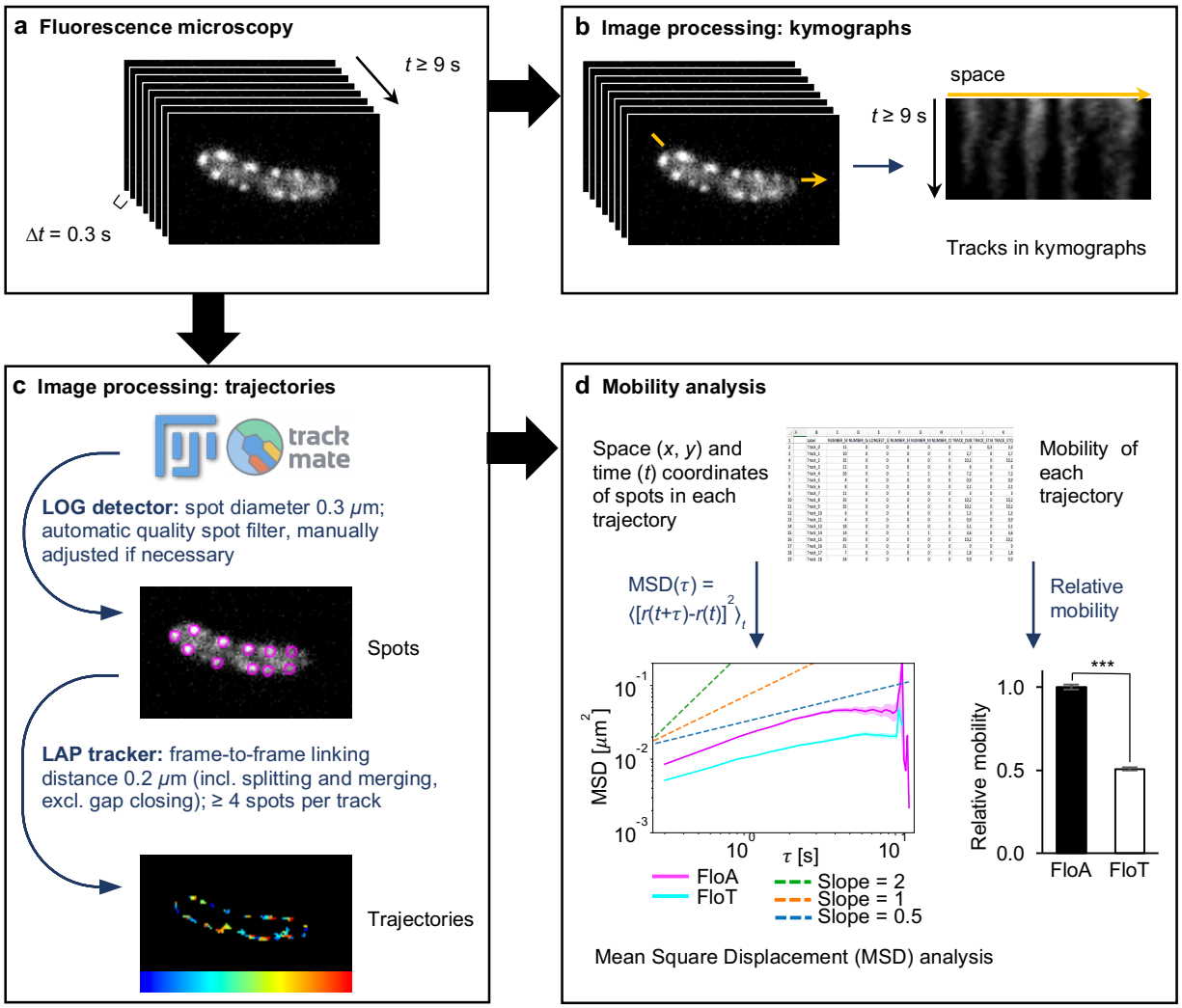

Figure 54: Schematic representation of image analysis and mobility determination. a) Schematic representation of the images acquired with fluorescence microscopy. Images are acquired every 300 ms for 9 s. b) Schematic representation of kymograph creation. The membrane signal that is used to generate the kymographs is marked with a yellow arrow. c) Schematic representation of trajectory analysis. The software Fiji (Schindelin et al., 2012) with the plugin Trackmate (Tinevez et al., 2017) is used to detect spots (LOG detector, top) and link them to trajectories (LAP tracker, bottom). Trajectories are overlaid with the fluorescence signal. Colors indicate elapsing time from blue to red. d) Schematic representation of mobility analysis. Space (x and y) and time (t) coordinates for each spot in a trajectory are collected during trajectory analysis, as well as its mobility. This information is used to calculate the mean square displacement (MSD) which is plotted against the time intervals τ. Plots show the means with shaded areas representing the 95% confidence intervals. Bar chart shows the mobility information from trajectory analysis normalized to FloA and represented in relative numbers.

The spatial (x and y) and temporal (t) information for each trajectory provided by Trackmate were then used to characterize the mobility profile by mean square displacement (MSD) analysis. Trajectories that included splitting and merging events were excluded from this analysis. MSD analyses were performed by biophysicists from the laboratory of Prof. PhD Ned Wingreen at Princeton University using a code written in Python. The trajectories r(t) = (x(t),y(t)) generated via Trackmate were used to calculate MSD as a function of time intervals τ, MSD(τ) = <[r(t+τ)-r(t)]^2>, where the mean is over time t. The mean of MSD is plotted against time intervals with the 95 % bootstrap confidence interval represented as shaded

areas. MSD plots reveal two characteristics for mobility analysis. Firstly, the y-intercept determines the level of the movement, the diffusion coefficient. The higher the diffusion coefficient, the faster the movement. In general, the diffusion coefficient depends on the temperature, the viscosity of the medium and the radius of the particle (Einstein, 1905), where the only difference of FloA and FloT supposedly is their radius. Secondly, the slope of the graph characterizes the movement further, with a slope of <1 corresponding to subdiffusion, a slope of =1 to normal diffusion, and a slope >1 to superdiffusion (Saxton, 2007). Subdiffusion results from impediments reducing diffusivity and superdiffusion occurs due to a local increase in diffusivity. Generally, only early and intermediate time points are paid attention to, as later time points are intrinsically less reliable. In every experiment an untreated control was included. As output parameters depend on the Trackmate input parameters, the experiments are only compared to their respective control (within the same plot) but not between each other (different plots).

TIRFM corrections

The TIRFM output consists of two-dimensional images of the curved surface of three-dimensional cells. To overcome this spatial discrepancy, in several studies that quantify the diffusion coefficients of membrane proteins, correction calculations have been used (Oswald et al., 2014, 2016; Lucena et al., 2018). However, in the present work, the diffusion of the membrane proteins was compared under different experimental conditions. No absolute diffusion coefficients were specified which obviated the need for any spatial correction of the TIRFM images.

7.5 Biochemistry methods

7.5.1 Cellular fractionation of *B. subtilis* cultures

Fast cell-extract

Cells were grown in 1 ml LB ON, pelleted, resuspended in 50 µl PBS and lysed with 1 mg/ml lysozyme for 30 min at 37 °C and 15 min boiling with 1x SDS sample buffer. Samples were used immediately, or kept at RT for short-term storage.

Cell fractionation and membrane harvest

Cells were grown in liquid cultures inoculated 1:100 from ONC. The duration of growth is specified for each experiment individually. Cell pellets were resuspended in PBS, lysed with lysozyme (0.1 mg/ml) for 30 min at 37 °C and sonication, supplemented with 1 mM PMSF for protease inhibition. Leftover cells that were not lysed were pelleted (12,000 x g, 30 min, 4 °C). The remaining cleared whole cell extract was ultracentrifuged (200,000 x g, 1 h, 4 °C) to separate the soluble cytosolic fraction from the pelleted membrane fraction. Membrane pellets were resuspended in PBS supplemented with 1 mM PMSF with or without DDM (n-dodecyl-B-D-maltoside (Glycon), the concentration for each experiment is specified) and homogenized in a sonication water bath. Membranes were used immediately or kept at 4 °C for short-term or at -20 °C for long-term storage.

Separation of detergent resistant and detergent sensitive membrane fractions

The CelLytic MEM Protein Extraction Kit (Sigma) was used to separate the detergent resistant membrane (DRM) from the detergent sensitive membrane (DSM) fraction (Brown, 2002). 600 µl of lysis

and separation buffer was added to 50 µl of resuspended membrane (corresponding to membrane harvested from roughly 10 ml culture of OD_{600} = 3) and incubated in agitation at 4 °C ON. Insolubilized membranes were pelleted (17,000 x g, 30 min, 4 °C) and the supernatant used for DRM/DSM separation. Samples were incubated for 20 min at 37°C and centrifuged (3000 x g, 3 min, RT) for phase separation. The upper DSM fraction was collected and the lower DRM fraction washed three times with 400 µl PBS (20 min on ice, 20 min at 37 °C, centrifugation for phase separation). The proteins of the DRM and DSM fractions were then precipitated with 20 % trichloroacetic acid (TCA) and resuspended in 0.25 V of 1x SDS sample buffer.

7.5.2 Protein separation

SDS-PAGE

Samples to be analyzed were denatured by adding 1x SDS sample buffer and boiling for 5 min. Samples were loaded on 12 % SDS-PAGE gels (1 mm, 15 wells, composition see chapter 7.1.3) and subjected to electrophoresis in 1x running buffer at 180 V for 1 h. To visualize the whole protein content of the gels, they were stained with BlueSafe (NZYTech) by addition of the protein dye and subsequent boiling in the microwave for 30 s and agitation at RT until protein bands were visible.

Western blot and immunodetection

To visualize specific proteins in SDS-PAGE, western blots were performed. Proteins from the gels were transferred to nitrocellulose membranes using the Trans-Blot Turbo Transfer System (Bio-Rad, Standard program). Membranes were blocked in 10 % skimmed milk in TBS-T, incubated with the primary antibody for 2 h at RT, washed three times for 10 min in TBS-T and incubated with the secondary antibody conjugated to horseradish-peroxidase (HRP) for 1 h at RT. HRP activity was detected with chemiluminescence (ChemiDoc™ Imaging System, Bio-Rad). Antibodies were used at the following dilutions: rabbit anti-GFP IgG (recombinant monoclonal, Invitrogen) 1:1000 for native blots; rabbit anti-GFP (polyclonal, Takara) 1:5000 for denatured blots; rabbit anti-mCherry IgG (polyclonal, BioVision) 1:5000; goat anti-rabbit IgG HRP-conjugate (Bio-Rad) 1:20,000.

Blue-native PAGE

The NativePAGE™ Novex system (Invitrogen) was used for blue-native (BN) PAGE (Swamy et al., 2006; Wittig et al., 2006). Cells were grown on MSgg plates at 30 °C for 24 h prior to membrane harvest. Membranes were incubated with 0.1 % DDM in 1x NativePAGE™ Sample Buffer with agitation at 4 °C ON. Insolubilized membrane was pelleted (17,000 x g, 30 min, 4 °C), and solubilized membrane samples stained with 0.5 % Coomassie G-250 Sample Additive. Samples were loaded on 3-12 % Bis-Tris gradient gels and subjected to electrophoresis in Dark Blue Cathode Buffer (1x Running Buffer with 1x blue Cathode Buffer Additive containing 0.02 % Coomassie G-250) at 150 V for 30 min. The Dark Blue Cathode Buffer was exchanged for Light Blue Cathode Buffer (1x Running Buffer with 0.1x Cathode Buffer Additive containing 0.02 % Coomassie G-250) and run at 250 V for 1 h. Gels were carefully removed from the cassette and incubated in 1 % SDS in 5 mM Tris-HCl pH 8 for 15 min. Proteins were transferred to PVDF membranes in a wet blot system (Bio-Rad, 0.35 A, 1.5 h) and fixed on membranes

by incubation in 8 % acetic acid for 15 min. Membranes were rinsed with water, dried, the Coomassie removed with methanol to visualize the marker, and then further processed like regular western blots.

7.5.3 Mass spectrometry, protein identification and analysis

Pull-down assays

For pull-down analysis, 500 µl of membranes from stationary cells were solubilized overnight with 1 % DDM in agitation. Insolubilized membranes were pelleted (17,000 x g, 30 min, 4 °C) and the supernatant incubated with 25 µl of GFP-Trap resin (ChromoTek) that was previously equilibrated with three washes of 500 µl PBS (2500 x g, 5 min, 4 °C). After 2 h at 4 °C in agitation, the flowthrough was collected by centrifugation and the resin washed three times with 500 µl PBS before elution with 50 µl of 2x SDS-loading buffer.

For targeted pull-down analysis, double-labeled strains were used. The elution fractions were subjected to SDS-PAGE and western blot with immunodetection. Conditions to be compared were blotted on the same membrane. Quantification was performed by normalizing the GFP signal intensity of the elution fraction and determining each mCherry signal intensity in relation to the GFP signal intensity.

For global pull-down analysis, a Δ*floA* Δ*floT* double knockout strain background with GFP-labeled flotillin was used. The elution fractions were subjected to SDS-PAGE and stained with Coomassie. Each individual lane was cut into several pieces and proteins fixed in the gel. The protein content of each sample was analyzed by mass spectrometry and its proteins identified. The results for each lane are the assembly of the results of the individual pieces examined.

Excised protein bands were subjected to in-gel digestion and processed automatically using a Proteineer DP device (Bruker Daltonics). Peptides were analyzed using a 1D-nano liquid chromatography apparatus coupled to a high-speed time-of-flight mass spectrometer with a nanospray III ionization source (Eksigent Technologies NanoLC Ultra 1D plus and TripleTOF 5600, SCIEX). Data were collected with Analyst TF v.1.7 software and processed with PeakView v.2.2 software (both SCIEX). The detected peptides were compared against the genome of *B. subtilis* PY79 using the Mascot Server v.2.6.1 (Matrix Science).

Only proteins with peptide-to-spectrum matches (PSM) of ≥2 were considered for data analysis. The PSM of each identified protein was normalized to the control (normalized spectral abundance factor, NSAF) and the fold change in abundance determined against the control. Proteins were identified in the UniProt and NCBI databases via the provided accession numbers. Attention was only given to membrane proteins and their functional categories assigned according to the *Subti*wiki (Zhu and Stülke, 2018) classification. If a protein was classified into several functional categories, the most suitable was selected. Some functional categories were subdivided into subcategories to further specify protein function. The subcategories ‘transporters’ and ‘cell envelope and cell division’ belong to the main category “cellular processes”, and the subcategories ‘coping with stress’, ‘exponential and early post-exponential lifestyles’ and ‘sporulation’ belong to the main category “lifestyles”. The binding of membrane proteins was considered enriched when the abundance in the sample exceeded the

abundance in the control. The binding of membrane proteins to FloA or FloT was considered preferential when a threshold 1:1.25-fold enrichment difference was surpassed. To visualize the binding of proteins to FloA, FloT, $FloT_{nt}A_{ct}$ and $FloA_{nt}T_{ct}$ globally, a heatmap was generated. Fold changes for membrane proteins were transformed to log_{10} scale (Table 6) and visualized using Heatmapper software (Babicki et al., 2016) with the following input parameters: expression, no scaling, no clustering. Proteins not identified in a sample were manually assigned to the lowest fold-change value (shown in dark blue). Pull-down raw data can be found in Table 7, Table 8, Table 9, Table 10 and Table 11.

Visualization of penicillin binding proteins in DRM/DSM fractions

Bocillin is a penicillin that covalently binds to the transpeptidase domain of PBPs (Kocaoglu et al., 2012). A fluorescent variant of bocillin, Bocillin-FL, was used to stain membranes isolated from exponential cultures. PBPs were labeled with 100 µg/ml Bocillin-FL (Invitrogen) for 30 min at 37 °C in agitation prior to the addition of the lysis and separation buffer and subsequent DRM/DSM separation and protein precipitation. Samples were subjected to SDS-PAGE and the signal of Bocillin-FL was visualized in-gel with the ChemiDoc Flamingo Application (Bio-Rad). The protein marker used for SDS-PAGE shows strong fluorescence in these conditions. Therefore, its use is reduced to a minimum (0.2 µl) and a barrier of several empty wells was necessary to avoid signal scattering. As the Bocillin-FL signal intensity was not very high, protein loading was maximized to 15 µl per well (opposing 1 µl for BlueSafe loading controls). The Bocillin-FL signal does not persist after BlueSafe staining or in-gel fixation. The Bocillin-FL bands were cut under UV-light, fixed, and identified by peptide mass fingerprinting.

Samples were in-gel digested and analyzed using MALDI-TOF/TOF (Abi 4800 MALDI TOF/TOF mass spectrometer, SCIEX). Data were acquired using ABi 4000 Series Explorer Spot Set Manager software and processed using ABi 4000 Series Explorer Software v.3.6 (both SCIEX). The detected peptides were compared against the genome of *B. subtilis* PY79 using the Mascot Server v.2.6.1 (Matrix Science). Only peptides with an individual score above the identity threshold were considered as correctly identified, and attention paid only to identified PBPs.

Due to the relatively low cellular abundance of several PBPs it was not possible to obtain an entire profile of all PBPs during DRM/DSM membrane separation. Likewise, due to high signal-to-noise ratio with non-Bocillin-FL-stained membrane proteins not all bands visible in DRM and DSM fractions could be unequivocally identified with mass spectrometry fingerprinting.

7.5.4 Analysis of membrane properties and composition

Analyzing membrane properties with fluorescent dyes

Several dyes were used to visualize and confirm the activity of membrane-active compounds. The dyes were added for the last 15 min of the treatments with NIS and VAL or simultaneously with BNZ treatment. The membrane potential was analyzed with the cytoplasmic dye 3,3'-diethyloxacarboxyanine iodide ($DiOC_2(3)$), added to a final concentration of 30 nM. In intact cells, the dye $DiOC_2(3)$ accumulates in the cytoplasm due to an intact membrane potential (Novo et al., 1999). The accumulation is accompanied by a fluorescent shift from green to red (Novo et al., 1999). The fraction of cells with a green fluorescent signal was monitored, corresponding to alterations in the membrane potential. The state of membrane

permeability was studied with the LIVE/DEAD BacLight Bacterial Viability Kit (Invitrogen) (Boulos et al., 1999). It contains two dyes, propidium iodine and SYTO-9 which emit red and green fluorescence, respectively. SYTO-9 is a nucleic-acid stain that labels all bacterial cells. Propidium iodine can only enter cells with compromised membrane permeability and accumulates in the cytoplasm where it conceals the green fluorescent signal. The two dyes of the kit were used at a 1:1 ratio at 1:1000 dilutions and the fraction of cells with a red fluorescent signal monitored, corresponding to alterations in membrane permeability.

Membrane lipid analysis

For analyses of polar lipids and the composition of cellular fatty acid, cells were grown until exponential phase and treated with AMP, VAN and VAL for 90 min. 200 mg of lyophilized cell pellet was used in analyses. The samples were subjected to gas chromatography coupled to mass spectrometry, to determine the fatty acid composition (Table 5). Polar lipids were analyzed by 2D thin layer chromatography and annotated according to known standards. Cellular fatty acid and polar lipid analyses were performed by the identification service of the German Collection of Microorganisms and Cell Cultures GmbH (DSMZ) in Braunschweig, Germany.

Lipoteichoic acid isolation and quantification with ELISA

To compare lipoteichoic acids (LTA) contents, existing protocols were modified (Lu et al., 2009). Cultures were harvested after treatment with AMP, FOS, TUN, VAN and VAL. Pellets were washed with 0.5 and 0.25 V of LTA buffer and resuspended in LTA buffer (1 ml for OD_{600} = 20). 700 µl sample was disrupted in a Geno/Grinder® (SPEX® SamplePrep) with 250 µl acid-washed glass beads and the glass beads sedimented (200 x g, 5 min, RT). The supernatant was incubated with an equal volume of n-butanol with agitation at RT for 30 min. After phase-separation (17,000 x g, 20 min, RT) the lower aqueous phase containing LTA was collected. 100 µl sample was added to each well of a high-binding 96-well plate (Sarstedt) and incubated overnight at RT to allow immobilization. The immobilized samples were blocked with 3 % skimmed milk in TBS-T for 2 h at RT and incubated with 50 µl lipoteichoic acid monoclonal antibody (clone 55, HycultBiotech) at 1:50 dilution for 2 h at RT. Wells were washed 5x 3 min with TBS-T and incubated with 50 µl 1:500 HRP-conjugated goat anti-mouse antibody (Thermo Fisher) for 2 h followed by 5x 3 min washes with TBS-T. 100 µl of developing solution was added, incubated in the dark, and the reaction stopped after 20 min with the addition of 50 µl H_2SO_4 1 M. The absorbance at 490 nm was then determined and the signal intensity of treated cultures was compared to the untreated control.

Detergent resistance after antibiotic pre-treatment

The resistance of cells to detergents was determined with or without pre-treatment with antibiotics. 5 ml cultures were harvested after antibiotic treatment with AMP, FOS, TUN and VAN, washed with PBS, and resuspended in 1 ml PBS. 1:10 dilution series in 96-well plates were made until dilution 10^{-7}. Additional wells were prepared with 100 µl PBS or 100 µl PBS with SDS at a final concentration of 0.05 %, and 100 µl of diluted culture added to these wells. After 15 min incubation time at RT, 10 µl samples were spotted on LB plates and incubated at 37 °C. Difference in survival between treatments

with or without SDS were determined and compared to the control that was not pre-treated with antibiotics.

7.6 Statistics

Sample size and error bars are specified in the figure legends of each experiment individually. The unpaired two-sample Student's t-test with Welch's correction was used to evaluate differences between sample and control. Significance was set at $p<0.05$. MSD plots show the mean with shaded areas representing 95 % bootstrap interval.

8 REFERENCES

Ambrose, E. J. (1956). A surface contact microscope for the study of cell movements. *Nature* 178, 1194. doi:10.1038/1781194a0.

Andrade, D. M., Clausen, M. P., Keller, J., Mueller, V., Wu, C., Bear, J. E., et al. (2015). Cortical actin networks induce spatio-temporal confinement of phospholipids in the plasma membrane - a minimally invasive investigation by STED-FCS. *Sci Rep* 5, 11454. doi:10.1038/srep11454.

Arnaud, M., Chastanet, A., and Debarbouille, M. (2004). New vector for efficient allelic replacement in naturally nontransformable, low-GC-content, gram-positive bacteria. *Appl Environ Microbiol* 70, 6887–6891. doi:70/11/6887.

Babicki, S., Arndt, D., Marcu, A., Liang, Y., Grant, J. R., Maciejewski, A., et al. (2016). Heatmapper: web-enabled heat mapping for all. *Nucleic Acids Res.* 44, W147-153. doi:10.1093/nar/gkw419.

Babuke, T., and Tikkanen, R. (2007). Dissecting the molecular function of reggie/flotillin proteins. *Eur J Cell Biol* 86, 525–532. doi:S0171-9335(07)00044-1.

Bach, J. N., and Bramkamp, M. (2013). Flotillins functionally organize the bacterial membrane. *Mol Microbiol* 88, 1205–1217. doi:10.1111/mmi.12252.

Bach, J. N., and Bramkamp, M. (2015). Dissecting the molecular properties of prokaryotic flotillins. *PloS one* 10, e0116750. doi:10.1371/journal.pone.0116750.

Baumgart, T., Hammond, A. T., Sengupta, P., Hess, S. T., Holowka, D. A., Baird, B. A., et al. (2007). Large-scale fluid/fluid phase separation of proteins and lipids in giant plasma membrane vesicles. *Proc. Natl. Acad. Sci. U.S.A.* 104, 3165–3170. doi:10.1073/pnas.0611357104.

Baumgartner, W., Schütz, G. J., Wiegand, J., Golenhofen, N., and Drenckhahn, D. (2003). Cadherin function probed by laser tweezer and single molecule fluorescence in vascular endothelial cells. *J. Cell. Sci.* 116, 1001–1011. doi:10.1242/jcs.00322.

Bergstrom, J. D., Kurtz, M. M., Rew, D. J., Amend, A. M., Karkas, J. D., Bostedor, R. G., et al. (1993). Zaragozic acids: a family of fungal metabolites that are picomolar competitive inhibitors of squalene synthase. *Proc Natl Acad Sci U S A* 90, 80–84. doi:10.1073/pnas.90.1.80.

Bernardino de la Serna, J., Schütz, G. J., Eggeling, C., and Cebecauer, M. (2016). There Is No Simple Model of the Plasma Membrane Organization. *Front Cell Dev Biol* 4. doi:10.3389/fcell.2016.00106.

Bhavsar, A. P., and Brown, E. D. (2006). Cell wall assembly in *Bacillus subtilis*: how spirals and spaces challenge paradigms. *Molecular microbiology* 60, 1077–90. doi:10.1111/j.1365-2958.2006.05169.x.

Bickel, P. E., Scherer, P. E., Schnitzer, J. E., Oh, P., Lisanti, M. P., and Lodish, H. F. (1997). Flotillin and epidermal surface antigen define a new family of caveolae-associated integral membrane proteins. *J Biol Chem* 272, 13793–13802. doi: 10.1074/bjc.272.21.13793.

Billaudeau, C., Yao, Z., and Chastanet, A. (2019). MreB Forms Subdiffraction Nanofilaments during Active Growth in Bacillus subtilis. *mBio* 10, 1–13. doi:10.1128/mBio.01879-18.

Bolte, S., and Cordelieres, F. (2006). A guided tour into subcellular colocalization analysis in light microscopy. *Journal of Microscopy* 224, 213–232. doi:10.1111/j.1365-2818.2006.01706.x.

Borner, G. H. H., Sherrier, D. J., Weimar, T., Michaelson, L. V., Hawkins, N. D., Macaskill, A., et al. (2005). Analysis of detergent-resistant membranes in Arabidopsis. Evidence for plasma membrane lipid rafts. *Plant Physiol.* 137, 104–116. doi:10.1104/pp.104.053041.

Bosak, T., Losick, R. M., and Pearson, A. (2008). A polycyclic terpenoid that alleviates oxidative stress. *Proc Natl Acad Sci U S A* 105, 6725–6729. doi:0800199105.

Boulos, L., Prévost, M., Barbeau, B., Coallier, J., and Desjardins, R. (1999). LIVE/DEAD BacLight : application of a new rapid staining method for direct enumeration of viable and total bacteria in drinking water. *J. Microbiol. Methods* 37, 77–86. doi:10.1016/s0167-7012(99)00048-2.

Bramkamp, M., and Lopez, D. (2015). Exploring the Existence of Lipid Rafts in Bacteria. *Microbiol Mol Biol Rev* 79, 81–100. doi:10.1128/MMBR.00036-14.

Bretscher, M. S., and Munro, S. (1993). Cholesterol and the Golgi apparatus. *Science* 261, 1280–1281. doi:10.1126/science.8362242.

REFERENCES

Browman, D. T., Hoegg, M. B., and Robbins, S. M. (2007). The SPFH domain-containing proteins: more than lipid raft markers. *Trends Cell Biol* 17, 394–402. doi:10.1016/j.tcb.2007.06.005.

Brown, D. A. (2002). Isolation and use of rafts. *Curr Protoc Immunol* Chapter 11, Unit 11 10. doi:10.1002/0471142735.im1110s51.

Brown, D. A., and Rose, J. K. (1992). Sorting of GPI-anchored proteins to glycolipid-enriched membrane subdomains during transport to the apical cell surface. *Cell* 68, 533–544. doi:10.1016/0092-8674(92)90189-j.

Bussell, S. J., Hammer, D. A., and Koch, D. L. (1994). The effect of hydrodynamic interactions on the tracer and gradient diffusion of integral membrane proteins in lipid bilayers. *Journal of Fluid Mechanics* 258, 167–190. doi:10.1017/S0022112094003289.

Bussell, S. J., Koch, D. L., and Hammer, D. A. (1995). Effect of hydrodynamic interactions on the diffusion of integral membrane proteins: diffusion in plasma membranes. *Biophysical Journal* 68, 1836–1849. doi:10.1016/S0006-3495(95)80360-7.

Campbell, J., Singh, A. K., Santa Maria, J. P., Kim, Y., Brown, S., Swoboda, J. G., et al. (2011). Synthetic lethal compound combinations reveal a fundamental connection between wall teichoic acid and peptidoglycan biosyntheses in Staphylococcus aureus. *ACS Chem Biol* 6, 106–116. doi:10.1021/cb100269f.

Chaudhuri, A., Bhattacharya, B., Gowrishankar, K., Mayor, S., and Rao, M. (2011). Spatiotemporal regulation of chemical reactions by active cytoskeletal remodeling. *PNAS* 108, 14825–14830. doi:10.1073/pnas.1100007108.

Chichili, G. R., and Rodgers, W. (2009). Cytoskeleton-membrane interactions in membrane raft structure. *Cellular and Molecular Life Sciences* 66, 2319–2328. doi:10.1007/s00018-009-0022-6.

Cho, H., Wivagg, C. N., Kapoor, M., Barry, Z., Rohs, P. D. A., Suh, H., et al. (2016). Bacterial cell wall biogenesis is mediated by SEDS and PBP polymerase families functioning semi-autonomously. *Nature Microbiology* 1, 1–8. doi:10.1038/nmicrobiol.2016.172.

Coling, D., and Kachar, B. (1997). Theory and Application of Fluorescence Microscopy. *Current Protocols in Neuroscience* 00, 2.1.1-2.1.11. doi:10.1002/0471142301.ns0201s00.

Combs, C. A. (2010). Fluorescence Microscopy: A Concise Guide to Current Imaging Methods. *Curr Protoc Neurosci* 0 2, Unit2.1. doi:10.1002/0471142301.ns0201s50.

Coskun, U., and Simons, K. (2011). Cell membranes: the lipid perspective. *Structure* 19, 1543–1548. doi:10.1016/j.str.2011.10.010.

Cronan, J. E. (2003). Bacterial membrane lipids: where do we stand? *Annu Rev Microbiol* 57, 203–224. doi:10.1146/annurev.micro.57.030502.090851.

Daley, D. O. (2008). The assembly of membrane proteins into complexes. *Curr Opin Struct Biol* 18, 420–424. doi:10.1016/j.sbi.2008.04.006.

Daněk, M., Angelini, J., Malínská, K., Andrejch, J., Amlerová, Z., Kocourková, D., et al. (2019). Cell wall contributes to the stability of plasma membrane nanodomain organization of Arabidopsis thaliana FLOTILLIN2 and HYPERSENSITIVE INDUCED REACTION1 proteins. *Plant Journal*. doi:10.1111/tpj.14566.

D'Elia, M. A., Millar, K. E., Beveridge, T. J., and Brown, E. D. (2006). Wall Teichoic Acid Polymers Are Dispensable for Cell Viability in Bacillus subtilis. *J Bacteriol* 188, 8313–8316. doi:10.1128/JB.01336-06.

Dempwolff, F., Möller, H. M., and Graumann, P. L. (2012). Synthetic Motility and Cell Shape Defects Associated with Deletions of Flotillin/Reggie Paralogs in *Bacillus subtilis* and Interplay of These Proteins with NfeD Proteins. *J Bacteriol* 194, 4652–4661. doi:10.1128/JB.00910-12.

Dempwolff, F., Schmidt, F. K., Hervás, A. B., Stroh, A., Rösch, T. C., Riese, C. N., et al. (2016). Super Resolution Fluorescence Microscopy and Tracking of Bacterial Flotillin (Reggie) Paralogs Provide Evidence for Defined-Sized Protein Microdomains within the Bacterial Membrane but Absence of Clusters Containing Detergent-Resistant Proteins. *PLoS Genetics* 12, 1–29. doi:10.1371/journal.pgen.1006116.

Dion, M. F., Kapoor, M., Sun, Y., Wilson, S., Ryan, J., Vigouroux, A., et al. (2019). *Bacillus subtilis* cell diameter is determined by the opposing actions of two distinct cell wall synthetic systems. *Nature Microbiology* 4, 1294–1305. doi:10.1038/s41564-019-0439-0.

Doherty, G. P., Bailey, K., and Lewis, P. J. (2010). Stage-specific fluorescence intensity of GFP and mCherry during sporulation in *Bacillus Subtilis*. *BMC Research Notes* 3, 303. doi:10.1186/1756-0500-3-303.

REFERENCES

Domínguez-Escobar, J., Chastanet, A., Crevenna, A. H., Fromion, V., Wedlich-Söldner, R., and Carballido-López, R. (2011). Processive movement of MreB-associated cell wall biosynthetic complexes in bacteria. *Science* 333, 225–228. doi:10.1126/science.1203466.

Donovan, C., and Bramkamp, M. (2009). Characterization and subcellular localization of a bacterial flotillin homologue. *Microbiology* 155, 1786–1799. doi:10.1099/mic.0.025312-0.

Ducret, A., Quardokus, E. M., and Brun, Y. V. (2016). MicrobeJ, a tool for high throughput bacterial cell detection and quantitative analysis. *Nature Microbiology* 1, 1–7. doi:10.1038/nmicrobiol.2016.77.

Earl, A. M., Losick, R., and Kolter, R. (2008). Ecology and genomics of *Bacillus subtilis*. *Trends Microbiol.* 16, 269–275. doi:10.1016/j.tim.2008.03.004.

Edidin, M. (2003). The state of lipid rafts: from model membranes to cells. *Annu Rev Biophys Biomol Struct* 32, 257–283. doi:10.1146/annurev.biophys.32.110601.142439.

Einstein, A. (1905). Über die von der molekularkinetischen Theorie der Wärme geforderte Bewegung von in ruhenden Flüssigkeiten suspendierten Teilchen. *Annalen der Physik* 322, 549–560. doi:10.1002/andp.19053220806.

Emami, K., Guyet, A., Kawai, Y., Devi, J., Wu, L. J., Allenby, N., et al. (2017). RodA as the missing glycosyltransferase in *Bacillus subtilis* and antibiotic discovery for the peptidoglycan polymerase pathway. *Nature Microbiology* 2, 1–8. doi:10.1038/nmicrobiol.2016.253.

Errington, J. (2015). Bacterial morphogenesis and the enigmatic MreB helix. *Nature Reviews Microbiology* 13, 241–248. doi:10.1038/nrmicro3398.

Falagas, M. E., Makris, G. C., Matthaiou, D. K., and Rafailidis, P. I. (2008). Statins for infection and sepsis: a systematic review of the clinical evidence. *J Antimicrob Chemother* 61, 774–785. doi:10.1093/jac/dkn019.

Feng, X., Hu, Y., Zheng, Y., Zhu, W., Li, K., Huang, C. H., et al. (2014). Structural and Functional Analysis of *Bacillus subtilis* YisP Reveals a Role of Its Product in Biofilm Production. *Chem Biol*. doi:10.1016/j.chembiol.2014.08.018.

Field, K. A., Holowka, D., and Baird, B. (1995). Fc epsilon RI-mediated recruitment of p53/56lyn to detergent-resistant membrane domains accompanies cellular signaling. *PNAS* 92, 9201–9205. doi:10.1073/pnas.92.20.9201.

Freese, E., Heinze, J. E., and Galliers, E. M. (1979). Partial purine deprivation causes sporulation of *Bacillus subtilis* in the presence of excess ammonia, glucose and phosphate. *J. Gen. Microbiol.* 115, 193–205. doi:10.1099/00221287-115-1-193.

Fujiwara, T. K., Iwasawa, K., Kalay, Z., Tsunoyama, T. A., Watanabe, Y., Umemura, Y. M., et al. (2016). Confined diffusion of transmembrane proteins and lipids induced by the same actin meshwork lining the plasma membrane. *Mol. Biol. Cell* 27, 1101–1119. doi:10.1091/mbc.E15-04-0186.

Fujiwara, T., Ritchie, K., Murakoshi, H., Jacobson, K., and Kusumi, A. (2002). Phospholipids undergo hop diffusion in compartmentalized cell membrane. *J. Cell Biol.* 157, 1071–1081. doi:10.1083/jcb.200202050.

Ganchev, D. N., Hasper, H. E., Breukink, E., and de Kruijff, B. (2006). Size and orientation of the lipid II headgroup as revealed by AFM imaging. *Biochemistry* 45, 6195–6202. doi:10.1021/bi051913e.

García-Betancur, J.-C., Goñi-Moreno, A., Horger, T., Schott, M., Sharan, M., Eikmeier, J., et al. (2017). Cell differentiation defines acute and chronic infection cell types in *Staphylococcus aureus*. *Elife* 6. doi:10.7554/eLife.28023.

García-Fernández, E., Koch, G., Wagner, R. M., Fekete, A., Stengel, S. T., Schneider, J., et al. (2017). Membrane Microdomain Disassembly Inhibits MRSA Antibiotic Resistance. *Cell* 171, 1354-1367.e20. doi:10.1016/j.cell.2017.10.012.

Garner, E. C., Bernard, R., Wang, W., Zhuang, X., Rudner, D. Z., and Mitchison, T. (2011). Coupled, circumferential motions of the cell wall synthesis machinery and MreB filaments in *B. subtilis*. *Science* 333, 222–225. doi:10.1126/science.1203285.

Gómez-Móuton, C., Abad, J. L., Mira, E., Lacalle, R. A., Gallardo, E., Jiménez-Baranda, S., et al. (2001). Segregation of leading-edge and uropod components into specific lipid rafts during T cell polarization. *Proc. Natl. Acad. Sci. U.S.A.* 98, 9642–9647. doi:10.1073/pnas.171160298.

Good, M. C., Zalatan, J. G., and Lim, W. A. (2011). Scaffold proteins: hubs for controlling the flow of cellular information. *Science* 332, 680–686. doi:332/6030/680.

REFERENCES

Goswami, D., Gowrishankar, K., Bilgrami, S., Ghosh, S., Raghupathy, R., Chadda, R., et al. (2008). Nanoclusters of GPI-Anchored Proteins Are Formed by Cortical Actin-Driven Activity. *Cell* 135, 1085–1097. doi:10.1016/j.cell.2008.11.032.

Grecco, H. E., Schmick, M., and Bastiaens, P. I. (2011). Signaling from the living plasma membrane. *Cell* 144, 897–909. doi:10.1016/j.cell.2011.01.029.

Green, J. B., Fricke, B., Chetty, M. C., von Düring, M., Preston, G. F., and Stewart, G. W. (2004). Eukaryotic and prokaryotic stomatins: the proteolytic link. *Blood Cells Mol. Dis.* 32, 411–422. doi:10.1016/j.bcmd.2004.01.016.

Gründling, A., Schneewind, O., Grundling, A., and Schneewind, O. (2007). Genes required for glycolipid synthesis and lipoteichoic acid anchoring in *Staphylococcus aureus*. *J Bacteriol* 189, 2521–2530. doi:10.1128/JB.01683-06.

Guerout-Fleury, A. M., Frandsen, N., and Stragier, N. P. (1996). Plasmids for ectopic integration in *Bacillus subtilis*. *Gene* 180, 57–61. doi:10.1016/s0378-1119(96)00404-0.

Gupta, N., Wollscheid, B., Watts, J. D., Scheer, B., Aebersold, R., and DeFranco, A. L. (2006). Quantitative proteomic analysis of B cell lipid rafts reveals that ezrin regulates antigen receptor-mediated lipid raft dynamics. *Nat. Immunol.* 7, 625–633. doi:10.1038/ni1337.

Guzmán-Flores, J. E., Steinemann-Hernández, L., González de la Vara, L. E., Gavilanes-Ruiz, M., Romeo, T., Alvarez, A. F., et al. (2019). Proteomic analysis of *Escherichia coli* detergent-resistant membranes (DRM). *PLoS One* 14. doi:10.1371/journal.pone.0223794.

Haas, R., Koch, H. U., and Fischer, W. (1984). Alanyl turnover from lipoteichoic acid to teichoic acid in *Staphylococcus aureus*. *FEMS Microbiology Letters* 21, 27–31. doi:10.1111/j.1574-6968.1084.tb00180.x.

Harris, L. K., and Theriot, J. A. (2016). Relative Rates of Surface and Volume Synthesis Set Bacterial Cell Size. *Cell* 165, 1479–1492. doi:10.1016/j.cell.2016.05.045.

Heerklotz, H. (2002). Triton promotes domain formation in lipid raft mixtures. *Biophys. J.* 83, 2693–2701. doi:10.1016/S0006-3495(02)75278-8.

Hinderhofer, M., Walker, C. A., Friemel, A., Stuermer, C. A., Moller, H. M., and Reuter, A. (2009). Evolution of prokaryotic SPFH proteins. *BMC Evol Biol* 9, 10. doi:10.1186/1471-2148-9-10.

Hussain, S., Wivagg, C. N., Szwedziak, P., Wong, F., Schaefer, K., Izoré, T., et al. (2018). MreB filaments align along greatest principal membrane curvature to orient cell wall synthesis. *eLife* 7, 1–45. doi:10.7554/eLife.32471.

Hutton, M. L., D'Costa, K., Rossiter, A. E., Wang, L., Turner, L., Steer, D. L., et al. (2017). A *Helicobacter pylori* Homolog of Eukaryotic Flotillin Is Involved in Cholesterol Accumulation, Epithelial Cell Responses and Host Colonization. *Front Cell Infect Microbiol* 7. doi:10.3389/fcimb.2017.00219.

Hyyryläinen, H. L., Vitikainen, M., Thwaite, J., Wu, H., Sarvas, M., Harwood, C. R., et al. (2000). D-alanine substitution of teichoic acids as a modulator of protein folding and stability at the cytoplasmic membrane/cell wall interface of *Bacillus subtilis*. *Journal of Biological Chemistry* 275, 26696–26703. doi:10.1074/jbc.M003804200.

Iino, R., Koyama, I., and Kusumi, A. (2001). Single molecule imaging of green fluorescent proteins in living cells: E-cadherin forms oligomers on the free cell surface. *Biophys J* 80, 2667–2677. doi:10.1016/S0006-3495(01)76236-4.

Ishino, F., Park, W., Tomioka, S., Tamaki, S., Takase, I., Kunugita, K., et al. (1986). Peptidoglycan synthetic activities in membranes of *Escherichia coli* caused by overproduction of penicillin-binding protein 2 and rodA protein. *J. Biol. Chem.* 261, 7024–7031.

Jorasch, P., Wolter, F. P., Zähringer, U., and Heinz, E. (1998). A UDP glucosyltransferase from *Bacillus subtilis* successively transfers up to four glucose residues to 1,2-diacylglycerol: expression of ypfP in *Escherichia coli* and structural analysis of its reaction products. *Molecular Microbiology* 29, 419–430. doi:10.1046/j.1365-2958.1998.00930.x.

Junková, P., Daněk, M., Kocourková, D., Brouzdová, J., Kroumanová, K., Zelazny, E., et al. (2018). Mapping of Plasma Membrane Proteins Interacting With *Arabidopsis thaliana* Flotillin 2. *Front. Plant Sci.* 9. doi:10.3389/fpls.2018.00991.

Kahne, D., Leimkuhler, C., Lu, W., and Walsh, C. (2005). Glycopeptide and Lipoglycopeptide Antibiotics. *Chem. Rev.* 105, 425–448. doi:10.1021/cr030103a.

REFERENCES

Kalay, Z., Parris, P. E., and Kenkre, V. M. (2008). Effects of disorder in location and size of fence barriers on molecular motion in cell membranes. *J. Phys.: Condens. Matter* 20, 245105. doi:10.1088/0953-8984/20/24/245105.

Kannenberg, E., and Poralla, K. (1982). The influence of hopanoids on growth of *Mycoplasma mycoides*. *Arch Microbiol* 133, 100–102. doi:10.1007/BF00413519.

Kawai, F., Shoda, M., Harashima, R., Sadaie, Y., Hara, H., and Matsumoto, K. (2004). Cardiolipin domains in *Bacillus subtilis* marburg membranes. *J Bacteriol* 186, 1475–1483. doi:10.1128/jb.186.5.1473-1483.2004.

Kawai, Y., Asai, K., and Errington, J. (2009). Partial functional redundancy of MreB isoforms, MreB, Mbl and MreBH, in cell morphogenesis of *Bacillus subtilis*. *Mol Microbiol* 73, 719–731. doi:10.1111./j.1365-2958.2009.06805.x.

Kawai, Y., Marles-Wright, J., Cleverley, R. M., Emmins, R., Ishikawa, S., Kuwano, M., et al. (2011). A widespread family of bacterial cell wall assembly proteins. *EMBO J* 30, 4931–4941. doi:10.1038/emboj.2011.358.

Kelley, L. A., Mezulis, S., Yates, C. M., Wass, M. N., and Sternberg, M. J. (2015). The Phyre2 web portal for protein modelling, prediction and analysis. *Nat Protoc* 10, 845–858. doi:10.1038/nprot.2015.053.

Kenkre, V. M., Giuggioli, L., and Kalay, Z. (2008). Molecular motion in cell membranes: analytic study of fence-hindered random walks. *Phys Rev E Stat Nonlin Soft Matter Phys* 77, 051907. doi:10.1103/PhysRevE.77.051907.

Klammt, C., and Lillemeier, B. F. (2012). How membrane structures control T cell signaling. *Front Immunol* 3. doi:10.3389/fimmu.2012.00291.

Klar, T. A., Jakobs, S., Dyba, M., Egner, A., and Hell, S. W. (2000). Fluorescence microscopy with diffraction resolution barrier broken by stimulated emission. *Proc Natl Acad Sci U S A* 97, 8206–8210. doi:10.1073/pnas.97.15.8206.

Klein, U., Gimpl, G., and Fahrenholz, F. (1995). Alteration of the Myometrial Plasma Membrane Cholesterol Content with .beta.-Cyclodextrin Modulates the Binding Affinity of the Oxytocin Receptor. *Biochemistry* 34, 13784–13793. doi:10.1021/bi00042a009.

Kocaoglu, O., Calvo, R. A., Sham, L. T., Cozy, L. M., Lanning, B. R., Francis, S., et al. (2012). Selective penicillin-binding protein imaging probes reveal substructure in bacterial cell division. *ACS Chemical Biology* 7, 1746–1753. doi:10.1021/cb300329r.

Koch, G., Wermser, C., Acosta, I. C., Kricks, L., Stengel, S. T., Yepes, A., et al. (2017). Attenuating *Staphylococcus aureus* Virulence by Targeting Flotillin Protein Scaffold Activity. *Cell Chemical Biology* 24, 845–857.e6. doi:10.1016/j.chembiol.2017.05.027.

Kohlrausch, U., and Höltje, J. V. (1991). Analysis of murein and murein precursors during antibiotic-induced lysis of *Escherichia coli*. *J. Bacteriol.* 173, 3425–3431. doi:10.1128/jb.173.11.3425-3431.1991.

Kong, K.-F., Schneper, L., and Mathee, K. (2010). Beta-lactam Antibiotics: From Antibiosis to Resistance and Bacteriology. *APMIS* 118, 1–36. doi:10.1111/j.1600-0463.2009.02563.x.

Konopásek, I., Strzalka, K., and Svobodová, J. (2000). Cold shock in *Bacillus subtilis*: Different effects of benzyl alcohol and ethanol on the membrane organisation and cell adaptation. *Biochimica et Biophysica Acta - Biomembranes* 1464, 18–26. doi:10.1016/S0005-2736(99)00240-0.

Kopterides, P., and Falagas, M. E. (2009). Statins for sepsis: a critical and updated review. *Clin Microbiol Infect* 15, 325–334. doi:10.1111/j.1469-0691.2009.02750.x.

Korber, D. R., Choi, A., Wolfaardt, G. M., and Caldwell, D. E. (1996). Bacterial plasmolysis as a physical indicator of viability. *Appl Environ Microbiol* 62, 3939–3947.

Krapf, D. (2018). Compartmentalization of the plasma membrane. *Current Opinion in Cell Biology* 53, 15–21. doi:10.1016/j.ceb.2018.04.002.

Kunst, F., Ogasawara, N., Moszer, I., Albertini, A. M., Alloni, G., Azevedo, V., et al. (1997). The complete genome sequence of the gram-positive bacterium *Bacillus subtilis*. *Nature* 390, 249–256. doi:10.1038/36786.

Kurrle, N., John, B., Meister, M., and Tikkanen, R. (2012). Function of Flotillins in Receptor Tyrosine Kinase Signaling and Endocytosis: Role of Tyrosine Phosphorylation and Oligomerization. *Protein Phosphorylation in Human Health*. doi:10.5772/48598.

Kusumi, A., Fujiwara, T. K., Morone, N., Yoshida, K. J., Chadda, R., Xie, M., et al. (2012). Membrane mechanisms for signal transduction: The coupling of the meso-scale raft domains to membrane-skeleton-induced compartments and dynamic protein complexes. *Seminars in Cell & Developmental Biology* 23, 126–144. doi:10.1016/j.semcdb.2012.01.018.

Kusumi, A., and Sako, Y. (1996). Cell surface organization by the membrane skeleton. *Curr. Opin. Cell Biol.* 8, 566–574. doi:10.1016/s0955-0674(96)80036-6.

Kusumi, A., Shirai, Y. M., Koyama-Honda, I., Suzuki, K. G. N., and Fujiwara, T. K. (2010). Hierarchical organization of the plasma membrane: Investigations by single-molecule tracking vs. fluorescence correlation spectroscopy. *FEBS Letters* 584, 1814–1823. doi:10.1016/j.febslet.2010.02.047.

Kuzmin, P. I., Akimov, S. A., Chizmadzhev, Y. A., Zimmerberg, J., and Cohen, F. S. (2005). Line tension and interaction energies of membrane rafts calculated from lipid splay and tilt. *Biophys. J.* 88, 1120–1133. doi:10.1529/biophysj.104.048223.

Lajoie, P., Partridge, E. A., Guay, G., Goetz, J. G., Pawling, J., Lagana, A., et al. (2007). Plasma membrane domain organization regulates EGFR signaling in tumor cells. *J Cell Biol* 179, 341–356. doi:10.1083/jcb.200611106.

Langhorst, M. F., Solis, G. P., Hannbeck, S., Plattner, H., and Stuermer, C. A. (2007). Linking membrane microdomains to the cytoskeleton: regulation of the lateral mobility of reggie-1/flotillin-2 by interaction with actin. *FEBS Lett* 581, 4697–4703. doi:S0014-5793(07)00961-1.

Lara, B., Mengin-Lecreulx, D., Ayala, J. A., and van Heijenoort, J. (2005). Peptidoglycan precursor pools associated with MraY and FtsW deficiencies or antibiotic treatments. *FEMS Microbiol Lett* 250, 195–200. doi:10.1016/j.femsle.2005.07.005.

Lazarevic, V., Soldo, B., Médico, N., Pooley, H., Bron, S., and Karamata, D. (2005). *Bacillus subtilis* α-Phosphoglucomutase Is Required for Normal Cell Morphology and Biofilm Formation. *Appl Environ Microbiol* 71, 39–45. doi:10.1128/AEM.71.1.39-45.2005.

Leaver, M., and Errington, J. (2005). Roles for MreC and MreD proteins in helical growth of the cylindrical cell wall in Bacillus subtilis. *Mol Microbiol* 57, 1196–1209. doi:10.1111/j.1365-2958.2005.04736.x.

Lee, Y. H., Kingston, A. W., and Helmann, J. D. (2012). Glutamate dehydrogenase affects resistance to cell wall antibiotics in *Bacillus subtilis*. *Journal of Bacteriology* 194, 993–1001. doi:10.1128/JB.06547-11.

Letunic, I., and Bork, P. (2018). 20 years of the SMART protein domain annotation resource. *Nucleic Acids Res.* 46, D493–D496. doi:10.1093/nar/gkx922.

Letunic, I., Doerks, T., and Bork, P. (2015). SMART: recent updates, new developments and status in 2015. *Nucleic Acids Res.* 43, D257-260. doi:10.1093/nar/gku949.

Levental, I., Lingwood, D., Grzybek, M., Coskun, U., and Simons, K. (2010). Palmitoylation regulates raft affinity for the majority of integral raft proteins. *Proc Natl Acad Sci U S A* 107, 22050–22054. doi:10.1073/pnas.1016184107.

Liappis, A. P., Kan, V. L., Rochester, C. G., and Simon, G. L. (2001). The effect of statins on mortality in patients with bacteremia. *Clin Infect Dis* 33, 1352–1357. doi:10.1086/323334.

Liese, J., Rooijakkers, S. H. M., van Strijp, J. A. G., Novick, R. P., and Dustin, M. L. (2013). Intravital two-photon microscopy of host-pathogen interactions in a mouse model of Staphylococcus aureus skin abscess formation. *Cell. Microbiol.* 15, 891–909. doi:10.1111/cmi.12085.

Lingwood, D., and Simons, K. (2010). Lipid rafts as a membrane-organizing principle. *Science (New York, N.Y.)* 327, 46–50. doi:10.1126/science.1174621.

Liu, J., Deyoung, S. M., Zhang, M., Dold, L. H., and Saltiel, A. R. (2005). The stomatin/prohibitin/flotillin/HflK/C domain of flotillin-1 contains distinct sequences that direct plasma membrane localization and protein interactions in 3T3-L1 adipocytes. *J. Biol. Chem.* 280, 16125–16134. doi:10.1074/jbc.M500940200.

Lopez, D., and Koch, G. (2017). Exploring functional membrane microdomains in bacteria: an overview. *Curr Opin Microbiol* 36, 76–84. doi:10.1016/j.mib.2017.02.001.

López, D., Kolter, R., Lopez, D., and Kolter, R. (2010). Functional microdomains in bacterial membranes. *Genes Dev* 24, 1893–1902. doi:10.1101/gad.1945010.

Lopez, D., Vlamakis, H., Losick, R., and Kolter, R. (2009). Cannibalism enhances biofilm development in *Bacillus subtilis*. *Mol Microbiol* 74, 609–618. doi:10.1111/j.1365-1958.2009.06882.x.

Lovering, A. L., Safadi, S. S., and Strynadka, N. C. J. (2012). Structural Perspective of Peptidoglycan Biosynthesis and Assembly. *Annual Review of Biochemistry* 81, 451–478. doi:10.1146/annurev-biochem-061809-112742.

Lu, D., Wörmann, M. E., Zhang, X., Schneewind, O., Gründiing, A., and Freemont, P. S. (2009). Structure-based mechanism of lipoteichoic acid synthesis by *Staphylococcus aureus* LtaS. *Proceedings of the National Academy of Sciences of the United States of America* 106, 1584–1589. doi:10.1073/pnas.0809020106.

Lucena, D., Mauri, M., Schmidt, F., Eckhardt, B., and Graumann, P. L. (2018). Microdomain formation is a general property of bacterial membrane proteins and induces heterogeneity of diffusion patterns. *BMC Biology* 16, 1–17. doi:10.1186/s12915-018-0561-0.

Ludwig, A., Otto, G. P., Riento, K., Hams, E., Fallon, P. G., and Nichols, B. J. (2010). Flotillin microdomains interact with the cortical cytoskeleton to control uropod formation and neutrophil recruitment. *J Cell Biol* 191, 771–781. doi:10.1083/jcb.201005140.

Lv, X., Jin, K., Wu, Y., Zhang, C., Cui, S., Zhu, X., et al. (2020a). Enzyme assembly guided by SPFH-induced functional inclusion bodies for enhanced cascade biocatalysis. *Biotechnol. Bioeng.* doi:10.1002/bit.27304.

Lv, X., Wu, Y., Tian, R., Gu, Y., Liu, Y., Li, J., et al. (2020b). Synthetic metabolic channel by functional membrane microdomains for compartmentalized flux control. *Metab. Eng.* 59, 106–118. doi:10.1016/j.ymben.2020.02.003.

Lv, X., Zhang, C., Cui, S., Xu, X., Wang, L., Li, J., et al. (2020c). Assembly of pathway enzymes by engineering functional membrane microdomain components for improved N-acetylglucosamine synthesis in *Bacillus subtilis*. *Metab. Eng.* doi:10.1016/j.ymben.2020.05.011.

Magnuson, R., Solomon, J., and Grossman, A. D. (1994). Biochemical and genetic characterization of a competence pheromone from *B. subtilis*. *Cell* 77, 207–216. doi:10.1016/0092-8674(94)90313-1.

Mann, J. M., Carabetta, V. J., Cristea, I. M., and Dubnau, D. (2013). Complex formation and processing of the minor transformation pilins of *Bacillus subtilis*. *Mol Microbiol* 90, 1201–1215. doi:10.1111/mmi.12425.

Matsuoka, S. (2017). Biological functions of glucolipids in *Bacillus subtilis*. *Genes & Genetic Systems* 92, 217–221. doi:10.1266/ggs.17-00017.

McKay Wood, B., Santa Maria, J. P., Matano, L. M., Vickery, C. R., and Walker, S. (2018). A partial reconstitution implicates DltD in catalyzing lipoteichoic acid D-alanylation. *Journal of Biological Chemistry* 293, 17985–17996. doi:10.1074/jbc.RA118.004561.

McKenney, P. T., Driks, A., and Eichenberger, P. (2013). The *Bacillus subtilis* endospore: assembly and functions of the multilayered coat. *Nat. Rev. Microbiol.* 11, 33–44. doi:10.1038/nrmicro2921.

McPherson, D. C., and Popham, D. L. (2003). Peptidoglycan synthesis in the absence of class A penicillin-binding proteins in *Bacillus subtilis*. *J. Bacteriol.* 185, 1423–1431. doi:10.1128/jb.185.4.1423-1431.2003.

Meeske, A. J., Riley, E. P., Robins, W. P., Uehara, T., Mekalanos, J. J., Kahne, D., et al. (2016). SEDS proteins are a widespread family of bacterial cell wall polymerases. *Nature* 537, 634–638. doi:10.1038/nature19331.

Meeske, A. J., Sham, L.-T., Kimsey, H., Koo, B.-M., Gross, C. A., Bernhardt, T. G., et al. (2015). MurJ and a novel lipid II flippase are required for cell wall biogenesis in *Bacillus subtilis*. *Proc. Natl. Acad. Sci. U.S.A.* 112, 6437–6442. doi:10.1073/pnas.1504967112.

Michel, V., and Bakovic, M. (2007). Lipid rafts in health and disease. *Biology of the cell / under the auspices of the European Cell Biology Organization* 99, 129–40. doi:10.1042/BC20060051.

Mielich-Süss, B., Schneider, J., and Lopez, D. (2013). Overproduction of flotillin influences cell differentiation and shape in *Bacillus subtilis*. *MBio* 4, e00719–13. doi:10.1128/mBio.00719-13.

Mielich-Süss, B., Wagner, R. M., Mietrach, N., Hertlein, T., Marincola, G., Ohlsen, K., et al. (2017). Flotillin scaffold activity contributes to type VII secretion system assembly in *Staphylococcus aureus*. *PLOS Pathogens* 13, e1006728. doi:10.1371/journal.ppat.1006728.

Mileykovskaya, E., and Dowhan, W. (2000). Visualization of phospholipid domains in *Escherichia coli* by using the cardiolipin-specific fluorescent dye 10-N-nonyl acridine orange. *J Bacteriol* 182, 1172–1175.

Moreau, R. A., Agnew, J., Hicks, K. B., and Powell, M. J. (1997). Modulation of lipoxygenase activity by bacterial hopanoids. *J Nat Prod* 60, 397–398. doi:10.1021/np960611y np960611y.

Morone, N., Fujiwara, T., Murase, K., Kasai, R. S., Ike, H., Yuasa, S., et al. (2006). Three-dimensional reconstruction of the membrane skeleton at the plasma membrane interface by electron tomography. *J Cell Biol* 174, 851–862. doi:10.1083/jcb.200606007.

REFERENCES

Morrow, I. C., and Parton, R. G. (2005). Flotillins and the PHB domain protein family: rafts, worms and anaesthetics. *Traffic* 6, 725–740. doi:10.1111/j.1600-0854.2005.00318.x.

Morrow, I. C., Rea, S., Martin, S., Prior, I. A., Prohaska, R., Hancock, J. F., et al. (2002). Flotillin-1/reggie-2 traffics to surface raft domains via a novel golgi-independent pathway. Identification of a novel membrane targeting domain and a role for palmitoylation. *J Biol Chem* 277, 48834–48841. doi:10.1074/jbc.M209082200 M209082200.

Mouritsen, O. G., and Bloom, M. (1984). Mattress model of lipid-protein interactions in membranes. *Biophys. J.* 46, 141–153. doi:10.1016/S0006-3495(84)84007-2.

Munro, S. (2003). Lipid rafts: elusive or illusive? *Cell* 115, 377–388. doi:10.1016/S0092-8674(03)00882-1.

Murase, K., Fujiwara, T., Umemura, Y., Suzuki, K., Iino, R., Yamashita, H., et al. (2004). Ultrafine membrane compartments for molecular diffusion as revealed by single molecule techniques. *Biophys. J.* 86, 4075–4093. doi:10.1529/biophysj.103.035717.

Murray, T., Popham, D. L., and Setlow, P. (1998). *Bacillus subtilis* cells lacking penicillin-binding protein 1 require increased levels of divalent cations for growth. *J. Bacteriol.* 180, 4555–4563.

Mutoh, T., Tokuda, A., Miyadai, T., Hamaguchi, M., and Fujiki, N. (1995). Ganglioside GM1 binds to the Trk protein and regulates receptor function. *PNAS* 92, 5087–5091. doi:10.1073/pnas.92.11.5087.

Nebl, T., Pestonjamasp, K. N., Leszyk, J. D., Crowley, J. L., Oh, S. W., and Luna, E. J. (2002). Proteomic analysis of a detergent-resistant membrane skeleton from neutrophil plasma membranes. *J. Biol. Chem.* 277, 43399–43409. doi:10.1074/jbc.M205386200.

Neuhaus, F. C., and Baddiley, J. (2003). A Continuum of Anionic Charge: Structures and Functions of d-Alanyl-Teichoic Acids in Gram-Positive Bacteria. *Microbiol Mol Biol Rev* 67, 686–723. doi:10.1128/MMBR.67.4.686-723.2003.

Neumann-Giesen, C., Falkenbach, B., Beicht, P., Claasen, S., Luers, G., Stuermer, C. A., et al. (2004). Membrane and raft association of reggie-1/flotillin-2: role of myristoylation, palmitoylation and oligomerization and induction of filopodia by overexpression. *Biochem J* 378, 509–518. doi:10.1042/BJ20031100 BJ20031100.

Neumann-Giesen, C., Fernow, I., Amaddii, M., and Tikkanen, R. (2007). Role of EGF-induced tyrosine phosphorylation of reggie-1/flotillin-2 in cell spreading and signaling to the actin cytoskeleton. *J Cell Sci* 120, 395–406. doi:10.1242/jcs.03336.

Ngugi, H. K., Dedej, S., Delaplane, K. S., Savelle, A. T., and Scherm, H. (2005). Effect of flower-applied Serenade biofungicide (*Bacillus subtilis*) on pollination-related variables in rabbiteye blueberry. *Biological Control* 33, 32–38. doi:10.1016/j.biocontrol.2005.01.002.

Niehaus, A. M. S., Vlachos, D. G., Edwards, J. S., Plechac, P., and Tribe, R. (2008). Microscopic simulation of membrane molecule diffusion on corralled membrane surfaces. *Biophys. J.* 94, 1551–1564. doi:10.1529/biophysj.107.106484.

Novikov, D. S., Fieremans, E., Jensen, J. H., and Helpern, J. A. (2011). Random walk with barriers. *Nat Phys* 7, 508–514. doi:10.1038/nphys1936.

Novo, D., Perlmutter, N. G., Hunt, R. H., and Shapiro, H. M. (1999). Accurate flow cytometric membrane potential measurement in bacteria using diethyloxacarbocyanine and a ratiometric technique. *Cytometry* 35, 55–63. doi:10.1002/(SICI)1097-0320(19990101)35:1<55::AID-CYTO8>3.0.CO;2-2.

Nykjaer, A., Kjøller, L., Cohen, R. L., Lawrence, D. A., Garni-Wagner, B. A., Todd, R. F., et al. (1994). Regions involved in binding of urokinase-type-1 inhibitor complex and pro-urokinase to the endocytic alpha 2-macroglobulin receptor/low density lipoprotein receptor-related protein. Evidence that the urokinase receptor protects pro-urokinase against binding to the endocytic receptor. *J. Biol. Chem.* 269, 25668–25676.

Oswald, F., L M Bank, E., Bollen, Y. J. M., and Peterman, E. J. G. (2014). Imaging and quantification of trans-membrane protein diffusion in living bacteria. *Phys Chem Chem Phys* 16, 12625–12634. doi:10.1039/c4cp00299g.

Oswald, F., Varadarajan, A., Lill, H., Peterman, E. J. G., and Bollen, Y. J. M. (2016). MreB-Dependent Organization of the *E. coli* Cytoplasmic Membrane Controls Membrane Protein Diffusion. *Biophysical Journal* 110, 1139–1149. doi:10.1016/j.bpj.2016.01.010.

Otto, G. P., and Nichols, B. J. (2011). The roles of flotillin microdomains–endocytosis and beyond. *Journal of cell science* 124, 3933–40. doi:10.1242/jcs.092015.

REFERENCES

Parsons, J. K., Pierce, J. P., Natarajan, L., Newman, V. A., Barbier, L., Mohler, J., et al. (2013). A randomized pilot trial of dietary modification for the chemoprevention of noninvasive bladder cancer: the dietary intervention in bladder cancer study. *Cancer Prev Res (Phila)* 6, 971–978. doi:10.1158/1940-6207.CAPR-13-0050.

Perego, M., Glaser, P., Minutello, A., Strauch, M. A., Leopold, K., and Fischer, W. (1995). Incorporation of D-alanine into lipoteichoic acid and wall teichoic acid in *Bacillus subtilis*. Identification of genes and regulation. *J Biol Chem* 270, 15598–15606. doi:10.1074/jbc.270.26.15598.

Piepenbreier, H., Diehl, A., and Fritz, G. (2019). Minimal exposure of lipid II cycle intermediates triggers cell wall antibiotic resistance. *Nature Communications* 10, 2733. doi:10.1038/s41467-019-10673-4.

Pike, L. J. (2009). The challenge of lipid rafts. *J. Lipid Res.* 50, S323–S328. doi:10.1194/jlr.R800040-JLR200.

Pike, L. J., Han, X., Chung, K.-N., and Gross, R. W. (2002). Lipid rafts are enriched in arachidonic acid and plasmenylethanolamine and their composition is independent of caveolin-1 expression: a quantitative electrospray ionization/mass spectrometric analysis. *Biochemistry* 41, 2075–2088. doi:10.1021/bi0156557.

Poralla, K., Muth, G., and Hartner, T. (2000). Hopanoids are formed during transition from substrate to aerial hyphae in *Streptomyces coelicolor* A3(2). *FEMS Microbiol Lett* 189, 93–95. doi:10.1111/j.1574-6968.2000.tb09212.x.

Powles, J. G., Mallett, M. J. D., Rickayzen, G., and Evans, W. a. B. (1992). Exact analytic solutions for diffusion impeded by an infinite array of partially permeable barriers. *Proceedings of the Royal Society of London. Series A: Mathematical and Physical Sciences* 436, 391–403. doi:10.1098/rspa.1992.0025.

Pralle, A., Keller, P., Florin, E. L., Simons, K., and Hörber, J. K. (2000). Sphingolipid-cholesterol rafts diffuse as small entities in the plasma membrane of mammalian cells. *J. Cell Biol.* 148, 997–1008. doi:10.1083/jcb.148.5.997.

Price, K. D., Roels, S., and Losick, R. (1997). A *Bacillus subtilis* gene encoding a protein similar to nucleotide sugar transferases influences cell shape and viability. *J Bacteriol* 179, 4959–4961. doi:10.1128/jb.179.15.4959-4961.1997.

Rajagopal, M., and Walker, S. (2017). Envelope Structures of Gram-Positive Bacteria. *Curr Top Microbiol Immunol* 404, 1–44. doi:10.1007/82_2015_5021.

Rajendran, L., and Simons, K. (2005). Lipid rafts and membrane dynamics. *J Cell Sci* 118, 1099–1102. doi:10.1242/jcs.01681.

Ramaniuk, O., Převorovský, M., Pospíšil, J., Vítovská, D., Kofroňová, O., Benada, O., et al. (2018). σI from *Bacillus subtilis*: Impact on Gene Expression and Characterization of σI-Dependent Transcription That Requires New Types of Promoters with Extended −35 and −10 Elements. *J Bacteriol* 200. doi:10.1128/JB.00251-18.

Ravier, M. A., Tsuboi, T., and Rutter, G. A. (2008). Imaging a target of Ca2+ signalling: Dense core granule exocytosis viewed by total internal reflection fluorescence microscopy. *Methods* 46, 233–238. doi:10.1016/j.ymeth.2008.09.016.

Reichmann, N. T., Cassona, C. P., and Gründling, A. (2013). Revised mechanism of D-alanine incorporation into cell wall polymers in Gram-positive bacteria. *Microbiology (United Kingdom)* 159, 1868–1877. doi:10.1099/mic.0.069898-0.

Renner, L. D., Eswaramoorthy, P., Ramamurthi, K. S., and Weibel, D. B. (2013). Studying Biomolecule Localization by Engineering Bacterial Cell Wall Curvature. *PLOS ONE* 8, e84143. doi:10.1371/journal.pone.0084143.

Reusch, R. N., Hiske, T. W., and Sadoff, H. L. (1986). Poly-beta-hydroxybutyrate membrane structure and its relationship to genetic transformability in *Escherichia coli*. *J Bacteriol* 168, 553–562. doi:10.1128/jb.168.2.553-562.1986.

Rodgers, W., and Zavzavadjian, J. (2001). Glycolipid-enriched membrane domains are assembled into membrane patches by associating with the actin cytoskeleton. *Exp. Cell Res.* 267, 173–183. doi:10.1006/excr.2001.5253.

Rudner, D. Z., and Losick, R. (2010). Protein subcellular localization in bacteria. *Cold Spring Harb Perspect Biol* 2, a000307. doi:10.1101/cshperspect.a000307.

Ruiz, N. (2008). Bioinformatics identification of MurJ (MviN) as the peptidoglycan lipid II flippase in *Escherichia coli*. *Proc. Natl. Acad. Sci. U.S.A.* 105, 15553–15557. doi:10.1073/pnas.0808352105.

Saffman, P. G., and Delbrück, M. (1975). Brownian motion in biological membranes. *PNAS* 72, 3111–3113. doi:10.1073/pnas.72.8.3111.

Sako, Y., and Kusumi, A. (1994). Compartmentalized structure of the plasma membrane for receptor movements as revealed by a nanometer-level motion analysis. *J. Cell Biol.* 125, 1251–1264. doi:10.1083/jcb.125.6.1251.

Sarkar, P., Yarlagadda, V., Ghosh, C., and Haldar, J. (2017). A review on cell wall synthesis inhibitors with an emphasis on glycopeptide antibiotics. *Medchemcomm* 8, 516–533. doi:10.1039/c6md00585c.

Sauvage, E., Kerff, F., Terrak, M., Ayala, J. A., and Charlier, P. (2008). The penicillin-binding proteins: Structure and role in peptidoglycan biosynthesis. *FEMS Microbiology Reviews* 32, 234–258. doi:10.1111/j.1574-6976.2008.00105.x.

Saxton, M. J. (2001). Chemically limited reactions on a percolation cluster. *J. Chem. Phys.* 116, 203–208. doi:10.1063/1.1424317.

Saxton, M. J. (2007). A Biological Interpretation of Transient Anomalous Subdiffusion. I. Qualitative Model. *Biophysical Journal* 92, 1178–1191. doi:10.1529/biophysj.106.092619.

Scheffers, D.-J. J., Jones, L. J. F. F., and Errington, J. (2004). Several distinct localization patterns for penicillin-binding proteins in *Bacillus subtilis*. *Mol Microbiol* 51, 749–764. doi:10.1046/j.1365-2958.2003.03854.x.

Schermelleh, L., Heintzmann, R., and Leonhardt, H. (2010). A guide to super-resolution fluorescence microscopy. *J Cell Biol* 190, 165–175. doi:10.1083/jcb.201002018.

Schindelin, J., Arganda-Carreras, I., Frise, E., Kaynig, V., Longair, M., Pietzsch, T., et al. (2012). Fiji: an open-source platform for biological-image analysis. *Nature methods* 9, 676–82. doi:10.1038/nmeth.2019.

Schirner, K., and Errington, J. (2009). The Cell Wall Regulator σI Specifically Suppresses the Lethal Phenotype of mbl Mutants in *Bacillus subtilis*. *Journal of Bacteriology* 191, 1404–1413. doi:10.1128/JB.01497-08.

Schirner, K., Eun, Y. J., Dion, M., Luo, Y., Helmann, J. D., Garner, E. C., et al. (2015). Lipid-linked cell wall precursors regulate membrane association of bacterial actin MreB. *Nature Chemical Biology* 11, 38–45. doi:10.1038/nchembio.1689.

Schirner, K., Marles-Wright, J., Lewis, R. J., and Errington, J. (2009). Distinct and essential morphogenic functions for wall- and lipo-teichoic acids in *Bacillus subtilis*. *The EMBO Journal* 28, 830–842. doi:10.1038/emboj.2009.25.

Schneider, J., Klein, T., Mielich-Süss, B., Koch, G., Franke, C., Kuipers, O. P., et al. (2015a). Spatio-temporal Remodeling of Functional Membrane Microdomains Organizes the Signaling Networks of a Bacterium. *PLoS Genet.* 11, e1005140. doi:10.1371/journal.pgen.1005140.

Schneider, J., Mielich-Suss, B., Bohme, R., and Lopez, D. (2015b). In vivo characterization of the scaffold activity of flotillin on the membrane kinase KinC of *Bacillus subtilis*. *Microbiology* 161, 1871–1887. doi:10.1099/mic.0.000137.

Schulte, T., Paschke, K. A., Laessing, U., Lottspeich, F., and Stuermer, C. A. (1997). Reggie-1 and reggie-2, two cell surface proteins expressed by retinal ganglion cells during axon regeneration. *Development* 124, 577–587.

Shah, M. B., and Sehgal, P. B. (2007). Nondetergent isolation of rafts. *Methods Mol Biol* 398, 21–28. doi:10.1007/978-1-59745-513-8_3.

Sham, L.-T., Butler, E. K., Lebar, M. D., Kahne, D., Bernhardt, T. G., and Ruiz, N. (2014). Bacterial cell wall. MurJ is the flippase of lipid-linked precursors for peptidoglycan biogenesis. *Science* 345, 220–222. doi:10.1126/science.1254522.

Shashkova, S., and Leake, M. C. (2017). Single-molecule fluorescence microscopy review: shedding new light on old problems. *Biosci Rep* 37. doi:10.1042/BSR20170031.

Silver, L. L. (2017). Fosfomycin: Mechanism and Resistance. *Cold Spring Harb Perspect Med* 7. doi:10.1101/cshperspect.a025262.

Simons, K., and Ikonen, E. (1997). Functional rafts in cell membranes. *Nature* 387, 569–72. doi:10.1038/42408.

Simons, K., and Sampaio, J. L. (2011). Membrane organization and lipid rafts. *Cold Spring Harbor perspectives in biology* 3, a004697. doi:10.1101/cshperspect.a004697.

Singer, S. J., and Nicolson, G. L. (1972). The fluid mosaic model of the structure of cell membranes. *Science* 175, 720–731. doi:10.1126/science.175.4023.720.

Smotrys, J. E., and Linder, M. E. (2004). Palmitoylation of intracellular signaling proteins: regulation and function. *Annu. Rev. Biochem.* 73, 559–587. doi:10.1146/annurev.biochem.73.011303.073954.

REFERENCES

Sohlenkamp, C., and Geiger, O. (2016). Bacterial membrane lipids: diversity in structures and pathways. *FEMS Microbiol. Rev.* 40, 133–159. doi:10.1093/femsre/fuv008.

Solis, G. P., Hoegg, M., Munderloh, C., Schrock, Y., Malaga-Trillo, E., Rivera-Milla, E., et al. (2007). Reggie/flotillin proteins are organized into stable tetramers in membrane microdomains. *Biochem J* 403, 313–322. doi:10.1042/BJ20061686.

Soufo, H. J. D., and Graumann, P. L. (2003). Actin-like proteins MreB and Mbl from *Bacillus subtilis* are required for bipolar positioning of replication origins. *Curr Biol* 13, 1916–1920. doi:10.1016/j.cub.2003.10.024.

Strahl, H., Bürmann, F., and Hamoen, L. W. (2014). The actin homologue MreB organizes the bacterial cell membrane. *Nature communications* 5, 3442. doi:10.1038/ncomms4442.

Strahl, H., and Hamoen, L. W. (2010). Membrane potential is important for bacterial cell division. *Proceedings of the National Academy of Sciences of the United States of America* 107, 12281–6. doi:10.1073/pnas.1005485107.

Stuermer, C. a O. (2010). The reggie/flotillin connection to growth. *Trends in cell biology* 20, 6–13. doi:10.1016/j.tcb.2009.10.003.

Swain, M. R., and Ray, R. C. (2009). Biocontrol and other beneficial activities of *Bacillus subtilis* isolated from cowdung microflora. *Microbiological Research* 164, 121–130. doi:10.1016/j.micres.2006.10.009.

Swamy, M., Siegers, G. M., Minguet, S., Wollscheid, B., and Schamel, W. W. (2006). Blue native polyacrylamide gel electrophoresis (BN-PAGE) for the identification and analysis of multiprotein complexes. *Sci STKE* 2006, pl4. doi:10.1126/stke.3452006pl4.

Swulius, M. T., Chen, S., Jane Ding, H., Li, Z., Briegel, A., Pilhofer, M., et al. (2011). Long helical filaments are not seen encircling cells in electron cryotomograms of rod-shaped bacteria. *Biochem Biophys Res Commun* 407, 650–655. doi:10.1016/j.bbrc.2011.03.062.

Takeshita, N., Diallinas, G., and Fischer, R. (2012). The role of flotillin FloA and stomatin StoA in the maintenance of apical sterol-rich membrane domains and polarity in the filamentous fungus *Aspergillus nidulans*. *Mol Microbiol* 83, 1136–1152. doi:10.1111/j.1365-2958.2012.07996.x.

Tinevez, J.-Y., Perry, N., Schindelin, J., Hoopes, G. M., Reynolds, G. D., Laplantine, E., et al. (2017). TrackMate: An open and extensible platform for single-particle tracking. *Methods* 115, 80–90. doi:10.1016/j.ymeth.2016.09.016.

Toledo, A., Perez, A., Coleman, J. L., and Benach, J. L. (2015). The lipid raft proteome of *Borrelia burgdorferi*. *Proteomics*. doi:10.1002/pmic.201500093.

Tomishige, M., Sako, Y., and Kusumi, A. (1998). Regulation Mechanism of the Lateral Diffusion of Band 3 in Erythrocyte Membranes by the Membrane Skeleton. *J Cell Biol* 142, 989–1000. doi:10.1083/jcb.142.4.989.

Treanor, B., Depoil, D., Gonzalez-Granja, A., Barral, P., Weber, M., Dushek, O., et al. (2010). The membrane skeleton controls diffusion dynamics and signaling through the B cell receptor. *Immunity* 32, 187–199. doi:10.1016/j.immuni.2009.12.005.

van den Ent, F., Amos, L. A., and Lowe, J. (2001). Prokaryotic origin of the actin cytoskeleton. *Nature* 413, 39–44. doi:10.1038/35092500.

van Dijl, J. M., and Hecker, M. (2013). *Bacillus subtilis*: from soil bacterium to super-secreting cell factory. *Microb Cell Fact* 12, 3. doi:10.1186/1475-2859-12-3.

van Meer, G., Voelker, D. R., and Feigenson, G. W. (2008). Membrane lipids: where they are and how they behave. *Nat Rev Mol Cell Biol* 9, 112–124. doi:10.1038/nrm2330.

Van Teeffelen, S., Wang, S., Furchtgott, L., Huang, K. C., Wingreen, N. S., Shaevitz, J. W., et al. (2011). The bacterial actin MreB rotates, and rotation depends on cell-wall assembly. *Proc Natl Acad Sci U S A* 108, 15822–15827. doi:10.1073/pnas.1108999108.

Vigouroux, A., Cordier, B., Aristov, A., Alvarez, L., Özbaykal, G., Chaze, T., et al. (2020). Class-A penicillin binding proteins do not contribute to cell shape but repair cell-wall defects. *eLife* 9. doi:10.7554/eLife.51998.

Viola, A., and Gupta, N. (2007). Tether and trap: regulation of membrane-raft dynamics by actin-binding proteins. *Nature reviews. Immunology* 7, 889–96. doi:10.1038/nri2193.

Wach, A. (1996). PCR-synthesis of marker cassettes with long flanking homology regions for gene disruptions in *S. cerevisiae*. *Yeast* 12, 259–265. doi:10.1002/(SICI)1097-0061(19960315)12:3<259::AID-YEA901>3.0.CO;2-C

REFERENCES

Wagner, R. M., Kricks, L., and Lopez, D. (2017). Functional Membrane Microdomains Organize Signaling Networks in Bacteria. *J Membrane Biol* 250, 367–378. doi:10.1007/s00232-016-9923-0.

Wagner, R. M., Setru, S. U., Machta, B., Wingreen, N. S., and Lopez, D. (2020). The Bacterial Cytoskeleton Spatially Confines Functional Membrane Microdomains. *bioRxiv*, 2020.04.25.060970. doi:10.1101/2020.04.25.060970.

Wang, J., Chen, H., and Brown, E. J. (2001). L-plastin peptide activation of alpha(v)beta(3)-mediated adhesion requires integrin conformational change and actin filament disassembly. *J. Biol. Chem.* 276, 14474–14481. doi:10.1074/jbc.M007324200.

Wecke, J., Perego, M., and Fischer, W. (1996). D-alanine deprivation of *Bacillus subtilis* teichoic acids is without effect on cell growth and morphology but affects the autolytic activity. *Microb. Drug Resist.* 2, 123–129. doi:10.1089/mdr.1996.2.123.

Weisswange, I., Bretschneider, T., and Anderson, K. I. (2005). The leading edge is a lipid diffusion barrier. *J. Cell. Sci.* 118, 4375–4380. doi:10.1242/jcs.02551.

White, D. C., and Frerman, F. E. (1967). Extraction, characterization, and cellular localization of the lipids of *Staphylococcus aureus*. *J Bacteriol* 94, 1854–1867.

Wittig, I., Braun, H. P., and Schagger, H. (2006). Blue native PAGE. *Nat Protoc* 1, 418–428. doi:10.1038/nprot.2006.62.

Wong, F., Garner, E. C., and Amir, A. (2019). Mechanics and dynamics of translocating mreb filaments on curved membranes. *eLife* 8, 1–30. doi:10.7554/eLife.40472.

Yasbin, R. E., and Young, F. E. (1974). Transduction in *Bacillus subtilis* by bacteriophage SPP1. *J Virol* 14, 1343–1348.

Yepes, A., Schneider, J., Mielich, B., Koch, G., Garcia-Betancur, J. C., Ramamurthi, K. S., et al. (2012). The biofilm formation defect of a *Bacillus subtilis* flotillin-defective mutant involves the protease FtsH. *Mol Microbiol* 86, 457–471. doi:10.1111/j.1365-2958.2012.08205.x.

Yokoyama, H., and Matsui, I. (2020). The lipid raft markers stomatin, prohibitin, flotillin, and HflK/C (SPFH)-domain proteins form an operon with NfeD proteins and function with apolar polyisoprenoid lipids. *Crit. Rev. Microbiol.*, 1–11. doi:10.1080/1040841X.2020.1716682.

Youngman, P., Perkins, J. B., and Losick, R. (1984). Construction of a cloning site near one end of Tn917 into which foreign DNA may be inserted without affecting transposition in *Bacillus subtilis* or expression of the transposon-borne erm gene. *Plasmid* 12, 1–9. doi:10.1016/0147-619x(84)90061-1.

Yu, J., Fischman, D. A., and Steck, T. L. (1973). Selective solubilization of proteins and phospholipids from red blood cell membranes by nonionic detergents. *J. Supramol. Struct.* 1, 233–248. doi:10.1002/jss.400010308.

Yu, M. J., Pisitkun, T., Wang, G., Aranda, J. F., Gonzales, P. A., Tchapyjnikov, D., et al. (2008). Large-scale quantitative LC-MS/MS analysis of detergent-resistant membrane proteins from rat renal collecting duct. *Am J Physiol Cell Physiol* 295, C661–78. doi:10.1152/ajpcell.90650.2007.

Zacharias, D. A., Violin, J. D., Newton, A. C., and Tsien, R. Y. (2002). Partitioning of lipid-modified monomeric GFPs into membrane microdomains of live cells. *Science* 296, 913–916. doi:10.1126/science.1068539.

Zhao, G., Meier, T. I., Kahl, S. D., Gee, K. R., and Blaszczak, L. C. (1999). BOCILLIN FL, a sensitive and commercially available reagent for detection of penicillin-binding proteins. *Antimicrobial Agents and Chemotherapy* 43, 1124–1128. doi:10.1128/aac.43.5.1124.

Zhao, H., Patel, V., Helmann, J. D., and Dörr, T. (2017). Don't let sleeping dogmas lie: new views of peptidoglycan synthesis and its regulation. *Molecular Microbiology* 106, 847–860. doi:10.1111/mmi.13853.

Zhao, J., Wu, J., and Veatch, S. L. (2013). Adhesion stabilizes robust lipid heterogeneity in supercritical membranes at physiological temperature. *Biophys. J.* 104, 825–834. doi:10.1016/j.bpj.2012.12.047.

Zhu, B., and Stülke, J. (2018). SubtiWiki in 2018: from genes and proteins to functional network annotation of the model organism *Bacillus subtilis*. *Nucleic Acids Res* 46, D743–D748. doi:10.1093/nar/gkx908.

Zielińska, A., Savietto, A., Borges, A. de S., Martinez, D., Berbon, M., Roelofsen, J. R., et al. (2020). Flotillin mediated membrane fluidity controls peptidoglycan synthesis and MreB movement. *bioRxiv*, 736819. doi:10.1101/736819.

9 APPENDIX I

9.1 Lists of contents

9.1.1 List of figures

9.1.2 List of tables

9.2 DNA sequence

FloA

Gene: BSU_25380

```
ATGGATCCGT CAACACTTAT GATTCTGGCA ATTGTCGCAG TAGCGATCAT TGTTTTGGCA GTATTTTTTA CATTTGTGCC
TGTAATGCTT TGGATTTCAG CTTTGGCAGC CGGAGTGAAA ATCAGCATTT TCACTCTAGT TGGGATGAGG CTTCGCCGCG
TCATTCCGAA TCGGGTTGTT AACCCGCTGA TTAAAGCGCA TAAAGCGGGA CTTAATGTTG GAACAAACCA GCTTGAAAGC
CACTATCTGG CTGGAGGTAA TGTTGACAGA GTCGTCAACG CGCTTATCGC CGCTCAGCGA GCTAACATTG AACTCACATT
CGAGCGCTGT GCTGCCATTG ATCTTGCAGG CCGGGACGTG TTGGAAGCTG TTCAAATGAG CGTTAATCCT AAGGTGATTG
AAACACCGTT CATTGCCGGC GTCGCAATGG ACGGGATTGA AGTGAAAGCG AAAGCGAGAA TCACAGTAAG AGCGAATATC
GAGCGCCTCG TCGGGGGAGC AGGGGAAGAA ACCATTGTAG CTCGTGTAGG TGAGGGAATC GTTTCTACAA TCGGTTCATC
TGATAATCAT AAAAAAGTGC TTGAAAACCC TGACATGATT TCTCAGACAG TCCTTGGAAA AGGATTGGAC TCAGGAACTG
CGTTTGAAAT TCTCTCAATT GATATTGCAG ATGTAGATAT CGGCAAAAAC ATCGGGGCAA TTTTACAAAC CGATCAGGCC
GAGGCTGATA AAAACATCGC GCAGGCAAAA GCGGAAGAAC GACGTGCGAT GGCTGTCGCT CAAGAACAGG AAATGCGTGC
CCGCGTAGAA GAAATGCGCG CGAAAGTAGT AGAAGCCGAG GCGGAAGTGC CGCTTGCGAT GGCAGAAGCT TTGCGTGAAG
GGAATATTGG CGTCATGGAT TACATGAATA TCAAGAACAT CGATGCTGAC ACAGAAATGC GTGATTCATT CGGCAAGCTG
ACGAAAGACC CTTCGGATGA AGACCGCAAA TCATAA
```

FloT

Gene: BSU_31010

```
ATGACAATGC CGATTATAAT GATCATCGGA GTTGTATTCT TTTTATTAAT TGCACTAATA GCTGTGTTTA TTACGAAGTA
TCGTACAGCA GGGCCTGATG AAGCGTTAAT TGTAACAGGG AGCTATCTGG GTAATAAAAA TGTTCATGTC GATGAAGGCG
GCAACCGTAT TAAAATCGTC CGCGGCGGAG GAACCTTTGT CCTTCCCGTC TTCCAGCAGG CAGAGCCGCT AAGCCTATTA
TCAAGCAAAC TCGATGTTTC GACACCTGAA GTCTATACAG AACAAGGAGT GCCAGTAATG GCCGATGGAA CTGCGATTAT
TAAAATCGGC GGTTCTATAG GAGAAATCGC TACAGCGGCC GAACAATTTT TAGGGAAATC AAAAGACGAC CGTGAGCAGG
AAGCGCGGGA GGTTTTAGAA GGCCACCTTC GTTCCATTCT CGGCTCAATG ACAGTAGAAG AAATCTATAA AAACAGAGAA
AAATTCTCTC AAGAGGTGCA GCGTGTCGCT TCACAGGATC TCGCGAAAAT GGGACTTGTA ATCGTCTCGT TTACCATTAA
AGATGTTCGT GATAAAAACG GTTATCTTGA ATCATTAGGG AAACCGAGAA TTGCCCAAGT AAAACGCGAT GCTGATATCG
CAACAGCAGA GGCTGATAAA GAAACCCGAA TTAAGCGGGC AGAAGCCGAT AAAGACGCAA AAAAATCAGA ACTTGAACGG
GCGACGGAAA TCGCTGAAGC TGAAAAAATC AATCAGCTCA AAATGGCTGA ATTCCGCAGA GAACAAGATA CGGCAAAAGC
GAATGCCGAC CAAGCATATG ATTTAGAGAC TGCCCGAGCG CGCCAGCAAG TCACAGAGCA GGAAATGCAG GTTAAAATTA
TCGAACGCCA AAAACAAATA GAACTAGAAG AAAAAGAAAT TCTTCGCCGT GAACGTCAAT ACGACTCAGA GGTAAAGAAA
AAAGCCGATG CAGACCGTTA TTCTGTTGAG CAGTCCGCAG CAGCTGAGAA AGCCAAACAG CTCGCGGAAG CCGATGCCAA
GAAGTACAGT ATTGAAGCAA TGGCAAAGGC TGAGGCGGAA AAAGTAAGAA TTGACGGGCT AGCAAAAGCA GAAGCGGAAA
AAGCGAAAGG AGAGACAGAA GCAGAGGTTA TCCGCCTGAA AGGTCTTGCA GAAGCGGAAG CAAAAGAGAA AATTGCGGCC
GCCTTTGAAC AGTACGGGCA GGCGGCGATT TTCGATATGA TTGTCAAAAT GCTTCCGGAA TACGCGAAAC AAGCAGCGGC
ACCTCTTTCA AATATTGATA AAATCACCGT TGTCGATACA GGAGGAAGCG GTGAATCAAG CGGAGCAAAC AAAGTAACCA
GCTATGCGAC GAACTTAATG TCAAGTCTGC AAGAAAGTTT AAAAGCATCC TCAGGAATTG ATGTAAAAGA AATGCTTGAG
AACTTTTCAG GAAAAGGAAA CGTAAAACAA AGCATTAATG AATTAACAAA TGAAATCAAA GAAGCCAAAA CGATCCAAAA
ATCAGAGTAA
```

$FloT_{nt}A_{ct}$

```
ATGACAATGC CGATTATAAT GATCATCGGA GTTGTATTCT TTTTATTAAT TGCACTAATA GCTGTGTTTA TTACGAAGTA
TCGTACAGCA GGGCCTGATG AAGCGTTAAT TGTAACAGGG AGCTATCTGG GTAATAAAAA TGTTCATGTC GATGAAGGCG
GCAACCGTAT TAAAATCGTC CGCGGCGGAG GAACCTTTGT CCTTCCCGTC TTCCAGCAGG CAGAGCCGCT AAGCCTATTA
TCAAGCAAAC TCGATGTTTC GACACCTGAA GTCTATACAG AACAAGGAGT GCCAGTAATG GCCGATGGAA CTGCGATTAT
TAAAATCGGC GGTTCTATAG GAGAAATCGC TACAGCGGCC GAACAATTTT TAGGGAAATC AAAAGACGAC CGTGAGCAGG
AAGCGCGGGA GGTTTTAGAA GGCCACCTTC GTTCCATTCT CGGCTCAATG ACAGTAGAAG AAATCTATAA AAACAGAGAA
AAATTCTCTC AAGAGGTGCA GCGTGTCGCT TCACAGGATC TCGCGAAAAT GGGACTTGTA ATCGTCTCGT TTACCATTAA
AGATGTTCGT GATAAAAACG GTTATCTTGA ATCATTAGGG AAACCGAGAA TTGCCCAAGT AAAACGCGAT GCTGATATCG
CAACAGCAGA GGCTGATAAA GAAACCCGAA TTAAGCGGGC AGAAGCCGAT AAAGACGCAA AAAAATCAGA ACTTGAACGG
GCGACGGAAA TCGCTGAAGC TGAAAAAATC AATCAGCTCA AAATGGCTGA ATTCCGCAGA GAACAAGATA CGGCAAAAGC
GAATGCCGAC CAAGCATATG ATTTAGAGAC TGCCCGAGCG CGCCAGCAAG TCACAGAGCA GGAAATGCAG GTTAAAATTA
TCGAACGCCA AAAACAAATA GAAGCAGATG TAGATATCGG CAAAAACATC GGGGCAATTT TACAAACCGA TCAGGCCGAG
GCTGATAAAA ACATCGCGCA GGCAAAAGCG GAAGAACGAC GTGCGATGGC TGTCGCTCAA GAACAGGAAA TGCGTGCCCG
CGTAGAAGAA ATGCGCGCGA AAGTAGTAGA AGCCGAGGCG GAAGTGCCGC TTGCGATGGC AGAAGCTTTG CGTGAAGGGA
ATATTGGCGT CATGGATTAC ATGAATATCA AGAACATCGA TGCTGACACA GAAATGCGTG ATTCATTCGG CAAGCTGACG
AAAGACCCTT CGGATGAAGA CCGCAAATCA TAA
```

$FloA_{nt}T_{ct}$

Type RW326

```
ATGGATCCGT CAACACTTAT GATTCTGGCA ATTGTCGCAG TAGCGATCAT TGTTTTGGCA GTATTTTTTA CATTTGTGCC
TGTAATGCTT TGGATTTCAG CTTTGGCAGC CGGAGTGAAA ATCAGCATTT TCACTCTAGT TGGGATGAGG CTTCGCCGCG
TCATTCCGAA TCGGGTTGTT AACCCGCTGA TTAAAGCGCA TAAAGCGGGA CTTAATGTTG GAACAAACCA GCTTGAAAGC
CACTATCTGG CTGGAGGTAA TGTTGACAGA GTCGTCAACG CGCTTATCGC CGCTCAGCGA GCTAACATTG AACTCACATT
CGAGCGCTGT GCTGCCATTG ATCTTGCAGG CCGGGACGTG TTGGAAGCTG TTCAAATGAG CGTTAATCCT AAGGTGATTG
AAACACCGTT CATTGCCGGC GTCGCAATGG ACGGGATTGA AGTGAAAGCG AAAGCGAGAA TCACAGTAAG AGCGAATATC
GAGCGCCTCG TCGGGGGAGC AGGGGAAGAA ACCATTGTAG CTCGTGTAGG TGAGGGAATC GTTTCTACAA TCGGTTCATC
TGATAATCAT AAAAAAGTGC TTGAAAACCC TGACATGATT TCTCAGACAG TCCTTGGAAA AGGATTGGAC TCAGGAACTG
CGTTTGAAAT TCTCTCAATT GATATTCTAG AAGAAAAAGA AATTCTTCGC CGTGAACGTC AATACGACTC AGAGGTAAAG
AAAAAAGCCG ATGCAGACCG TTATTCTGTT GAGCAGTCCG CAGCAGCTGA GAAAGCCAAA CAGCTCGCGG AAGCCGATGC
CAAGAAGTAC AGTATTGAAG CAATGGCAAA GGCTGAGGCG GAAAAAGTAA GAATTGACGG GCTAGCAAAA GCAGAAGCGG
```

AAAAAGCGAA AGGAGAGACA GAAGCAGAGG TTATCCGCCT GAAAGGTCTT GCAGAAGCGG AAGCAAAAGA GAAAATTGCG
GCCGCCTTTG AACAGTACGG GCAGGCGGCG ATTTTCGATA TGATTGTCAA AATGCTTCCG GAATACGCGA AACAAGCAGC
GGCACCTCTT TCAAATATTG ATAAAATCAC CGTTGTCGAT ACAGGAGGAA GCGGTGAATC AAGCGGAGCA AACAAAGTAA
CCAGCTATGC GACGAACTTA ATGTCAAGTC TGCAAGAAAG TTTAAAAGCA TCCTCAGGAA TTGATGTAAA AGAAATGCTT
GAGAACTTTT CAGGAAAAGG AAACGTAAAA CAAAGCATTA ATGAATTAAC AAATGAAATC AAAGAAGCCA AAACGATCCA
AAAATCAGAG TAA

Type RW375

ATGGATCCGT CAACACTTAT GATTCTGGCA ATTGTCGCAG TAGCGATCAT TGTTTTGGCA GTATTTTTTA CATTTGTGCC
TGTAATGCTT TGGATTTCAG CTTTGGCAGC CGGAGTGAAA ATCAGCATTT TCACTCTAGT TGGGATGAGG CTTCGCCGCG
TCATTCCGAA TCGGGTTGTT AACCCGCTGA TTAAAGCGCA TAAAGCGGGA CTTAATGTTG GAACAAACCA GCTTGAAAGC
CACTATCTGG CTGGAGGTAA TGTTGACAGA GTCGTCAACG CGCTTATCGC CGCTCAGCGA GCTAACATTG AACTCACATT
CGAGCGCTGT GCTGCCATTG ATCTTGCAGG CCGGGACGTG TTGGAAGCTG TTCAAATGAG CGTTAATCCT AAGGTGATTG
AAACACCGTT CATTGCCGGC GTCGCAATGG ACGGGATTGA AGTGAAAGCG AAAGCGAGAA TCACAGTAAG AGCGAATATC
GAGCGCCTCG TCGGGGGAGC AGGGGAAGAA ACCATTGTAG CTCGTGTAGG TGAGGGAATC GTTTCTACAA TCGGTTCATC
TGATAATCAT AAAAAAGTGC TTGAAAACCC TGACATGATT TCTCAGACAG TCCTTGGAAA AGGATTGGAC TCAGGAACTG
CGTTTGAAAT TCTCTCAATT GATATTATTC TTCGCCGTGA ACGTCAATAC GACTCAGAGG TAAAGAAAAA AGCCGATGCA
GACCGTTATT CTGTTGAGCA GTCCGCAGCA GCTGAGAAAG CCAAACAGCT CGCGGAAGCC GATGCCAAGA AGTACAGTAT
TGAAGCAATG GCAAAGGCTG AGGCGGAAAA AGTAAGAATT GACGGGCTAG CAAAAGCAGA AGCGGAAAAA GCGAAAGGAG
AGACAGAAGC AGAGGTTATC CGCCTGAAAG GTCTTGCAGA AGCGGAAGCA AAAGAGAAAA TTGCGGCCGC CTTTGAACAG
TACGGGCAGG CGGCGATTTT CGATATGATT GTCAAAATGC TTCCGGAATA CGCGAAACAA GCAGCGGCAC CTCTTTCAAA
TATTGATAAA ATCACCGTTG TCGATACAGG AGGAAGCGGT GAATCAAGCG GAGCAAACAA AGTAACCAGC TATGCGACGA
ACTTAATGTC AAGTCTGCAA GAAAGTTTAA AAGCATCCTC AGGAATTGAT GTAAAAGAAA TGCTTGAGAA CTTTTCAGGA
AAAGGAAACG TAAAACAAAG CATTAATGAA TTAACAAATG AAATCAAAGA AGCCAAAACG ATCCAAAAAT CAGAGTAA

GFP

ATGAGTAAAG GAGAAGAACT TTTCACTGGA GTTGTCCCAA TTCTTGTTGA ATTAGATGGT GATGTTAATG GGCACAAATT
TTCTGTCAGT GGAGAGGGTG AAGGTGATGC AACATACGGA AAACTTACCC TTAAATTTAT TTGCACTACT GGAAAACTAC
CTGTTCCATG GCCAACACTT GTCACTACTT TCGCGTATGG TCTTCAATGC TTTGCGAGAT ACCCAGATCA TATGAAACAG
CATGACTTTT TCAAGAGTGC CATGCCCGAA GGTTATGTAC AGGAAAGAAC TATATTTTTC AAAGATGACG GGAACTACAA
GACACGTGCT GAAGTCAAGT TTGAAGGTGA TACCCTTGTT AATAGAATCG AGTTAAAAGG TATTGATTTT AAAGAAGATG
GAAACATTCT TGGACACAAA TTGGAATACA ACTATAACTC ACACAATGTA TACATCATGG CAGACAAACA AAAGAATGGA
ATCAAAGTTA ACTTCAAAAT TAGACACAAC ATTGAAGATG GAAGCGTTCA ACTAGCAGAC CATTATCAAC AAAATACTCC
AATTGGCGAT GGCCCTGTCC TTTTACCAGA CAACCATTAC CTGTCCACAC AATCTGCCCT TTCGAAAGAT CCCAACGAAA
AGAGAGACCA CATGGTCCTT CTTGAGTTTG TAACAGCTGC TGGGATTACA CATGGCATGG ATGAACTATA CAAATAA

mCherry

ATGGTGAGCA AGGGCGAGGA GGATAACATG GCCATCATCA AGGAGTTCAT GCGCTTCAAG GTGCACATGG AGGGCTCCGT
GAACGGCCAC GAGTTCGAGA TCGAGGGCGA GGGCGAGGGC CGCCCCTACG AGGGCACCCA GACCGCCAAG CTGAAGGTGA
CCAAGGGTGG CCCCCTGCCC TTCGCCTGGG ACATCCTGTC CCCTCAGTTC ATGTACGGCT CCAAGGCCTA CGTGAAGCAC
CCCGCCGACA TCCCCGACTA CTTGAAGCTG TCCTTCCCCG AGGGCTTCAA GTGGGAGCGC GTGATGAACT TCGAGGACGG
CGGCGTGGTG ACCGTGACCC AGGACTCCTC CCTGCAGGAC GGCGAGTTCA TCTACAAGGT GAAGCTGCGC GGCACCAACT
TCCCCTCCGA CGGCCCCGTA ATGCAGAAGA AGACCATGGG CTGGGAGGCC TCCTCCGAGC GGATGTACCC CGAGGACGGC
GCCCTGAAGG GCGAGATCAA GCAGAGGCTG AAGCTGAAGG ACGGCGGCCA CTACGACGCT GAGGTCAAGA CCACCTACAA
GGCCAAGAAG CCCGTGCAGC TGCCCGGCGC CTACAACGTC AACATCAAGT TGGACATCAC CTCCCACAAC GAGGACTACA
CCATCGTGGA ACAGTACGAA CGCGCCGAGG GCCGCCACTC CACCGGCGGC ATGGACGAGC TGTACAAGTA G

pRW001-4

pRW001 (*ermC*)

TTTGCGGAAA GAGTTAATAA GTTAACAGAA GATGAACCAA AACTAAATGG TTTAGCAGGA AACTTAGATA AAAAAATGAA
TCCAGAATTA TATTCAGAAC AGGAACAGCA ACAAGAACAA CAAAAGAATC AAAAACGAGA TAGAGGTATG CACTTATAGA
ACATGCATTT ATGCCGAGAA AACTTATTGG TTGGAATGGG CTATGTGTTA GCTAACTTGT TAGCGAGTTG GTTGGACTTG
AATTGGGATT AATCCCAAGA AAGTACCAAC TCAACAACAC ATAAAGCCCT GTAGGTTCCG ACCAATAAGG AAATTGGAAT
AAAGCAATAA AAGGAGTTGA AGAAATGAAA TTCAGAGAAG CCTTTGAGAA TTTTATAACA AGTAAGTATG TACTTGGTGT
TTTAGTAGTT TTAACTGTTT ACCAGATAAT ACAAATGCTT AAATAAAAAA AGACTTGATC TGATTAGACC AAATCTTTTG
ATAGTGTTAT ATTAATAACA AAATAAAAAG GAGTCGCTCA CGCCCTGACC AAAGTTTGTG AACGACATCA TTCAAAGAAA
AAAACACTGA GTTGTTTTTA TAATCTTGTA TATTTAGATA TTAAACGATA TTTAAATATA CATCAAGATA TATATTTGGG
TGAGCGATTC CTTAAACGAA ATTGAGATTA AGGAGTCGAT TTTTTATGTA TAAAAACAAT CATGCAAATC ATTCAAATCA
TTTGGAAAAT CACGATTTAG ACAATTTTTC TAAAACCGGC TACTCTAATA GCCGGTTGGA CGCACATACT GTGTGCATAT
CTGATCCAAA ATTAAGTTTT GATGCAATGA CGATCGTTGG AAATCTCAAC CGAGACAACG CTCAAGCCCT TTCTAAATTT
ATGAGTGTAG AGCCCCAAAT AAGACTTTGG GATATTCTTC AAACAAAGTT TAAAGCTAAA GCACTTCAAG AAAAAGTTTA
TATTGAATAT GACAAAGTGA AAGCAGATAG TTGGGATAGA CGTAATATGC GTATTGAATT TAATCCAAAC AAACTTACAC
GAGATGAAAT GATTTGGTTA AAACAAAATA TAATAAGCTA CATGGAAGAT GACGGTTTTA CAAGATTAGA TTTAGCCTTT
GATTTTGAAG ATGATTTGAG TGACTACTAT GCAATGTCTG ATAAAGCAGT TAAGAAAACT ATTTTTTATG GTCGTAATGG
TAAGCCAGAA ACAAAATATT TTGGCGTGAG AGATAGTAAT AGATTTATTA GAATTTATAA TAAAAAGCAA GAACGTAAAG
ATAATGCAGA TGCTGAAGTT ATGTCTGAAC ATTTATGGCG TGTAGAAATC GAACTTAAAA GAGATATGGT GGATTACTGG
AATGATTGCT TTAGTGATTT ACATATCTTG CAACCAGATT GGAAAACTAT CCAACGCACT GCGGATAGAG CAATAGTTTT
TATGTTATTG AGTGATGAAG AAGAATGGGG AAAGCTTCAC AGAAATTCTA GAACAAAATA TAAGAATTTG ATAAAAGAAA
TTTCGCCAGT CGATTTAACG GACTTAATGA AATCGACTTT AAAAGCGAAC GAAAAACAAT TGCAAAAACA AATCGATTTT
TGGCAACATG AATTTAAATT TTGGAAATAG TGTACATATT AATATTACTG AACAAAAATG ATATATTTAA ACTATTCTAA
TTTAGGAGGA TTTTTTTATG AAGTGTCTAT TTAAAAATTT GGGGAATTTA TATGAGGTGA AAGAATAATT TACCCCTATA
AACTTTAGTC ACCTCAAGTA AAGAGGTAAA ATTGTTTAGT TTATATAAAA AATTTAAAGG TTTGTTTTAT AGCGTTTTAT
TTTGGCTTTG TATTCTTTCA TTTTTTAGTG TATTAAATGA AATGGTTTTA AATGTTTCTT TACCTGATAT TGCAAATCAT
TTTAATACTA CTCCTGGAAT TACAAACTGG GTAAACACTG CATATATGTT AACTTTTTCG ATAGGAACAG CAGTATATGG

APPENDIX I

AAAATTATCT GATTATATAA ATATAAAAAA ATTGTTAATT ATTGGTATTA GTTTGAGCTG TCTTGGTTCA TTGATTGCTT
TTATTGGGCC C**ACCTAGGAA TTGAATGAGA CATGCTACAC CTCCGGATAA TAAATATATA TAAACGTATA TAGATTTCAT**
AAAGTCTAAC ACACTAGACT TATTTACTTC GTAATTAAGT CGTTAAACCG TGTGCTCTAC GACCAAAACT ATAAAACCTT
TAAGAACTTT CTTTTTTTAC AAGAAAAAAG AAATTAGATA AATCTCTCAT ATCTTTTATT CAATAATCGC ATCCGATTGC
AGTATAAATT TAACGATCAC TCATCATGTT CATATTTATC AGAGCTCGTG CTATAATTAT ACTAATTTTA TAAGGAGGAA
AAAATATGGG CATTTTTAGT ATTTTTGTAA TCAGCACAGT TCATTATCAA CCAAACAAAA AATAAGTGGT TATAATGAAT
CGTTAATAAG CAAAATTCAT ATAACCAAAT TAAAGAGGGT TATAATGAAC GAGAAAAATA TAAAACACAG TCAAAACTTT
ATTACTTCAA AACATAATAT AGATAAAATA ATGACAAATA TAAGATTAAA TGAACATGAT AATATCTTTG AAATCGGCTC
AGGAAAAGGC CATTTTACCC TTGAATTAGT AAAGAGGTGT AATTTCGTAA CTGCCATTGA AATAGACCAT AAATTATGCA
AAACTACAGA AAATAAACTT GTTGATCACG ATAATTTCCA AGTTTTAAAC AAGGATATAT TGCAGTTTAA ATTTCCTAAA
AACCAATCCT ATAAAATATA TGGTAATATA CCTTATAACA TAAGTACGGA TATAATACGC AAAATTGTTT TTGATAGTAT
AGCTAATGAG ATTTATTTAA TCGTGGAATA CGGGTTTGCT AAAAGATTAT TAAATACAAA ACGCTCATTG GCATTACTTT
TAATGGCAGA AGTTGATATT TCTATATTAA GTATGGTTCC AAGAGAATAT TTTCATCCTA AACCTAAAGT GAATAGCTCA
CTTATCAGAT TAAGTAGAAA AAAATCAAGA ATATCACACA AAGATAAACA AAAGTATAAT TATTTCGTTA TGAAATGGGT
TAACAAAGAA TACAAGAAAA TATTTACAAA AAATCAATTT AACAATTCCT TAAAACATGC AGGAATTGAC GATTTAAACA
ATATTAGCTT TGAACAATTC TTATCTCTTT TCAATAGCTA TAAATTATTT AATAAGTAAG TTAAGGGATG CATAAACTGC
ATCCCTTAAC TTGTTTTTCG TGTGCCTATT TTTTGTGAAT CGATTATGTC TTTTGCGCAG TCGGCTTAAA CCAGTTTTCC
GCGGCGCTCG AGCGGCCGCA TAGTTAAGCC AGCCCCGACA CCCGCCAACA CCCGCTGACG CGCCCTGACG GGCTTGTCTG
CTCCCGGCAT CCGCTTACAG ACAAGCTGTG ACCGTCTCCG GGAGCTGCAT GTGTCAGAGG TTTTCACCGT CATCACCGAA
ACGCGCGAGA CGAAAGGGCC TCGTGATACG CCTATTTTTA TAGGTTAATG TCATGATAAT AATGGTTTCT TAGACGTCAG
GTGGCACTTT TCGGGGAAAT GTGCGCGGAA CCCCTATTTG TTTATTTTTC TAAATACATT CAAATATGTA TCCGCTCATG
AGACAATAAC CCTGATAAAT GCTTCAATAA TATTGAAAAA GGAAGAGTAT GAGTATTCAA CATTTCCGTG TCGCCCTTAT
TCCCTTTTTT GCGGCATTTT GCCTTCCTGT TTTTGCTCAC CCAGAAACGC TGGTGAAAGT AAAAGATGCT GAAGATCAGT
TGGGTGCACG AGTGGGTTAC ATCGAACTGG ATCTCAACAG CGGTAAGATC CTTGAGAGTT TTCGCCCCGA AGAACGTTTT
CCAATGATGA GCACTTTTAA AGTTCTGCTA TGTGGCGCGG TATTATCCCG TATTGACGCC GGGCAAGAGC AACTCGGTCG
CCGCATACAC TATTCTCAGA ATGACTTGGT TGAGTACTCA CCAGTCACAG AAAAGCATCT TACGGATGGC ATGACAGTAA
GAGAATTATG CAGTGCTGCC ATAACCATGA GTGATAACAC TGCGGCCAAC TTACTTCTGA CAACGATCGG AGGACCGAAG
GAGCTAACCG CTTTTTTGCA CAACATGGGG GATCATGTAA CTCGCCTTGA TCGTTGGGAA CCGGAGCTGA ATGAAGCCAT
ACCAAACGAC GAGCGTGACA CCACGATGCC TGTAGCAATG GCAACAACGT TGCGCAAACT ATTAACTGGC GAACTACTTA
CTCTAGCTTC CCGGCAACAA TTAATAGACT GGATGGAGGC GGATAAAGTT GCAGGACCAC TTCTGCGCTC GGCCCTTCCG
GCTGGCTGGT TTATTGCTGA TAAATCTGGA GCCGGTGAGC GTGGGTCTCG CGGTATCATT GCAGCACTGG GGCCAGATGG
TAAGCCCTCC CGTATCGTAG TTATCTACAC GACGGGGAGT CAGGCAACTA TGGATGAACG AAATAGACAG ATCGCTGAGA
TAGGTGCCTC ACTGATTAAG CATTGGTAAC TGTCAGACCA AGTTTACTCA TATATACTTT AGATTGATTT AAAACTTCAT
TTTTAATTTA AAAGGATCTA GGTGAAGATC CTTTTTGATA ATCTCATGAC CAAAATCCCT TAACGTGAGT TTTCGTTCCA
CTGAGCGTCA GACCCCGTAG AAAAGATCAA AGGATCTTCT TGAGATCCTT TTTTTCTGCG CGTAATCTGC TGCTTGCAAA
CAAAAAAACC ACCGCTACCA GCGGTGGTTT GTTTGCCGGA TCAAGAGCTA CCAACTCTTT TTCCGAAGGT AACTGGCTTC
AGCAGAGCGC AGATACCAAA TACTGTTCTT CTAGTGTAGC CGTAGTTAGG CCACCACTTC AAGAACTCTG TAGCACCGCC
TACATACCTC GCTCTGCTAA TCCTGTTACC AGTGGCTGCT GCCAGTGGCG ATAAGTCGTG TCTTACCGGG TTGGACTCAA
GACGATAGTT ACCGGATAAG GCGCAGCGGT CGGGCTGAAC GGGGGGTTCG TGCACACAGC CCAGCTTGGA GCGAACGACC
TACACCGAAC TGAGATACCT ACAGCGTGAG CTATGAGAAA GCGCCACGCT TCCCGAAGGG AGAAAGGCGG ACAGGTATCC
GGTAAGCGGC AGGGTCGGAA CAGGAGAGCG CACGAGGGAG CTTCCAGGGG GAAACGCCTG GTATCTTTAT AGTCCTGTCG
GGTTTCGCCA CCTCTGACTT GAGCGTCGAT TTTTGTGATG CTCGTCAGGG GGGCGGAGCC TATGGAAAAA CGCCAGCAAC
GCGGCCTTTT TACGGTTCCT GGCCTTTTGC TGGCCTTTTG CTCACATGTT CTTTCCTGCG TTATCCCCTG ATTCTGTGGA
TAACCGTATT ACCGCCTTTG AGTGAGCTGG CGGCCGCTGC ATGCTAGCAG ATCTCCATGG TACCCGGGAG CTCGAATTCT
AGAAGCTTCT GCAGACGCGT CGACGTCATA TGGATCCGAT ATCGGCGCC

Sequence that is bolded corresponds to *ermC* resistance cassette that is exchanged for other antibiotic cassettes in the pRW002-4 derivates. For these, only the sequence of the antibiotic cassette will be displayed.

pRW002 (*km*)

CAGCGAACCA TTTGAGGTGA TAGGTAAGAT TATACCGAGG TATGAAAACG AGAATTGGAC CTTTACAGAA TTACTCTATG
AAGCGCCATA TTTAAAAAGC TACCAAGACG AAGAGGATGA AGAGGATGAG GAGGCAGATT GCCTTGAATA TATTGACAAT
ACTGATAAGA TAATATATCT TTTATATAGA AGATATCGCC GTATGTAAGG ATTTCAGGGG GCAAGGCATA GGCAGCGCGC
TTATCAATAT ATCTATAGAA TGGGCAAAGC ATAAAAACTT GCATGGACTA ATGCTTGAAA CCCAGGACAA TAACCTTATA
GCTTGTAAAT TCTATCATAA TTGTGGTTTC AAAATCGGCT CCGTCGATAC TATGTTATAC GCCAACTTTC AAAACAACTT
TGAAAAAGCT GTTTTCTGGT ATTTAAGGTT TTAGAATGCA AGGAACAGTG AATTGGAGTT CGTCTTGTTA TAATTAGCTT
CTTGGGGTAT CTTTAAATAC TGTAGAAAAG AGGAAGGAAA TAATAAATGG CTAAAATGAG AATATCACCG GAATTGAAAA
AACTGATCGA AAAATACCGC TGCGTAAAAG ATACGGAAGG AATGTCTCCT GCTAAGGTAT ATAAGCTGGT GGGAGAAAAT
GAAAACCTAT ATTTAAAAAT GACGGACAGC CGGTATAAAG GGACCACCTA TGATGTGGAA CGGGAAAAGG ACATGATGCT
ATGGCTGGAA GGAAAGCTGC CTGTTCCAAA GGTCCTGCAC TTTGAACGGC ATGATGGCTG GAGCAATCTG CTCATGAGTG
AGGCCGATGG CGTCCTTTGC TCGGAAGAGT ATGAAGATGA ACAAAGCCCT GAAAAGATTA TCGAGCTGTA TGCGGAGTGC
ATCAGGCTCT TTCACTCCAT CGACATATCG GATTGTCCCT ATACGAATAG CTTAGACAGC CGCTTAGCCG AATTGGATTA
CTTACTGAAT AACGATCTGG CCGATGTGGA TTGCGAAAAC TGGGAAGAAG ACACTCCATT TAAAGATCCG CGCGAGCTGT
ATGATTTTTT AAAGACGGAA AAGCCCGAAG AGGAACTTGT CTTTTCCCAC GGCGACCTGG GAGACAGCAA CATCTTTGTG
AAAGATGGCA AAGTAAGTGG CTTTATTGAT CTTGGGAGAA GCGGCAGGGC GGACAAGTGG TATGACATTG CCTTCTGCGT
CCGGTCGATC AGGGAGGATA TCGGGGAAGA ACAGTATGTC GAGCTATTTT TTGACTTACT GGGGATCAAG CCTGATTGGG
AGAAAATAAA ATATTATATT TTACTGGATG AATTGTTTTA GTACCTAGAT TTAGATGTCT AAAAAGCTTT AACTACAAGC
TTTTTAGACA TCTAATCTTT TCTGAAGTAC ATCCGCAACT GTCCATACTC TGATGTTTTA TATCTTTTCT AAAAGTTCGC
TAGATAGGGG TCCCGAGCGC CTACGAGGAA TTTGTATCG

pRW003 (*tet*)

TCTTGCAATG GTGCAGGTTG TTCTCAATGT CGAAAATATG TATTTGTATT TAACGCACGA GAGCAAGGAC GCTATTGCTA
AGAAGAAACA TGTTTATGAT AAGGCTGATA TAAAGCTAAT CAATAATTTT GATATTGACC GTTATGTGAC GTTAGATGTC
GAGGAAAAGA CCGAACTTTT CAATGTGGTT GTATCGCTTA TTCGTGCGTA CACTCTCCAA AATATTTTTG ATTTGTATGA

APPENDIX I

TTTCATTGAC GAAAATGGAG AAACTTATGG GTTGACTATA AATTTGGTTA ACGAAGTTAT TGCAGGGAAA ACTGGTTTTA
TGAAATTGTT GTTTGACGGA GCTTATCAAC GTAGTAAGCG TGGAACAAAG AACGAAGAGA GATAAAAAGT TGATCTTTGT
GAAAACTACA GAAAGTAAAG AATGAAAAGA GTAATGCTAA CATAGCATTA CGGATTTTAT GACCGATGAT GAAGAAAAGA
ATTTGAAACT TAGTTTATAT GTGGTAAAAT GTTTTAATCA AGTTTAGGAG GAATTAATTA TGAAGTGTAA TTAATGTAAC
AGGGTTCAAT TAAAAGAGGG AAGCGTATCA TTAACCCTAT AAACTACGTC TGCCCTCATT ATTGGAGGGT GAAATGTGAA
TACATCCTAT TCACAATCGA ATTTACGACA CAACCAAATT TTAATTTGGC TTTGCATTTT ATCTTTTTTT AGCGTATTAA
ATGAAATGGT TTTGAACGTC TCATTACCTG ATATTGCAAA TGATTTTAAT AAACCACCTG CGAGTACAAA CTGGGTGAAC
ACAGCCTTTA TGTTAACCTT TTCCATTGGA ACAGCTGTAT ATGGAAAGCT ATCTGATCAA TTAGGCATCA AAAGGTTACT
CCTATTTGGA ATTATAATAA ATTGTTTCGG GTCGGTAATT GGGTTTGTTG GCCATTCTTT CTTTTCCTTA CTTATTATGG
CTCGTTTTAT TCAAGGGGCT GGTGCAGCTG CATTTCCAGC ACTCGTAATG GTTGTAGTTG CGCGCTATAT TCCAAAGGAA
AATAGGGGTA AAGCATTTGG TCTTATTGGA TCGATAGTAG CCATGGGAGA AGGAGTCGGT CCAGCGATTG GTGGAATGAT
AGCCCATTAT ATTCATTGGT CCTATCTTCT ACTCATTCCT ATGATAACAA TTATCACTGT TCCGTTTCTT ATGAAATTAT
TAAAGAAAGA AGTAAGGATA AAAGGTCATT TTGATATCAA AGGAATTATA CTAATGTCTG TAGGCATTGT ATTTTTTATG
TTGTTTACAA CATCATATAG CATTTCTTTT CTTATCGTTA GCGTGCTGTC ATTCCTGATA TTTGTAAAAC ATATCAGGAA
AGTAACAGAT CCTTTTGTTG ATCCCGGATT AGGGAAAAAT ATACCTTTTA TGATTGGAGT TCTTTGTGGG GGAATTATAT
TTGGAACAGT AGCAGGGTTT GTCTCTATGG TTCCTTATAT GATGAAAGAT GTTCACCAGC TAAGTACTGC CGAAATCGGA
AGTGTAATTA TTTTCCCTGG AACAATGAGT GTCATTATTT TCGGCTACAT TGGTGGGATA CTTGTTGATA GAAGAGGTCC
TTTATACGTG TTAAACATCG GAGTTACATT TCTTTCTGTT AGCTTTTTAA CTGCTTCCTT TCTTTTAGAA ACAACATCAT
GGTTCATGAC AATTATAATC GTATTTGTTT TAGGTGGGCT TTCGTTCACC AAAACAGTTA TATCAACAAT TGTTTCAAGT
AGCTTGAAAC AGCAGGAAGC TGGTGCTGGA ATGAGTTTGC TTAACTTTAC CAGCTTTTTA TCAGAGGGAA CAGGTATTGC
AATTGTAGGT GGTTTATTAT CCATACCCTT ACTTGATCAA AGGTTGTTAC CTATGGAAGT TGATCAGTCA ACTTATCTGT
ATAGTAATTT GTTATTACTT TTTTCAGGAA TCATTGTCAT TAGTTGGCTG GTTACCTTGA ATGTATATAA ACATTCTCAA
AGGGATTTCT AAATCGTTAA GGGATCAACT TTGGGAGAGA GTTC

pRW004 (*cm*)

CGGCAATAGT TACCCTTATT ATCAAGATAA GAAAGAAAAG GATTTTTCGC TACGCTCAAA TCCTTTAAAA AAACACAAAA
GACCACATTT TTTAATGTGG TCTTTATTCT TCAACTAAAG CACCCATTAG TTCAACAAAC GAAAATTGGA TAAAGTGGGA
TATTTTTAAA ATATATATTT ATGTTACAGT AATATTGACT TTTAAAAAAG GATTGATTCT AATGAAGAAA GCAGACAAGT
AAGCCTCCTA AATTCACTTT AGATAAAAAT TTAGGAGGCA TATCAAATGA ACTTTAATAA AATTGATTTA GACAATTGGA
AGAGAAAAGA GATATTTAAT CATTATTTGA ACCAACAAAC GACTTTTAGT ATAACCACAG AAATTGATAT TAGTGTTTTA
TACCGAAACA TAAAACAAGA AGGATATAAA TTTTACCCTG CATTTATTTT CTTAGTGACA AGGGTGATAA ACTCAAATAC
AGCTTTTAGA ACTGGTTACA ATAGCGACGG AGAGTTAGGT TATTGGGATA AGTTAGAGCC ACTTTATACA ATTTTTGATG
GTGTATCTAA AACATTCTCT GGTATTTGGA CTCCTGTAAA GAATGACTTC AAAGAGTTTT ATGATTTATA CCTTTCTGAT
GTAGAGAAAT ATAATGGTTC GGGGAAATTG TTTCCCAAAA CACCTATACC TGAAAATGCT TTTTCTCTTT CTATTATTCC
ATGGACTTCA TTTACTGGGT TTAACTTAAA TATCAATAAT AATAGTAATT ACCTTCTACC CATTATTACA GCAGGAAAAT
TCATTAATAA AGGTAATTCA ATATATTTAC CGCTATCTTT ACAGGTACAT CATTCTGTTT GTGATGGTTA TCATGCAGGA
TTGTTTATGA ACTCTATTCA GGAATTGTCA GATAGGCCTA ATGACTGGCT TTTATAATAT GAGATAATGC CGACTGTACT
TTTTACAGTC GGTTTTCTAA TGTCACTAAC CTGCCCCGTT AGTTGAAGAA GGTTTTTATA TTACAGCTCC AGATC

9.3 Flotillin secondary structure and domain prediction

9.3.1 Secondary structure prediction with Phyre[2]

The secondary structures of flotillins were predicted with Phyre[2] (Kelley et al., 2015).

FloA

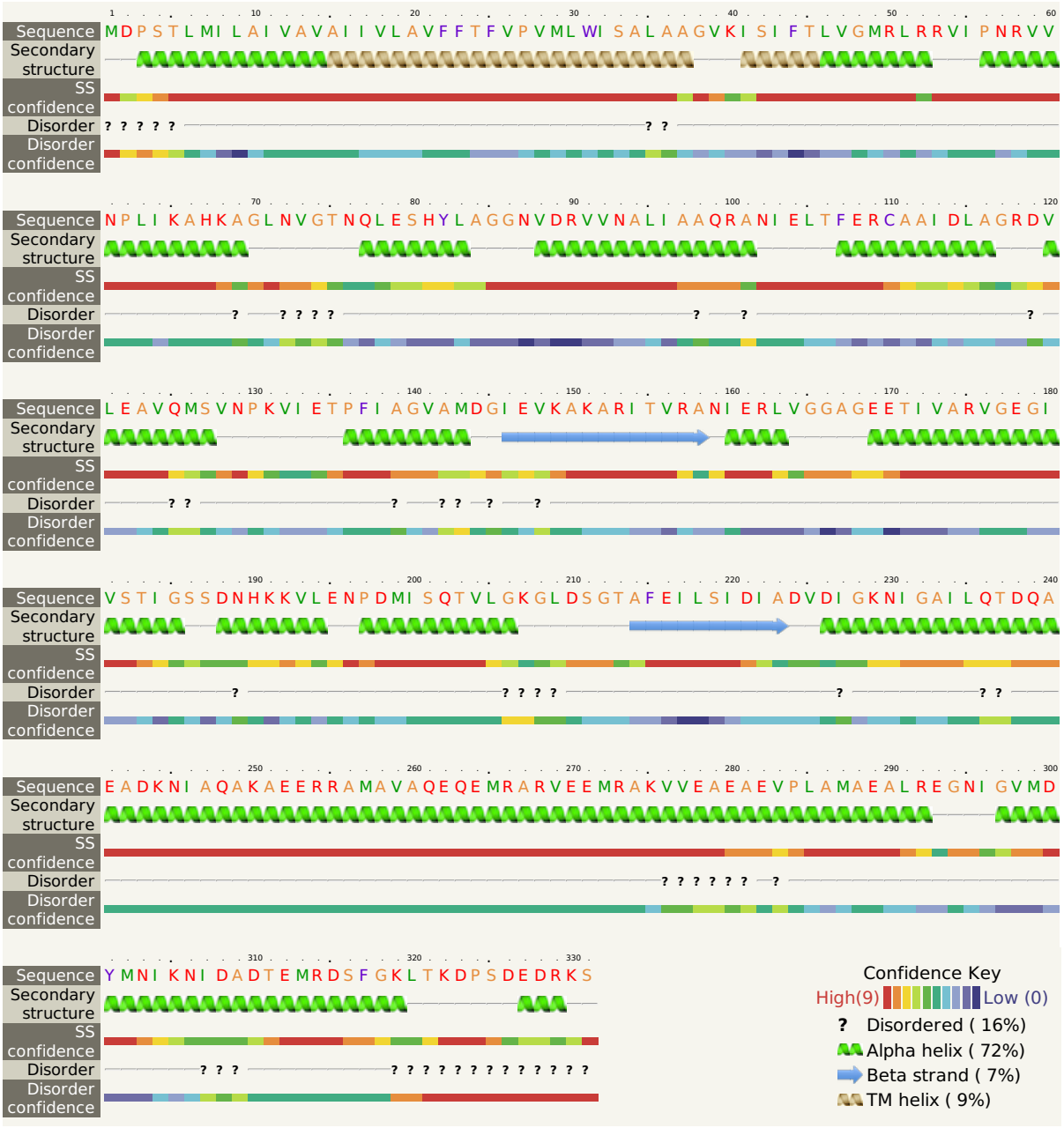

FloT


Sequence
Secondary structure
SS confidence
Disorder
Disorder confidence
MTMPIIMIIGVVFFLLIALIAVFITKYRTAGPDEALIVTGSYLGNKNVHVDEGGNRIKIV
RGGGTFVLPVFQQAEPLSLLSSKLDVSTPEVYTEQGVPVMADGTAIIKIGGSIGEIATAA
EQFLGKSKDDREQEAREVLEGHLRSILGSMTVEEIYKNREKFSQEVQRVASQDLAKMGLV
IVSFTIKDVRDKNGYLESLGKPRIAQVKRDADIATAEADKETRIKRAEADKDAKKSELER
ATEIAEAEKINQLKMAEFRREQDTAKANADQAYDLETARARQQVTEQEMQVKIIERQKQI
ELEEKEILRRERQYDSEVKKKADADRYSVEQSAAAEKAKQLAEADAKKYSIEAMAKAEAE
KVRIDGLAKAEAEKAKGETEAEVIRLKGLAEAEAKEKIAAAFEQYGQAAIFDMIVKMLPE
YAKQAAAPLSNIDKITVVDTGGSGESSGANKVTSYATNLMSSLQESLKASSGIDVKEMLE


490
500
Sequence
N F S G K G N V K Q S I N E L T N E I K E A K T I Q K S E
Secondary structure
SS confidence
Disorder
? ?
Disorder confidence
Confidence Key
High(9) Low (0)
? Disordered (15%)
Alpha helix (69%)
Beta strand (11%)
TM helix (4%)

FloT$_{nt}$A$_{ct}$

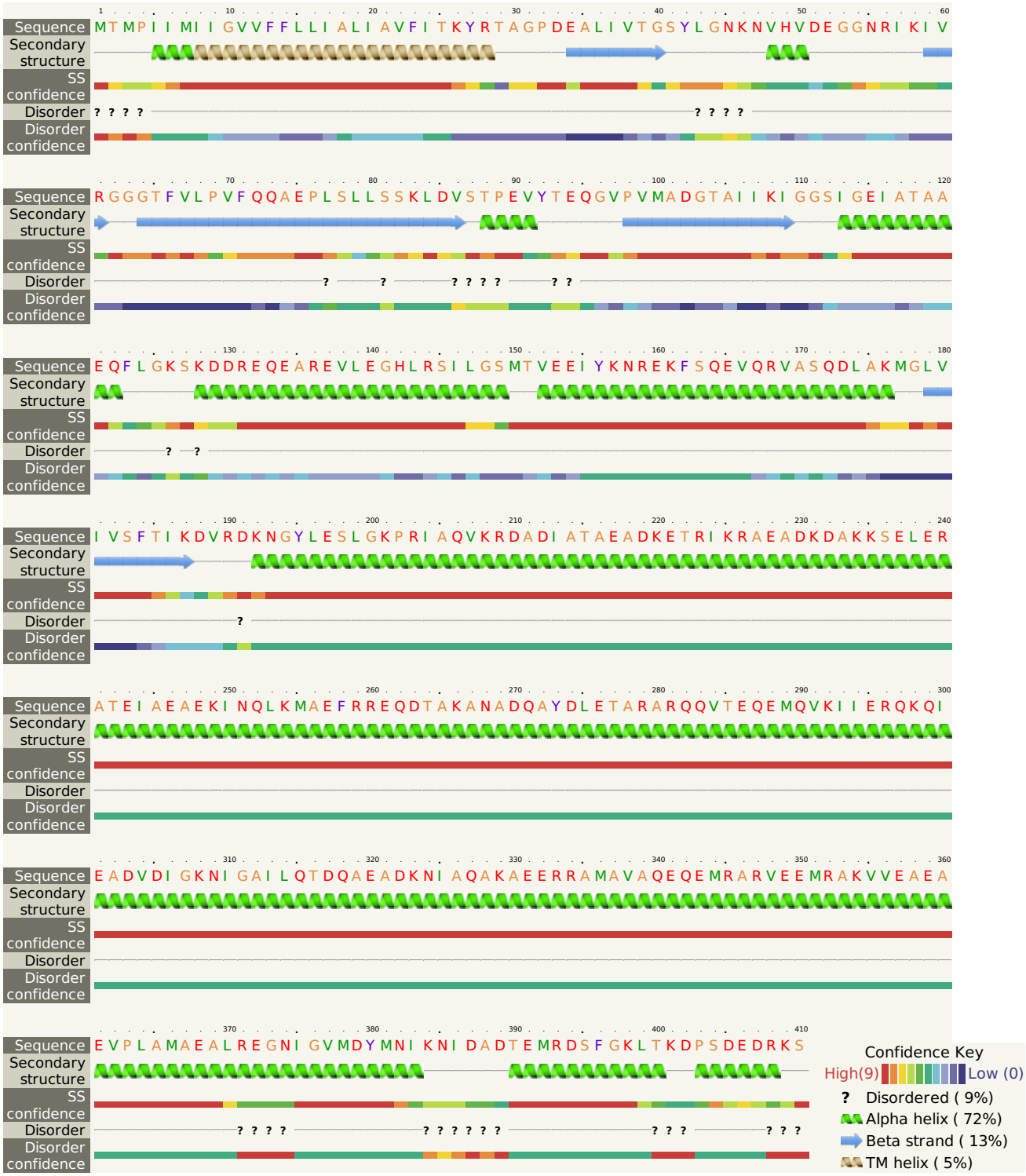
1 10 20 30 40 50 60
Sequence
M T M P I I M I I G V V F F L L I A L I A V F I T K Y R T A G P D E A L I V T G S Y L G N K N V H V D E G G N R I K I V
Secondary structure
SS confidence
Disorder
? ? ? ?
? ? ? ?
Disorder confidence
70 80 90 100 110 120
Sequence
R G G G T F V L P V F Q Q A E P L S L L S S K L D V S T P E V Y T E Q G V P V M A D G T A I I K I G G S I G E I A T A A
Secondary structure
SS confidence
Disorder
? ? ? ? ? ? ? ?
Disorder confidence
130 140 150 160 170 180
Sequence
E Q F L G K S K D D R E Q E A R E V L E G H L R S I L G S M T V E E I Y K N R E K F S Q E V Q R V A S Q D L A K M G L V
Secondary structure
SS confidence
Disorder
? ?
Disorder confidence
190 200 210 220 230 240
Sequence
I V S F T I K D V R D K N G Y L E S L G K P R I A Q V K R D A D I A T A E A D K E T R I K R A E A D K D A K K S E L E R
Secondary structure
SS confidence
Disorder
?
Disorder confidence
250 260 270 280 290 300
Sequence
A T E I A E A E K I N Q L K M A E F R R E Q D T A K A N A D Q A Y D L E T A R A R Q Q V T E Q E M Q V K I I E R Q K Q I
Secondary structure
SS confidence
Disorder
Disorder confidence
310 320 330 340 350 360
Sequence
E A D V D I G K N I G A I L Q T D Q A E A D K N I A Q A K A E E R R A M A V A Q E Q E M R A R V E E M R A K V V E A E A
Secondary structure
SS confidence
Disorder
Disorder confidence
370 380 390 400 410
Sequence
E V P L A M A E A L R E G N I G V M D Y M N I K N I D A D T E M R D S F G K L T K D P S D E D R K S
Secondary structure
SS confidence
Disorder
? ? ? ?
? ? ? ? ? ?
? ? ?
? ? ?
Disorder confidence
Confidence Key
High(9) Low (0)
? Disordered (9%)
Alpha helix (72%)
Beta strand (13%)
TM helix (5%)

$FloA_{nt}T_{ct}$ Type RW326

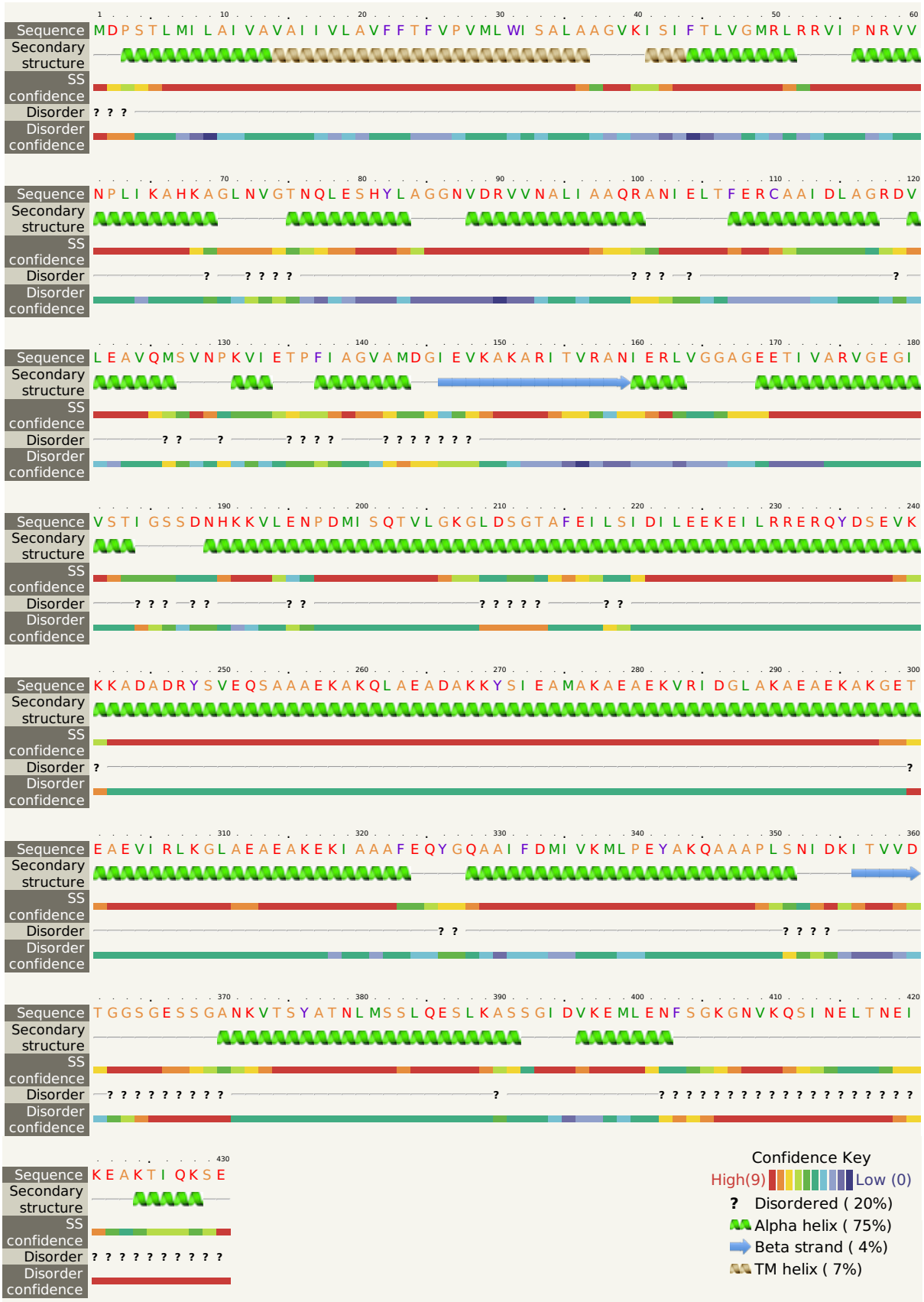

$FloA_{nt}T_{ct}$ Type RW375

9.3.2 Domain prediction with SMART

Protein domains of flotillins were predicted with SMART (Letunic et al., 2015; Letunic and Bork, 2018).

FloA

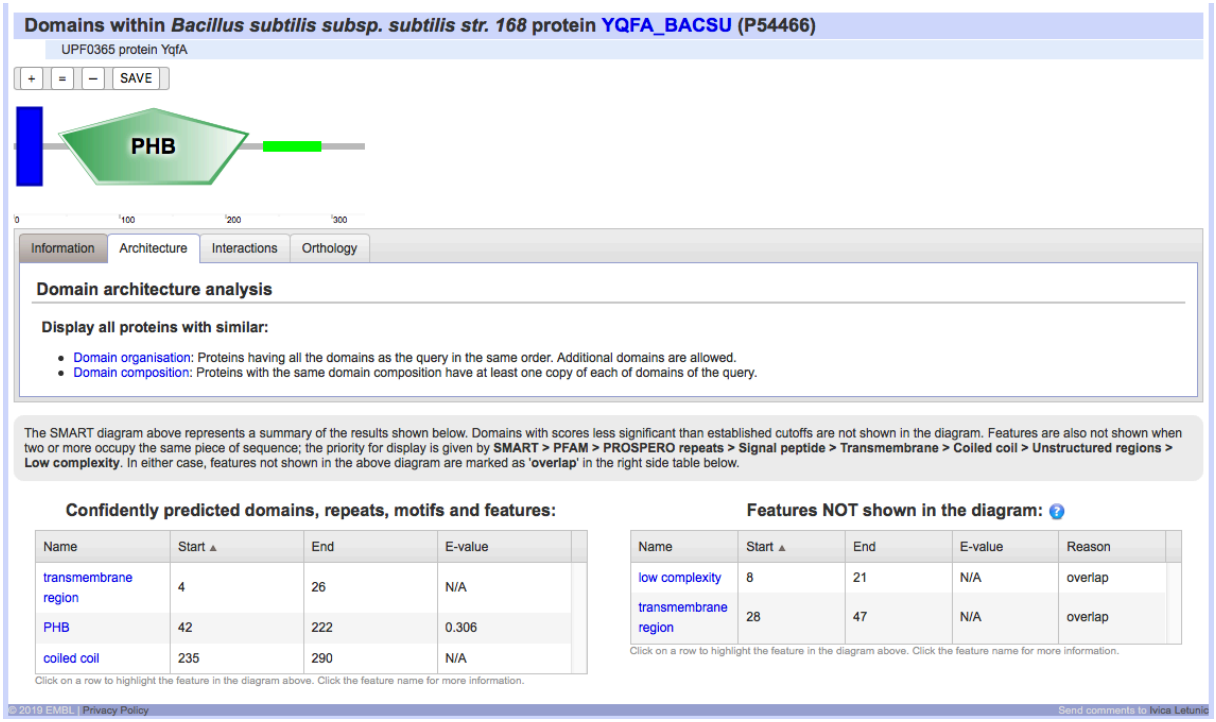

Domains within *Bacillus subtilis subsp. subtilis str. 168* protein YQFA_BACSU (P54466)

UPF0365 protein YqfA

+ = − SAVE

PHB

0 100 200 300

Information | Architecture | Interactions | Orthology

Domain architecture analysis

Display all proteins with similar:

- Domain organisation: Proteins having all the domains as the query in the same order. Additional domains are allowed.
- Domain composition: Proteins with the same domain composition have at least one copy of each of domains of the query.

The SMART diagram above represents a summary of the results shown below. Domains with scores less significant than established cutoffs are not shown in the diagram. Features are also not shown when two or more occupy the same piece of sequence; the priority for display is given by **SMART > PFAM > PROSPERO repeats > Signal peptide > Transmembrane > Coiled coil > Unstructured regions > Low complexity**. In either case, features not shown in the above diagram are marked as '**overlap**' in the right side table below.

Confidently predicted domains, repeats, motifs and features:

Name	Start ▲	End	E-value
transmembrane region	4	26	N/A
PHB	42	222	0.306
coiled coil	235	290	N/A

Click on a row to highlight the feature in the diagram above. Click the feature name for more information.

Features NOT shown in the diagram:

Name	Start ▲	End	E-value	Reason
low complexity	8	21	N/A	overlap
transmembrane region	28	47	N/A	overlap

Click on a row to highlight the feature in the diagram above. Click the feature name for more information.

© 2019 EMBL | Privacy Policy — Send comments to Ivica Letunic

FloT

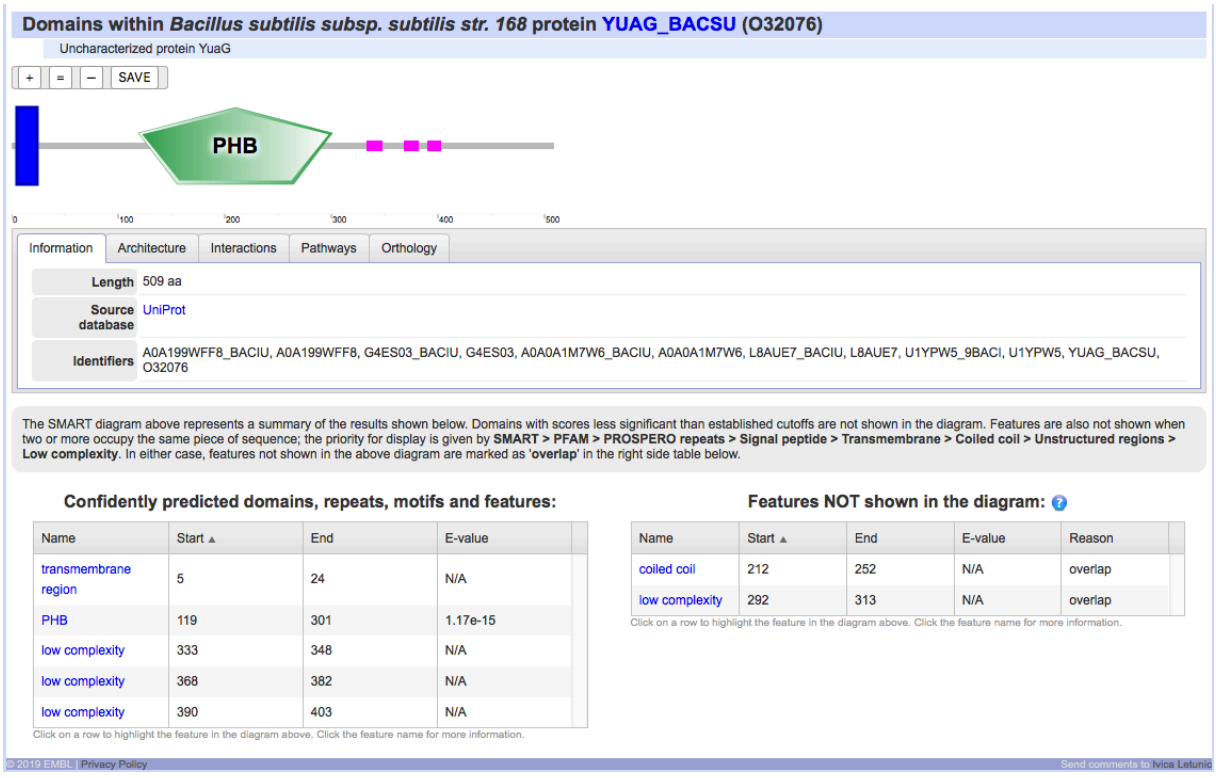

Domains within *Bacillus subtilis subsp. subtilis str. 168* protein YUAG_BACSU (O32076)

Uncharacterized protein YuaG

+ = − SAVE

PHB

0 100 200 300 400 500

Information | Architecture | Interactions | Pathways | Orthology

Length	509 aa
Source database	UniProt
Identifiers	A0A199WFF8_BACIU, A0A199WFF8, G4ES03_BACIU, G4ES03, A0A0A1M7W6_BACIU, A0A0A1M7W6, L8AUE7_BACIU, L8AUE7, U1YPW5_9BACI, U1YPW5, YUAG_BACSU, O32076

The SMART diagram above represents a summary of the results shown below. Domains with scores less significant than established cutoffs are not shown in the diagram. Features are also not shown when two or more occupy the same piece of sequence; the priority for display is given by **SMART > PFAM > PROSPERO repeats > Signal peptide > Transmembrane > Coiled coil > Unstructured regions > Low complexity**. In either case, features not shown in the above diagram are marked as '**overlap**' in the right side table below.

Confidently predicted domains, repeats, motifs and features:

Name	Start ▲	End	E-value
transmembrane region	5	24	N/A
PHB	119	301	1.17e-15
low complexity	333	348	N/A
low complexity	368	382	N/A
low complexity	390	403	N/A

Click on a row to highlight the feature in the diagram above. Click the feature name for more information.

Features NOT shown in the diagram:

Name	Start ▲	End	E-value	Reason
coiled coil	212	252	N/A	overlap
low complexity	292	313	N/A	overlap

Click on a row to highlight the feature in the diagram above. Click the feature name for more information.

© 2019 EMBL | Privacy Policy — Send comments to Ivica Letunic

9.4 Fatty acid composition

Table 5: Raw data of fatty acid composition analysis.

	Ctrl	AMP	VAN	VAL
PEAK	**Relative Abundance**			
10:0	0,12	0,10	0,12	0,10
12:0	0,00	0,00	0,00	0,14
13:0 iso	0,27	0,33	0,27	0,25
13:0 anteiso	0,20	0,19	0,16	0,16
14:0 iso	1,67	1,49	1,63	1,67
14:0	0,81	0,64	0,94	1,09
15:0 iso	20,60	23,22	19,35	17,88
15:0 anteiso	41,59	40,02	40,62	39,88
15:0 2OH	0,00	0,00	0,13	0,16
16:0 iso	4,19	3,83	4,57	4,92
16:0	6,88	5,28	8,65	10,26
16:0 iso 3OH	0,00	0,20	0,25	0,23
17:0 iso	10,81	12,06	9,97	9,50
17:0 anteiso	11,88	11,95	11,78	11,29
17:0	0,30	0,23	0,42	0,50
17:0 2OH	0,00	0,00	0,00	0,15
18:0 iso	0,00	0,00	0,00	0,12
18:0	0,68	0,45	0,92	1,18
18:1	0,00	0,00	0,00	0,28
TYPE	**Sum of relative abundances**			
C15	62,19	63,24	60,10	57,92
C17	22,99	24,24	22,17	21,44
iso	37,54	41,13	36,04	34,45
anteiso	53,67	52,16	52,56	51,33
	Ratio			
C17/C15	0,37	0,38	0,37	0,37
iso/anteiso	0,70	0,79	0,69	0,67

9.5 Pull-down raw data

Table 6: Pull-down log_{10}-fold change heatmap.

Protein	$FloT_{nt}A_{ct}$	FloA	FloT	$FloA_{nt}T_{ct}$	Functional Category (Zhu and Stülke, 2018)
Ndh	0,61641	0,60578	0,61841	0,39827	Metabolism
MurG	0,47028	0,36275	0,07434	-1,2	Metabolism
PlsX	0,47028	0,45966	0,25043	-1,2	Metabolism
QoxA	0,24843	0,36275	0,07434	-1,2	Metabolism
ResE	0,72555	0,36275	0,07434	-1,2	Metabolism
NupN	0,07234	0,06172	0,47228	-1,2	Metabolism
FadE	0,07234	0,60578	-1,2	0,09724	Metabolism
PhoR	0,47028	0,06172	-1,2	-1,2	Metabolism
FruA	0,07234	-1,2	-1,2	-1,2	Metabolism
Vpr	-1,2	-1,2	-0,95071	-1,2	Metabolism
FecC	-1,2	-1,2	0,07434	-1,2	Metabolism
MsmX	-1,2	-1,2	0,07434	-1,2	Metabolism
CtaD	-1,2	-1,2	-1,2	0,09724	Metabolism
Eno	-1,2	-1,2	-1,2	0,09724	Metabolism
ResB	0,07234	-1,2	-1,2	0,09724	Metabolism
HemY	0,24843	-1,2	-1,2	0,49518	Metabolism
AtpG	0,24843	-1,2	0,07434	-1,2	Metabolism
CtaC	-0,16769	-0,46399	-0,15483	-0,42431	Metabolism
OdhB	-0,19765	0,01314	-0,25174	-0,16107	Metabolism
Icd	-0,36606	-0,30428	-0,33092	-0,35736	Metabolism
GapA	-0,56563	-0,37684	-0,55277	-0,12328	Metabolism
AtpD	-0,57899	-0,41040	-0,49150	-0,38652	Metabolism
AtpA	-0,77951	-0,71926	-0,50701	-0,37855	Metabolism
PdhB	-0,68373	-0,61987	-0,39787	-0,54241	Metabolism
QcrC	-0,74172	-0,81617	-0,58273	-0,69731	Metabolism
SdhA	-0,13966	-0,07581	-0,07565	0,09857	Metabolism
SdhB	-1,2	-1,2	0,61841	0,09724	Metabolism
Hom	-1,2	0,23781	-1,2	-1,2	Metabolism
PycA	-1,2	0,23781	-1,2	-1,2	Metabolism
CdaA	-1,2	0,06172	-1,2	-1,2	Metabolism
AppD	0,07234	-1,2	0,07434	-1,2	Transporters
MetN	-1,2	0,06172	0,07434	-1,2	Transporters
AppF	-1,2	0,06172	0,25043	-1,2	Transporters
MetQ	-0,74172	-0,71926	-0,18479	-0,50349	Transporters
MntB	-1,2	-0,69123	-0,30289	-0,60040	Transporters
AlbC	-0,51987	-0,69123	-0,36088	-0,47546	Transporters
MntA	-0,66917	-0,65344	-0,56613	-0,94282	Transporters
RbsC	-1,2	-1,2	-0,72886	-0,60040	Transporters
EcsA	-0,91781	-1,2	-0,60392	-0,77649	Transporters
TcyA	-1,2	-1,2	0,25043	0,09724	Transporters
DppE	0,07234	-1,2	0,25043	0,27333	Transporters
YhfQ	0,47028	0,53884	0,25043	0,27333	Transporters
ArtP	0,07234	0,36275	0,47228	0,57436	Transporters
FhuD	0,54946	0,45966	0,72755	0,49518	Transporters
FeuA	0,67440	0,53884	0,88725	0,39827	Transporters
RbsB	0,77131	0,71493	0,61841	0,49518	Transporters
YxeB	0,24843	0,66378	0,72755	0,39827	Transporters
ManP	0,94740	0,36275	0,47228	0,09724	Transporters
RbsA	1,21847	0,80208	0,77331	1,09724	Transporters
PfeT	-0,00136	0,05889	-0,12680	-0,29937	Transporters
EzrA	-1,2	0,23781	0,07434	-1,2	Cell envelope and cell division
MinD	-1,2	0,06172	0,25043	-1,2	Cell envelope and cell division
FtsH	-0,16769	-0,46399	-0,72886	-0,29937	Cell envelope and cell division
FtsZ	0,24843	0,76069	0,47228	0,27333	Cell envelope and cell division

APPENDIX I

Protein	$FloT_{nt}A_{ct}$	FloA	FloT	$FloA_{nt}T_{ct}$	Functional Category (Zhu and Stülke, 2018)
TagU	0,37337	0,45966	0,61841	0,09724	Cell envelope and cell division
TagF	-1,2	0,06172	-1,2	-1,2	Cell envelope and cell division
RodZ	0,54946	-1,2	0,67640	-1,2	Cell envelope and cell division
PBP5	-0,21884	-0,33905	-0,30289	-0,12328	Cell envelope and cell division
MreB	-0,31575	-0,51514	-0,30289	-0,60040	Cell envelope and cell division
DltD	-1,2	-1,2	0,37537	-1,2	Cell envelope and cell division
Mbl	-0,74172	-0,64008	-0,55277	-0,29937	Cell envelope and cell division
RasP	0,07234	0,06172	-1,2	0,09724	Cell envelope and cell division
FtsA	-1,2	-1,2	-1,2	-0,12328	Cell envelope and cell division
MreC	0,24843	0,06172	0,07434	-1,2	Cell envelope and cell division
PBP3	0,07234	0,36275	0,25043	-1,2	Cell envelope and cell division
FloA	0,73952	1,00991	-0,19375	0,45213	Cell envelope and cell division
Hag	-0,88002	-1,15859	-0,53980	-0,86364	Exponential and early post-exponential lifestyles
FlgE	-0,74172	-0,81617	-0,42783	-0,60040	Exponential and early post-exponential lifestyles
FloT	1,06615	-1,2	1,34760	1,06236	Exponential and early post-exponential lifestyles
MotB	0,24843	0,45966	0,25043	0,09724	Exponential and early post-exponential lifestyles
OppA	-0,11847	-0,23638	0,00353	-0,06892	Exponential and early post-exponential lifestyles
OppD	0,37337	-1,2	0,47228	-1,2	Exponential and early post-exponential lifestyles
CheA	-1,2	0,36275	-1,2	0,09724	Exponential and early post-exponential lifestyles
MotA	0,24843	0,23781	0,25043	-1,2	Exponential and early post-exponential lifestyles
McpA	0,07234	0,53884	-1,2	0,09724	Exponential and early post-exponential lifestyles
McpB	0,07234	0,76069	-1,2	0,27333	Exponential and early post-exponential lifestyles
McpC	0,37337	0,23781	-1,2	-1,2	Exponential and early post-exponential lifestyles
FliY	0,07234	0,23781	-1,2	-1,2	Exponential and early post-exponential lifestyles
FliF	0,07234	0,23781	-1,2	-1,2	Exponential and early post-exponential lifestyles
SrfAB	-0,11102	-0,03149	-0,20205	-0,09773	Coping with stress
SrfAA	0,19613	0,35992	-0,25174	0,17775	Coping with stress
AhpF	0,67440	0,71493	0,07434	0,49518	Coping with stress
YknX	-0,44069	-0,81617	-0,33092	-0,60040	Coping with stress
SwrC	-1,2	0,53884	-1,2	-1,2	Coping with stress
SrfAC	-0,44069	-0,16296	-1,2	0,00166	Coping with stress
YdcC	0,07234	-1,2	0,55146	-1,2	Sporulation
YycH	0,07234	-1,2	-1,2	-1,2	Information processing
WalK	0,07234	-1,2	-1,2	-1,2	Information processing
RpoB	-1,2	0,45966	-1,2	-1,2	Information processing
KinC	-1,2	-1,2	-0,42783	-0,42431	Information processing
BdbD	-0,64481	-0,81617	-0,55277	-0,60040	Information processing
PrsA	-0,57899	-0,53534	-0,39004	-0,68755	Information processing
FtsY	-0,31575	-0,51514	-0,90495	-0,60040	Information processing
CshA	0,61641	0,06172	0,07434	0,57436	Information processing
Rny	0,37337	0,66378	0,55146	0,57436	Information processing
PdhC	-0,17745	-0,21411	-0,16459	0,06861	Information processing
RpsB	-0,26460	-0,16296	-0,25174	-0,20246	Information processing
SecA	-0,26460	-0,16296	-1,2	-0,20246	Information processing
WprA	-0,79971	-1,02029	-0,85380	-0,38955	Information processing
YclK	0,07234	-1,2	0,07434	-1,2	Information processing
SecY	0,24843	-1,2	0,07434	-1,2	Information processing
TufA	-0,56563	0,02893	-0,33092	0,24470	Information processing
RpoC	-1,2	0,60578	-1,2	0,09724	Information processing
YbfF	-1,2	-1,2	0,07434	-1,2	Proteins of unknown function
YhgE	-1,2	0,06172	-1,2	-1,2	Proteins of unknown function
YxkC	0,07234	-1,2	-1,2	-1,2	Proteins of unknown function
YdjG	0,24843	-1,2	0,07434	0,09724	Proteins of unknown function

Table 7: Pull-down raw data of control.

Protein	Prot_AC [a]	Description	MW (Da)	pI	Functional Category [b]
AtpA	WP_003243657.1	ATP synthase subunit alpha [Bacillus]	54679	5,22	Metabolism
AtpD	WP_003227686.1	ATP synthase subunit beta [Bacillus]	51388	4,8	Metabolism
PrsA	WP_003245079.1	foldase [Bacillus]	32547	8,77	Information processing
MntA	WP_003229060.1	manganese-binding lipoprotein MntA [Bacillus]	33454	6,16	Transporters
SrfAB	WP_010886403.1	surfactin non-ribosomal peptide synthetase SrfAB [Bacillus]	401377	5,07	Coping with stress
Hag	WP_003228021.1	flagellin [Bacillus]	32607	4,97	Exponential and early post-exponential lifestyles
Icd	WP_003229433.1	isocitrate dehydrogenase (NADP(+)) [Bacillus]	46503	5,03	Metabolism
WprA	WP_003244653.1	peptidase S8 [Bacillus]	96485	9,2	Information processing
PdhB	WP_003232313.1	pyruvate dehydrogenase E1 component subunit beta [Bacillus]	35452	4,74	Metabolism
FloA	WP_003230026.1	UPF0365 family protein [Bacillus]	35676	5,1	Cell envelope and cell division
RpsB	WP_003220918.1	30S ribosomal protein S2 [Bacillales]	28007	6,27	Information processing
OppA	WP_003232957.1	peptide ABC transporter substrate-binding protein [Bacillus]	61510	5,83	Exponential and early post-exponential lifestyles
Vpr	WP_003227419.1	minor protease vpr [Bacillus]	85556	5,87	Metabolism
QcrC	WP_003225562.1	menaquinol-cytochrome c reductase cytochrome b/c subunit [Bacillus]	28258	6,92	Metabolism
FtsH	WP_003243881.1	ATP-dependent zinc metalloprotease FtsH [Bacillus]	71064	5,92	Cell envelope and cell division
FloT	WP_003228960.1	flotillin family protein [Bacillus]	55959	5,34	Exponential and early post-exponential lifestyles
BdbD	WP_003228414.1	thioredoxin [Bacillus]	25004	5,27	Information processing
MetQ	WP_003228595.1	methionine-binding lipoprotein MetQ [Bacillus]	30393	8,26	Transporters
CtaC	WP_003232248.1	cytochrome c oxidase subunit 2 [Bacillus]	40354	8,71	Metabolism
OdhB	WP_004399364.1	dihydrolipoyllysine-residue succinyltransferase component of 2-oxoglutarate dehydrogenase complex [Bacillus]	45975	5,05	Metabolism
GapA	WP_003219957.1	aldehyde dehydrogenase [Bacillales]	35924	5,2	Metabolism
PBP5	AHA75966.1	D-alanyl-D-alanine carboxypeptidase dacA [Bacillus subtilis PY79 PY79]	45951	5,43	Cell envelope and cell division
MreB	WP_003229650.1	rod shape-determining protein [Bacillus]	36008	5,09	Cell envelope and cell division
SrfAA	WP_010886402.1	surfactin non-ribosomal peptide synthetase SrfAA [Bacillus]	402750	5	Coping with stress
PdhC	WP_003232311.1	dihydrolipoyllysine-residue acetyltransferase component of pyruvate dehydrogenase complex [Bacillus]	47567	5,04	Information processing
FtsY	WP_003232026.1	signal recognition particle-docking protein FtsY [Bacillus]	36377	5,27	Information processing
AlbC	WP_003227564.1	ABC transporter ATP-binding protein [Bacillus]	27387	5,4	Transporters
EcsA	WP_003233230.1	ABC transporter ATP-binding protein [Bacillales]	27818	5,72	Transporters
MntB	WP_004398644.1	manganese transport system ATP-binding protein MntB [Bacillus]	27921	9,11	Transporters
FtsA	WP_009967186.1	cell division protein FtsA [Bacillus]	48333	5,17	Cell envelope and cell division
Mbl	WP_003227776.1	rod shape-determining protein [Bacillus]	36009	5,77	Cell envelope and cell division
SrfAC	WP_003234570.1	surfactin non-ribosomal peptide synthetase SrfAC [Bacillus]	144237	5,18	Coping with stress
YknX	WP_003244902.1	efflux RND transporter periplasmic adaptor subunit [Bacillus]	41682	5,37	Coping with stress
FlgE	WP_003231968.1	flagellar basal body rod protein FlgG [Bacillus]	27439	4,92	Exponential and early post-exponential lifestyles
SecA	WP_003228033.1	protein translocase subunit SecA [Bacillus]	95698	5,49	Information processing
KinC	WP_003232333.1	PAS domain-containing sensor histidine kinase [Bacillus]	48986	6,23	Information processing
TufA	WP_003235058.1	elongation factor Tu [Bacillus]	43680	4,92	Information processing
SdhA	WP_003229567.1	succinate dehydrogenase flavoprotein subunit [Bacillus]	65395	5,77	Metabolism
PfeT	WP_003245873.1	cadmium-translocating P-type ATPase [Bacillus]	68864	5,12	Transporters
RbsC	WP_009968282.1	ribose ABC transporter permease [Bacillus]	33823	9,95	Transporters

APPENDIX I

Protein	Protein score	PSMs [c]	Num. pept	emPAI [d]	Coverage	NSAF [e] (FloA)	NSAF (FloT)	NSAF ($FloT_{nt}A_{ct}$)	NASF ($FloA_{nt}T_{ct}$)
AtpA	503	**12**	12	1,5	24,5	45,293	38,138	39,103	29,909
AtpD	634	**11**	11	1,65	30	41,519	34,959	35,845	27,416
PrsA	635	**11**	9	2,57	40,1	41,519	34,959	35,845	27,416
MntA	385	**11**	8	1,69	22,9	41,519	34,959	35,845	27,416
SrfAB	316	**11**	7	0,11	2,7	41,519	34,959	35,845	27,416
Hag	366	**11**	5	0,66	15,5	41,519	34,959	35,845	27,416
Icd	326	**8**	8	1,24	23,2	30,196	25,425	26,069	19,939
WprA	300	**8**	6	0,36	7,4	30,196	25,425	26,069	19,939
PdhB	307	**7**	7	1,27	21,8	26,421	22,247	22,810	17,447
FloA	320	**7**	5	1,01	23,9	26,421	22,247	22,810	17,447
RpsB	136	**6**	3	0,8	14,2	22,647	19,069	19,552	14,954
OppA	278	**5**	5	0,4	9,2	18,872	15,891	16,293	12,462
Vpr	216	**5**	5	0,28	7,1		15,891		
QcrC	280	**5**	5	1,07	16,5	18,872	15,891	16,293	12,462
FtsH	131	**4**	4	0,27	5,8	15,098	12,713	13,034	9,970
FloT	233	**4**	4	0,35	7,9		12,713	13,034	9,970
BdbD	229	**4**	4	0,94	23,4	15,098	12,713	13,034	9,970
MetQ	160	**4**	4	0,72	12,8	15,098	12,713	13,034	9,970
CtaC	162	**4**	3	0,67	11,2	15,098	12,713	13,034	9,970
OdhB	81	**4**	2	0,31	7,7	15,098	12,713	13,034	9,970
GapA	106	**4**	2	0,26	8,1	15,098	12,713	13,034	9,970
PBP5	97	**3**	3	0,31	6,5	11,323	9,534	9,776	7,477
MreB	103	**3**	3	0,41	7,1	11,323	9,534	9,776	7,477
SrfAA	179	**3**	3	0,03	1	11,323	9,534	9,776	7,477
PdhC	128	**3**	3	0,42	7,5	11,323	9,534	9,776	7,477
FtsY	103	**3**	3	0,41	8,2	11,323	9,534	9,776	7,477
AlbC	128	**3**	3	0,57	12,6	11,323	9,534	9,776	7,477
EcsA	80	**3**	3	0,56	10,1		9,534	9,776	7,477
MntB	129	**3**	3	0,56	12,4	11,323	9,534		7,477
FtsA	64	**2**	2	0,19	4,1				4,985
Mbl	110	**2**	2	0,26	5,4	7,549	6,356	6,517	4,985
SrfAC	99	**2**	2	0,06	2,3	7,549		6,517	4,985
YknX	60	**2**	2	0,35	6,6	7,549	6,356	6,517	4,985
FlgE	94	**2**	2	0,35	9,8	7,549	6,356	6,517	4,985
SecA	86	**2**	2	0,09	2,4	7,549		6,517	4,985
KinC	114	**2**	2	0,19	5,8		6,356		4,985
TufA	151	**2**	2	0,21	6,8	7,549	6,356	6,517	4,985
SdhA	69	**2**	2	0,14	2,9	7,549	6,356	6,517	4,985
PfeT	73	**2**	2	0,2	4,7	7,549	6,356	6,517	4,985
RbsC	110	**2**	2	0,28	5,3		6,356		4,985

Table 8: Pull-down raw data of FloA.

Protein	Prot_AC	Description	MW (Da)	pI	Functional Category
FloA	WP_003230026.1	UPF0365 family protein [Bacillus]	35676	5,1	Cell envelope and cell division
RbsA	WP_003244379.1	ribose import ATP-binding protein RbsA [Bacillus]	54612	6,2	Transporters
FtsZ	WP_003232167.1	cell division protein FtsZ [Bacillales]	40370	5,01	Cell envelope and cell division
McpB	WP_003243461.1	methyl-accepting chemotaxis protein McpB [Bacillus]	71857	5,18	Exponential and early post-exponential lifestyles
RbsB	WP_003242760.1	D-ribose ABC transporter substrate-binding protein [Bacillus]	32264	6,15	Transporters
AhpF	WP_003243077.1	alkyl hydroperoxide reductase subunit F [Bacillus]	55125	4,89	Coping with stress
YxeB	WP_003243725.1	iron(3+)-hydroxamate-binding protein [Bacillus]	35541	6,25	Transporters
Rny	WP_003221010.1	ribonuclease Y [Bacillales]	58940	5,51	Information processing
RpoC	WP_004399688.1	DNA-directed RNA polymerase subunit beta~ [Bacillus]	134795	8,79	Information processing
Ndh	WP_003232765.1	NADH dehydrogenase [Bacillus]	41927	6,28	Metabolism
FadE	WP_003244094.1	acyl-CoA dehydrogenase [Bacillus]	65352	5,31	Metabolism
McpA	AHA79044.1	Methyl-accepting chemotaxis protein mcpA [Bacillus subtilis PY79 PY79]	72400	5,14	Exponential and early post-exponential lifestyles
YhfQ	WP_003233159.1	ABC transporter substrate-binding protein [Bacillus]	35524	9,06	Transporters
FeuA	WP_003234978.1	iron-uptake system-binding protein [Bacillus]	35143	7,66	Transporters
SwrC	O31501.2	Swarming motility protein SwrC [Bacillus subtilis subsp. subtilis str. 168 168]	113435	4,98	Coping with stress
TagU	WP_003227949.1	LytR family transcriptional regulator [Bacillus]	34565	9,18	Cell envelope and cell division
MotB	WP_003232473.1	motility protein B [Bacillus]	29464	6,57	Exponential and early post-exponential lifestyles
RpoB	WP_009966326.1	DNA-directed RNA polymerase subunit beta [Bacillus subtilis PY79 PY79]	128184	4,89	Information processing
PlsX	WP_003232041.1	phosphate acyltransferase [Bacillus]	35798	5,61	Metabolism
FhuD	WP_003243220.1	iron(3+)-hydroxamate-binding protein FhuD [Bacillus]	34462	8,85	Transporters
PBP3	WP_003246590.1	penicillin-binding protein 3 [Bacillus]	74531	6,24	Cell envelope and cell division
CheA	WP_003245734.1	chemotaxis protein CheA [Bacillus]	74994	4,67	Exponential and early post-exponential lifestyles
ResE	WP_003230520.1	PAS domain-containing sensor histidine kinase [Bacillus]	66730	5,47	Metabolism
MurG	WP_003232184.1	undecaprenyldiphospho-muramoylpentapeptide beta-N-acetylglucosaminyltransferase [Bacillus]	40025	9,18	Metabolism
QoxA	ADV94634.1	cytochrome aa3-600 quinol oxidase (subunit II) [Bacillus subtilis BSn5 BSn5]	35942	5	Metabolism
ArtP	WP_004398706.1	arginine ABC transporter substrate-binding protein [Bacillus]	28409	5,28	Transporters
ManP	WP_023592766.1	PTS mannose EIIBCA component [Bacillus subtilis]	69154	6,1	Transporters
SrfAA	WP_010886402.1	surfactin non-ribosomal peptide synthetase SrfAA [Bacillus]	402750	5	Coping with stress
EzrA	WP_003229320.1	septation ring formation regulator EzrA [Bacillus]	65013	4,95	Cell envelope and cell division
FliF	WP_010886506.1	Flagellar M-ring protein [Bacillus subtilis PY79 PY79]	58648	4,55	Exponential and early post-exponential lifestyles
McpC	WP_003245443.1	methyl-accepting chemotaxis protein McpC [Bacillus]	71986	5,07	Exponential and early post-exponential lifestyles
FliY	WP_003231962.1	flagellar motor switch phosphatase FliY [Bacillus]	41027	4,31	Exponential and early post-exponential lifestyles
MotA	WP_003244739.1	motility protein A [Bacillus]	29321	5,19	Exponential and early post-exponential lifestyles

APPENDIX I

Protein	Protein score	PSMs	Num. pept	emPAI	Coverage	NSAF	fold change [f]	log_{10} (fold change)
FloA	2433	469	31	24,99	66,5	270,308	10,231	**1,0099**
RbsA	235	11	6	0,99	18,1	6,340	6,340	**0,8021**
FtsZ	432,35	10	8	1,27	19,6	5,763	5,763	**0,7607**
McpB	249	10	3	0,26	8,8	5,763	5,763	**0,7607**
RbsB	607	9	9	3,1	38,7	5,187	5,187	**0,7149**
AhpF	286	9	7	0,7	14,9	5,187	5,187	**0,7149**
YxeB	363	8	8	1,86	35,5	4,611	4,611	**0,6638**
Rny	241	8	5	0,42	9,2	4,611	4,611	**0,6638**
RpoC	248	7	7	0,28	5,5	4,034	4,034	**0,6058**
Ndh	375,53	7	7	0,99	18,1	4,034	4,034	**0,6058**
FadE	197	7	5	0,38	9,3	4,034	4,034	**0,6058**
McpA	313	6	6	0,5	11,5	3,458	3,458	**0,5388**
YhfQ	282	6	6	1,55	25,7	3,458	3,458	**0,5388**
FeuA	243	6	6	1,57	23,3	3,458	3,458	**0,5388**
SwrC	146	6	3	0,12	2,6	3,458	3,458	**0,5388**
TagU	329	5	5	1,32	22,2	2,882	2,882	**0,4597**
MotB	281	5	5	1,33	17,6	2,882	2,882	**0,4597**
RpoB	182	5	5	0,3	6,2	2,882	2,882	**0,4597**
PlsX	246,84	5	5	0,78	18	2,882	2,882	**0,4597**
FhuD	247	5	5	0,83	19,4	2,882	2,882	**0,4597**
PBP3	208	4	4	0,32	7,2	2,305	2,305	**0,3627**
CheA	199	4	4	0,25	6,2	2,305	2,305	**0,3627**
ResE	206	4	4	0,45	10,4	2,305	2,305	**0,3627**
MurG	141,52	4	4	0,86	13,8	2,305	2,305	**0,3627**
QoxA	210	4	4	0,59	15,7	2,305	2,305	**0,3627**
ArtP	163	4	4	0,79	21,6	2,305	2,305	**0,3627**
ManP	76	4	2	0,35	8,8	2,305	2,305	**0,3627**
SrfAA	1581	45	32	0,47	12	25,936	2,290	**0,3599**
EzrA	114	3	3	0,29	5,9	1,729	1,729	**0,2378**
FliF	121	3	3	0,33	5,8	1,729	1,729	**0,2378**
McpC	94	3	3	0,19	4,7	1,729	1,729	**0,2378**
FliY	135,16	3	3	0,5	9,8	1,729	1,729	**0,2378**
MotA	113	3	3	0,53	14,1	1,729	1,729	**0,2378**

APPENDIX I

Protein	Prot_AC	Description	MW (Da)	pI	Functional Category
PycA	WP_003244778.1	pyruvate carboxylase [Bacillus]	128141	5,53	Metabolism
Hom	WP_003228694.1	homoserine dehydrogenase [Bacillus]	47579	5,08	Metabolism
TagF	WP_003243463.1	CDP-glycerol--poly(glycerophosphate) glycerophosphotransferase [Bacillus]	88236	9,13	Cell envelope and cell division
RasP	AHA77684.1	Zinc metalloprotease rasP [Bacillus subtilis PY79 PY79]	46525	5,31	Cell envelope and cell division
MreC	AHA78700.1	Rod shape-determining protein mreC [Bacillus subtilis PY79 PY79]	30073	5,92	Cell envelope and cell division
MinD	WP_004398624.1	septum site-determining protein MinD [Bacillus]	29559	5,16	Cell envelope and cell division
CshA	P96614.2	DEAD-box ATP-dependent RNA helicase CshA [Bacillus subtilis subsp. subtilis str. 168 168]	55296	9,49	Information processing
PhoR	WP_004398493.1	PAS domain-containing sensor histidine kinase [Bacillus]	65309	6	Metabolism
NupN	WP_003228831.1	BMP family ABC transporter substrate-binding protein [Bacillus]	38395	5,26	Metabolism
CdaA	WP_003223651.1	membrane protein [Bacillales]	30584	7,79	Metabolism
YhgE	WP_003245424.1	YhgE/Pip domain-containing protein [Bacillus subtilis]	84042	5,18	Proteins of unknown function
MetN	WP_003242531.1	methionine import ATP-binding protein MetN [Bacillus]	37976	7,08	Transporters
AppF	WP_003232964.1	dipeptide ABC transporter ATP-binding protein [Bacillus]	37348	9,38	Transporters
PfeT	WP_003245873.1	cadmium-translocating P-type ATPase [Bacillus]	68864	5,12	Transporters
TufA	WP_003235058.1	elongation factor Tu [Bacillus]	43680	4,92	Information processing
OdhB	WP_004399364.1	dihydrolipoyllysine-residue succinyltransferase component of 2-oxoglutarate dehydrogenase complex [Bacillus]	45975	5,05	Metabolism
SrfAB	WP_010886403.1	surfactin non-ribosomal peptide synthetase SrfAB [Bacillus]	401377	5,07	Coping with stress
SdhA	WP_003229567.1	succinate dehydrogenase flavoprotein subunit [Bacillus]	65395	5,77	Metabolism
SrfAC	WP_003234570.1	surfactin non-ribosomal peptide synthetase SrfAC [Bacillus]	144237	5,18	Coping with stress
SecA	WP_003228033.1	protein translocase subunit SecA [Bacillus]	95698	5,49	Information processing
RpsB	WP_003220918.1	30S ribosomal protein S2 [Bacillales]	28007	6,27	Information processing
PdhC	WP_003232311.1	dihydrolipoyllysine-residue acetyltransferase component of pyruvate dehydrogenase complex [Bacillus]	47567	5,04	Information processing
OppA	WP_003232957.1	peptide ABC transporter substrate-binding protein [Bacillus]	61510	5,83	Exponential and early post-exponential lifestyles
Icd	WP_003229433.1	isocitrate dehydrogenase (NADP(+)) [Bacillus]	46503	5,03	Metabolism
PBP5	AHA75966.1	D-alanyl-D-alanine carboxypeptidase dacA [Bacillus subtilis PY79 PY79]	45951	5,43	Cell envelope and cell division
GapA	WP_003219957.1	aldehyde dehydrogenase [Bacillales]	35924	5,2	Metabolism
AtpD	WP_003227686.1	ATP synthase subunit beta [Bacillus]	51388	4,8	Metabolism
FtsH	WP_003243881.1	ATP-dependent zinc metalloprotease FtsH [Bacillus]	71064	5,92	Cell envelope and cell division
CtaC	WP_003232248.1	cytochrome c oxidase subunit 2 [Bacillus]	40354	8,71	Metabolism
MreB	WP_003229650.1	rod shape-determining protein [Bacillus]	36008	5,09	Cell envelope and cell division
FtsY	WP_003232026.1	signal recognition particle-docking protein FtsY [Bacillus]	36377	5,27	Information processing
PrsA	WP_003245079.1	foldase [Bacillus]	32547	8,77	Information processing
PdhB	WP_003232313.1	pyruvate dehydrogenase E1 component subunit beta [Bacillus]	35452	4,74	Metabolism
MbI	WP_003227776.1	rod shape-determining protein [Bacillus]	36009	5,77	Cell envelope and cell division
MntA	WP_003229060.1	manganese-binding lipoprotein MntA [Bacillus]	33454	6,16	Transporters
AlbC	WP_003227564.1	ABC transporter ATP-binding protein [Bacillus]	27387	5,4	Transporters
MntB	WP_004398644.1	manganese transport system ATP-binding protein MntB [Bacillus]	27921	9,11	Transporters
MetQ	WP_003228595.1	methionine-binding lipoprotein MetQ [Bacillus]	30393	8,26	Transporters
AtpA	WP_003243657.1	ATP synthase subunit alpha [Bacillus]	54679	5,22	Metabolism

APPENDIX I

Protein	Protein score	PSMs	Num. pept	emPAI	Coverage	NSAF	fold change	log_{10} (fold change)
PycA	114	3	3	0,18	6	1,729	1,729	**0,2378**
Hom	170	3	3	0,42	9,2	1,729	1,729	**0,2378**
TagF	50	2	2	0,1	2,4	1,153	1,153	**0,0617**
RasP	58,49	2	2	0,31	5,7	1,153	1,153	**0,0617**
MreC	67	2	2	0,51	9,6	1,153	1,153	**0,0617**
MinD	74	2	2	0,32	9	1,153	1,153	**0,0617**
CshA	111	2	2	0,16	6,7	1,153	1,153	**0,0617**
PhoR	61	2	2	0,29	7,4	1,153	1,153	**0,0617**
NupN	80,83	2	2	0,38	9,2	1,153	1,153	**0,0617**
CdaA	94	2	2	0,31	6,6	1,153	1,153	**0,0617**
YhgE	65	2	2	0,16	4,1	1,153	1,153	**0,0617**
MetN	66,42	2	2	0,24	5,3	1,153	1,153	**0,0617**
AppF	57	2	2	0,56	10,3	1,153	1,153	**0,0617**
PfeT	154	15	4	0,35	7,7	8,645	1,145	**0,0589**
TufA	454,02	14	8	1,13	26,8	8,069	1,069	**0,0289**
OdhB	631	27	13	2,24	38,1	15,561	1,031	**0,0131**
SrfAB	2115	67	42	0,6	13,5	38,615	0,930	**-0,0315**
SdhA	499	11	11	1,02	18,1	6,340	0,840	**-0,0758**
SrfAC	426	9	9	0,38	7,1	5,187	0,687	**-0,1630**
SecA	380	9	9	0,62	13,2	5,187	0,687	**-0,1630**
RpsB	833	27	14	8,19	52,8	15,561	0,687	**-0,1630**
PdhC	542	12	11	1,61	31	6,916	0,611	**-0,2141**
OppA	845	19	15	2,16	31,4	10,951	0,580	**-0,2364**
Icd	817,79	26	15	3,54	37,4	14,985	0,496	**-0,3043**
PBP5	376,91	9	9	1,46	22,7	5,187	0,458	**-0,3390**
GapA	507,88	11	7	1,23	29	6,340	0,420	**-0,3768**
AtpD	741,01	28	13	2,35	43,1	16,138	0,389	**-0,4104**
FtsH	384	9	8	0,8	15,2	5,187	0,344	**-0,4640**
CtaC	327,39	9	6	1,05	16	5,187	0,344	**-0,4640**
MreB	252,14	6	6	0,99	23,7	3,458	0,305	**-0,5151**
FtsY	310,12	6	6	1,21	23,1	3,458	0,305	**-0,5151**
PrsA	851	21	13	4,96	46,2	12,103	0,292	**-0,5353**
PdhB	554,49	11	11	2,6	39,4	6,340	0,240	**-0,6199**
Mbl	126	3	3	0,41	8,7	1,729	0,229	**-0,6401**
MntA	410	16	8	1,7	22,9	9,222	0,222	**-0,6534**
AlbC	218	4	4	0,83	18,4	2,305	0,204	**-0,6912**
MntB	204	4	4	1,09	18,8	2,305	0,204	**-0,6912**
MetQ	196	5	5	1,26	21,9	2,882	0,191	**-0,7193**
AtpA	547,17	15	13	1,68	24,1	8,645	0,191	**-0,7193**

Protein	Prot_AC	Description	MW (Da)	pI	Functional Category
QcrC	WP_003225562.1	menaquinol-cytochrome c reductase cytochrome b/c subunit [Bacillus]	28258	6,92	Metabolism
BdbD	WP_003228414.1	thioredoxin [Bacillus]	25004	5,27	Information processing
YknX	WP_003244902.1	efflux RND transporter periplasmic adaptor subunit [Bacillus]	41682	5,37	Coping with stress
FlgE	WP_003231968.1	flagellar basal body rod protein FlgG [Bacillus]	27439	4,92	Exponential and early post-exponential lifestyles
WprA	WP_003244653.1	peptidase S8 [Bacillus]	96485	9,2	Information processing
Hag	WP_003228021.1	flagellin [Bacillus]	32607	4,97	Exponential and early post-exponential lifestyles

Table 9: Pull-down raw data of FloT.

Protein	Prot_AC	Description	MW (Da)	pI	Functional Category
FloT	WP_003228960.1	flotillin family protein [Bacillus]	55959	5,34	Exponential and early post-exponential lifestyles
FeuA	WP_003234978.1	iron-uptake system-binding protein [Bacillus]	35143	7,66	Transporters
RbsA	WP_003244379.1	ribose import ATP-binding protein RbsA [Bacillus]	54612	6,2	Transporters
FhuD	WP_003243220.1	iron(3+)-hydroxamate-binding protein FhuD [Bacillus]	34462	8,85	Transporters
YxeB	WP_003243725.1	iron(3+)-hydroxamate-binding protein [Bacillus]	35541	6,25	Transporters
RodZ	WP_003244699.1	helix-turn-helix domain-containing protein [Bacillus]	34271	5,56	Cell envelope and cell division
TagU	WP_003227949.1	LytR family transcriptional regulator [Bacillus]	34565	9,18	Cell envelope and cell division
Ndh	WP_003232765.1	NADH dehydrogenase [Bacillus]	41927	6,28	Metabolism
SdhB	WP_003229569.1	succinate dehydrogenase iron-sulfur subunit [Bacillus]	29026	8,47	Metabolism
RbsB	WP_003242760.1	D-ribose ABC transporter substrate-binding protein [Bacillus]	32264	6,15	Transporters
Rny	WP_003221010.1	ribonuclease Y [Bacillales]	58940	5,51	Information processing
YdcC	AFQ56402.1	Putative lipoprotein [Bacillus subtilis QB928 QB928]	42219	9,22	Sporulation
FtsZ	WP_003232167.1	cell division protein FtsZ [Bacillales]	40370	5,01	Cell envelope and cell division
OppD	AHA77124.1	Oligopeptide transport ATP-binding protein OppD [Bacillus subtilis PY79 PY79]	39329	5,92	Exponential and early post-exponential lifestyles
NupN	WP_003228831.1	BMP family ABC transporter substrate-binding protein [Bacillus]	38395	5,26	Metabolism
ArtP	WP_004398706.1	arginine ABC transporter substrate-binding protein [Bacillus]	28409	5,28	Transporters
ManP	WP_023592766.1	PTS mannose EIIBCA component [Bacillus subtilis]	69154	6,1	Transporters
DltD	WP_003227323.1	D-alanyl-lipoteichoic acid biosynthesis protein DltD [Bacillus]	44780	9,51	Cell envelope and cell division
PBP3	WP_003246590.1	penicillin-binding protein 3 [Bacillus]	74531	6,24	Cell envelope and cell division
MinD	WP_004398624.1	septum site-determining protein MinD [Bacillus]	29559	5,16	Cell envelope and cell division
MotB	WP_003232473.1	motility protein B [Bacillus]	29464	6,57	Exponential and early post-exponential lifestyles
MotA	WP_003244739.1	motility protein A [Bacillus]	29321	5,19	Exponential and early post-exponential lifestyles
PlsX	WP_003232041.1	phosphate acyltransferase [Bacillus]	35798	5,61	Metabolism
DppE	P26906.4	Dipeptide-binding protein DppE [Bacillus subtilis subsp. subtilis str. 168 168]	61837	5,36	Transporters
AppF	WP_003232964.1	dipeptide ABC transporter ATP-binding protein [Bacillus]	37348	9,38	Transporters
YhfQ	WP_003233159.1	ABC transporter substrate-binding protein [Bacillus]	35524	9,06	Transporters

Protein	Protein score	PSMs	Num. pept	emPAI	Coverage	NSAF	fold change	log_{10} (fold change)
QcrC	213	5	4	1,08	20,8	2,882	0,153	**-0,8162**
BdbD	306	4	4	0,94	23,4	2,305	0,153	**-0,8162**
YknX	68,11	2	2	0,35	8	1,153	0,153	**-0,8162**
FlgE	99	2	2	0,35	7,6	1,153	0,153	**-0,8162**
WprA	87	5	3	0,19	3,9	2,882	0,095	**-1,0203**
Hag	362,45	5	5	1,13	22	2,882	0,069	**-1,1586**

Protein	Protein score	PSMs	Num. pept	emPAI	Coverage	NSAF	fold change	log_{10} (fold change)
FloT	4647	477	68	69,66	70,7	283,027	22,264	**1,3476**
FeuA	393	13	8	1,28	19,6	7,714	7,714	**0,8873**
RbsA	329	10	7	0,7	15,8	5,933	5,933	**0,7733**
FhuD	390	9	8	1,63	27,3	5,340	5,340	**0,7276**
YxeB	234	9	5	0,79	14	5,340	5,340	**0,7276**
RodZ	354	8	7	1,33	24,3	4,747	4,747	**0,6764**
TagU	348	7	7	1,32	20,6	4,153	4,153	**0,6184**
Ndh	317	7	7	1	18,1	4,153	4,153	**0,6184**
SdhB	433	7	7	2,61	37,9	4,153	4,153	**0,6184**
RbsB	380	7	6	1,16	23,6	4,153	4,153	**0,6184**
Rny	218	6	6	0,53	9,8	3,560	3,560	**0,5515**
YdcC	298	6	6	0,8	16,4	3,560	3,560	**0,5515**
FtsZ	254	5	5	0,67	12,8	2,967	2,967	**0,4723**
OppD	272	5	5	0,69	13,2	2,967	2,967	**0,4723**
NupN	211	5	5	0,71	15	2,967	2,967	**0,4723**
ArtP	329	5	4	1,39	25,1	2,967	2,967	**0,4723**
ManP	118	5	3	0,35	6,6	2,967	2,967	**0,4723**
DltD	117	4	4	0,45	12,5	2,373	2,373	**0,3754**
PBP3	153	3	3	0,18	6	1,780	1,780	**0,2504**
MinD	91	3	3	0,52	18,3	1,780	1,780	**0,2504**
MotB	145	3	3	0,53	12,6	1,780	1,780	**0,2504**
MotA	167	3	3	1,02	22,2	1,780	1,780	**0,2504**
PlsX	128	3	3	0,41	8,4	1,780	1,780	**0,2504**
DppE	115	3	3	0,22	4,2	1,780	1,780	**0,2504**
AppF	135	3	3	0,56	10,6	1,780	1,780	**0,2504**
YhfQ	113	3	3	0,6	14,6	1,780	1,780	**0,2504**

APPENDIX I

Protein	Prot_AC	Description	MW (Da)	pI	Functional Category
TcyA	WP_003246699.1	L-cystine-binding protein TcyA [Bacillus]	29553	8,61	Transporters
EzrA	WP_003229320.1	septation ring formation regulator EzrA [Bacillus]	65013	4,95	Cell envelope and cell division
MreC	AHA78700.1	Rod shape-determining protein mreC [Bacillus subtilis PY79 PY79]	30073	5,92	Cell envelope and cell division
AhpF	WP_003243077.1	alkyl hydroperoxide reductase subunit F [Bacillus]	55125	4,89	Coping with stress
CshA	P96614.2	DEAD-box ATP-dependent RNA helicase CshA [Bacillus subtilis subsp. subtilis str. 168 168]	55296	9,49	Information processing
YclK	AHA76342.1	Sensor histidine kinase yclK [Bacillus subtilis PY79 PY79]	54936	6,16	Information processing
SecY	WP_004399662.1	protein translocase subunit SecY [Bacillus]	47213	9,88	Information processing
ResE	WP_003230520.1	PAS domain-containing sensor histidine kinase [Bacillus]	66730	5,47	Metabolism
MurG	WP_003232184.1	undecaprenyldiphospho-muramoylpentapeptide beta-N-acetylglucosaminyltransferase [Bacillus]	40025	9,18	Metabolism
MsmX	WP_003242648.1	maltodextrin import ATP-binding protein MsmX [Bacillus]	41397	7,11	Metabolism
QoxA	ADV94634.1	cytochrome aa3-600 quinol oxidase (subunit II) [Bacillus subtilis BSn5 BSn5]	35942	5	Metabolism
FecC	WP_003243996.1	Fe(3+)-citrate-binding protein YfmC [Bacillus]	35113	7,68	Metabolism
AtpG	WP_003244388.1	ATP synthase subunit gamma [Bacillus]	31635	6,56	Metabolism
YdjG	AHA76571.1	Uncharacterized protein ydjG [Bacillus subtilis PY79 PY79]	37400	5,5	Proteins of unknown function
YbfF	WP_003246251.1	hypothetical protein [Bacillus]	35458	9,39	Proteins of unknown function
AppD	WP_003232965.1	oligopeptide transport ATP-binding protein AppD [Bacillus]	36744	5,51	Transporters
MetN	WP_003242531.1	methionine import ATP-binding protein MetN [Bacillus]	37976	7,08	Transporters
OppA	WP_003232957.1	peptide ABC transporter substrate-binding protein [Bacillus]	61510	5,83	Exponential and early post-exponential lifestyles
SdhA	WP_003229567.1	succinate dehydrogenase flavoprotein subunit [Bacillus]	65395	5,77	Metabolism
PfeT	WP_003245873.1	cadmium-translocating P-type ATPase [Bacillus]	68864	5,12	Transporters
CtaC	WP_003232248.1	cytochrome c oxidase subunit 2 [Bacillus]	40354	8,71	Metabolism
PdhC	WP_003232311.1	dihydrolipoyllysine-residue acetyltransferase component of pyruvate dehydrogenase complex [Bacillus]	47567	5,04	Information processing
MetQ	WP_003228595.1	methionine-binding lipoprotein MetQ [Bacillus]	30393	8,26	Transporters
FloA	WP_003230026.1	UPF0365 family protein [Bacillus]	35676	5,1	Cell envelope and cell division
SrfAB	WP_010886403.1	surfactin non-ribosomal peptide synthetase SrfAB [Bacillus]	401377	5,07	Coping with stress
RpsB	WP_003220918.1	30S ribosomal protein S2 [Bacillales]	28007	6,27	Information processing
SrfAA	WP_010886402.1	surfactin non-ribosomal peptide synthetase SrfAA [Bacillus]	402750	5	Coping with stress
OdhB	WP_004399364.1	dihydrolipoyllysine-residue succinyltransferase component of 2-oxoglutarate dehydrogenase complex [Bacillus]	45975	5,05	Metabolism
PBP5	AHA75966.1	D-alanyl-D-alanine carboxypeptidase dacA [Bacillus subtilis PY79 PY79]	45951	5,43	Cell envelope and cell division
MreB	WP_003229650.1	rod shape-determining protein [Bacillus]	36008	5,09	Cell envelope and cell division
MntB	WP_004398644.1	manganese transport system ATP-binding protein MntB [Bacillus]	27921	9,11	Transporters
Icd	WP_003229433.1	isocitrate dehydrogenase (NADP(+)) [Bacillus]	46503	5,03	Metabolism
YknX	WP_003244902.1	efflux RND transporter periplasmic adaptor subunit [Bacillus]	41682	5,37	Coping with stress
TufA	WP_003235058.1	elongation factor Tu [Bacillus]	43680	4,92	Information processing
AlbC	WP_003227564.1	ABC transporter ATP-binding protein [Bacillus]	27387	5,4	Transporters
PrsA	WP_003245079.1	foldase [Bacillus]	32547	8,77	Information processing
PdhB	WP_003232313.1	pyruvate dehydrogenase E1 component subunit beta [Bacillus]	35452	4,74	Metabolism
FlgE	WP_003231968.1	flagellar basal body rod protein FlgG [Bacillus]	27439	4,92	Exponential and early post-exponential lifestyles

APPENDIX I

Protein	Protein score	PSMs	Num. pept	emPAI	Coverage	NSAF	fold change	log_{10} (fold change)
TcyA	150	3	3	1,01	20,1	1,780	1,780	**0,2504**
EzrA	83	2	2	0,14	2,8	1,187	1,187	**0,0743**
MreC	105	2	2	0,51	11,4	1,187	1,187	**0,0743**
AhpF	91	2	2	0,25	6,1	1,187	1,187	**0,0743**
CshA	55	2	2	0,16	4,5	1,187	1,187	**0,0743**
YclK	81	2	2	0,16	3	1,187	1,187	**0,0743**
SecY	100	2	2	0,3	4,9	1,187	1,187	**0,0743**
ResE	75	2	2	0,21	5,3	1,187	1,187	**0,0743**
MurG	89	2	2	0,36	6,9	1,187	1,187	**0,0743**
MsmX	81	2	2	0,22	5,2	1,187	1,187	**0,0743**
QoxA	91	2	2	0,41	8,2	1,187	1,187	**0,0743**
FecC	65	2	2	0,43	14	1,187	1,187	**0,0743**
AtpG	77	2	2	0,3	8	1,187	1,187	**0,0743**
YdjG	85	2	2	0,39	7,9	1,187	1,187	**0,0743**
YbfF	49	2	2	0,26	5,9	1,187	1,187	**0,0743**
AppD	67	2	2	0,4	8,2	1,187	1,187	**0,0743**
MetN	95	2	2	0,24	5,3	1,187	1,187	**0,0743**
OppA	1108	27	19	2,86	32,1	16,020	1,008	**0,0035**
SdhA	375	9	9	1,14	22,2	5,340	0,840	**-0,0756**
PfeT	213	8	4	0,27	7,4	4,747	0,747	**-0,1268**
CtaC	591	15	13	4,16	26,4	8,900	0,700	**-0,1548**
PdhC	480	11	10	1,61	26,9	6,527	0,685	**-0,1646**
MetQ	639	14	11	4,86	44,2	8,307	0,653	**-0,1848**
FloA	545	24	10	1,85	39,9	14,240	0,640	**-0,1937**
SrfAB	885	37	22	0,33	9,2	21,954	0,628	**-0,2021**
RpsB	462	18	9	2,79	30,5	10,680	0,560	**-0,2517**
SrfAA	208	9	6	0,11	3,7	5,340	0,560	**-0,2517**
OdhB	241	12	6	0,72	14,1	7,120	0,560	**-0,2517**
PBP5	350	8	8	1,48	21,1	4,747	0,498	**-0,3029**
MreB	307	8	8	1,82	27,3	4,747	0,498	**-0,3029**
MntB	457	8	6	1,43	27,6	4,747	0,498	**-0,3029**
Icd	507	20	12	2,48	32,2	11,867	0,467	**-0,3309**
YknX	175	5	5	0,65	11,7	2,967	0,467	**-0,3309**
TufA	174	5	3	0,33	9,6	2,967	0,467	**-0,3309**
AlbC	323	7	5	1,12	25,5	4,153	0,436	**-0,3609**
PrsA	760	24	12	5,78	46,9	14,240	0,407	**-0,3900**
PdhB	627	15	11	2,62	35,7	8,900	0,400	**-0,3979**
FlgE	229	4	4	1,47	36	2,373	0,373	**-0,4278**

Protein	Prot_AC	Description	MW (Da)	pI	Functional Category
KinC	WP_003232333.1	PAS domain-containing sensor histidine kinase [Bacillus]	48986	6,23	Information processing
AtpD	WP_003227686.1	ATP synthase subunit beta [Bacillus]	51388	4,8	Metabolism
AtpA	WP_003243657.1	ATP synthase subunit alpha [Bacillus]	54679	5,22	Metabolism
Hag	WP_003228021.1	flagellin [Bacillus]	32607	4,97	Exponential and early post-exponential lifestyles
BdbD	WP_003228414.1	thioredoxin [Bacillus]	25004	5,27	Information processing
GapA	WP_003219957.1	aldehyde dehydrogenase [Bacillales]	35924	5,2	Metabolism
Mbl	WP_003227776.1	rod shape-determining protein [Bacillus]	36009	5,77	Cell envelope and cell division
MntA	WP_003229060.1	manganese-binding lipoprotein MntA [Bacillus]	33454	6,16	Transporters
QcrC	WP_003225562.1	menaquinol-cytochrome c reductase cytochrome b/c subunit [Bacillus]	28258	6,92	Metabolism
EcsA	WP_003233230.1	ABC transporter ATP-binding protein [Bacillales]	27818	5,72	Transporters
FtsH	WP_003243881.1	ATP-dependent zinc metalloprotease FtsH [Bacillus]	71064	5,92	Cell envelope and cell division
RbsC	WP_009968282.1	ribose ABC transporter permease [Bacillus]	33823	9,95	Transporters
WprA	WP_003244653.1	peptidase S8 [Bacillus]	96485	9,2	Information processing
FtsY	WP_003232026.1	signal recognition particle-docking protein FtsY [Bacillus]	36377	5,27	Information processing
Vpr	WP_003227419.1	minor protease vpr [Bacillus]	85556	5,87	Metabolism

Table 10:Pull-down raw data of $FloT_{nt}A_{ct}$.

Protein	Prot_AC	Description	MW (Da)	pI	Functional Category
RbsA	WP_003244379.1	ribose import ATP-binding protein RbsA [Bacillus]	54612	6,2	Transporters
FloT	WP_003228960.1	flotillin family protein [Bacillus]	55959	5,34	Exponential and early post-exponential lifestyles
ManP	WP_023592766.1	PTS mannose EIIBCA component [Bacillus subtilis]	69154	6,1	Transporters
RbsB	WP_003242760.1	D-ribose ABC transporter substrate-binding protein [Bacillus]	32264	6,15	Transporters
FloA	WP_003230026.1	UPF0365 family protein [Bacillus]	35676	5,1	Cell envelope and cell division
ResE	WP_003230520.1	PAS domain-containing sensor histidine kinase [Bacillus]	66730	5,47	Metabolism
AhpF	WP_003243077.1	alkyl hydroperoxide reductase subunit F [Bacillus]	55125	4,89	Coping with stress
FeuA	WP_003234978.1	iron-uptake system-binding protein [Bacillus]	35143	7,66	Transporters
CshA	P96614.2	DEAD-box ATP-dependent RNA helicase CshA [Bacillus subtilis subsp. subtilis str. 168 168]	55296	9,49	Information processing
Ndh	WP_003232765.1	NADH dehydrogenase [Bacillus]	41927	6,28	Metabolism
RodZ	WP_003244699.1	helix-turn-helix domain-containing protein [Bacillus]	34271	5,56	Cell envelope and cell division
FhuD	WP_003243220.1	iron(3+)-hydroxamate-binding protein FhuD [Bacillus]	34462	8,85	Transporters
PhoR	WP_004398493.1	PAS domain-containing sensor histidine kinase [Bacillus]	65309	6	Metabolism
PlsX	WP_003232041.1	phosphate acyltransferase [Bacillus]	35798	5,61	Metabolism
MurG	WP_003232184.1	undecaprenyldiphospho-muramoylpentapeptide beta-N-acetylglucosaminyltransferase [Bacillus]	40025	9,18	Metabolism
YhfQ	WP_003233159.1	ABC transporter substrate-binding protein [Bacillus]	35524	9,06	Transporters
TagU	WP_003227949.1	LytR family transcriptional regulator [Bacillus]	34565	9,18	Cell envelope and cell division
McpC	WP_003245443.1	methyl-accepting chemotaxis protein McpC [Bacillus]	71986	5,07	Exponential and early post-exponential lifestyles
OppD	AHA77124.1	Oligopeptide transport ATP-binding protein OppD [Bacillus subtilis PY79 PY79]	39329	5,92	Exponential and early post-exponential lifestyles
Rny	WP_003221010.1	ribonuclease Y [Bacillales]	58940	5,51	Information processing

APPENDIX I

Protein	Protein score	PSMs	Num. pept	emPAI	Coverage	NSAF	fold change	log_{10} (fold change)
KinC	81	4	2	0,18	4,2	2,373	0,373	**-0,4278**
AtpD	496	19	9	1,08	24,5	11,274	0,322	**-0,4915**
AtpA	519	20	13	1,91	24,1	11,867	0,311	**-0,5070**
Hag	850	17	11	3,03	45,4	10,087	0,289	**-0,5398**
BdbD	403	6	6	2,18	35,6	3,560	0,280	**-0,5528**
GapA	342	6	6	0,99	19,1	3,560	0,280	**-0,5528**
Mbl	112	3	3	0,78	16,8	1,780	0,280	**-0,5528**
MntA	665	16	11	2,92	32,7	9,494	0,272	**-0,5661**
QcrC	198	7	4	1,4	22,4	4,153	0,261	**-0,5827**
EcsA	123	4	4	0,81	13,4	2,373	0,249	**-0,6039**
FtsH	200	4	4	0,34	7,1	2,373	0,187	**-0,7289**
RbsC	98	2	2	0,44	8,1	1,187	0,187	**-0,7289**
WprA	180	6	4	0,3	6,5	3,560	0,140	**-0,8538**
FtsY	113	2	2	0,41	8,8	1,187	0,124	**-0,9050**
Vpr	112	3	3	0,22	7,4	1,780	0,112	**-0,9507**

Protein	Protein score	PSMs	Num. pept	emPAI	Coverage	NSAF	fold change	log_{10} (fold change)
RbsA	527	28	11	1,31	23,3	16,538	16,538	**1,2185**
FloT	2645	257	37	9,83	41,8	151,791	11,645	**1,0662**
ManP	580	15	11	1,06	20,5	8,859	8,859	**0,9474**
RbsB	492	10	8	1,79	28,9	5,906	5,906	**0,7713**
FloA	1290	212	20	5,44	25,4	125,213	5,489	**0,7395**
ResE	379	9	9	1,11	21,9	5,316	5,316	**0,7256**
AhpF	341	8	8	0,97	18,9	4,725	4,725	**0,6744**
FeuA	226	8	5	0,8	15,8	4,725	4,725	**0,6744**
CshA	367	7	7	0,69	16	4,134	4,134	**0,6164**
Ndh	250	7	6	0,81	16,1	4,134	4,134	**0,6164**
RodZ	193	6	6	1,06	20,1	3,544	3,544	**0,5495**
FhuD	300	6	6	1,32	21,9	3,544	3,544	**0,5495**
PhoR	251	5	5	0,37	12,6	2,953	2,953	**0,4703**
PlsX	217	5	5	1	21	2,953	2,953	**0,4703**
MurG	176	5	5	0,86	14	2,953	2,953	**0,4703**
YhfQ	207	5	5	1,01	20,1	2,953	2,953	**0,4703**
TagU	206	4	4	0,82	14,1	2,363	2,363	**0,3734**
McpC	173	4	4	0,26	8,9	2,363	2,363	**0,3734**
OppD	180	4	4	0,52	13,2	2,363	2,363	**0,3734**
Rny	146	4	4	0,53	11	2,363	2,363	**0,3734**

APPENDIX I

Protein	Prot_AC	Description	MW (Da)	pI	Functional Category
FtsZ	WP_003232167.1	cell division protein FtsZ [Bacillales]	40370	5,01	Cell envelope and cell division
MreC	AHA78700.1	Rod shape-determining protein mreC [Bacillus subtilis PY79 PY79]	30073	5,92	Cell envelope and cell division
MotB	WP_003232473.1	motility protein B [Bacillus]	29464	6,57	Exponential and early post-exponential lifestyles
MotA	WP_003244739.1	motility protein A [Bacillus]	29321	5,19	Exponential and early post-exponential lifestyles
SecY	WP_004399662.1	protein translocase subunit SecY [Bacillus]	47213	9,88	Information processing
HemY	WP_003245394.1	protoporphyrinogen oxidase [Bacillus]	51399	8,13	Metabolism
QoxA	ADV94634.1	cytochrome aa3-600 quinol oxidase (subunit II) [Bacillus subtilis BSn5 BSn5]	35942	5	Metabolism
AtpG	WP_003244388.1	ATP synthase subunit gamma [Bacillus]	31635	6,56	Metabolism
YdjG	AHA76571.1	Uncharacterized protein ydjG [Bacillus subtilis PY79 PY79]	37400	5,5	Proteins of unknown function
YxeB	WP_003243725.1	iron(3+)-hydroxamate-binding protein [Bacillus]	35541	6,25	Transporters
SrfAA	WP_010886402.1	surfactin non-ribosomal peptide synthetase SrfAA [Bacillus]	402750	5	Coping with stress
PBP3	WP_003246590.1	penicillin-binding protein 3 [Bacillus]	74531	6,24	Cell envelope and cell division
RasP	AHA77684.1	Zinc metalloprotease rasP [Bacillus subtilis PY79 PY79]	46525	5,31	Cell envelope and cell division
FliF	WP_010886506.1	Flagellar M-ring protein [Bacillus subtilis PY79 PY79]	58648	4,55	Exponential and early post-exponential lifestyles
McpA	AHA79044.1	Methyl-accepting chemotaxis protein mcpA [Bacillus subtilis PY79 PY79]	72400	5,14	Exponential and early post-exponential lifestyles
McpB	WP_003243461.1	methyl-accepting chemotaxis protein McpB [Bacillus]	71857	5,18	Exponential and early post-exponential lifestyles
FliY	WP_003231962.1	flagellar motor switch phosphatase FliY [Bacillus]	41027	4,31	Exponential and early post-exponential lifestyles
WalK	WP_009968432.1	cell wall metabolism sensor histidine kinase WalK [Bacillus]	69990	4,96	Information processing
YclK	AHA76342.1	Sensor histidine kinase yclK [Bacillus subtilis PY79 PY79]	54936	6,16	Information processing
YycH	WP_003242498.1	two-component system YycF/YycG regulatory protein YycH [Bacillus]	52183	5,7	Information processing
ResB	WP_003230515.1	cytochrome c biogenesis protein [Bacillus]	62007	9,23	Metabolism
FruA	WP_003232350.1	PTS fructose EIIABC component [Bacillus]	67255	5,38	Metabolism
FadE	WP_003244094.1	acyl-CoA dehydrogenase [Bacillus]	65352	5,31	Metabolism
NupN	WP_003228831.1	BMP family ABC transporter substrate-binding protein [Bacillus]	38395	5,26	Metabolism
YxkC	WP_003242670.1	DUF4352 domain-containing protein [Bacillus]	23170	9,09	Proteins of unknown function
YdcC	AFQ56402.1	Putative lipoprotein [Bacillus subtilis QB928 QB928]	42219	9,22	Sporulation
DppE	P26906.4	Dipeptide-binding protein DppE [Bacillus subtilis subsp. subtilis str. 168 168]	61837	5,36	Transporters
AppD	WP_003232965.1	oligopeptide transport ATP-binding protein AppD [Bacillus]	36744	5,51	Transporters
ArtP	WP_004398706.1	arginine ABC transporter substrate-binding protein [Bacillus]	28409	5,28	Transporters
PfeT	WP_003245873.1	cadmium-translocating P-type ATPase [Bacillus]	68864	5,12	Transporters
SrfAB	WP_010886403.1	surfactin non-ribosomal peptide synthetase SrfAB [Bacillus]	401377	5,07	Coping with stress
OppA	WP_003232957.1	peptide ABC transporter substrate-binding protein [Bacillus]	61510	5,83	Exponential and early post-exponential lifestyles
SdhA	WP_003229567.1	succinate dehydrogenase flavoprotein subunit [Bacillus]	65395	5,77	Metabolism
CtaC	WP_003232248.1	cytochrome c oxidase subunit 2 [Bacillus]	40354	8,71	Metabolism
FtsH	WP_003243881.1	ATP-dependent zinc metalloprotease FtsH [Bacillus]	71064	5,92	Cell envelope and cell division

APPENDIX I

Protein	Protein score	PSMs	Num. pept	emPAI	Coverage	NSAF	fold change	log_{10} (fold change)
FtsZ	143	3	3	0,51	12,8	1,772	1,772	**0,2484**
MreC	137	3	3	0,73	11,8	1,772	1,772	**0,2484**
MotB	169	3	3	0,76	12,6	1,772	1,772	**0,2484**
MotA	127	3	3	0,53	14,1	1,772	1,772	**0,2484**
SecY	91	3	3	0,42	7,7	1,772	1,772	**0,2484**
HemY	104	3	3	0,28	5,3	1,772	1,772	**0,2484**
QoxA	128	3	3	0,41	10,7	1,772	1,772	**0,2484**
AtpG	120	3	3	0,92	17,4	1,772	1,772	**0,2484**
YdjG	138	3	3	0,56	9,8	1,772	1,772	**0,2484**
YxeB	170	3	3	0,59	14	1,772	1,772	**0,2484**
SrfAA	782	26	17	0,23	6,1	15,356	1,571	**0,1961**
PBP3	79	2	2	0,18	4,5	1,181	1,181	**0,0723**
RasP	64	2	2	0,2	3,8	1,181	1,181	**0,0723**
FliF	81	2	2	0,15	3,4	1,181	1,181	**0,0723**
McpA	89	2	2	0,12	4,4	1,181	1,181	**0,0723**
McpB	82	2	2	0,12	3,3	1,181	1,181	**0,0723**
FliY	74	2	2	0,23	4,8	1,181	1,181	**0,0723**
WalK	77	2	2	0,13	4,1	1,181	1,181	**0,0723**
YclK	60	2	2	0,16	3	1,181	1,181	**0,0723**
YycH	68	2	2	0,17	4,4	1,181	1,181	**0,0723**
ResB	73	2	2	0,14	3,7	1,181	1,181	**0,0723**
FruA	74	2	2	0,2	4,9	1,181	1,181	**0,0723**
FadE	142	2	2	0,29	10,9	1,181	1,181	**0,0723**
NupN	50	2	2	0,24	4,5	1,181	1,181	**0,0723**
YxkC	73	2	2	0,43	8,9	1,181	1,181	**0,0723**
YdcC	62	2	2	0,22	4,8	1,181	1,181	**0,0723**
DppE	63	2	2	0,14	3,7	1,181	1,181	**0,0723**
AppD	96	2	2	0,4	8,2	1,181	1,181	**0,0723**
ArtP	71	2	2	0,34	15,7	1,181	1,181	**0,0723**
PfeT	542	11	9	0,83	22,4	6,497	0,997	**-0,0014**
SrfAB	1250	47	28	0,46	11,1	27,759	0,774	**-0,1110**
OppA	1087	21	17	2,61	37,6	12,403	0,761	**-0,1185**
SdhA	443	8	8	0,89	17,9	4,725	0,725	**-0,1397**
CtaC	611	15	11	3,2	27,2	8,859	0,680	**-0,1677**
FtsH	259	15	6	0,51	11	8,859	0,680	**-0,1677**

Protein	Prot_AC	Description	MW (Da)	pI	Functional Category
PdhC	WP_003232311.1	dihydrolipoyllysine-residue acetyltransferase component of pyruvate dehydrogenase complex [Bacillus]	47567	5,04	Information processing
OdhB	WP_004399364.1	dihydrolipoyllysine-residue succinyltransferase component of 2-oxoglutarate dehydrogenase complex [Bacillus]	45975	5,05	Metabolism
PBP5	AHA75966.1	D-alanyl-D-alanine carboxypeptidase dacA [Bacillus subtilis PY79 PY79]	45951	5,43	Cell envelope and cell division
RpsB	WP_003220918.1	30S ribosomal protein S2 [Bacillales]	28007	6,27	Information processing
SecA	WP_003228033.1	protein translocase subunit SecA [Bacillus]	95698	5,49	Information processing
MreB	WP_003229650.1	rod shape-determining protein [Bacillus]	36008	5,09	Cell envelope and cell division
FtsY	WP_003232026.1	signal recognition particle-docking protein FtsY [Bacillus]	36377	5,27	Information processing
Icd	WP_003229433.1	isocitrate dehydrogenase (NADP(+)) [Bacillus]	46503	5,03	Metabolism
YknX	WP_003244902.1	efflux RND transporter periplasmic adaptor subunit [Bacillus]	41682	5,37	Coping with stress
SrfAC	WP_003234570.1	surfactin non-ribosomal peptide synthetase SrfAC [Bacillus]	144237	5,18	Coping with stress
AlbC	WP_003227564.1	ABC transporter ATP-binding protein [Bacillus]	27387	5,4	Transporters
GapA	WP_003219957.1	aldehyde dehydrogenase [Bacillales]	35924	5,2	Metabolism
TufA	WP_003235058.1	elongation factor Tu [Bacillus]	43680	4,92	Information processing
PrsA	WP_003245079.1	foldase [Bacillus]	32547	8,77	Information processing
AtpD	WP_003227686.1	ATP synthase subunit beta [Bacillus]	51388	4,8	Metabolism
BdbD	WP_003228414.1	thioredoxin [Bacillus]	25004	5,27	Information processing
MntA	WP_003229060.1	manganese-binding lipoprotein MntA [Bacillus]	33454	6,16	Transporters
PdhB	WP_003232313.1	pyruvate dehydrogenase E1 component subunit beta [Bacillus]	35452	4,74	Metabolism
QcrC	WP_003225562.1	menaquinol-cytochrome c reductase cytochrome b/c subunit [Bacillus]	28258	6,92	Metabolism
MetQ	WP_003228595.1	methionine-binding lipoprotein MetQ [Bacillus]	30393	8,26	Transporters
Mbl	WP_003227776.1	rod shape-determining protein [Bacillus]	36009	5,77	Cell envelope and cell division
FlgE	WP_003231968.1	flagellar basal body rod protein FlgG [Bacillus]	27439	4,92	Exponential and early post-exponential lifestyles
AtpA	WP_003243657.1	ATP synthase subunit alpha [Bacillus]	54679	5,22	Metabolism
WprA	WP_003244653.1	peptidase S8 [Bacillus]	96485	9,2	Information processing
Hag	WP_003228021.1	flagellin [Bacillus]	32607	4,97	Exponential and early post-exponential lifestyles
EcsA	WP_003233230.1	ABC transporter ATP-binding protein [Bacillales]	27818	5,72	Transporters

Table 11: Pull-down raw data of $FloA_{nt}T_{ct}$.

Protein	Prot_AC	Description	MW (Da)	pI	Functional Category
RbsA	WP_003244379.1	ribose import ATP-binding protein RbsA [Bacillus]	54612	6,2	Transporters
FloT	WP_003228960.1	flotillin family protein [Bacillus]	55959	5,34	Exponential and early post-exponential lifestyles
CshA	P96614.2	DEAD-box ATP-dependent RNA helicase CshA [Bacillus subtilis subsp. subtilis str. 168 168]	55296	9,49	Information processing
Rny	WP_003221010.1	ribonuclease Y [Bacillales]	58940	5,51	Information processing
ArtP	WP_004398706.1	arginine ABC transporter substrate-binding protein [Bacillus]	28409	5,28	Transporters
AhpF	WP_003243077.1	alkyl hydroperoxide reductase subunit F [Bacillus]	55125	4,89	Coping with stress
HemY	WP_003245394.1	protoporphyrinogen oxidase [Bacillus]	51399	8,13	Metabolism
RbsB	WP_003242760.1	D-ribose ABC transporter substrate-binding protein [Bacillus]	32264	6,15	Transporters
FhuD	WP_003243220.1	iron(3+)-hydroxamate-binding protein FhuD [Bacillus]	34462	8,85	Transporters
FloA	WP_003230026.1	UPF0365 family protein [Bacillus]	35676	5,1	Cell envelope and cell division
FeuA	WP_003234978.1	iron-uptake system-binding protein [Bacillus]	35143	7,66	Transporters

APPENDIX I

Protein	Protein score	PSMs	Num. pept	emPAI	Coverage	NSAF	fold change	log_{10} (fold change)
PdhC	592	11	11	1,61	26,9	6,497	0,665	**-0,1775**
OdhB	593	14	10	1,46	31,7	8,269	0,634	**-0,1977**
PBP5	416	10	10	1,72	24,2	5,906	0,604	**-0,2188**
RpsB	549	18	10	4,89	47,2	10,631	0,544	**-0,2646**
SecA	230	6	6	0,3	7,6	3,544	0,544	**-0,2646**
MreB	285	8	8	1,82	26,4	4,725	0,483	**-0,3158**
FtsY	262	8	6	1,22	18,2	4,725	0,483	**-0,3158**
Icd	614	19	12	2,48	33,3	11,222	0,430	**-0,3661**
YknX	176	4	4	0,49	11,9	2,363	0,363	**-0,4407**
SrfAC	74	4	2	0,06	2,9	2,363	0,363	**-0,4407**
AlbC	247	5	5	1,12	23	2,953	0,302	**-0,5199**
GapA	353	6	6	0,99	23,3	3,544	0,272	**-0,5656**
TufA	197	3	3	0,33	9,3	1,772	0,272	**-0,5656**
PrsA	599	16	10	3,61	39,4	9,450	0,264	**-0,5790**
AtpD	386	16	8	0,92	18,4	9,450	0,264	**-0,5790**
BdbD	375	5	5	1,28	28,4	2,953	0,227	**-0,6448**
MntA	304	13	6	1,1	19,3	7,678	0,214	**-0,6692**
PdhB	463	8	8	1,55	29,8	4,725	0,207	**-0,6837**
QcrC	264	5	5	1,08	16,5	2,953	0,181	**-0,7417**
MetQ	192	4	4	0,97	16,1	2,363	0,181	**-0,7417**
Mbl	44	2	2	0,26	7,8	1,181	0,181	**-0,7417**
FlgE	102	2	2	0,35	7,6	1,181	0,181	**-0,7417**
AtpA	464	11	11	1,32	19,5	6,497	0,166	**-0,7795**
WprA	149	7	4	0,19	3,9	4,134	0,159	**-0,7997**
Hag	387	8	5	0,88	21,7	4,725	0,132	**-0,8800**
EcsA	65	2	2	0,35	7,3	1,181	0,121	**-0,9178**

Protein	Protein score	PSMs	Num. pept	emPAI	Coverage	NSAF	fold change	log_{10} (fold change)
RbsA	409	20	9	1,32	23,9	12,510	12,510	**1,0972**
FloT	1657	184	27	5,91	31,2	115,088	11,544	**1,0624**
CshA	247	6	6	0,57	10,9	3,753	3,753	**0,5744**
Rny	220	6	5	0,42	8,1	3,753	3,753	**0,5744**
ArtP	204	6	5	0,79	18	3,753	3,753	**0,5744**
AhpF	224	5	5	0,46	10,8	3,127	3,127	**0,4952**
HemY	134	5	5	0,5	10,4	3,127	3,127	**0,4952**
RbsB	280,24	5	5	0,9	21,3	3,127	3,127	**0,4952**
FhuD	214,4	5	5	0,83	14,6	3,127	3,127	**0,4952**
FloA	857	79	12	2,6	35,6	49,413	2,832	**0,4521**
FeuA	173	4	4	0,6	12,6	2,502	2,502	**0,3983**

APPENDIX I

Protein	Prot_AC	Description	MW (Da)	pI	Functional Category
YxeB	WP_003243725.1	iron(3+)-hydroxamate-binding protein [Bacillus]	35541	6,25	Transporters
Ndh	WP_003232765.1	NADH dehydrogenase [Bacillus]	41927	6,28	Metabolism
FtsZ	WP_003232167.1	cell division protein FtsZ [Bacillales]	40370	5,01	Cell envelope and cell division
McpB	WP_003243461.1	methyl-accepting chemotaxis protein McpB [Bacillus]	71857	5,18	Exponential and early post-exponential lifestyles
YhfQ	WP_003233159.1	ABC transporter substrate-binding protein [Bacillus]	35524	9,06	Transporters
DppE	P26906.4	Dipeptide-binding protein DppE [Bacillus subtilis subsp. subtilis str. 168 168]	61837	5,36	Transporters
TufA	WP_003235058.1	elongation factor Tu [Bacillus]	43680	4,92	Information processing
SrfAA	WP_010886402.1	surfactin non-ribosomal peptide synthetase SrfAA [Bacillus]	402750	5	Coping with stress
SrfAA	WP_010886402.1	surfactin non-ribosomal peptide synthetase SrfAA [Bacillus]	402750	5	Coping with stress
SdhA	WP_003229567.1	succinate dehydrogenase flavoprotein subunit [Bacillus]	65395	5,77	Metabolism
RasP	AHA77684.1	Zinc metalloprotease rasP [Bacillus subtilis PY79 PY79]	46525	5,31	Cell envelope and cell division
TagU	WP_003227949.1	LytR family transcriptional regulator [Bacillus]	34565	9,18	Cell envelope and cell division
McpA	AHA79044.1	Methyl-accepting chemotaxis protein mcpA [Bacillus subtilis PY79 PY79]	72400	5,14	Exponential and early post-exponential lifestyles
CheA	WP_003245734.1	chemotaxis protein CheA [Bacillus]	74994	4,67	Exponential and early post-exponential lifestyles
MotB	WP_003232473.1	motility protein B [Bacillus]	29464	6,57	Exponential and early post-exponential lifestyles
RpoC	WP_004399688.1	DNA-directed RNA polymerase subunit beta~ [Bacillus]	134795	8,79	Information processing
FadE	WP_003244094.1	acyl-CoA dehydrogenase [Bacillus]	65352	5,31	Metabolism
ResB	WP_003230515.1	cytochrome c biogenesis protein [Bacillus]	62007	9,23	Metabolism
Eno	WP_003228333.1	enolase [Bacillus]	46610	4,68	Metabolism
CtaD	WP_003232245.1	cytochrome ubiquinol oxidase subunit I [Bacillus]	68982	6,88	Metabolism
SdhB	WP_003229569.1	succinate dehydrogenase iron-sulfur subunit [Bacillus]	29026	8,47	Metabolism
YdjG	AHA76571.1	Uncharacterized protein ydjG [Bacillus subtilis PY79 PY79]	37400	5,5	Proteins of unknown function
ManP	WP_023592766.1	PTS mannose EIIBCA component [Bacillus subtilis]	69154	6,1	Transporters
TcyA	WP_003246699.1	L-cystine-binding protein TcyA [Bacillus]	29553	8,61	Transporters
PdhC	WP_003232311.1	dihydrolipoyllysine-residue acetyltransferase component of pyruvate dehydrogenase complex [Bacillus]	47567	5,04	Information processing
SrfAC	WP_003234570.1	surfactin non-ribosomal peptide synthetase SrfAC [Bacillus]	144237	5,18	Coping with stress
OppA	WP_003232957.1	peptide ABC transporter substrate-binding protein [Bacillus]	61510	5,83	Exponential and early post-exponential lifestyles
SrfAB	WP_010886403.1	surfactin non-ribosomal peptide synthetase SrfAB [Bacillus]	401377	5,07	Coping with stress
PBP5	AHA75966.1	D-alanyl-D-alanine carboxypeptidase dacA [Bacillus subtilis PY79 PY79]	45951	5,43	Cell envelope and cell division
GapA	WP_003219957.1	aldehyde dehydrogenase [Bacillales]	35924	5,2	Metabolism
FtsA	WP_009967186.1	cell division protein FtsA [Bacillus]	48333	5,17	Cell envelope and cell division
OdhB	WP_004399364.1	dihydrolipoyllysine-residue succinyltransferase component of 2-oxoglutarate dehydrogenase complex [Bacillus]	45975	5,05	Metabolism
RpsB	WP_003220918.1	30S ribosomal protein S2 [Bacillales]	28007	6,27	Information processing
SecA	WP_003228033.1	protein translocase subunit SecA [Bacillus]	95698	5,49	Information processing
FtsH	WP_003243881.1	ATP-dependent zinc metalloprotease FtsH [Bacillus]	71064	5,92	Cell envelope and cell division
MbI	WP_003227776.1	rod shape-determining protein [Bacillus]	36009	5,77	Cell envelope and cell division

APPENDIX I

Protein	Protein score	PSMs	Num. pept	emPAI	Coverage	NSAF	fold change	log_{10} (fold change)
YxeB	145,75	4	4	0,6	11,5	2,502	2,502	**0,3983**
Ndh	179	4	3	0,35	7,9	2,502	2,502	**0,3983**
FtsZ	94	3	3	0,36	5,8	1,876	1,876	**0,2733**
McpB	120	3	3	0,19	5,1	1,876	1,876	**0,2733**
YhfQ	121,72	3	3	0,42	9,3	1,876	1,876	**0,2733**
DppE	71	3	2	0,14	2,8	1,876	1,876	**0,2733**
TufA	669	14	12	2,79	37,6	8,757	1,757	**0,2447**
SrfAA	583	18	12	0,13	3,8	11,259	1,506	**0,1777**
SrfAA	161	2	3	0,06	1,6	11,259	1,506	**0,1777**
SdhA	468	10	10	1,01	18,9	6,255	1,255	**0,0986**
RasP	78	2	2	0,2	6,2	1,251	1,251	**0,0972**
TagU	113,69	2	2	0,27	5,9	1,251	1,251	**0,0972**
McpA	75	2	2	0,12	2,6	1,251	1,251	**0,0972**
CheA	57	2	2	0,12	2,5	1,251	1,251	**0,0972**
MotB	98,32	2	2	0,76	12,6	1,251	1,251	**0,0972**
RpoC	49	2	2	0,1	2,3	1,251	1,251	**0,0972**
FadE	48	2	2	0,14	5,9	1,251	1,251	**0,0972**
ResB	67	2	2	0,14	6,3	1,251	1,251	**0,0972**
Eno	100	2	2	0,2	7,4	1,251	1,251	**0,0972**
CtaD	70	2	2	0,2	3,7	1,251	1,251	**0,0972**
SdhB	77	2	2	0,54	11,5	1,251	1,251	**0,0972**
YdjG	90	2	2	0,25	4,9	1,251	1,251	**0,0972**
ManP	108	2	2	0,2	4,5	1,251	1,251	**0,0972**
TcyA	67	2	2	0,52	11,9	1,251	1,251	**0,0972**
PdhC	539	14	9	1,19	25,1	8,757	1,171	**0,0686**
SrfAC	293	8	8	0,26	5,9	5,004	1,004	**0,0017**
OppA	737	17	12	1,41	26,2	10,633	0,853	**-0,0689**
SrfAB	776	35	19	0,24	6,6	21,892	0,798	**-0,0977**
PBP5	329	9	9	1,48	21,3	5,629	0,753	**-0,1233**
GapA	425	12	8	1,24	26	7,506	0,753	**-0,1233**
FtsA	221	6	6	0,83	15,2	3,753	0,753	**-0,1233**
OdhB	314	11	7	1,26	29,3	6,880	0,690	**-0,1611**
RpsB	493,58	15	8	4,1	35,4	9,382	0,627	**-0,2025**
SecA	211	5	5	0,24	5,2	3,127	0,627	**-0,2025**
FtsH	319	8	7	0,51	10,5	5,004	0,502	**-0,2994**
Mbl	189	4	4	1	16,8	2,502	0,502	**-0,2994**

APPENDIX I

Protein	Prot_AC [a]	Description	MW (Da)	pI	Functional Category [b]
PfeT	WP_003245873.1	cadmium-translocating P-type ATPase [Bacillus]	68864	5,12	Transporters
Icd	WP_003229433.1	isocitrate dehydrogenase (NADP(+)) [Bacillus]	46503	5,03	Metabolism
AtpA	WP_003243657.1	ATP synthase subunit alpha [Bacillus]	54679	5,22	Metabolism
AtpD	WP_003227686.1	ATP synthase subunit beta [Bacillus]	51388	4,8	Metabolism
WprA	WP_003244653.1	peptidase S8 [Bacillus]	96485	9,2	Information processing
CtaC	WP_003232248.1	cytochrome c oxidase subunit 2 [Bacillus]	40354	8,71	Metabolism
KinC	WP_003232333.1	PAS domain-containing sensor histidine kinase [Bacillus]	48986	6,23	Information processing
AlbC	WP_003227564.1	ABC transporter ATP-binding protein [Bacillus]	27387	5,4	Transporters
MetQ	WP_003228595.1	methionine-binding lipoprotein MetQ [Bacillus]	30393	8,26	Transporters
PdhB	WP_003232313.1	pyruvate dehydrogenase E1 component subunit beta [Bacillus]	35452	4,74	Metabolism
BdbD	WP_003228414.1	thioredoxin [Bacillus]	25004	5,27	Information processing
MreB	WP_003229650.1	rod shape-determining protein [Bacillus]	36008	5,09	Cell envelope and cell division
FtsY	WP_003232026.1	signal recognition particle-docking protein FtsY [Bacillus]	36377	5,27	Information processing
FlgE	WP_003231968.1	flagellar basal body rod protein FlgG [Bacillus]	27439	4,92	Exponential and early post-exponential lifestyles
MntB	WP_004398644.1	manganese transport system ATP-binding protein MntB [Bacillus]	27921	9,11	Transporters
RbsC	WP_009968282.1	ribose ABC transporter permease [Bacillus]	33823	9,95	Transporters
PrsA	WP_003245079.1	foldase [Bacillus]	32547	8,77	Information processing
QcrC	WP_003225562.1	menaquinol-cytochrome c reductase cytochrome b/c subunit [Bacillus]	28258	6,92	Metabolism
EcsA	WP_003233230.1	ABC transporter ATP-binding protein [Bacillales]	27818	5,72	Transporters
Hag	WP_003228021.1	flagellin [Bacillus]	32607	4,97	Exponential and early post-exponential lifestyles
MntA	WP_003229060.1	manganese-binding lipoprotein MntA [Bacillus]	33454	6,16	Transporters

[a] Protein Accession Number
[b] Functional Category was assigned with *Subti*wiki (Zhu and Stülke, 2018).

APPENDIX I

Protein	Protein score	PSMs [c]	Num. pept	emPAI [d]	Coverage	NSAF [e]	fold change [f]	log_{10} (fold change)
PfeT	181	4	4	0,27	6,3	2,502	0,502	**-0,2994**
Icd	365	14	7	0,87	19,4	8,757	0,439	**-0,3574**
AtpA	871	20	17	2,66	36,3	12,510	0,418	**-0,3786**
AtpD	753	18	15	2,12	42,3	11,259	0,411	**-0,3865**
WprA	514	13	9	0,68	13,3	8,131	0,408	**-0,3895**
CtaC	371	6	6	1,28	20,2	3,753	0,376	**-0,4243**
KinC	140	3	3	0,4	10,5	1,876	0,376	**-0,4243**
AlbC	175	4	4	1,13	23	2,502	0,335	**-0,4755**
MetQ	243	5	5	1,59	20,1	3,127	0,314	**-0,5035**
PdhB	369	8	8	1,56	26,2	5,004	0,287	**-0,5424**
BdbD	263	4	4	0,64	22,5	2,502	0,251	**-0,6004**
MreB	134	3	3	0,41	9,8	1,876	0,251	**-0,6004**
FtsY	147	3	3	0,41	10,9	1,876	0,251	**-0,6004**
FlgE	137	2	2	0,35	7,6	1,251	0,251	**-0,6004**
MntB	69	3	2	0,34	7,6	1,876	0,251	**-0,6004**
RbsC	101	2	2	0,28	5,3	1,251	0,251	**-0,6004**
PrsA	450,54	9	7	1,77	29,1	5,629	0,205	**-0,6876**
QcrC	199	4	4	1,08	16,5	2,502	0,201	**-0,6973**
EcsA	102	2	2	0,35	7,3	1,251	0,167	**-0,7765**
Hag	309	6	4	0,66	15,5	3,753	0,137	**-0,8636**
MntA	296,45	5	5	0,86	19,6	3,127	0,114	**-0,9428**

[c] Peptide Spectra Match

[d] Exponentially modified Protein Abundance Index

[e] Normalized Spectral Abundance Factor

[f] Fold change is determined compared to the control

9.6 Compiled microscopy of mobility analysis

This is a summary of the mobility analysis performed in this work sorted chronologically according to the results presented. The corresponding figure is indicated. The mobility pattern of a representative cell at the beginning and the end of the image sequence will be displayed on the left. Kymograph analysis and trajectories of this cell are shown in the middle. The MSD plot corresponding to the experimental setup is shown on the left. Kymographs were generated with the membrane signal indicated with the yellow arrow in the left. Blue triangles indicate neighboring cell poles. Horizontal scale bars represent 2 µm, vertical scale bars represent 3 s. Colors in trajectories show elapsing time from blue to red. Representative trajectories are highlighted. Numbers in the plots indicate the numbers of trajectories used in MSD analysis.

9.6.1 FloA and FloT

Epifluorescence microscopy control (Figure 13)

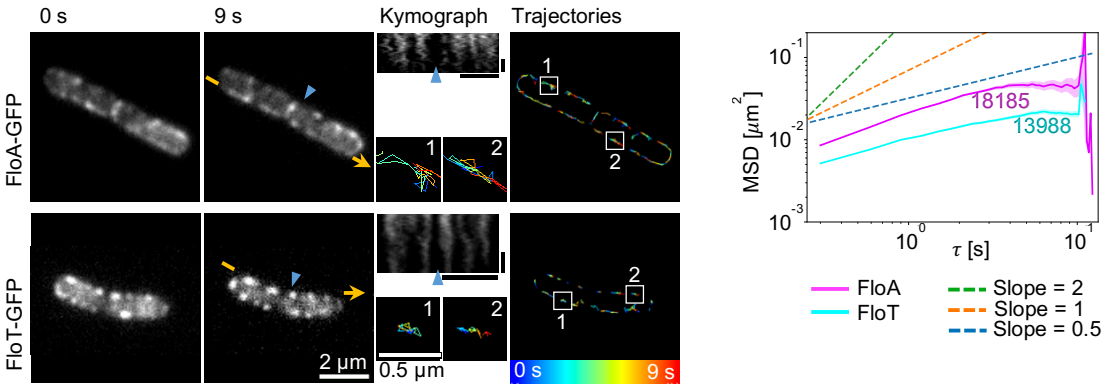

TIRFM (Figure 11, Figure 12)

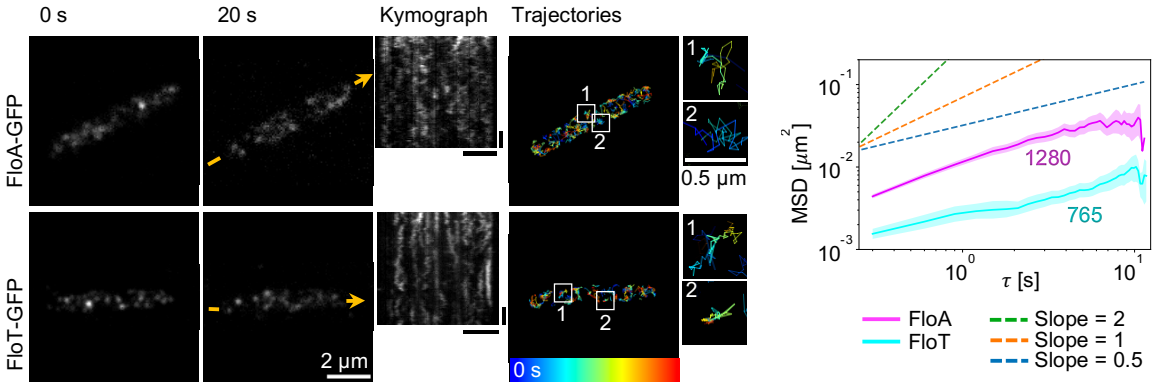

Deletion of the other flotillin operon (Figure 14)

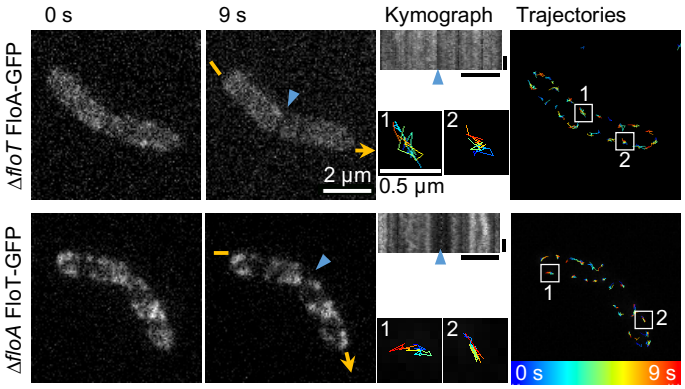

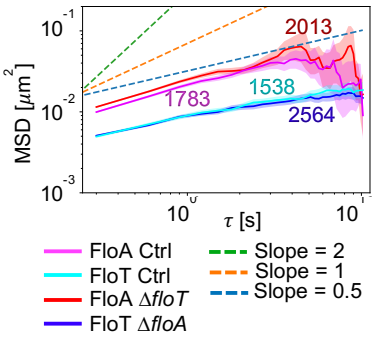

Benzyl alcohol (Figure 15)

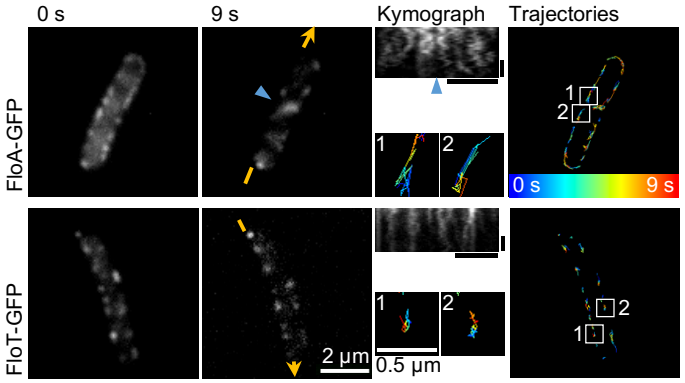

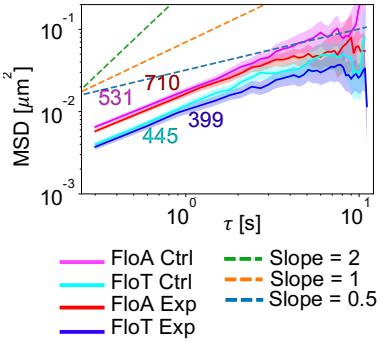

Nisin (Figure 15)

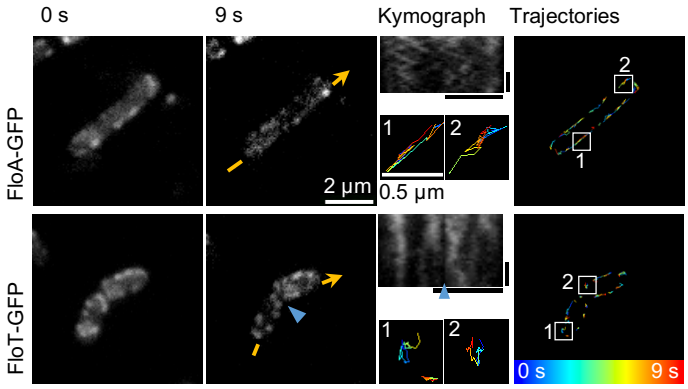

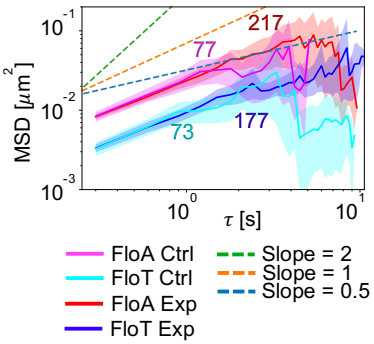

Valinomycin (Figure 15)

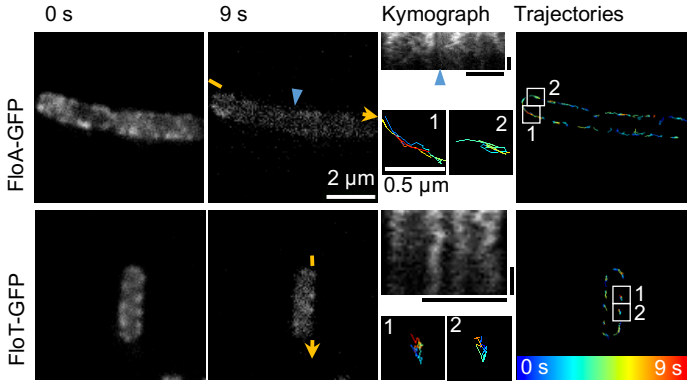

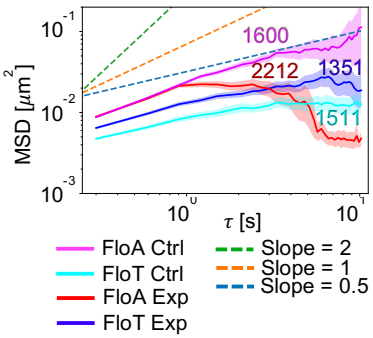

Chimeric flotillins (Figure 20, Figure 21)

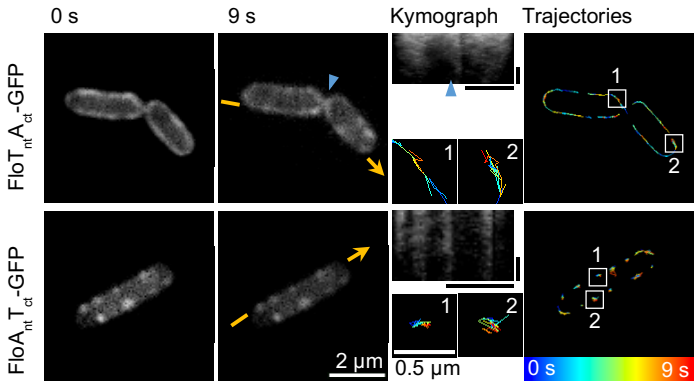

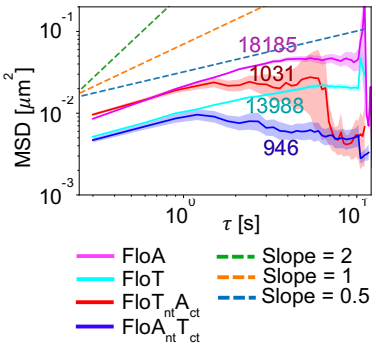

Δ*pbpC* (Figure 28)

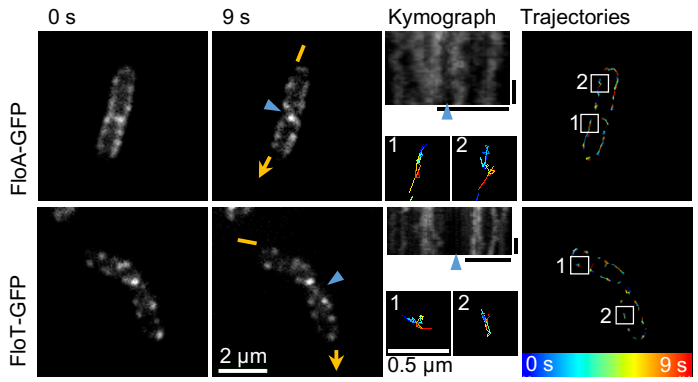

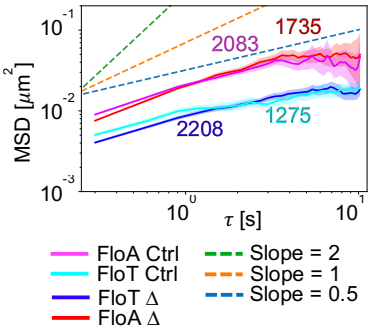

Δ*dltA-E* (Figure 33)

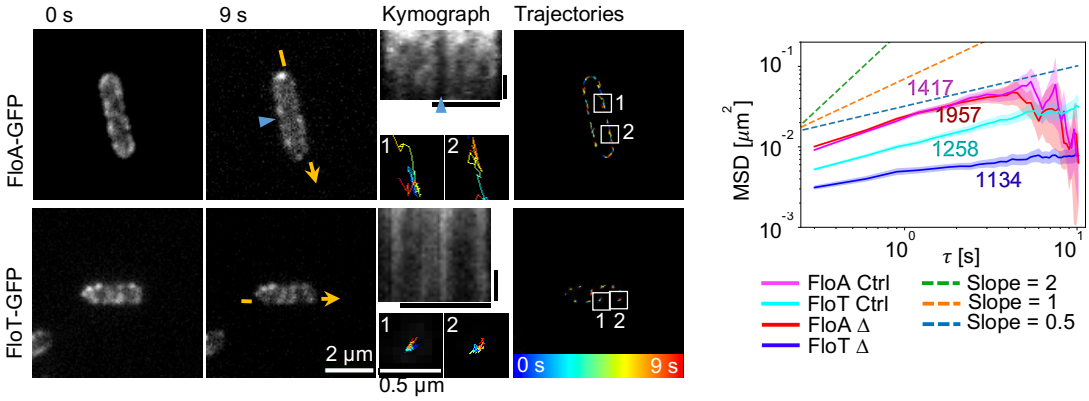

Δ*tagU* (Figure 34)

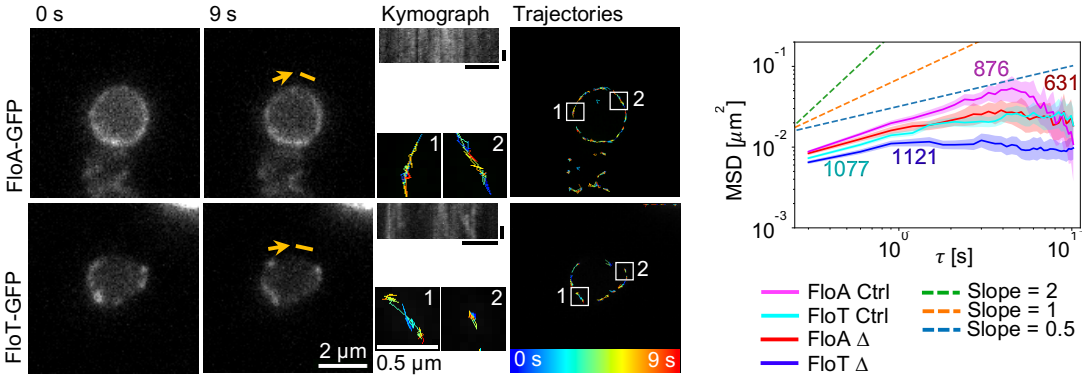

Δ*ugtP* (Figure 34)

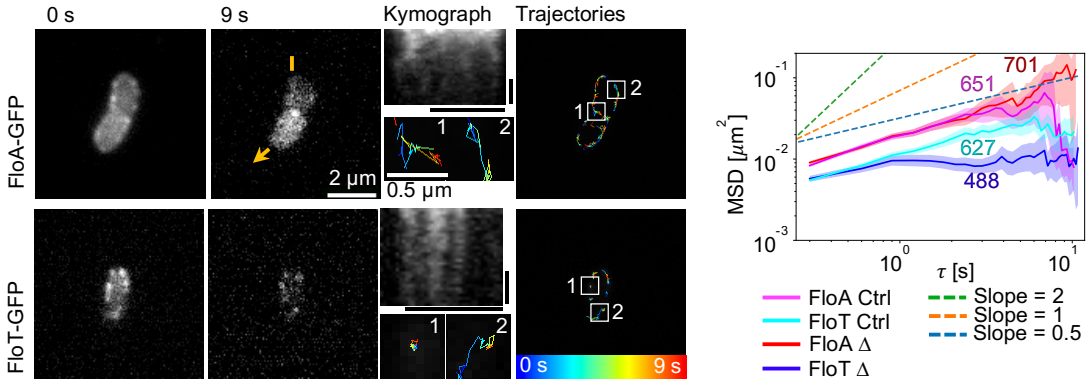

FloT controls for Δ*dltA-E* (Figure 35)

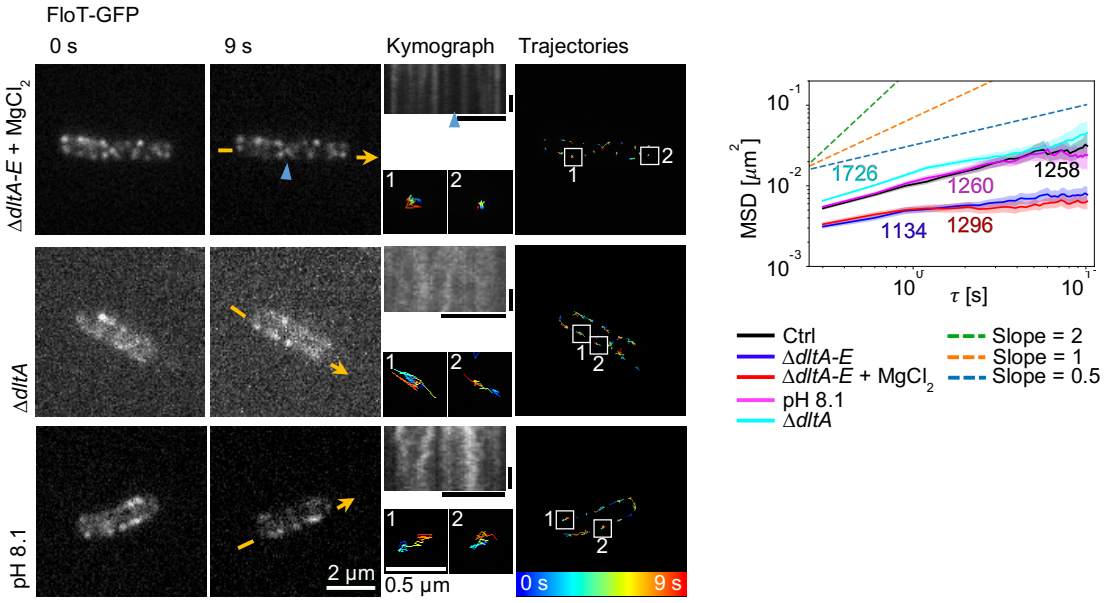

Fosfomycin (Figure 37)

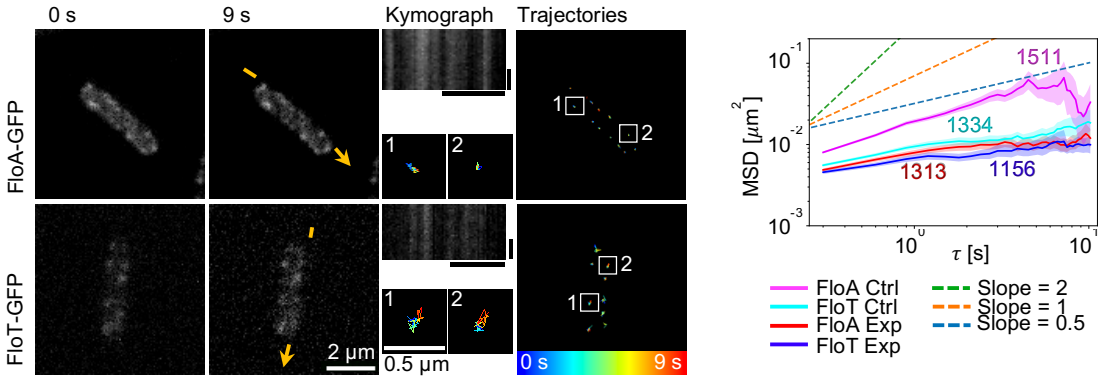

Tunicamycin: TUN 2.5 μg/ml (Figure 37)

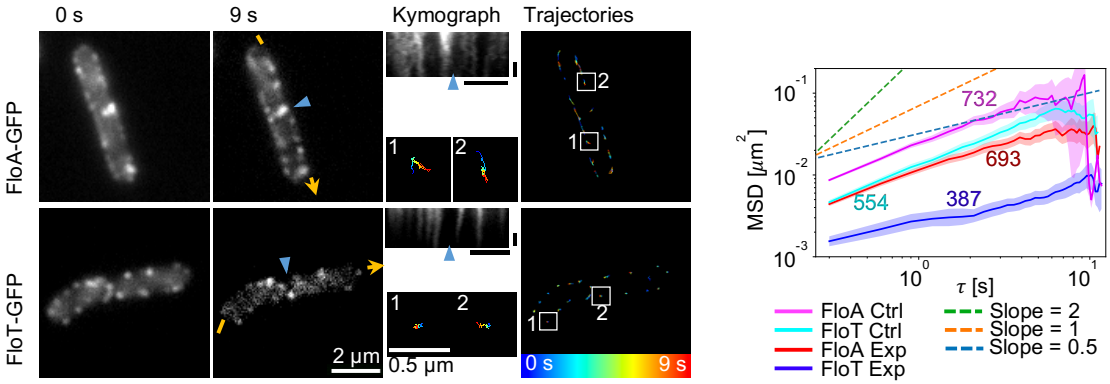

Ampicillin (Figure 37)

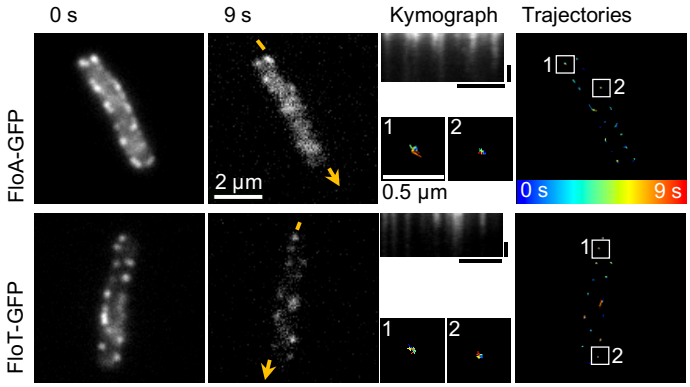

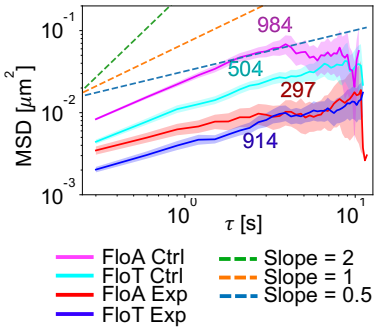

Vancomycin (Figure 37)

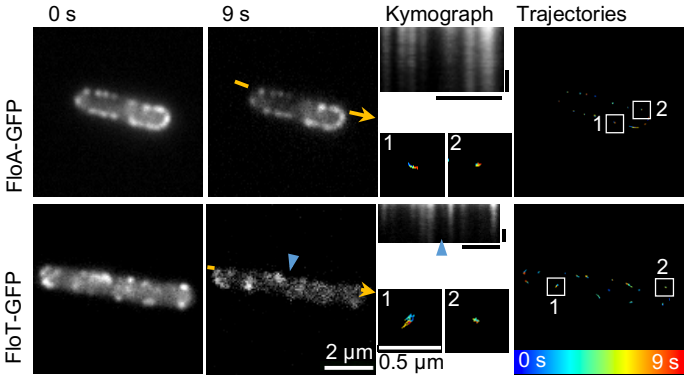

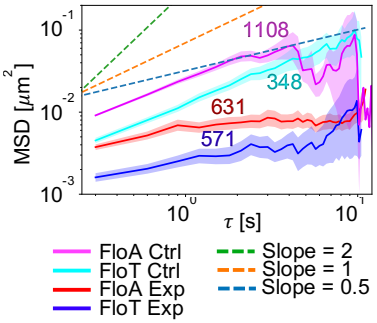

Tunicamycin: TunWTA 0.025µg/ml (Figure 38)

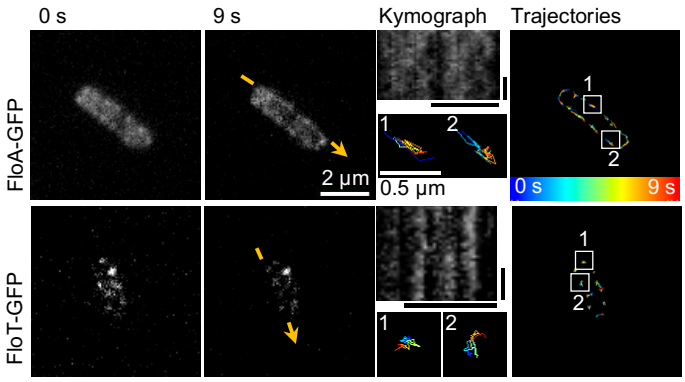

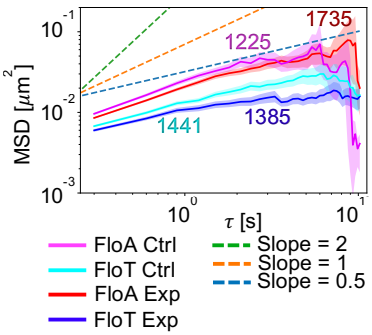

DMSO (Figure 38)

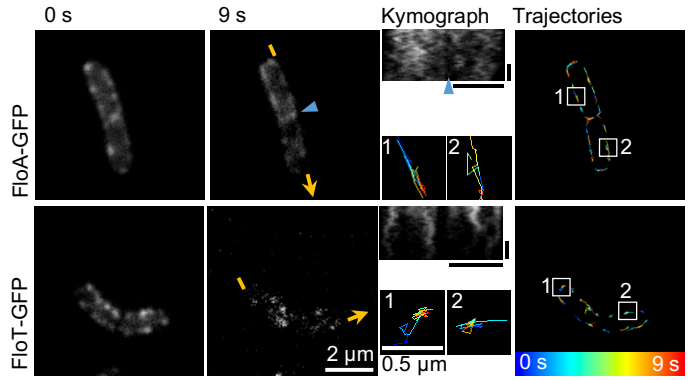

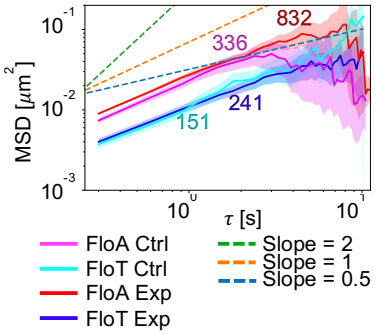

Cytoskeleton-disrupting conditions (Figure 45)

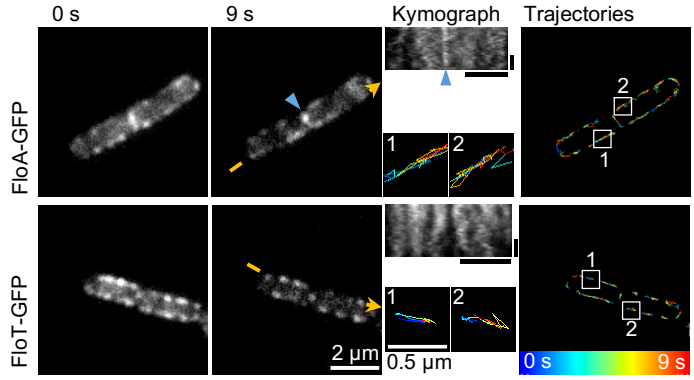

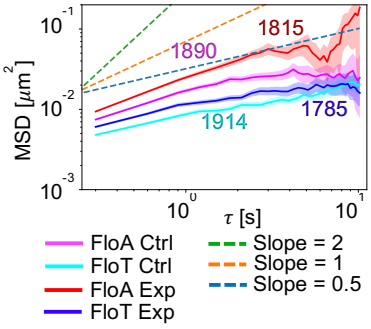

Δ*rsgI* (Figure 46)

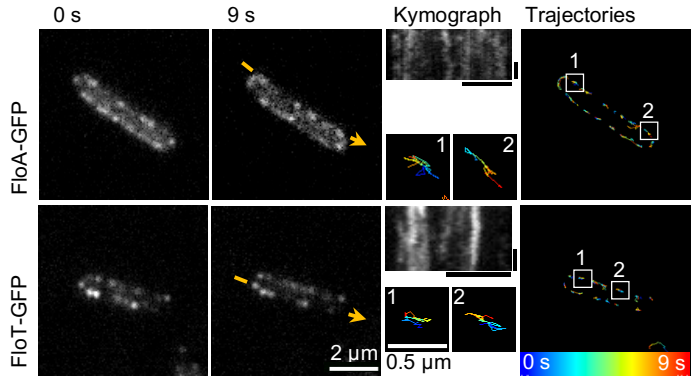

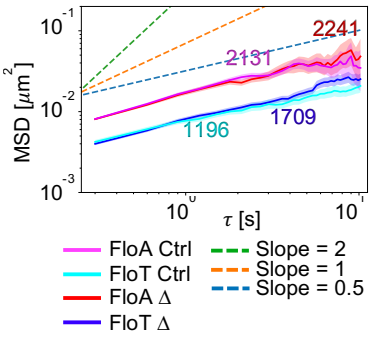

Δ*mreB* Δ*mreBH* Δ*mbl* (Figure 47)

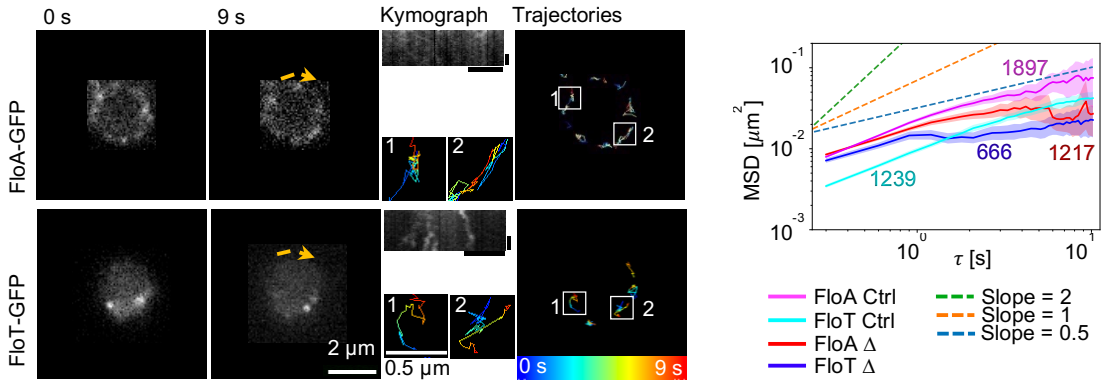

Protoplasts (Figure 49)

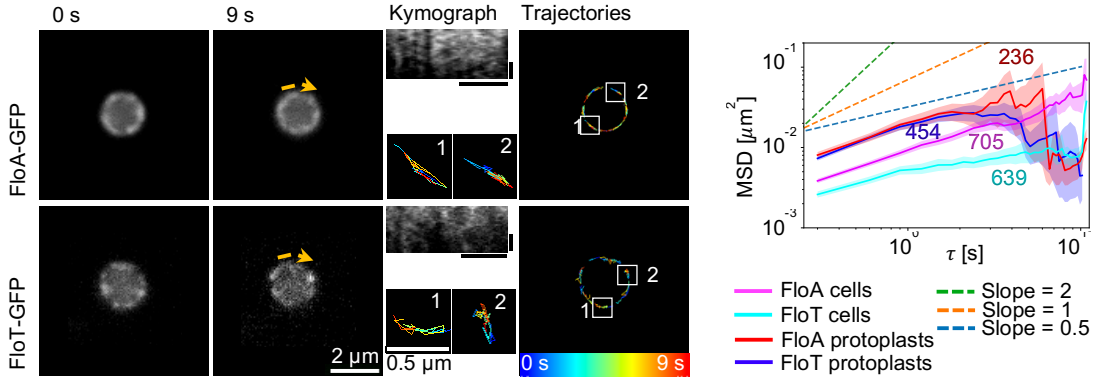

9.6.2 PBP3

Flotillin deletion mutants (Figure 29)

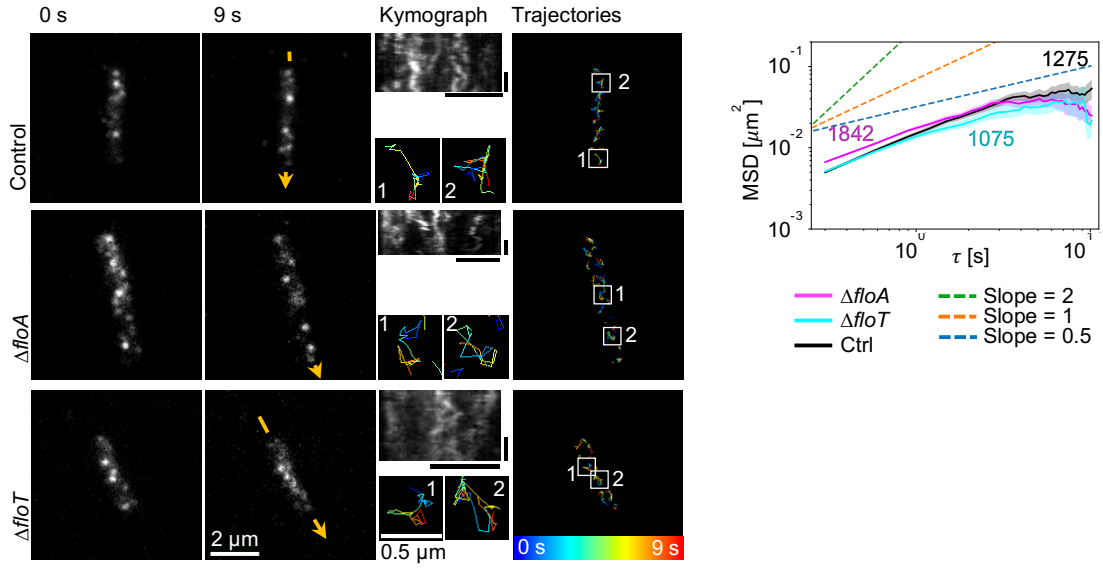

9.6.3 DltD

Flotillin deletion mutants (Figure 32)

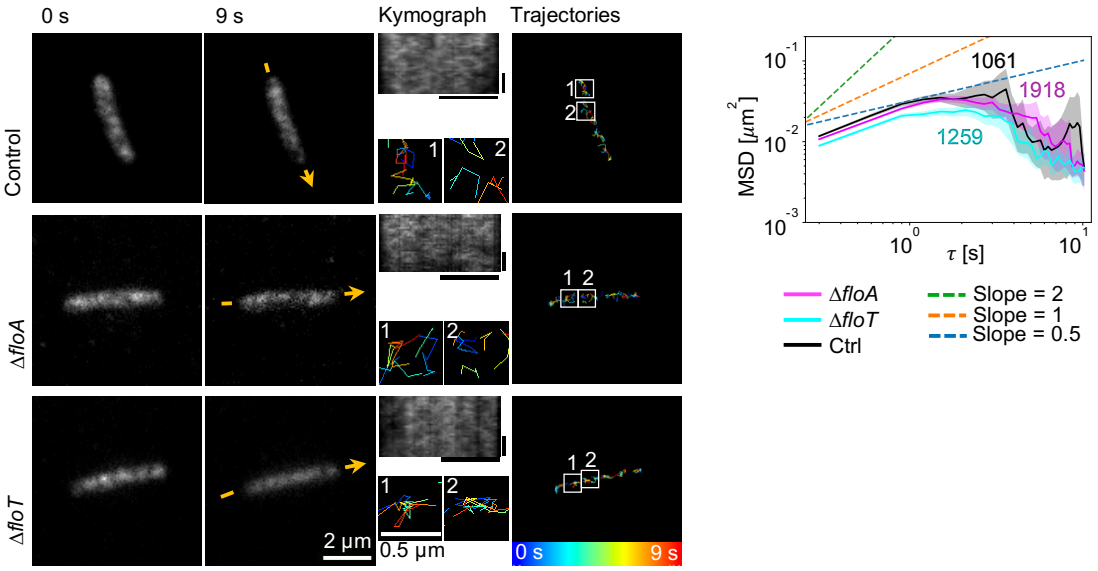

9.6.4 MreB

Protoplasts (Figure 41, Figure 48)

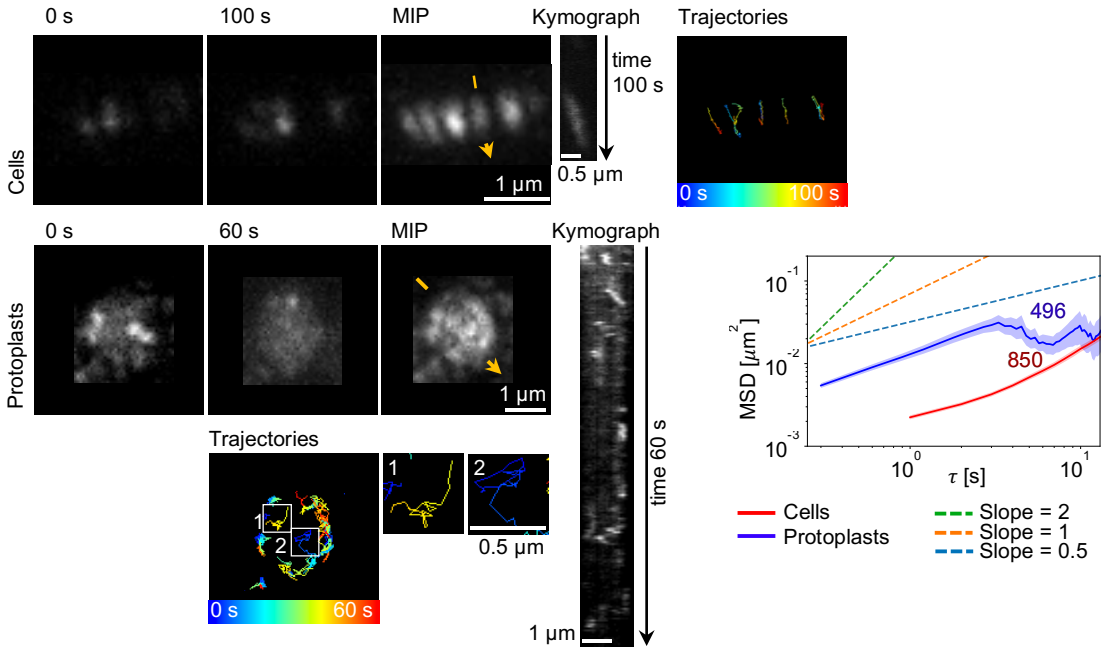

10 APPENDIX II

10.1 Contributions by others

This doctoral thesis was performed under the supervision of Dr. Daniel Lopez in part at the Institute of Infection Biology (IMIB) at the University of Würzburg, Germany, and in part at the Spanish National Center for Biotechnology (CNB-CSIC) in Madrid, Spain. Listed below are contributions by others that have led to the successful completion of this doctoral thesis.

- Biophysical and bioinformatical support was given by the collaboration partners Prof. PhD Ned Wingreen, Sagar Setru (both Princeton University) and Prof. PhD Benjamin Machta (Yale University). They bioinformatically created the plots of mean square displacement analysis and provided support in their interpretation.
- The microscopy facilities of the IMIB in Würzburg (especially Hilde Merkert) and the CNB-CSIC in Madrid (especially Sylvia Gutiérrez Erlandsson and Ana Oña Blanco) provided technical support with maintenance of the fluorescence microscopes and expertise.
- Technical support with purchases and especially with a continuous access to plates, medium and gels was provided by Isa Westedt, Carmen Ortega Plaza and Marina Cabrerizo Alonso.
- Scienseed contributed with the graphic implementation of the model in Figure 52.
- The proteomics facility at the CNB-CSIC in Madrid performed the mass-spectrometry experiments of this work and provided guidance in data processing (especially Sergio Ciordia Higuera).
- The German Collection of Microorganisms and Cell Cultures GmbH (DSMZ) in Braunschweig, Germany, performed the analysis of the fatty acid composition and the polar lipids.

10.2 License for the use of published figures

Figure 1: Hop-diffusion can be explained with the picket-fence model.

Figure 4a, b of Kusumi et al., 2012

Order Summary

Licensee:	Mrs. Rabea Wagner
Order Date:	May 19, 2020
Order Number:	4832391432666
Publication:	Seminars in Cell & Developmental Biology
Title:	Membrane mechanisms for signal transduction: The coupling of the meso-scale raft domains to membrane-skeleton-induced compartments and dynamic protein complexes
Type of Use:	reuse in a thesis/dissertation

Figure 3: Lipid rafts can coexist within the picket-fence model.

Figure 1 of Kusumi et al., 2012

Order Summary

Licensee:	Mrs. Rabea Wagner
Order Date:	May 18, 2020
Order Number:	4832010120947
Publication:	Seminars in Cell & Developmental Biology
Title:	Membrane mechanisms for signal transduction: The coupling of the meso-scale raft domains to membrane-skeleton-induced compartments and dynamic protein complexes
Type of Use:	reuse in a thesis/dissertation

Figure 7: Lateral cell wall is synthesized independently by the Rod-complex and aPBPs.

Figure 1a of Dion et al., 2019

Order Summary

Licensee:	Mrs. Rabea Wagner
Order Date:	May 18, 2020
Order Number:	4832020958835
Publication:	Nature Microbiology
Title:	Bacillus subtilis cell diameter is determined by the opposing actions of two distinct cell wall synthetic systems
Type of Use:	Thesis/Dissertation

Figure 30: The DltABCDE proteins modify LTA and WTA in the cell wall.

Figure 1 of McKay Wood et al., 2018

1. Journal of biological chemistry

Billing Status: Open

Print License

Order license ID	1035893-1
Order detail status	Completed
ISSN	1083-351X
Type of use	Republish in a thesis/dissertation
Publisher	AMERICAN SOCIETY FOR BIOCHEMISTRY AND ...
Portion	Chart/graph/table/figure

11 APPENDIX III

11.1 Acknowledgements

Endless people contributed in one way or another to this work, be it scientific support in the lab, emotional support from the distance or just simple distraction. Each one of you participated in bringing this work to a completion. Thank you! Danke! Gracias! Grazie! Dziękuję! धन्यवाद

First of all, I want to thank my sponsor and supervisor Daniel Lopez for giving me the opportunity to work on this interesting project for my PhD thesis. Dani was always positive and helped to make me see the whole picture and believe in the project even when things seemed hopeless. He always gave me the freedom to follow my own ideas and to independently develop the project.

I further want to thank the members of my thesis committee, Prof. PhD Samuel Wagner (Universität Tübingen) and Prof. Dr. Nicolai Siegel (LMU München) for their constructive feedback and new ideas that were implemented in the project. In the course of this I also want to thank the members of the GSLS (Universität Würzburg) for their support and especially for the workshops they organized.

A special thanks goes to all current and previous members of AG DL in Würzburg and Lab 211 in Madrid. Thank you for your trust, your advice and your scientific and emotional support and particularly the distractions in P2 gossip sessions. Special thanks go to: the Geibels for hosting me in their lab; Joe for patience in introducing me to microscopy; Diana, Mar, Esther and Elvira for overcoming Spanish bureaucracy again and again; Lara for going through all of these ups and downs with me together – frei nach dem Motto: geteiltes Leid ist halbes Leid; Charly and Ben for kindly welcoming me again when I had to go back to the microscope; Nicky, Ivan and Ilaria for the early-morning and Julia for the late-afternoon conversations; Marina for her DJ qualities and finally Anabel, Gaurav, Charly and Nicky for editing of this thesis.

Ein ganz besonderer Dank geht an meine Familie für ihre Unterstützung und ihr Vertrauen, dass ich das schon meistern werde, auch wenn sie nicht genau verstanden haben, was ich da eigentlich genau mache. Und auch für ihr Fingerspitzengefühl, dass sie wussten, wann Zeit war, das Thema zu wechseln.

Außerdem möchte ich meinen Freunden danken: den Mädels von daheim mit ihren Buben (und Kindern) für Verständnis, Ablenkung und Gossip und besonders Julia und Selina für ihr Vertrauen; der Freisinger Seppen Abgangsgruppe für ihren schwarzen Humor und all die nerdigen Ergüsse; der immer noch anhaltenden Verbindung zu Würzburg (Charly, Gabri, Nicky und Tonja) für die Gastfreundschaft, gemeinsame (TV-) Erlebnisse und IMIB Gossip und zum Schluss ganz besonders allen die Kosten und Mühen nicht gescheut haben, um mich in Madrid besuchen zu kommen.

Last but not least I want to thank Gaurav for his endless support and understanding. Thank you for always being there! Finally, the time has come for us to start a life together!

11.2 List of Publications

Wagner, R. M., Setru, S. U., Machta, B., Wingreen, N. S., and Lopez, D. (2020). The Bacterial Cytoskeleton Spatially Confines Functional Membrane Microdomains. *In revision*. Preprint in bioRxiv, 2020.04.25.060970. doi:10.1101/2020.04.25.060970.

García-Fernández, E., Koch, G., **Wagner, R. M.**, Fekete, A., Stengel, S. T., Schneider, J., et al. (2017). Membrane Microdomain Disassembly Inhibits MRSA Antibiotic Resistance. *Cell* 171, 1354-1367.e20. doi:10.1016/j.cell.2017.10.012.

Mielich-Süss, B., **Wagner, R. M.**, Mietrach, N., Hertlein, T., Marincola, G., Ohlsen, K., et al. (2017). Flotillin scaffold activity contributes to type VII secretion system assembly in *Staphylococcus aureus*. *PLOS Pathogens* 13, e1006728. doi:10.1371/journal.ppat.1006728.

Wagner, R. M., Kricks, L., and Lopez, D. (2017). Functional Membrane Microdomains Organize Signaling Networks in Bacteria. *J Membrane Biol* 250, 367–378. doi:10.1007/s00232-016-9923-0.

11.3 List of Presentations

06/2020 **Talk** at Subtillery – Virtual International Conference to distill, understand, and appreciate the biology of Bacillus subtilis and related endospore-forming organisms
Wagner, R. M., Setru, S. U., Machta, B., Wingreen, N. S., and Lopez, D. *'The Bacterial Cytoskeleton Spatially Confines Functional Membrane Microdomains'*

03/2019 **Short talk** at the German Association of General and Applied Microbiology (VAAM) Annual Conference 2019 in Mainz, Germany
' **Wagner, R. M.**, and Lopez, D. *'Cytoskeletal confinement of membrane microdomains'*

09/2018 **Short talk** at the Rafts4Biotech Symposium on Lipid Membrane Eukaryotic & Prokaryotic Biology in Madrid, Spain
Wagner, R. M., and Lopez, D. *'Dynamics of functional membrane microdomains in Bacillus subtilis'*

05/2018 **Short talk** at the Microbial Biotechnology department seminar at the Spanish National Center for Biotechnology in Madrid, Spain
Wagner, R. M., and Lopez, D. '*Structure and dynamics of bacterial lipid rafts'*

04/2018 **E-Poster** at the German Association of General and Applied Microbiology (VAAM) Annual Conference 2018 in Wolfsburg, Germany
Wagner, R. M., and Lopez, D. *'Functional membrane microdomain dynamics in B. subtilis'*

07/2017 **Poster** at the Federation of European Microbiological Societies (FEMS) 2017 conference in Valencia, Spain
Wagner, R. M., and Lopez, D. *'Molecular characterization of microdomain dynamics in bacterial membranes'*

11.4 *Curriculum Vitae*

Cover:
Bacillus subtilis expressing FloA-GFP (green)
DNA stained with Hoechst (blue)
Scale bar represents 2 μm